Genetic, pathologic, and radiographic correlations in multiple sclerosis

Richard L. Yates

Pembroke College, University of Oxford



Nuffield Department of Clinical Neurosciences

Medical Sciences Division

University of Oxford

A thesis submitted for the degree of Doctor of Philosophy

Trinity Term, 2016

Genetic, pathologic, and radiographic correlations in multiple sclerosis

Richard L. Yates, Pembroke College, Oxford

A thesis submitted for the degree of Doctor of Philosophy, Trinity Term, 2016

Abstract

Substantial evidence suggests that cortical tissue injury plays a key role in the progression of permanent disability in multiple sclerosis (MS). A greater knowledge of factors that drive pathology in the MS cortex is therefore desperately needed in order to develop novel medicines that can ameliorate disease burden in the progressive stage. In the current thesis, we undertake a robust and quantitative analysis of motor cortical neuropathology in a large cohort of post-mortem MS cases. We find that genetic variation at the *HLA-DRB1* locus is associated with the extent of cortical demyelinating and inflammatory disease, especially in younger cases. Relevant to cortical neurodegeneration, we identify fibrinogen deposition as a novel component of MS cortical pathology that associates with neuronal loss, show that carriage of *HLA-DRB1*15* has a critical impact on the relationship between microglia/macrophage inflammation and cortical neuronal density, and demonstrate disease-relevant changes to motor cortical neuronal glutamic acid decarboxylase expression. Given the myriad subcortical connections of the motor cortex, we have also undertaken an extensive assessment of corticospinal tract lesional burden throughout the neuraxis and find that motor cortical neurodegeneration appears independent of subcortical tissue injury. Taken together, this thesis highlights the importance of genetic variation at the *HLA-DRB1* locus to cortical pathologic outcome, and the fundamental contribution of fibrinogen deposition and cortical parenchymal inflammatory factors to neuronal fate.

Publications related to thesis

Yates RL, Esiri MM, Palace J, DeLuca GC. The influence of *HLA-DRB1*15* on motor cortical pathology in multiple sclerosis. *Neuropathol Appl Neurobiol* 2015; 41: 371-84.

Yates RL, DeLuca GC. Comment: *HLA-DRB1*1501* associations with magnetic resonance imaging measures of grey matter pathology in multiple sclerosis. *Mult Scler Relat Disord* 2016 (in press).

Yates RL, Esiri MM, Palace J, Jacobs B, Perera R, DeLuca GC. Fibrinogen associates with degeneration in the multiple sclerosis motor cortex (submitted).

Yates RL, Esiri MM, Palace J, Perera R, Li Q, Orlowski P, DeLuca GC. The influence of *HLA-DRB1*15* on motor cortical neurodegeneration in multiple sclerosis (in preparation).

Publications unrelated to thesis

Grussu F, Schneider T, **Yates RL**, Zhang H, Wheeler-Kingshott CA, DeLuca GC, Alexander DC. A framework for optimal whole-sample histological quantification of neurite orientation dispersion in the human spinal cord. *J Neurosci Methods* 2016; 273:20-32.

James RE, Hillis J, Adorján I, Gration B, Mundim MV, Iqbal AJ, Majumdar MM, **Yates RL**, Richards MM, Goings GE, DeLuca GC, Greaves DR, Miller SD, Szele FG. Loss of galectin-3 decreases the number of immune cells in the subventricular zone and restores proliferation in a viral model of multiple sclerosis. *Glia* 2016; 64: 105-21.

DeLuca GC, **Yates RL,** Beale H, Morrow SA. Cognitive impairment in multiple sclerosis: clinical, radiologic and pathologic insights. *Brain Pathol* 2015; 25: 79-98.

DeLuca GC, Joseph A, George J, **Yates RL**, Hamard M, Hofer M, Esiri MM. Olfactory Pathology in Central Nervous System Demyelinating Diseases. *Brain Pathol* 2015; 25: 543-51.

Book chapter

DeLuca GC, **Yates RL**, Sadovnik D. Genetics and Epidemiology of multiple sclerosis. Primer on MS (2016). Oxford University Press (USA).

Acknowledgements

This thesis would not have been possible without the continual support and encouragement of all those around me during the last four years. First and foremost, I would like to thank my supervisors, Dr Gabriele DeLuca and Dr Jacqueline Palace. I will be eternally grateful for the time invested in my education, and I look forward to their continuing mentorship as I embark on my clinical and research career. I would also like to thank Professor Margaret Esiri, for her excellent advice and critical analysis, whenever requested. Thanks is also given to my lab mates, Bryan Adriaanse, Dr Damian Jenkins and Dr Ruth Geraldes, for the positive and scholastic atmosphere that always pervades the lab, and that I have come to cherish throughout my DPhil.

I would also like to to thank individuals who contributed to the body of work contained within this thesis. Thanks are offered to J.L. Martin, R. Alterman, and K. Morrison, for the many hours spent genotyping the multiple sclerosis cases used in this study. I would also like to thank S. Foxley, for acquiring such high-quality radiographic images of our post-mortem cohort. Thanks to P. Orlowski and Q. Li, for their excellent work optimising the algorithm used in this thesis to quantify inhibitory synaptic coverage. Finally, thanks to A. Rudzitis, for help proof-reading.

Last, but certainly not least, I would like to thank my parents. Their unconditional support is never taken for granted. I owe them dearly.

Contents

List of Figures 11
List of Tables 13
Abbreviations 14
1. Introduction 17
1.1 Overview of MS 17
1.2. Clinical Summary 18
1.2.1. Diagnosis 18
1.2.2. Natural history 19
1.2.3. *HLA-DRB1*15* and clinical outcome 20
1.3. Environmental Epidemiology 21
1.3.1. Geographic distribution 21
1.3.2. Vitamin D 22
1.3.3. Viral infectious agents 23
1.3.4. Bacterial infectious agents 24
1.3.5. Lifestyle factors 25
1.4. Genetics 26
1.4.1. Genetic epidemiology 26
1.4.2. Genetic susceptibility 26
1.5. Immunology 29
1.5.1. Peripheral lymphocyte activation 29
1.5.2. Lymphocyte migration into the CNS 30
1.5.3. Activation of brain microglia 31
1.6. Neuroimaging 33
1.6.1. Magnetic resonance imaging (MRI) Physics 33
1.6.2. MRI assessment of white matter lesions 34
1.6.3. MRI assessment of grey matter lesions 35
1.6.4. MRI assessment of non-lesional parenchyma 36
1.6.5. *HLA-DRB1*15* and MRI outcome 39
1.7. Neuropathology 40
1.7.1. Histologic assessment of white matter lesions 40
1.7.2. Histologic assessment of grey matter lesions 41
1.7.3. Histologic assessment of neurodegeneration 43

1.7.4. Mechanisms of neurodegeneration 44
1.7.5. *HLA-DRB1*15* and neuropathology outcome 47
1.7.6. MRI-pathology studies 48
1.8. Overview of Thesis 49
2. The influence of *HLA-DRB1*15* status on motor cortical inflammatory pathology in multiple sclerosis 52
2.1. Introduction 52
2.2. Materials and Methods 54
2.2.1. Study Population 54
2.2.2. Genetics 54
2.2.3. Neuropathological Evaluation 55
2.2.4. Assessment of motor cortical demyelination 56
2.2.5. Assessment of motor cortical inflammation 57
2.2.6. Statistical Analyses 61
2.3. Results 62
2.3.1. Genetics 62
2.3.2. Neuropathological findings: MS versus controls 63
2.3.2.1 Demyelination 63
2.3.2.2 Lymphocytic inflammation 65
2.3.2.3. Microglial/macrophage inflammation 65
2.3.2.4. Relationship of motor cortical lesions, inflammation and demographic factors 67
2.3.3. Genetic-pathology relationships in MS 67
2.3.3.1. Demyelination 67
2.3.3.2. Parenchymal lymphocytic inflammation 70
2.3.3.3. Perivascular lymphocytic inflammation 72
2.3.3.4. Meningeal lymphocytic inflammation 74
2.3.3.5. Microglial/macrophage inflammation 74
2.3.4. Relationships between motor cortical lesion load, inflammation, demographic factors and *HLA-DRB1*15* status 76
2.3.5. Correlations between motor cortical and spinal cord MS pathology, and the influence of *HLA-DRB1*15* status 76
2.3.5.1. Demyelination 76
2.3.5.2. Parenchymal lymphocytic inflammation 77
2.3.5.3. Parenchymal microglia/macrophage inflammation 77

2.3.5.4. Meningeal Inflammation 78
2.4. Discussion 79
3. Fibrinogen deposition associates with neurodegeneration in the multiple sclerosis motor cortex 86
3.1 Introduction 86
3.2. Materials and Methods 89
3.2.1. Study population 89
3.2.2. Tissue sampling 89
3.2.3. Immunohistochemistry 89
3.2.4 Assessment of motor cortical demyelination 91
3.2.5 Assessment of motor cortical fibrinogen deposition, microglial/macrophage inflammation, and neuronal density 91
3.2.6. Quantitation of fibrinogen deposition 94
3.2.7. Quantitation of microglial/macrophage inflammation 94
3.2.8. Quantitation of neuronal density 94
3.2.9. Assessment of motor cortical PAI-1 95
3.2.10. Statistical analyses 96
3.3. Results 97
3.3.1. Demographic features of MS and control cohort 97
3.3.2. Fibrinogen deposition: MS vs. controls 98
3.3.2.1. Distribution and extent of fibrinogen deposition 98
3.3.2.2. Extracellular fibrinogen 98
3.3.2.3. Cell Body Fibrinogen 99
3.3.2.4. Neuritic/glial-process fibrinogen 99
3.3.2.5. Validation of (monoclonal) fibrinogen findings with additional (polyclonal) fibrinogen antibody 105
3.3.3. Influence of *HLA-DRB1*15* on motor cortical fibrinogen deposition 108
3.3.4. Relationships between MS motor cortical pathology and fibrinogen deposition 110
3.3.4.1. Demyelination and fibrinogen deposition 110
3.3.4.2. Microglial/macrophage inflammation and fibrinogen deposition 110
3.3.4.3. Neuronal density and fibrinogen deposition 113
3.3.5. Assessment of motor cortical PAI-1 in MS cases and controls 117
3.4 Discussion 119
4. The influence of *HLA-DRB1*15* on motor cortical neurodegeneration in multiple sclerosis 124

4.1. Introduction 124
4.2. Materials and Methods 128
4.2.1. Study population 128
4.2.2. Immunohistochemistry and Immunofluorescence 128
4.2.3. Assessment strategy of motor cortical inflammation and neuronal density 130
4.2.3.1. Lymphocytic inflammation 130
4.2.3.2. Microglia/macrophage inflammation 130
4.2.3.3. Neuronal density 131
4.2.4. Assessment strategy of motor cortical meningeal inflammation 131
4.2.5. Assessment strategy of motor cortical GAD 131
4.2.5.1. Synaptic GAD 132
4.2.5.2. Cytoplasmic GAD 135
4.2.6. Statistical analyses 136
4.3. Results 136
4.3.1. Clinical features of MS cases and controls 136
4.3.2. Neuropathological findings: MS vs. controls 139
4.3.2.1. Parenchymal microglia/macrophage inflammation in MS versus control motor cortex 139
4.3.2.2. Parenchymal and perivascular lymphocytic inflammation in MS versus control motor cortex 139
4.3.2.3. Meningeal inflammation in MS versus control motor cortex 140
4.3.2.4. Neuronal density in MS versus control motor cortex 142
4.3.3. Relationships between meningeal, perivascular and parenchymal inflammation in MS and control 142
4.3.4. Relationships between parenchymal inflammation and neuronal density in MS and control motor cortex 144
4.3.5. Influence of *HLA-DRB1*15* status on the relationship between parenchymal microglia/macrophage inflammation and neuronal density 146
4.3.6. GAD in the MS motor cortex 154
Synaptic GAD+ neurons 154
4.3.6.1. Membrane-associated GAD+ synaptic density in MS and control 154
4.3.6.2. Relationships between membrane-associated GAD+ synaptic density, microglia/macrophage inflammation and neuronal density in MS and controls 155
4.3.6.3. Assessment of GAD+ neuronal size 156

4.3.6.4. Relationships between GAD+ neuronal size, microglia/macrophage inflammation, neuronal density, and GAD synapse in MS and controls 156
Cytoplasmic GAD+ neurons 158
4.3.6.5. Cytoplasmic GAD density in MS and control 158
4.3.6.6. Relationships between cytoplasmic GAD, microglia/macrophage inflammation and neuronal density in MS and controls 158
4.3.6.7. Influence of HLA-DRB1*15 on the relationship between cytoplasmic GAD and microglia/macrophage inflammation 159
4.4. Discussion 161
5. MRI-pathology correlations in the multiple sclerosis corticospinal tract 167
5.1. Introduction 167
5.2. Materials and Methods 170
5.2.1. Study population 170
5.2.2. Histology 170
5.2.2.1. Tissue sampling 170
5.2.2.2. Immunohistochemistry 170
5.2.2.3. Assessment of motor cortical demyelination 171
5.2.2.4. Assessment strategy of motor cortical layer 5 microglia/macrophage inflammation and neuronal density 171
5.2.2.5. Motor cortical layer 5 microglia/macrophage inflammation 172
5.2.2.6. Motor cortical layer 5 neuronal density 172
5.2.2.7. Subgroup analysis of spinal cord LCST demyelination, microglia/macrophage inflammation and axonal density/number 173
5.2.3. Cerebral hemispheric MRI 175
5.2.3.1. Cerebral hemispheric radiographic image acquisition 175
5.2.3.2. Cerebral hemispheric radiographic image analysis 175
5.2.4. Spinal cord MRI 176
5.2.4.1. Spinal cord radiographic image acquisition 176
5.2.4.2. Spinal cord image analysis 178
5.2.5. Statistical analyses 180
5.3. Results 181
5.3.1. Demographic features of cohort 181
5.3.2. Motor cortical neuropathological findings 182
5.3.2.1. Cortical lesions 182
5.3.2.2. Layer 5 microglia/macrophage inflammation 182
5.3.2.3. Layer 5 Neuronal density 183

5.3.2.4. Relationships between cortical lesions and layer 5 microglia/macrophage inflammation and neuronal density 183
5.3.3. Spinal cord sub-group analysis 189
5.3.3.1. Radiographic and pathologic characteristics of MS1 and MS2 189
5.3.3.2. Relationship between microglia/macrophage inflammation and axonal density in MS1 and MS2 190
5.3.4. Cerebral hemispheric CST radiographic findings 192
5.3.5. Spinal cord LCST radiographic findings 192
5.3.6. Relationship between motor cortical histology and CST radiographic findings 193
5.3.6.1. Relationship between motor cortical demyelination and CST radiographic lesional burden 193
5.3.6.2. Relationship between motor cortical neuropathology and CST radiographic lesional burden 194
5.4. Discussion 196
6. Summary 202
6.1 The influence of *HLA-DRB1*15* on motor cortical inflammatory pathology in multiple sclerosis 202
6.2. Fibrinogen deposition associates with neurodegeneration in the multiple sclerosis motor cortex 204
6.3. The influence of *HLA-DRB1*15* on neurodegeneration in the multiple sclerosis motor cortex 207
6.4. MRI-pathology correlations in the MS corticospinal tract 210
7. Future work 212
7.1. Genetic-pathology correlations 212
7.2. Fibrinogen deposition and BBB disruption 214
7.3. MRI-pathology correlations 215
8. Bibliography 216
Appendix 1 - Protocol for DAB immunohistochemistry 254
Appendix 2 - Protocol for immunofluorescence 255

List of Figures

Figure 2.1: Quantitative neuropathological methods 59
Figure 2.2: Quantitation of microglial/macrophage inflammation. 60
Figure 2.3: Photomicrographs of proteo-lipid protein (PLP) stained cortical tissue 64
Figure 2.4: Motor cortical inflammation in MS cases and controls 66
Figure 2.5: Relationship of age, HLA-DRB1*15 status and motor cortical lesion load 69
Figure 2.6: HLA-DRB1*15 status and parenchymal T-cell inflammation 71
Figure 2.7: HLA-DRB1*15 status and perivascular T-cell inflammation 73
Figure 2.8: HLA-DRB1*15 status and microglial/macrophage inflammation 75
Figure 3.1: Assessment strategy of motor cortical pathology 93
Figure 3.2: Quantitation of motor cortical neuronal density 95
Figure 3.3: Semi-quantitative scoring of fibrinogen deposition 102
Figure 3.4: Fibrinogen deposition in the MS motor cortex 103
Figure 3.5: Fluorescent double-labelling of fibrinogen to demonstrate cellular localisation 104
Figure 3.6: Fibrinogen deposition detected with polyclonal antibody 106
Figure 3.7: Direct Comparison of fibrinogen deposition detected with monoclonal and polyclonal antibodies 106
Figure 3.8: Quantitation of fibrinogen deposition using polyclonal fibrinogen antibody 107
Figure 3.9: Association of HLA-DRB1*15 status with fibrinogen deposition 109
Figure 3.10: Iba1+ inflammation in MS and controls 111
Figure 3.11: CD68+ inflammation in MS and controls 111
Figure 3.12: Microglial/macrophage inflammation in MS NAGM and lesions 112
Figure 3.13: Neuronal density in MS and controls 113
Figure 3.14: Neuronal density in MS NAGM and lesions 114
Figure 3.15: Association of fibrinogen deposition with motor cortical neuronal loss 116
Figure 3.16: Motor cortical PAI-1 118
Figure 4.1: Immunolabelling of synaptic GAD (left) and cytoplasmic GAD (right) 132
Figure 4.2: Quantitation of GAD+ synaptic coverage of layer 5 neurons. 134
Figure 4.3: Cytoplasmic GAD quantitation 135

Figure 4.4: Meningeal, perivascular and parenchymal inflammation in MS cases and controls 141

Figure 4.5: Relationship between microglia/macrophage inflammation and neuronal density 145

Figure 4.6: Relationship between microglia/macrophage inflammation and neuronal density in MS cases below and above the median age of the cohort (median age = 62 years) 145

Figure 4.7: Impact of HLA-DRB1*15 status on neuronal density in all MS cases, MS cases under 62 years, and MS cases over 62 years 146

Figure 4.8: Relationship between microglia/macrophage inflammation and neuronal density in HLA-DRB1*15+ and HLA-DRB1*15- genotype groups ... 147

Figure 4.9: Relationship between microglia/macrophage inflammation and neuronal density in HLA-DRB1*15+ and HLA-DRB1*15- MS cases under 62 years 152

Figure 4.10: Relationship between microglia/macrophage inflammation and neuronal density in HLA-DRB1*15+ and HLA-DRB1*15- MS cases over 62 years 153

Figure 4.11: GAD+ neurons in MS and control. 157

Figure 5.1: Neuronal counting method. 172

Figure 5.2: Spinal cord histology. 174

Figure 5.3: Spinal cord MRI acquisition 177

Figure 5.4: Summary of analysis strategy for motor cortex, cerebral hemispheres, and spinal cord 179

Figure 5.5: Demyelination in different motor cortical regions 184

Figure 5.6: Iba1+ inflammation in different motor cortical regions 185

Figure 5.7: CD68+ inflammation in different motor cortical regions 186

Figure 5.8: Neuronal density in different motor cortical regions 187

Figure 5.9: Pathologic outcomes throughout the length of the motor cortex. 188

Figure 5.10: Comparison of microglia/macrophage and neuronal relationships in motor cortex and spinal cord 191

Figure 5.11: Comparison of radiographic lesion burden impinging on the CST of the brain and spinal cord 193

Figure 5.12: Relationships between CST radiographic lesional burden and motor cortical layer 5 neuronal density 195

List of Tables

Table 2.1: Details of antibodies used in chapter 2 56

Table 2.2: Clinical details of cohort used in chapter 2 63

Table 3.1: Summary of antibodies used for DAB immunohistochemistry in chapter 3 90

Table 3.2: Summary of antibodies used for fluorescent immunohistochemistry in chapter 3 91

Table 3.3: Clinical details of cohort used in chapter 3 97

Table 3.4: Summary of fibrinogen deposition in MS and control motor cortex 101

Table 4.1: Antibodies used for DAB immunohistochemistry in chapter 4 .. 129

Table 4.2: Antibodies used for immunofluorescence in chapter 4 129

Table 4.3: Clinical details of cohort used in chapter 4 137

Table 4.4: Clinical details of cohort for synaptic GAD analysis 138

Table 4.5: Multiple linear regression analysis showing the interaction of *HLA-DRB1*15* status and Iba1+ inflammation to predict neuronal density 149

Table 4.6: Multiple linear regression analysis showing the interaction *of HLA-DRB1*15* status and CD68+ inflammation to predict neuronal density 150

Table 5.1: Clinical details of cohort used in chapter 5 181

Abbreviations

ANOVA	analysis of variance
ATP	adenosine triphosphate
BBB	blood-brain-barrier
BDNF	brain-derived neurotropic factor
Ca	calcium
CD	cluster of differentiation
CIS	clinically isolated syndrome
CNS	central nervous system
CREB	cAMP response element binding protein
CSF	cerebrospinal fluid
CST	corticospinal tract
DAB	diaminobenzidine
DAPI	4', 6-diamidino-2-phenylindole
DMT	disease modifying therapy
DNA	deoxyribonucleic acid
DTI	diffusion tensor imaging
EAE	experimental autoimmune encephalomyelitis
EBV	Epstein-Barr virus
EC	extracellular
EDTA	ethylenediaminetetraacetic acid
ETX	epsilon toxin
FMRIB	Oxford centre for functional MRI of the brain
FOV	field of view
GABA	gamma amino butyric acid
GAD	glutamic acid decarboxylase
GM	grey matter

GWAS	genome-wide association studies
H&E	haemotoxylin and eosin
HLA	human leukocyte antigen
Iba	ionised calcium-binding adaptor molecule
K	potassium
LC-MS/MS	liquid-chromatography tandem mass spectrometry
LCST	lateral corticospinal tract
MHC	major histocompatibility complex
MRI	magnetic resonance imaging
MRS	magnetic resonance spectroscopy
MS	multiple sclerosis
MTR	magnetisation transfer ratio
MWI	myelin water imaging
Na	sodium
NAA	N-acetyl aspartate
NAGM	normal appearing grey matter
NAWM	normal appearing white matter
NeuN	neuronal nuclei
NMDA	N-methyl-D-aspartate
NODDI	neurite orientation and dispersion imaging
OPC	oligodendrocyte precursor cell
PAI	plasminogen activator inhibitor
PD	proton-density
PLP	proteo-lipid protein
PPMS	primary progressive multiple sclerosis
PSIR	phase-sensitive inversion-recovery
RF	radio frequency
RIS	radiologically isolated syndrome

ROS	reactive oxygen species
RRMS	relapsing-remitting multiple sclerosis
SEM	standard error of the mean
SNP	single nucleotide polymorphism
SPMS	secondary progressive multiple sclerosis
SQ	semi-quantitative
TE	echo time
TR	repetition time
UK	United Kingdom
US	United States
UV	ultraviolet
VDRE	vitamin D response element
WM	white matter

1. Introduction

1.1 Overview of MS

Multiple sclerosis (MS) is a chronic inflammatory, demyelinating and degenerative disease of the central nervous system (CNS), and a leading cause of non-traumatic disability in young adults (Compston and Coles, 2008). Despite decades of research, the aetiology of MS remains elusive. Current consensus suggests that disease onset likely occurs when a genetically predisposed individual is exposed to an unknown environmental trigger (Milo and Kahana, 2010). Whilst several genetic and environmental factors have been associated with MS risk, it is carriage of the *HLA-DRB1*15* extended haplotype that presents the greatest risk of disease development (Sawcer *et al.*, 2011).

The pathologic substrate of permanent disability in MS is not well understood. Whilst demyelination is the pathologic hallmark of the disease, the conflation of evidence suggests that its correlation with neuroaxonal loss is poor (DeLuca *et al.*, 2006; Klaver *et al.*, 2015). In contrast, inflammation appears linked to neurodegeneration at all disease stages (Frischer *et al.*, 2009). This being said, the complexity of the inflammatory response in MS has made it difficult to define specific immune components that promote neurodegeneration and our knowledge of factors that associate with disease outcome subsequently remains poor.

One approach to identifying disease mechanisms that contribute to permanent disability in MS is to assess how genetic loci associated with disease susceptibility impacts on disease burden. Given the established contribution of *HLA-DRB1*15* to MS risk, allelic diversity at the *HLA-DRB1* locus may also associate with inflammatory phenotypes relevant to disability accrual. A greater understanding of how *HLA-DRB1*15* associates with clinical, radiographic and pathologic disease may allow stratification of patients for therapeutic benefit, greater understanding of the biologic substrates of disease activity, and elucidation of novel drug targets.

1.2. Clinical Summary

1.2.1. Diagnosis

MS is a neurologic disorder that typically presents in young adults around the age of 30 years, and verges on being 3 times more common in women (Orton *et al.*, 2006). Initially, MS is characterised by episodes of neurologic dysfunction that are functionally related to CNS blood-brain-barrier (BBB) disruption and lesions of focal inflammatory demyelination (Filippi *et al.*, 2012). A diagnosis of MS can be made if objective clinical evidence is gained of two or more CNS lesions disseminated in time and space. Magnetic resonance imaging (MRI) is often used to provide evidence of MS lesions, but is not a prerequisite. If an episode of neurologic dysfunction referable to the CNS is confined in time it is considered a clinically isolated syndrome (CIS). Approximately 45% of CIS patients convert to clinically definite MS within 2 years (Miller *et al.*, 2012), though this number increases if brain lesions are detected on MRI (Fisniku *et al.*,

2008). Incidental identification of a CNS lesion is termed "radiologically isolated syndrome (RIS)" (Okuda *et al.*, 2009). Factors that promote the conversion of RIS to clinically definite MS are not well defined and remains an active area of research, though spinal cord lesions appear predictive (Okuda *et al.*, 2011).

1.2.2. Natural history

Functional domains affected by MS can be motor, sensory and cognitive, with common manifestations including visual impairment, weakness, spasticity, paraesthesias and numbness. Motor deficit may also extend to sphincteric function, and urinary and bowel problems are common complaints (Compston and Coles, 2008). The early phase of MS is characterised by intermittent episodes of neurologic dysfunction, with partial or complete recovery between relapses (relapsing-remitting MS [RRMS]). The nature of RRMS can be highly variable between patients, with some experiencing largely quiescent disease, and others reporting frequent disabling relapses with only partial recovery.

Despite the marked clinical heterogeneity of RRMS, 80% of patients begin to experience an unrelenting accumulation of permanent disability (secondary progressive MS [SPMS]) within 20 years of disease onset (Kremenchutzky *et al.*, 2006), typically around the age of 40 years (Kremenchutzky *et al.*, 2006). Although some evidence suggests that the frequency of relapses in very early disease predicts shorter times to permanent disability (Scalfari *et al.*, 2010), for the most part SPMS appears to proceed at a similar rate regardless of initial relapsing-remitting disease course (Confavreux *et al.*, 2000). Consistent with this, evidence that disease modifying therapies (DMTs) effective at reducing the

frequency and severity of relapses in RRMS benefit long-term disability accrual is lacking (Coles *et al.*, 1999).

A subset of MS patients (10-20%) present with a progressive disease course in the absence of an initial RRMS phenotype (primary progressive MS [PPMS])(Koch *et al.*, 2009). The natural history of PPMS does not appear to markedly differ from SPMS, except that it is more common in males (Ebers, 2004).

The apparent inability of DMTs to limit permanent disability has led many to question the contribution of focal inflammatory attacks to neurodegeneration (Confavreux *et al.*, 2000). However, a wealth of radiographic (Ingle *et al.*, 2005) and pathologic evidence (Frischer *et al.*, 2009) implicates inflammatory processes occurring within the CNS of progressive MS patients. An increasing awareness of this has led to the re-appraisal of how we define MS in the progressive stage in order to differentiate patients with and without active inflammatory disease burden, who may respond to DMT therapy differently (Lublin *et al.*, 2014). A greater understanding of how inflammation contributes to permanent disability in progressive MS is urgently needed.

1.2.3. *HLA-DRB1*15* and clinical outcome

Given the role of inflammation throughout the disease, genetic risk factors that are implicated in immune system function, such as the *HLA-DRB1*15* extended haplotype, may also associate with disease outcomes and therefore allow stratification of patients for therapeutic benefit (Ramagopalan *et al.*, 2008).

Carriage of *HLA-DRB1*15* has been associated with a lower age of onset (Masterman *et al.*, 2000), female sex (Hensiek *et al.*, 2002) and the presence of oligoclonal bands (Idiman *et al.*, 2009). Studies that have assessed the impact of *HLA-DRB1*15* on disability outcome have reported inconsistent results. Whilst many studies have found no impact of *HLA-DRB1*15* on the extent of disability (Barcellos *et al.*, 2006; Isobe *et al.*, 2016; Smestad *et al.*, 2007), an equally large number of studies have detected an over-representation of severe MS in *HLA-DRB1*15* positive cohorts (Barcellos *et al.*, 2003; DeLuca *et al.*, 2007; Duquette *et al.*, 1985) and greater cognitive impairment (Okuda *et al.*, 2009). These inconsistent findings may be due to the insensitivity of disability scales to accurately reflect functional deficit and disease activity. More sensitive metrics, such as MRI and pathologic findings, are better able to reflect inflammatory and demyelinating pathology and are discussed in section 1.6.5 and 1.7.5, respectively.

1.3. Environmental Epidemiology

1.3.1. Geographic distribution

A peculiar feature of MS that has been noted in epidemiologic studies is a marked geographic variability. MS is relatively common in Northern Europe, the United States, Canada and New Zealand, where prevalence is approximately 1 in 1000 individuals. In contrast, MS is relatively rare in equatorial regions and in Asia (Rosati, 2001). When the prevalence of MS is depicted globally, a positive correlation with distance from the equator is observed (Kurtzke, 2005). Indeed, the Orkney Islands, located off the northern coast of Scotland, report the highest

global prevalence of MS (Pugliatti *et al.*, 2002). Whilst there are likely to be regional differences in the reporting and diagnosis of MS that relate to socioeconomic factors, this is unlikely to fully explain the global distribution of the disease. Studies carried out within Australia and New Zealand, where medical infrastructure is largely consistent throughout the country, have shown that MS prevalence is still significantly greater in the south compared to the north (Miller *et al.*, 1990).

1.3.2. Vitamin D

The heterogeneous global prevalence of MS, and its relationship with latitude, is incompletely understood. However, it is likely underpinned by the presence or absence of an environmental factor that impacts on disease susceptibility and differs according to distance from the equator. Given global variations in sunlight exposure (Acheson *et al.*, 1960), ultraviolet (UV) light and vitamin D are considered prime candidates (Holick, 2007). A large prospective study of US military personnel found that replete serum vitamin D was associated with lower risk of MS later on (Munger *et al.*, 2006), and supplementation of vitamin D also appears protective (Munger *et al.*, 2004). Unfortunately, research trials involving vitamin D have so far failed to provide any evidence of clinical benefit (Salari *et al.*, 2015; Sotirchos *et al.*, 2016), suggesting that vitamin D exposure contributes to MS risk but not disease outcome.

The timing of exposure may influence the effect of vitamin D on MS risk. Movement of individuals from areas of contrasting MS prevalence before the age of ~15 years appears to lead to an acquirement of MS risk inherent to their

destination (Dean and Elian, 1997), though this finding has proved difficult to replicate (Hammond *et al.*, 2000). That being said, a potential role for very early vitamin D exposure in dictating MS risk is further supported by the observation that disease susceptibility is higher in individuals born in April compared to November, even after controlling for seasonality of birth rate in the general population (Rodríguez Cruz *et al.*, 2016).

The mechanism by which vitamin D contributes to MS pathology is not completely understood. Vitamin D deficiency disrupts T-cell homeostasis in healthy rats and leads to a pro-inflammatory T-cell phenotype (Harvey *et al.*, 2010). Vitamin D administration prevents the onset of experimental autoimmune encephalomyelitis (EAE) (Lemire and Archer, 1991), a rodent model of MS, as well as the progression of clinical signs (Cantorna *et al.*, 1996). These effects are blocked when the vitamin D receptor is knocked-out (Meehan and DeLuca, 2002). The impact of vitamin D on the immune system is corroborated by human studies. Activation of monocytes in the presence of vitamin D leads to reduced pro-inflammatory cytokine secretion, and co-stimulation of T-cells by vitamin D-treated monocytes results in reduced T-cell proliferation (Almerighi *et al.*, 2009). Taken together, these studies suggest that insufficient vitamin D may lead to perturbed immunity that predisposes to MS development.

1.3.3. Viral infectious agents

Another environmental risk factor associated with MS risk is the Epstein-Barr virus (EBV). Seropositivity for EBV is found in approximately 99% of MS

patients, with a recent study suggesting that this figure may even be 100% (Pakpoor *et al.*, 2013). This contrasts with an EBV seropositivity of 90% in the general adult population (Ascherio and Munch, 2000). As with vitamin D, it appears that exposure to EBV needs to occur at a critical developmental time point for an impact on MS risk to be appreciated. Evidence suggests that severe symptomatic infection with EBV in early adulthood, i.e. infectious mononucleosis, increases the risk of MS 2.3x (Thacker *et al.*, 2006). Whilst the mechanism of this effect is not understood, it is notable that EBV proteins mimic myelin antigens (Mameli *et al.*, 2014). Active EBV infection may promote an autoimmune environment that leads to an aberrant anti-myelin immune response when combined with other environmental and genetic risk factors.

1.3.4. Bacterial infectious agents

In addition to viruses, bacterial agents may also have a role in MS susceptibility. It has recently been shown that *clostridium perfringens* subtype B epsilon toxin (ETX) damages the BBB of rodents and targets oligodendrocytes to induce demyelination (Linden *et al.*, 2015). Subclinical doses of ETX appear to be ubiquitous in the environment, and anti-ETX antibodies are 10x more prevalent in MS patients when compared to controls (Rumah *et al.*, 2013). Pathologic ETX exposure may therefore be a feature of a least a subset of the MS population. Other bacterial infections have also been associated with MS, including human herpes virus 6 (Voumvourakis *et al.*, 2010) and chlamydia pneumonia (Sriram *et al.*, 1999). Given emerging evidence of a perturbed microbiome in MS, the role of subclinical bacterial infections in MS aetiology deserves further study (Jangi *et al.*, 2016).

1.3.5. Lifestyle factors

Modifiable lifestyle factors may also increase MS risk. Cigarette smoke has been shown to dose-dependently increase MS susceptibility, with increased disease risk subsiding if exposure is ceased (Hedström *et al.*, 2013). Age of cigarette exposure does not appear to impact on this effect, and neither does mode of exposure, with both direct and passive smoking shown to influence disease risk similarly (Mikaeloff *et al.*, 2007). Smoking is also recognised as a negative modifier of disease outcome. Disability tends to be worse at baseline in smokers, with lesion burden more severe and disease progression faster (Healy *et al.*, 2009). Interestingly, it has been shown in animal models of MS that T-cells may initially be "licensed" to migrate to the CNS in the lung (Odoardi *et al.*, 2012). The presence of cigarette smoke in the airways may therefore heighten inflammation and influence critical T-cell interactions with antigen presenting cells that are relevant to disease onset and clinical outcome (Öckinger *et al.*, 2016).

A role of increased systemic inflammation on MS risk is exemplified by the fact that disease susceptibility is also increased in the adolescent obese, which has been associated with a greater than 2-fold increased risk of disease (Munger *et al.*, 2009). The increased basal inflammatory milieu of both smokers and the obese may increase the odds of developing an aberrant immune response such as that which is characteristic of MS. This being said, both smoking and obesity are also associated with reduced physical activity. Reduced sunlight exposure and vitamin D synthesis are therefore important confounding factors that should be considered in addition to diet (Kleinewietfeld *et al.*, 2013) and socioeconomic

status (Goulden *et al.*, 2015) when evaluating the role of lifestyle factors on disease risk.

1.4. Genetics

1.4.1. Genetic epidemiology

Environmental risk factors fail to fully explain susceptibility to MS, and it is clear that genetic factors also play a key role in dictating overall disease risk. MS tends to cluster in families, with a 30% concordance rate in monozygotic twins that declines with degree of kinship (Sadovnick *et al.*, 1993). MS concordance in step-siblings is greater if a mother is shared, highlighting an important contribution of maternal transmission of genes in disease susceptibility (Ebers *et al.*, 2004). The shared environment of families can make it difficult to disentangle genes from environment. However, the observation that disease risk is not increased in spouses, adoptees or step-siblings of those affected by MS would argue against environmental factors explaining familial aggregation (Dyment *et al.*, 2006; Ebers *et al.*, 1995). That being said, substantial discord of disease in monozygotic twins reinforces the important contribution of both environmental and genetic factors to overall MS risk.

1.4.2. Genetic susceptibility

The appreciation of heritable MS susceptibility stimulated interest in elucidating which genetic loci are associated with disease. Genome-wide association studies (GWAS) have been employed to investigate genetic risk in many diseases. GWAS identify single nucleotide polymorphisms (SNPs) that are over-represented in disease states compared to controls. The assessment of thousands of individuals

enables the identification of SNPs even with very small effect sizes. By elucidating which genes are co-inherited with disease-associated SNPs, it is possible to infer candidate susceptibility genes. In total, 14 GWA studies have been completed in MS, with over 100 genetic loci so far identified (Beecham *et al.*, 2013). The majority of candidate loci are implicated in immunity, with a preponderance of genes involved in T-cell regulation, thus providing support to the view that primary immune pathology is inextricably linked to the aetiology of MS (Sawcer *et al.*, 2011).

Whilst most candidate susceptibility genes have very small effect sizes (odd ratios < 1.3), the extended *HLA* class II risk haplotype (*HLA-DQA1*0102-DQB1*0602-DRB1*1501-DRB5*0101)* increases MS risk 3x (rising to 6x in homozygotes) and therefore presents a greater risk of disease development than all other GWA hits combined (Sawcer *et al.*, 2011). It is not entirely clear which specific locus of the extended risk haplotype directly contributes to MS risk, as intense linkage disequilibrium within the class II major histocompatibility complex (MHC) means that *HLA-DQA1*01*, *HLA-DQB1*0602* and *HLA-DRB1*15* are usually inherited together in Northern European populations (Fogdell *et al.*, 1995). Studies of MS in African Americans, in which there are distinct patters of linkage disequilibrium, implicates a selective association of *HLA-DRB1*15* (Oksenberg *et al.*, 2004). However, this may not be consistent across all ethnic groups (Alves-Leon *et al.*, 2007). The observation that certain *HLA* alleles appear protective only when combined with specific other *HLA* alleles suggests that it is

probably the complete *HLA* haplotype that dictates over disease risk (Dyment *et al.*, 2005).

Understanding the mechanism by which class II HLA impacts on MS susceptibility may uncover novel insights into pathophysiology. Class II HLA presents peptides to CD4+ T-cells to generate an immune response. Genetic variation of HLA class II may therefore dictate MS risk by influencing the T-cell repertoire via the quality and/or quantity of antigen presentation that could influence the induction or failure of immune tolerance. This hypothesis is supported by transgenic murine studies that have shown *HLA-DRB1*15* expressing T-cells react avidly with myelin proteins (Altmann *et al.*, 1995; Rich *et al.*, 2004) and can induce spontaneous EAE (Madsen *et al.*, 1999). However, this is likely an over-simplification. *HLA-DRB1*15* expression is up-regulated in MS patients (Alcina *et al.*, 2012), and autologous proliferation of *HLA-DRB1*15*+ T-cells is greater than T-cells not expressing this allele even in controls (Mohme *et al.*, 2013). In addition, a conserved vitamin D response element (VDRE) is found in the promoter region of *HLA-DRB1*15* and experimental work has shown that the expression of *HLA-DRB1*15* can be influenced by exogenous administration of vitamin D (Ramagopalan *et al.*, 2009). Whether vitamin D insufficiency impacts on MS susceptibility only in *HLA-DRB1*15*+ cases remains uncertain. However, a complex interaction between *HLA-DRB1*15*, smoking, EBV seropositivity, and vitamin D in dictating MS risk suggests critical gene-environment interactions may centre on HLA class II (Handunnetthi *et al.*, 2010; Simon *et al.*, 2010; Wergeland *et al.*, 2016). Whether these interactions lead to

aberrant antigen presentation of epitopes relevant to myelin autoimmunity requires further research.

1.5. Immunology

Much of what is understood about the immunology of MS has arisen from studying animal models of the disease, such as rodent EAE (Croxford *et al.*, 2011). In this experimental system, rodents are inoculated peripherally with myelin antigen and Freund's adjuvant to induce a demyelinating syndrome that resembles many of the clinical and pathologic features of early human disease. EAE does not recapitulate MS in its entirety, particularly later disease stages (Lassmann, 2007), and so observations made using this model should be interpreted with caution (Sriram and Steiner, 2005). That being said, disease modifying treatments that successfully quell inflammatory disease activity have entered the clinic as a result of animal model investigations (Teitelbaum *et al.*, 1971; Yednock *et al.*, 1992). As such, the sequence of immunologic events that characterise EAE onset represent our current best understanding of what might happen in the early stages of MS.

1.5.1. Peripheral lymphocyte activation

EAE induction may replicate human MS if central and/or peripheral tolerance mechanisms fail to induce anergy of anti-myelin lymphocytes. If these cells then interact with proteins containing epitopes cross-reactive with myelin in the context of ongoing inflammation, a specific anti-myelin immune response may ensue. Damage to the BBB through specific pathogen exposure may also lead to access of myelin to peripheral lymphoid organs and auto-reactive lymphocytes.

In either case, loss of peripheral tolerance to myelin appears to be an early feature of MS pathophysiology, as evidenced by the increased activation status of myelin reactive lymphocytes in MS cases compared to controls (Van der Aa *et al.*, 2003; Markovic-Plese *et al.*, 2001) and the apparently perturbed regulatory T-cell response (Zozulya and Wiendl, 2008).

1.5.2. Lymphocyte migration into the CNS

Due to the specific CNS expression of myelin, it is necessary for activated myelin-reactive T-cells to migrate across the blood-cerebral spinal fluid (CSF) and BBB before they are able to induce disease. Exactly how T-cells migrate into the meninges and CNS parenchyma is unclear. Recent evidence has suggested that T-cells initially enter the CSF from leptomeningeal vessels in EAE (Schläger *et al.*, 2016). Lymphocytic surveillance of the sub-arachnoid space is an important physiologic process that protects the meninges from pathogenic colonisation (Ransohoff and Engelhardt, 2012). Surveying self-reactive lymphocytes may re-encounter myelin in the subarachnoid space, or be presented antigen by perivascular macrophages (Bartholomäus *et al.*, 2009). Resultant T-cell activation, and differentiation into CD4+ Th1 and Th17 subsets, activates the endothelium and allows diapedesis across the BBB and migration deep into the CNS parenchyma (Flügel *et al.*, 2007).

Activated T-cells may also stimulate an intra-thecal B-cell response, as evidenced by CSF oligoclonal bands that are observed in up to 95% of MS patients (Chu *et al.*, 1983). The contribution of antibody production to MS pathogenesis is not known, though an important role is suggested by the fact that therapeutic

modulation of B-cells decreases inflammatory disease activity and lesion formation (Hauser *et al.*, 2008). Oligoclonal CSF immunoglobulins have recently been shown to primarily react to cellular debris (Brändle *et al.*, 2016), perhaps suggesting a secondary B-cell response to primary CNS damage. Reinforcing this view, CSF antibody responses to neurofilament likely also reflect neuroaxonal injury (Eikelenboom *et al.*, 2003). Whilst the specific detection of antibodies targeting KIR4.1, a neuronal protein, was met with enthusiasm (Srivastava *et al.*, 2012), this has not been replicated to date (Brickshawana *et al.*, 2014). These observations, and the finding that anti-myelin immunoglobulins are present in both MS cases and controls (Sun *et al.*, 1991), have led to the suggestion that B-cells predominantly contribute to MS pathogenesis via antigen presentation to T-cells (Parker Harp *et al.*, 2015). Further experimental work is needed to clarify the role of B-cells in MS.

1.5.3. Activation of brain microglia

The diffusion of cytokines into the brain parenchyma from meningeal inflammatory infiltrates activate parenchymal microglia (Goverman, 2009). Microglial cells are the resident innate immune cells of the CNS and the first responders to brain or spinal cord pathology (Chen and Trapp, 2016). Confined behind a closed BBB and therefore unable to recruit peripheral progenitors, microglia maintain the ability to expand and self-renew throughout life (Ajami *et al.*, 2007). A unique characteristic of microglia is their ability to extend highly motile processes throughout the CNS parenchyma in order to survey the microenvironment for signs of injury or infection (Nimmerjahn *et al.*, 2005). When activated, microglial cell bodies becomes larger and more ovoid and there

is a retraction and redistribution of their processes (Hanisch and Kettenmann, 2007). Activated microglia phagocytose cellular debris and infectious agents and can take part in antigen presentation to extravasated lymphocytes (Kettenmann *et al.*, 2013). As a result, proteins involved in phagocytosis and exogenous peptide processing, such as the lysosomal membrane protein CD68 (Holness and Simmons, 1993) and HLA class II (Xu and Ling, 1994), respectively, are up-regulated by activated microglia.

In EAE, activation of parenchymal microglia leads to the secretion of a multitude of pro-inflammatory molecules that activates the brain endothelium and disrupts the BBB to allow an influx of CD4+ and CD8+ T-cells as well as B-cells, macrophages and dendritic cells (Goverman, 2009). Microglia-mediated perpetuation of the T-cell response causes demyelination and clinical sequelae that proceeds until accessible myelin is exhausted. Concomitant extravasation of fibrinogen into the brain parenchyma directly activates microglia and leads to the secretion of neurotoxic factors that injure axons even before the onset of clinical signs (Davalos *et al.*, 2012).

Studying microglia in EAE suggests a promotion of CNS damage. However, this is likely an oversimplification of human MS given the diverse CNS regions affected by the human disease, global senescence of inflammation that occurs with age, and decades long disease duration (Bogie *et al.*, 2014). Indeed, it is now recognised that microglia demonstrate marked immunologic heterogeneity that relates to anatomic location, microenvironmental cues, and the chronological age

of their host (Grabert *et al.*, 2016). The contribution of microglia inflammation to MS pathology in different regions of the neuraxis, and relationships therein with neurodegeneration, is therefore likely to be heterogeneous and age-dependant. Whilst microglial inflammation is a salient feature of MS pathology throughout the neuraxis, neurodegeneration is highly variable even across very small anatomic distances. It therefore follows that microglial inflammation is not ubiquitously destructive in chronic CNS inflammatory diseases (Chen and Trapp, 2016).

Taken together, the immunopathology of MS is complex and involves both innate and adaptive arms. Studies of EAE implicate a critical role for inflammation in disease onset and early disease activity, reinforcing the findings of GWA studies noted earlier (Sawcer *et al.*, 2011). The relevance of inflammation to later disease stages, when neurodegeneration is greatest, is largely impervious to animal studies. It is therefore likely that a greater understanding of this critical unanswered question will come only from studying human disease, both with a combination of *in vivo* and *ex vivo* imaging, and post-mortem pathology.

1.6. Neuroimaging

1.6.1. MRI Physics

MRI can visualise the MS disease processes *in vivo* (Fazekas *et al.*, 1999) and has proved to be an invaluable tool in the diagnosis, management and research of MS. MRI scanners generate contrast within the soft tissues of the body by exposing protons (hydrogen) to strong magnetic fields to cause an alignment of

their nuclear spins. Subsequent application of energy in the form of "radiofrequency (RF) pulses" displaces protons from this uniform spin. The time taken for protons to relax back to their uniform position is dictated by local tissue properties, including those that may be due to pathological conditions, and can be detected and transformed into a radiographic image. The parameters of scan sequences can be varied to reveal specific aspects of tissue architecture and have led to a plethora of imaging modalities used in both clinical and research settings.

1.6.2. MRI assessment of white matter lesions

White matter demyelination is clearly visible as hyper-intense foci on "proton-density (PD)-weighted" and "T_2-weighted" imaging sequences in both brain and spinal cord tissue. A minority of lesions (10-30%) identified on T_2-weighted scans may also appear using "T_1-weighted" sequences as well-defined *hypo*-intensities. MS lesions typically have an ovoid shape, ranging in size from a few millimetres to 1cm (Filippi *et al.*, 2012). Whilst the anatomic location of radiographic lesions often functionally relates to neurologic deficit, MRI signal change may also be clinically silent (Okuda *et al.*, 2009). Radiographic lesions can resolve with abatement of inflammation and remyelination. However, persistence of lesions is common and probably reflects permanent tissue destruction (van Waesberghe *et al.*, 1999). In addition to focal lesions, subtle white matter abnormalities are also detectable with conventional MRI modalities and appear to have a different pathologic correlate (Laule *et al.*, 2011). However,

the contribution of subtle MRI signal change to the clinical expression of MS remains largely unexplored.

T_1-weighted MRI scans can be enhanced by peripheral administration of gadolinium that enters the brain parenchyma if the BBB is disrupted and therefore suggests ongoing inflammation and serum extravasation (Grossman *et al.*, 1986). Not all T_1 lesions show evidence of gadolinium enhancement. However, this may merely reflect the fact that radiographic evidence of BBB disruption is only a feature of the first 2-6 weeks of lesion development that is not required for lesion persistence or enlargement in later disease stages (Cotton *et al.*, 2003). These observations have led to the suggestion that BBB disruption is not a chronic feature of MS pathology (Hochmeister *et al.*, 2006). However, subtle BBB abnormalities that are beyond the resolution of MRI could be an underappreciated aspect of progressive disease, even in non-lesional parenchyma (Kirk *et al.*, 2003; Leech *et al.*, 2007). The role of chronic BBB disruption in MS therefore warrants further study, especially considering the wealth of evidence implicating serum proteins, such as fibrinogen, in inflammatory and neurotoxic pathways (Davalos *et al.*, 2012; Davalos and Akassoglou, 2012).

1.6.3. MRI assessment of grey matter lesions

Radiographic lesions impinging on deep grey nuclei (Harrison *et al.*, 2015), and cortical grey matter (M Calabrese *et al.*, 2010), can be visualised in MS. However, in contrast to white matter lesions, grey matter lesions are difficult to detect with conventional MRI sequences and are therefore likely under-represented

(Seewann *et al.*, 2011). Cortical lesions are particularly difficult to resolve, even with advanced sequences (Kilsdonk *et al.*, 2016). This is largely due to the relatively small area occupied by the cortical ribbon and high signal arising from subjacent white matter and overlying meninges.

Cortical lesions can be detected in early disease phases (Popescu *et al.*, 2011), can occur in the absence of white matter lesions (Calabrese and Gallo, 2009), and are most common in progressive MS (Harrison *et al.*, 2015). A critical contribution of cortical lesions to disease outcome is evidenced by the fact that cortical lesions are associated with the progression of permanent disability (Calabrese *et al.*, 2012; Calabrese *et al.*, 2010), including the extent of cognitive impairment (Calabrese *et al.*, 2009; Nelson *et al.*, 2011), and appear particularly common in the motor cortex (Calabrese *et al.*, 2010). Improved imaging sequences that can better detect the full extent of cortical lesional burden are therefore desperately needed (Ciccarelli and Chen, 2012; Seewann *et al.*, 2012). This is particularly pertinent with regards to subpial lesions that dominate the neuropathology of progressive disease (Kutzelnigg and Lassmann, 2005) and have been specifically associated with physical decline (Harrison *et al.*, 2015), yet remain poorly resolved with MRI (Kilsdonk *et al.*, 2016).

1.6.4. MRI assessment of non-lesional parenchyma

A considerable limitation of conventional MRI metrics is their inability to detect disease processes beyond the focal lesion. To this end, radiographic surrogates of diffuse inflammatory and degenerative processes occurring in non-lesional areas

of the CNS, in so-called “normal-appearing white/grey matter” (NAW/GM), have provided insight.

Magnetic transfer ratio (MTR) is a quantitative index derived from the ability of CNS macromolecules to exchange magnetisation with surrounding water molecules. MTR therefore reflects non-specific tissue damage, but is largely dictated by myelin given the relative contribution of myelin to CNS macromolecules (Horsfield *et al.*, 2003). MTR is reduced in lesions (Filippi and Agosta, 2007), but also in NAWM (Loevner *et al.*, 1995), suggesting that myelin loss can occur independently of overt demyelination. Evidence for abnormalities in NAWM has been corroborated by magnetic resonance spectroscopy (MRS), a technique capable of characterising metabolic perturbations in the CNS. Detection of N-acetylaspartate (NAA) by MRS has gained particular attention given its almost exclusive expression by neurons and axons (Sajja *et al.*, 2009). NAA is reduced in NAWM and correlates with the extent of physical disability (Fu *et al.*, 1998).

Brain and spinal cord atrophy are further imaging metrics that relate to abnormalities partly independently of demyelination. Atrophy is a prominent feature of MS progression, with brain volume reducing 0.7-1% per year (Miller *et al.*, 2002). Grey matter atrophy in both the brain and spinal cord occurs early (Chard *et al.*, 2002), progresses over time, and correlates with physical disability and cognitive decline (Benedict *et al.*, 2006) to a greater extent that white matter

atrophy (Sanfilipo *et al.*, 2005), wherein the majority of radiographic lesions are detected.

The conflation of radiographic evidence suggests that a diffuse inflammatory process drives neuroaxonal loss throughout the CNS in progressive MS largely independently of demyelination. However, these studies do not take account of the extensive connectivity of the nervous system and the potential for pathology to spread within CNS tracts (Kolasinski *et al.*, 2012). Diffusion tensor imaging (DTI) assesses the diffusion of water molecules and can provide information regarding the integrity of white matter bundles. DTI has shown disruption of tracts in MS (Ciccarelli *et al.*, 2001), that in some studies correlate with lesions in connected brain regions (Ciccarelli *et al.*, 2003). These observations perhaps suggest that axonal loss in NAWM is in part due to Wallerian degeneration of axons distant to demyelination. However, the inability of radiographic studies to assess pathologically confirmed neurodegeneration limits the interpretation of this work. Novel imaging sequences, such as neurite density and dispersion imaging (NODDI), promise to improve the ability to specifically detect radiographic neuroaxonal abnormalities (Grussu *et al.*, 2016). Work is now needed to validate these techniques with post-mortem pathology so that histologic correlates of non-conventional MRI signal change can be defined.

1.6.5. *HLA-DRB1*15* and MRI outcome

Several studies have assessed the impact of *HLA-DRB1*15* on white matter radiographic outcome. Carriage of *HLA-DRB1*15* has been shown to associate with more severe T_2 lesion burden at disease onset (Horakova *et al.*, 2011), as well as in later disease stages (Okuda *et al.*, 2009), wherein a greater reduction of brain parenchymal volume and NAA are also detected in *HLA-DR1*15*+ cases (Okuda *et al.*, 2009). *HLA-DRB1*15* may also impact the distribution of lesions (Gourraud *et al.*, 2013) and the progression of brain pathology in PPMS (Tur *et al.*, 2014), and has been associated with more severe lesion burden in the spinal cord (Sombekke *et al.*, 2009).

In contrast to white matter, the influence of *HLA-DRB1*15* on grey matter pathology is unknown, despite substantial evidence that now implicates cortical tissue injury in the progression of permanent disability in MS (Calabrese *et al.*, 2012). One reason this critical question remains unanswered is the significant technical challenges associated with assessing cortical pathology radiographically, as conventional MRI techniques fail to provide adequate resolution of cortical lesions (Seewann *et al.*, 2012). However, advanced techniques can improve this ability (Harel *et al.*, 2016), and a recent study employed phase-sensitive inversion-recovery (PSIR) to investigate cortical injury in a cohort of MS cases genotyped for *HLA-DRB1*15* (Yaldizli *et al.*, 2016). The study failed to detect any difference in MRI-visible cortical disease between the genotyped cohorts. However, a major limitation of this work was that subpial lesions, the major cortical lesion type identified by neuropathology studies,

remain undetected by PSIR (Harel *et al.*, 2016). Therefore, the ability of advanced MRI sequences to detect subtle, yet clinically relevant, cortical abnormalities that associate with specific genotype groups remains limited. As such, post-mortem pathology will continue to be the most robust way to assess and quantify cortical tissue injury in MS.

1.7. Neuropathology

The neuropathology of MS is complex. All MS phenotypes display chronic lymphocytic and microglia/macrophage inflammation of the parenchyma and meninges along with demyelination, gliosis and variable degrees of neuroaxonal and oligodendrocyte damage and loss (Matthews *et al.*, 2016). Whilst neuropathology studies continue to be fundamental in improving our understanding of human disease through their ability to detect cellular and subcellular changes beyond the resolution of MRI, they remain inherently limited by their inability to obtain a "global" view of MS.

1.7.1. Histologic assessment of white matter lesions

White matter lesions can be found in all MS subtypes and at all disease stages, with predilection sites including brainstem, optic nerves, periventricular white matter, cerebellum, and spinal cord (Noseworthy *et al.*, 2000). Active white matter lesions appear hyper-cellular due to dense microglia/macrophage infiltrates that associate with myelin destruction and contain intracellular myelin deposits (Brück *et al.*, 1995). BBB disruption with resultant complement, antibody and lymphocyte extravasation may also be evident (Esiri, 1977; Gay

and Esiri, 1991). Chronic active lesions are hypo-cellular in the centre but maintain a rim of activated microglia/macrophages that continues to drive demyelination at the lesion edge. Both active and chronic active lesions are common in early disease phases (Frischer *et al.*, 2015). Oligodendrocyte precursor cells (OPCs) can migrate into demyelinated plaques and differentiate into mature oligodendrocytes to mediate variable levels of remyelination (Patrikios *et al.*, 2006), though this may only be transient as remyelinated plaques appear more vulnerable to new demyelination (Bramow *et al.*, 2010). Remyelination can occur in MS cases with long disease duration (Patani *et al.*, 2007), though it also often fails for reasons that are not clear (Franklin, 2002). Age-related senescence of inflammation (Frischer *et al.*, 2009) and subsequent decline in new lesion formation means that in post-mortem pathologic studies chronic inactive plaques predominate (Frischer *et al.*, 2015), and describe areas of demyelination without evidence of inflammatory infiltration or ongoing myelin destruction.

1.7.2. Histologic assessment of grey matter lesions

Despite traditionally being considered a disease solely of white matter, grey matter pathology has nonetheless been a long-recognised feature of MS (Brownwell and Hughes, 1962) that has been explored in detail with the advent of modern immunohistochemical techniques (Bø *et al.*, 2003). Evidence of grey matter pathology can be gained in early MS but is most severe in progressive disease, with the cerebral cortex particularly affected (Kutzelnigg *et al.*, 2005). Four major cortical lesion subtypes have been described. Leukocortical (type I) lesions extend from deep cortical layers into subcortical white matter,

intracortical (type II) lesions are small areas of demyelination typically around a central vessel, subpial (type III) lesions are large areas of demyelination that extend from the pial surface into cortical layers 3/4 and type IV lesions extend from the pial surface to the grey/white matter boundary (L Bø *et al.*, 2003). Subpial lesions are the most common cortical lesion type identified in neuropathologic studies and can sometimes affect large areas of the cortical ribbon across adjacent gyri in progressive disease (Kutzelnigg *et al.*, 2005). Cingulate, temporal, insular, and cerebellar cortex appear to be particularly vulnerable to subpial lesions for reasons that are not understood (Kutzelnigg and Lassmann, 2006), but that may relate to differences in CSF flow and stasis (Kutzelnigg *et al.*, 2007). Extensive remyelination can take place in the cortical grey matter that appears to extend into old age and is more substantive than white matter remyelination (Chang *et al.*, 2012).

Despite occasionally extensive demyelination, only sparse parenchymal lymphocytic inflammation and microglia/macrophage activation are detected in the progressive MS cortex (L Bø *et al.*, 2003; Peterson *et al.*, 2001), though this may not be the case in earlier disease stages (Lucchinetti *et al.*, 2011). This observation has led to the suggestion that the pathogenesis of cortical lesions is different to white matter plaques, and may be driven by diffuse inflammation in the meninges, rather than parenchymal factors. Cortical lesions have been topographically associated with meningeal infiltrates in SPMS cases harbouring tertiary lymphoid-like structures in the sub-arachnoid space (Howell *et al.*, 2011; Magliozzi *et al.*, 2007). These findings have led to the hypothesis that a

myelinotoxic substance may diffuse into the brain parenchyma and mediate tissue destruction (Gardner *et al.*, 2013). Superficial neuronal loss and microglia/macrophage activation in cases wherein tertiary lymphoid-like structures can be detected (Magliozzi *et al.*, 2010), and a positive correlation between meningeal inflammation and spinal cord axonal loss reinforces this view (Androdias *et al.*, 2010). However, an association between meningeal inflammation and subpial lesions has not been found in all studies (Kooi *et al.*, 2009), and so the relationship between meningeal and parenchymal pathology requires further study.

1.7.3. Histologic assessment of neurodegeneration

Whilst demyelination and chronic inflammation are striking features of MS pathology, it is neurodegeneration that is the most likely correlate of disability (De Stefano *et al.*, 1998; Tallantyre *et al.*, 2010). Histology studies have demonstrated neuroaxonal loss to varying degrees throughout the neuraxis (DeLuca *et al.*, 2004; Klaver *et al.*, 2015; Vercellino *et al.*, 2009). In active white matter plaques, axons are relatively well preserved alongside variable levels of axonal damage (Ferguson *et al.*, 1997) and transection (Trapp *et al.*, 1998) that appears correlated with microglia/macrophage and CD8+ T-cell inflammation (Bitsch *et al.*, 2000). A substantial and progressive axonal loss may also occur in chronic lesions when inflammation has resolved (Kornek *et al.*, 2000). Axonal loss can be profound in MS lesions, with histologic series reporting up to 80% of axons lost in spinal cord tissue (Bjartmar *et al.*, 2000) that appears tract and size specific (DeLuca *et al.*, 2004). Axonal loss has also been demonstrated in NAWM (Evangelou *et al.*, 2000).

Neuronal loss is also a feature of MS pathology, with a 30-40% reduction described in deep grey matter nuclei, both in lesions and normal-appearing areas (Cifelli *et al.*, 2002; Vercellino *et al.*, 2009). Studies assessing cortical neuronal loss have been conflicting. Early immunohistochemical studies noted increased apoptotic neurons in demyelinated cortex (Peterson *et al.*, 2001), and some studies have reported neuronal loss of up to 25% in both lesions (Vercellino *et al.*, 2005) and NAGM (Klaver *et al.*, 2015). However, other studies have reported a more modest reduction in cortical neurons, with Wegner et al., reporting 10% neuronal loss confined to lesional parenchyma and associated with a marked reduction in synaptic density (Wegner *et al.*, 2006). In one of the largest assessments of cortical neuronal loss to date, significant neurodegeneration was only detected in cases harbouring lymphoid-like follicles in the sub-arachnoid space and was confined to superficial cortical layers (Magliozzi *et al.*, 2010). These discrepancies likely arise from a marked heterogeneity in neuronal loss between cases (Vercellino *et al.*, 2005), unknown follicle status of examined cohorts, and different cortical regions being assessed that are affected by the MS disease process differently (Kutzelnigg and Lassmann, 2006). Taken together, these considerations highlight the critical importance of systematic sampling when assessing the post-mortem MS cortex to minimise the effect of intra-cortical pathologic heterogeneity.

1.7.4. Mechanisms of neurodegeneration

Factors that drive neuroaxonal loss in MS are not well described. The inability of histology studies to correlate the extent of demyelination with axonal loss

(DeLuca *et al.*, 2006), and the substantial neurodegeneration observed in non-lesional parenchyma (Evangelou, Esiri, *et al.*, 2000; Klaver *et al.*, 2015), has shifted attention away from the focal lesion. In contrast, diffuse inflammation appears linked to the extent of axonal loss at all disease stages (Frischer *et al.*, 2009). Substantial evidence suggests a role for inflammation-induced reactive oxygen and nitrogen species-mediated neuroaxonal damage in MS (Haider *et al.*, 2011), including in the cortex (Fischer *et al.*, 2013). Activated microglia/macrophages secrete reactive oxygen species (ROS) (Colton and Gilbert, 1993) that can inhibit the mitochondrial respiratory chain and induce a failure of ATP production and subsequent virtual hypoxia and cellular energy deficiency (Mahad *et al.*, 2008). Recent animal model studies have shown that genuine hypoxia is also a feature of MS lesions that contributes to energy deficit (Desai *et al.*, 2016). Impairment of the Na/K ATPase results in axonal loading of sodium that stimulates reversal of the Na/Ca exchanger and subsequent activation of calcium dependent cytolytic enzymes that ultimately results in apoptosis of neurons and axons (Witte *et al.*, 2014). Up-regulation and redistribution of ion channels due to demyelination and iron liberation from microglia/macrophages that is partly age-associated may also exacerbate this process in lesions (Hametner *et al.*, 2013). Activated microglia/macrophages also secrete glutamate, and so excitotoxicity likely also damages axons via the over-activation of ionotropic glutamate receptors (Pitt *et al.*, 2000).

Taken together, these observations implicate an important role for microglia/macrophages in driving neurodegeneration in MS. However, a

limitation of neuropathology studies is their inability to distinguish resident microglia from extravasated macrophages. To this end, the potentially contrasting contribution of microglia and macrophages to neurodegeneration in MS are unknown. Study of the MS cortex may shed light on this critical knowledge gap, as peripheral leukocyte extravasation is not a cardinal feature of cortical pathology. Morphologic differences between white matter microglia/macrophages and cortical microglia/macrophages have been noted in MS, and likely relate to the vast over-representation of activated phagocytic macrophages in white matter lesions compared to their relative absence in grey matter lesions (Peterson *et al.*, 2001).

Emerging evidence suggests that microglia may have a neuroprotective role in MS. Increased neuronal density is associated with activated microglia in white matter MS lesions (Chang *et al.*, 2008) and microglia-mediated inhibitory synaptic stripping in a model of CNS inflammation rescued cortical neurons from apoptosis (Chen *et al.*, 2014). Microglia have also been demonstrated to promote remyelination (Miron *et al.*, 2013). These observations are consistent with the notion that microglia/macrophage phenotypes are heterogeneous in MS (Peferoen *et al.*, 2015), and likely contribute to both tissue destruction and repair. A greater understanding of the determinants of microglia/macrophage phenotype, and relationships therein with neurodegeneration are urgently needed.

Taken together, diffuse inflammatory processes in progressive MS likely underlie often profound neurodegeneration largely independently of demyelination. However, neuroaxonal loss induced by demyelination distant to the site of injury likely also contributes to neurodegeneration but has been relatively difficult to study (Ciccarelli *et al.*, 2003; Evangelou *et al.*, 2000). This is due, in part, to the inherent limitation of assessing associations of remote tissue injury using histology of MRI metrics alone, and calls for the combined assessment of radiographic and pathologic data within the same cases. It also remains possible that a primary neurodegenerative phenomenon stimulates the diffuse inflammation characteristic of MS (Stys, 2013). This being said, the conflation of clinical, radiographic and pathologic evidence does not support primary neurodegeneration fully explaining disability in MS (Frischer *et al.*, 2009).

1.7.5. *HLA-DRB1*15* and neuropathology outcome

Due to the shortcomings of current MRI modalities in detecting cortical disease in MS, robust and quantitative pathologic outcomes will play a vital role the evaluation of how genetic variation impacts MS cortical disease severity (Yates and DeLuca, 2016). The ability of histologic assessment to resolve genetic differences that associate with carriage of *HLA-DRB1*15* has already been demonstrated in the spinal cord, where *HLA-DRB1*15*+ MS cases were shown to have more severe demyelination and inflammation (DeLuca *et al.*, 2013). Divergent relationships between inflammation and neurodegeneration were also observed, as meningeal inflammation correlated with small fibre axonal loss only in *HLA-DRB1*15*+ cases (DeLuca *et al.*, 2013). Work is now required to assess

whether *HLA-DRB1*15* impacts pathologic outcome in the cortex, given the emerging role of cortical tissue injury to MS progression (Calabrese *et al.*, 2012).

1.7.6. MRI-pathology studies

A caveat of the vast majority of MS neuropathology studies is their dependence on autopsy cohorts, which are inherently biased towards older cases and end-stage disease. Whilst MRI can be used to assess tissue injury *in vivo*, our understanding of how radiographic signal change relates to specific aspects of MS pathology is limited. One approach to narrowing this critical knowledge gap is to correlate MRI metrics with MS pathology post-mortem.

MRI-pathology correlational studies have been instrumental in improving our understanding of the pathologic correlates of radiographic signal change. Examples of this include the demonstration that T_2 hyper-intense lesions in the brain represent oedema and inflammation, in addition to demyelination (De Groot *et al.*, 2001) and that areas of intermediate MRI signal change, so called "dirty appearing white matter", relate to specific loss of myelin lipid (Laule *et al.*, 2011). Such studies have also highlighted the inability of conventional radiographic sequences to detect all lesions (Geurts *et al.*, 2005), and a regional complexity in the interpretation of MRI signal change. In the spinal cord, myelin content and axonal density are only weakly correlated with T_2-metrics, yet robustly associated with MTR, T_1 and PD-weighted indices (Nijeholt *et al.*, 2001; Mottershead *et al.*, 2003). This convolution is further exemplified in the cortex, where high-field 9.4T has shown T_2-indices to be related to myelin

abnormalities, in contrast to T_1 signal change that appears related more to cortical neuronal density (Schmierer *et al.*, 2010). Taken together, the pathologic correlates of MRI signal change appear multi-factorial and region-specific. Further work in complete specimens, with brain and spinal cord material derived from the same cases, is therefore needed to assess how radiographic signal change relates to pathologic outputs throughout the length of the neuraxis.

1.8. Overview of Thesis

This thesis aims to improve our understanding of the pathogenesis of motor cortical pathology in MS. We achieve this using two approaches. In the first, we correlate robust and quantitative motor cortical pathologic outcomes with the primary genetic risk factor for the disease, *HLA-DRB1*15*. In the second approach, we quantify global radiographic lesional burden impinging on the brain and spinal cord corticospinal tract (CST) and relate this to pathologic outcomes gained in the motor cortex. Using this combined genetic, pathologic and radiographic approach, we have been able to improve our understanding of cortical pathologic heterogeneity and define novel factors that associate with motor cortical neurodegeneration that are potentially relevant to MS progression.

This thesis is presented as a series of results chapters that each include the following:

- Introduction
- Materials and Methods
- Results
- Discussion

Chapter 2: In this chapter it is hypothesised that carriage of *HLA-DRB1*15* associates with more severe motor cortical inflammatory pathology. The extent of demyelination and inflammation is quantified in the motor cortex of our MS cohort (n=47) and related to *HLA-DRB1*15* status. Comparisons of MS pathology are also made to a control cohort (n=9).

Chapter 3: In this chapter it is hypothesised that *HLA-DRB1*15* influences the extent of motor cortical fibrinogen deposition, a surrogate marker of BBB disruption. The extent and distribution of fibrinogen deposition is assessed in the motor cortex of our MS cohort (n=47) and related to *HLA-DRB1*15* status and neuronal loss. Comparisons are also made with a control cohort (n=10).

Chapter 4: In this chapter it is hypothesised that *HLA-DRB1*15* impacts the extent of motor cortical neurodegeneration and relationships therein with parenchymal inflammation, and putative neuroprotective mechanisms involving glutamic acid decarboxylase (GAD). Relationships between neuronal density, microglia/macrophage, lymphocytic inflammation and GAD are explored in the

context of *HLA-DRB1*15* in our MS cohort (n=47). Comparisons are also made with a control cohort (n=10).

Chapter 5: In this chapter it is hypothesised that the extent of global radiographic lesion burden impinging on the CST impacts on motor cortical MS pathology. Motor cortical demyelination, microglia/macrophage inflammation, and neuronal density is quantified in the motor cortex and related to radiographic lesion burden impinging on the CST throughout the neuraxis.

2. The influence of *HLA-DRB1*15* status on motor cortical inflammatory pathology in multiple sclerosis

2.1. Introduction

MS is a common, and chronic, inflammatory disease of the central nervous system (Compston and Coles, 2008). Grey matter pathology (Geurts *et al.*, 2012), in particular that affecting the cortex (Calabrese *et al.*, 2010), is increasingly recognised as a common feature of MS. Cortical lesions have been shown to occur at disease onset (Giorgio *et al.*, 2011; Lucchinetti *et al.*, 2011), and they appear to be an important feature of progressive disease (Kutzelnigg *et al.*, 2005; Reynolds *et al.*, 2011). The clinical relevance of cortical pathology is clear, as demyelination and atrophy here associate more with cognitive and physical disability than does white matter pathology (Calabrese *et al.*, 2012).

Whilst the etiology of MS remains elusive, current consensus states that initiation occurs when a genetically susceptible individual is exposed to an unknown environmental trigger (Milo and Kahana, 2010). Many genetic loci have been implicated in MS susceptibility, however the HLA class II region (namely the *HLA-DRB1*15* extended haplotype) confers the most significant risk. This implicates the involvement of an aberrant T-cell mediated inflammatory response directed against the myelin sheath that results in focal demyelination (Sawcer *et al.*, 2011).

There is emerging evidence to suggest that not only does *HLA-DRB1*15* influence disease susceptibility, but also the severity of disease (DeLuca *et al.*, 2007),

including in the cerebrum (Okuda *et al.*, 2009). A comprehensive study showed that patients positive for this allele tended to have more significant cognitive impairment, reduced brain parenchymal volume and levels of NAA, and greater T_2 subcortical lesion load (Okuda *et al.*, 2009). The limited resolution of current MRI techniques has precluded investigation of the nature and extent of cortical pathology, particularly in the subpial zone where disease is most extensive (Ciccarelli and Chen, 2012). Therefore, the influence of *HLA-DRB1*15* on motor cortical disease severity is unknown.

The current study employs a novel strategy to address this critical knowledge gap by evaluating the extent of motor cortical pathology in a post-mortem cohort of MS cases genotyped for *HLA-DRB1*15*. We provide evidence that *HLA-DRB1*15* significantly associates with the extent of inflammation in the MS motor cortex. In addition, we show that *HLA-DRB1*15* also associates with the extent of demyelination in the MS motor cortex of younger cases. These findings are the first to associate a genetic factor with the extent and distribution of motor cortical pathology in MS.

2.2. Materials and Methods

2.2.1. Study Population

A human autopsy cohort (n=47) of pathologically confirmed MS cases derived from the UK MS tissue bank, Imperial College, London and age- and sex- matched controls (n=9) from the Thomas Willis Oxford Brain Collection, Oxford University Hospitals NHS Trust, was used. All autopsy material was obtained with relevant ethics committee approval according to regulations outlined in the UK Human Tissue Act. Consent for use of archival post-mortem tissue prior to 2006 is given for research activity on tissue at the Thomas Willis Oxford Brain Collection where no explicit objection for research use is given by the patient or next of kin in accordance with UK Human Tissue Act regulations.

Each MS case had DNA available for genetic analyses and all cases had fixed material available for detailed pathologic characterisation. Several of the MS cases used in this study (n=42) were also used in a previous study of genetic-pathology correlations in the MS spinal cord (DeLuca *et al.*, 2013).

2.2.2. Genetics

Fresh frozen cerebellar tissue from all cases with MS was used for high-resolution genotyping of the *HLA-DRB1* locus using established methods (Bonin *et al.*, 2003). Two independent observers confirmed genotype scores. Genotyping of MS cohort was completed before the commencement of this thesis and was not carried out by the current author (DeLuca *et al.*, 2013).

2.2.3. Neuropathological Evaluation

Adjacent formalin-fixed paraffin-embedded sections of motor cortex, sampled from mesial precentral gyrus, were immunostained with primary antibodies for myelin (PLP), T-cells (CD3), cytotoxic T-cells (CD8), B-cells (CD20), microglia (Iba1) and activated microglia (CD68) (Table 2.1), using established methods (Appendix 1). Experiments with omission of primary and secondary antibodies were used as negative controls. Mesial precental gyrus was selected for study as this region supplies fibres destined to the leg, an area known to be predominately affected in the progressive phase of MS where spastic paraparesis is a common feature. This systematic sampling method (i.e. matching a specific motor cortical region between cases) was employed to control for possible intra-individual cortical heterogeneity.

Quantitative neuropathologic outcome data derived from the motor cortex was combined with that from three levels of the spinal cord (i.e. cervical, thoracic, and lumbar levels), previously acquired and published by DeLuca *et al*. (DeLuca *et al.*, 2013). Comparisons between motor cortical and total and lateral column spinal cord pathology were undertaken.

H&E staining was used to confirm the presence of Betz cells (specific to motor cortex) in layer 5 of each motor cortical block. Our analyses focused on cortical regions in which Betz cells could be definitively observed. Operators were blinded to the clinical details of each case.

Table 2.1: Details of antibodies used in chapter 2

Antibody	Clone	Classification	Pretreatment	Dilution	Supplier	Catalogue Number
PLP	plpc1	Monoclonal mouse	Microwave, citrate pH 6.0	1:1000	AbD Serotec	MCA8399
CD3		Polyclonal rabbit	Autoclave, tris-EDTA pH 9.0	1:100	Dako	A0452
CD8	C8/C114B	Monoclonal mouse	Autoclave, citrate pH 6.0	1:5	Dako	IS623
CD20	L26	Monoclonal mouse	Microwave, citrate pH 6.0	None	Dako	IS604
Iba1		Polyclonal rabbit	Autoclave, tris-EDTA pH 9.0	1:1000	Wako	019-19741
CD68	PG-M1	Monoclonal mouse	Microwave, citrate pH 6.0	1:100	Dako	M0876

2.2.4. Assessment of motor cortical demyelination

Cortical lesions were defined as well-demarcated areas of complete demyelination and were measured in mm^2 using ImageJ software. Areas of demyelination were related to sampled cortical length (mm) and not total sampled cortical area. This was because in many instances cortical thickness was incomplete, precluding measures of cortical lesion load relative to cortical area in those areas where all cortical layers were not present. In contrast, by relating cortical lesion burden to measures of cortical length, a more consistent and comprehensive sampling strategy was possible (Figure 2.1). To validate this approach, we compared cortical lesion burden/cortical area measures to cortical

lesion burden/cortical length measures and found they correlated significantly ($r=0.892$, $p<0.001$). Cortical lesion burden relative to cortical length was used in all subsequent analyses.

2.2.5. Assessment of motor cortical inflammation

Lymphocytes (CD3+, CD8+ and CD20+ cells) were quantified in the parenchyma, perivascular space and meninges. Parenchymal and perivascular lymphocytes were quantified at 200x magnification in field of views (FOVs) spaced in predefined and systematically spaced intervals throughout sampled motor cortex. The number of FOVs used for quantification depended on the size of the available tissue section, but was typically between 28 and 44 for each antibody per tissue block. FOVs were systematically spaced 6 fields apart at 200x magnification along the subpial surface of the cortex. At each of these points along the cortical surface, adjacent (but non-overlapping) FOVs at 200x magnification were assessed in a trajectory perpendicular to the cortical surface. Data derived from FOVs that localised to either NAGM or cortical lesions were analysed. Parenchymal lymphocytes were manually counted in each FOV (data expressed as cells/mm^2). Perivascular lymphocytic inflammation was scored semi-quantitatively using the following criteria (0 = no cells; 1 = 1 - 3 cells; 2 = 3+ cells; 3 = one or more perivascular cuff(s)) (Figure 2.1). Perivascular lymphocyte inflammation assessment was restricted to the vessel with the most severe lymphocyte infiltration within a given FOV. Semi-quantitative analysis of the most inflamed vessel within an FOV removes the confounding issue of parenchymal vessel diameter size that limits the applicability of quantitative analysis. Meningeal lymphocytes were manually counted in available

leptomeninges at 200x magnification and related to available meningeal length (data expressed as cells/mm meninges).

Microglial/macrophage inflammation (Iba1+ and CD68+ cells) was quantified in the same FOVs as those used for lymphocytic inflammation using an optimised semi-automated colour-based extraction method (expressed as millions pixels/mm^2) (Figure 2.2).

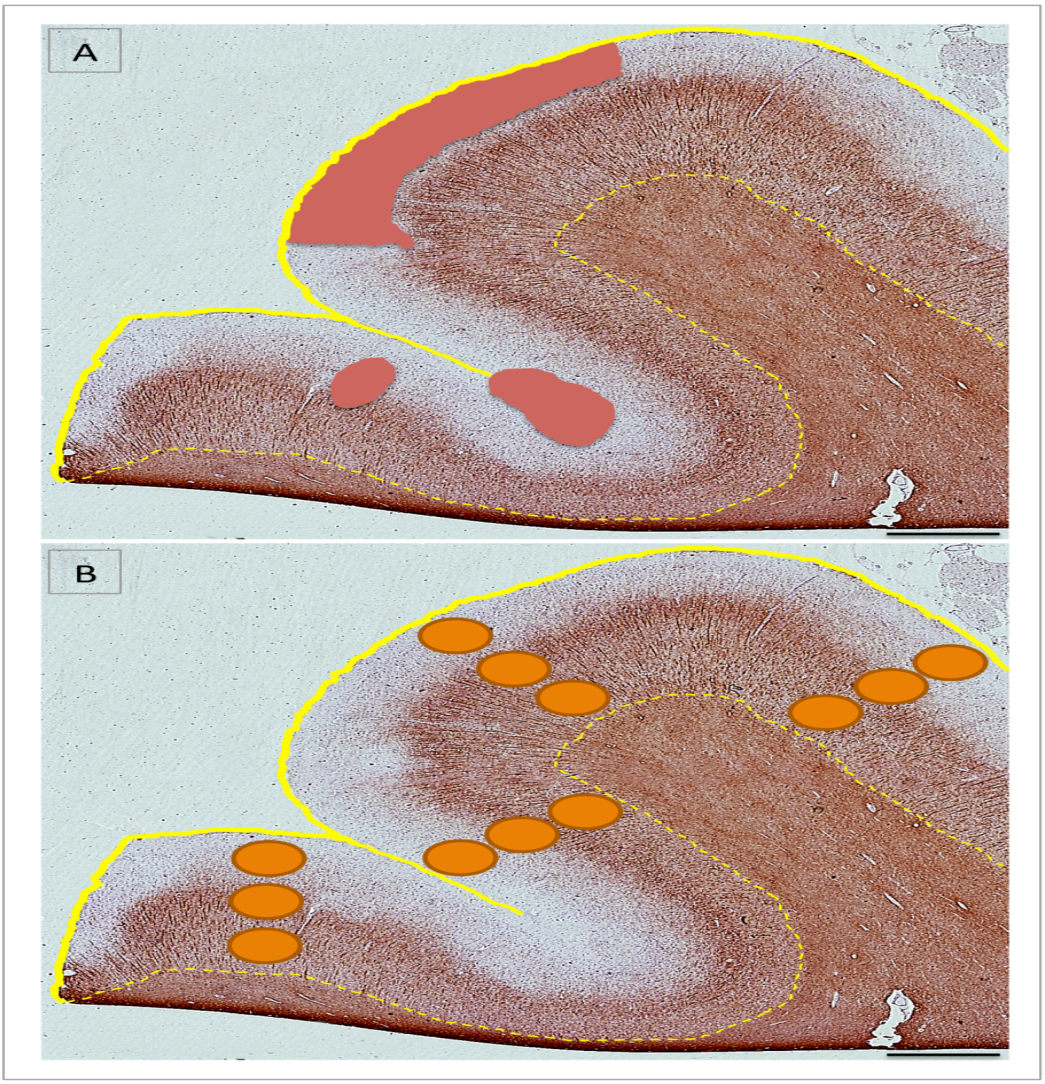


Figure 2.1: Quantitative neuropathological methods. Total sampled motor cortical area is outlined by a solid yellow line (subpial surface) and dashed yellow line (white/grey matter boundary). Cortical lesions (schematically represented as red areas) were measured in mm^2 and related to cortical length (mm) (A). Parenchymal and perivascular inflammation (CD3+, CD8+, CD20+, Iba1+ and CD68+) was quantified within field of views (orange circles) (B), as described in the main text. Meningeal lymphocytic inflammation was quantified by manually counting positively labeled cells (CD3+, CD8+ and CD20+) at 200x magnification in available leptomeninges and relating these counts to the meningeal length (cells/mm meninges). Scale bars represent 1mm.

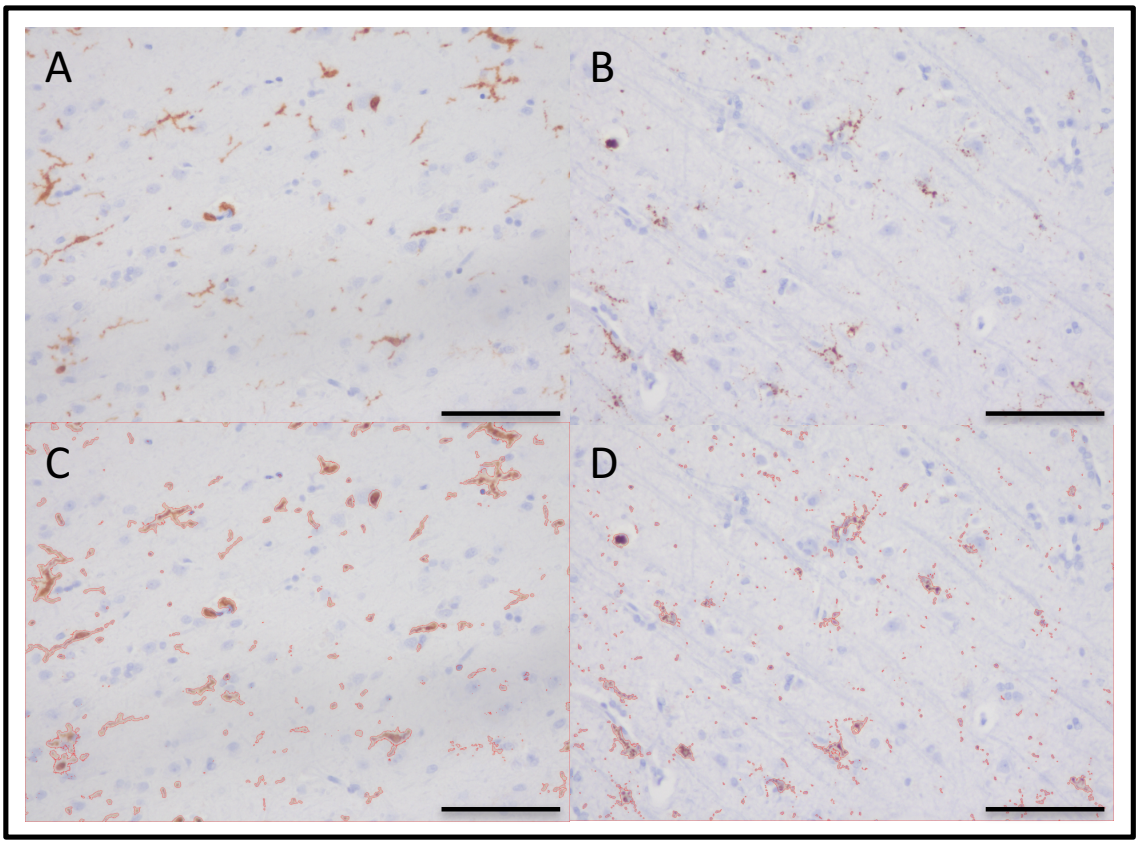


Figure 2.2: Quantitation of microglial/macrophage inflammation. Photomicrographs of Iba1+ (A) and CD68+ (B) stained cells in MS motor cortex (positively labelled cells with brown chromogen). Panels C and D show corresponding masked photomicrographs of A and B respectively, after application of an optimised semi-automated colour based extraction method to quantify positively labelled pixels per unit area (millions pixels/mm^2).

The semi-automatic colour based extraction method detects positively stained pixels above an optimised threshold applied in a consistent way across all cases. Given the complex morphology of microglial/macrophages, we found that this method provided the best estimate of microglia/macrophage burden.

The extent and distribution of motor cortical demyelination and inflammation (normal-appearing parenchyma, lesional, and meningeal) was compared to the same pathologic outcomes (i.e. extent of demyelination, parenchymal and meningeal inflammation) obtained from three spinal cord levels (i.e. cervical, thoracic, and lumbar) derived from the same MS cases reported in a previously published study (DeLuca *et al.*, 2013).

2.2.6. Statistical Analyses

Linear regression models were fitted to evaluate the influence of *HLA-DRB1*15* status on continuous pathologic outcome measures whilst controlling for age, disease duration, sex and post-mortem interval as appropriate. Distribution of data was assessed analytically and graphically and transformed as required. Data is presented ± standard error of the mean (SEM). All tests of hypotheses were carried out using two-sided tests. Correlations between continuous pathologic variables were assessed using Spearman rank correlation coefficients. In all analyses, P-values less than 0.05 were considered significant. Statistical analyses were done using SPSS v21 software.

2.3. Results

2.3.1. Genetics

Extraction of DNA and genotyping of the *HLA-DRB1* locus was carried out prior to this thesis, and was successful in all *HLA-DRB1*15*+ (n=21) and *HLA-DRB1*15*- (n=26) MS cases in our cohort. Age, duration of disease, post-mortem interval and disease course did not differ significantly between genotype groups. Clinical details of the cases used in this study can be found in Table 2.2.

In summary, the majority of MS cases were clinically classified as secondary progressive (38/47 = 80.9%) with 4/47 (8.5%) being primary progressive and only 1/47 (2.1%) being relapsing-remitting. The clinical course was unknown in 4 (8.5%) cases.

Table 2.2: Clinical details of cohort used in chapter 2

	MS cases (n=47)	***HLA-DRB1*15+* (n=21)**	***HLA-DRB1*15-* (n=26)**	**Controls (n=9)**
Age of death (yrs)	63 (range: 40-92)	65 (range: 40- 92)	62 (range: 43-86)	67 (range: 32-87)
Duration of disease (yrs)	31 (range: 11-58)	32 (range: 12-58)	30 (range: 11-55)	n/a
Sex	M=13, F=34	M=7, F=14	M=6, F=20	F=4, M=5
Clinical Course	PPMS: 4, SPMS: 38, RRMS: 1, Unknown: 4	PPMS: 3, SPMS: 17, RRMS: 0, Unknown: 1	PPMS: 1, SPMS: 21, RRMS: 1, Unknown: 3	n/a
Brain weight (g)	1157 (range: 894-1380)	1163 (range: 1000-1364)	1152 (range: 894-1380)	1319 (range: 1160-1462)
PM interval (hrs)	18 (range: 7-38)	18 (range: 7-38)	18 (range: 8-28)	54 (range: 24-72)

2.3.2. Neuropathological findings: MS versus controls

2.3.2.1 Demyelination

In total, 64% of MS cases (30/47) demonstrated motor cortical lesions. Of the total 78 cortical lesions recorded in our MS cohort, 93% (71/78) were subpial (Type III), 4% (3/78) were intracortical (Type II), 1% (1/78) were leukocortical (Type I) and 4% (3/78) spanned the full cortical depth (Type IV) according to

established criteria (L Bø *et al.*, 2003) (Figure 2.3). Subpial lesions typically did not extend beyond superficial cortical layers (layers 1-3) but often involved multiple gyri. Deeper cortical layers (layers 4-6) usually displayed normal myelin staining, even when subjacent to a subpial lesion. All cortical lesions were chronic inactive with the exception of one leukocortical lesion which was border-active, as classified by established criteria (Bö *et al.*, 1994). No evidence of demyelination was observed in control sections.

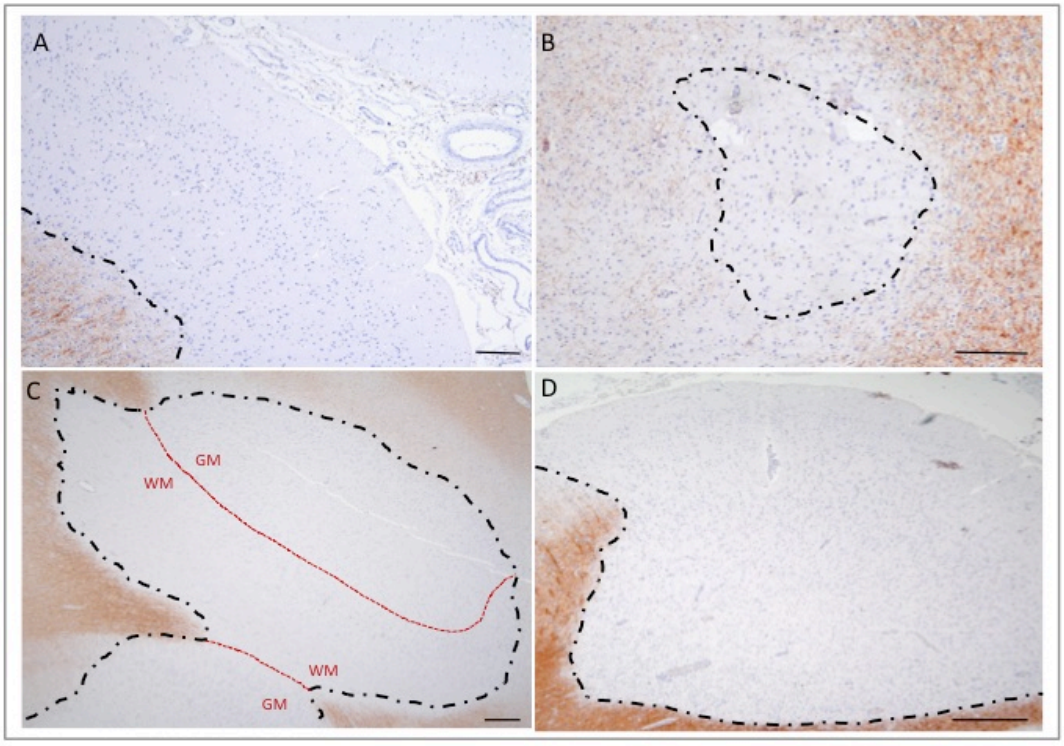


Figure 2.3: Photomicrographs of proteo-lipid protein (PLP) stained cortical tissue. In our MS cohort, subpial lesions (A) were the most common lesion type observed. Intracortical lesions (B), leukocortical lesions (C), and lesions that spanned the full cortical depth (i.e. type IV lesions) (D) were only rarely noted. Scale bars represent 200μm for Panels A and B, and 500μm for Panels C and D.

2.3.2.2 Lymphocytic inflammation

Motor cortical T-cell inflammation in MS cases was scarce. However, both CD3+ and CD8+ cells were significantly increased in the NAGM of MS cases compared to controls (CD3: MS: 4.25 ± 0.66 cells/mm^2 versus control: 0 ± 0 cells/mm^2, p=0.013) (CD8: 3.1 ± 0.66 cells/mm^2 versus control: 0.16 ± 0.16 cells/mm^2, p=0.012). The majority of CD3+ cells in MS parenchyma were also CD8+. Perivascular T-cell inflammation significantly increased in MS cases compared to controls (CD3: MS: 0.201 ± 0.02 versus control: 0.00 ± 0.0, p=0.001) (CD8: MS: 0.144 ± 0.01 versus control: 0.00 ± 0.0, p=0.003).

Meningeal T-cell inflammation was significantly increased in MS cases compared to controls (CD3: MS: 3.9 ± 0.5 cells/mm meninges versus control: 0.26 ± 0.05 cells/mm meninges, p=0.008) (CD8: MS: 2.7 ± 0.48 cells/mm meninges versus control: 0.5 ± 0.15 cells/mm meninges, p=0.029) (Figure 2.4). The majority of meningeal T-cells were CD8+.

CD20+ cells were virtually absent from the motor cortex of both MS cases and controls and were not analysed further.

2.3.2.3. Microglial/macrophage inflammation

Microglial/macrophage inflammation (Iba1+ and CD68+ cells) was significantly increased in the NAGM of MS cases compared to controls (Iba1+: MS: 1.83 ± 0.15 million pixels/mm^2 versus control: 0.94 ± 0.24 million pixels/mm^2, p=0.014) (CD68+: MS: 0.52 ± 0.12 millions pixels/mm^2 versus control: 0.09 ± 0.02 million pixels/mm^2, p=0.007) (Figure 2.4). Iba1+ and CD68+ cells were found diffusely

throughout the motor cortex, with Iba1+ inflammation being significantly more severe. Total motor cortical Iba1+ cells significantly correlated with total motor cortical CD68+ cells in MS cases (r=0.562, P<0.01).

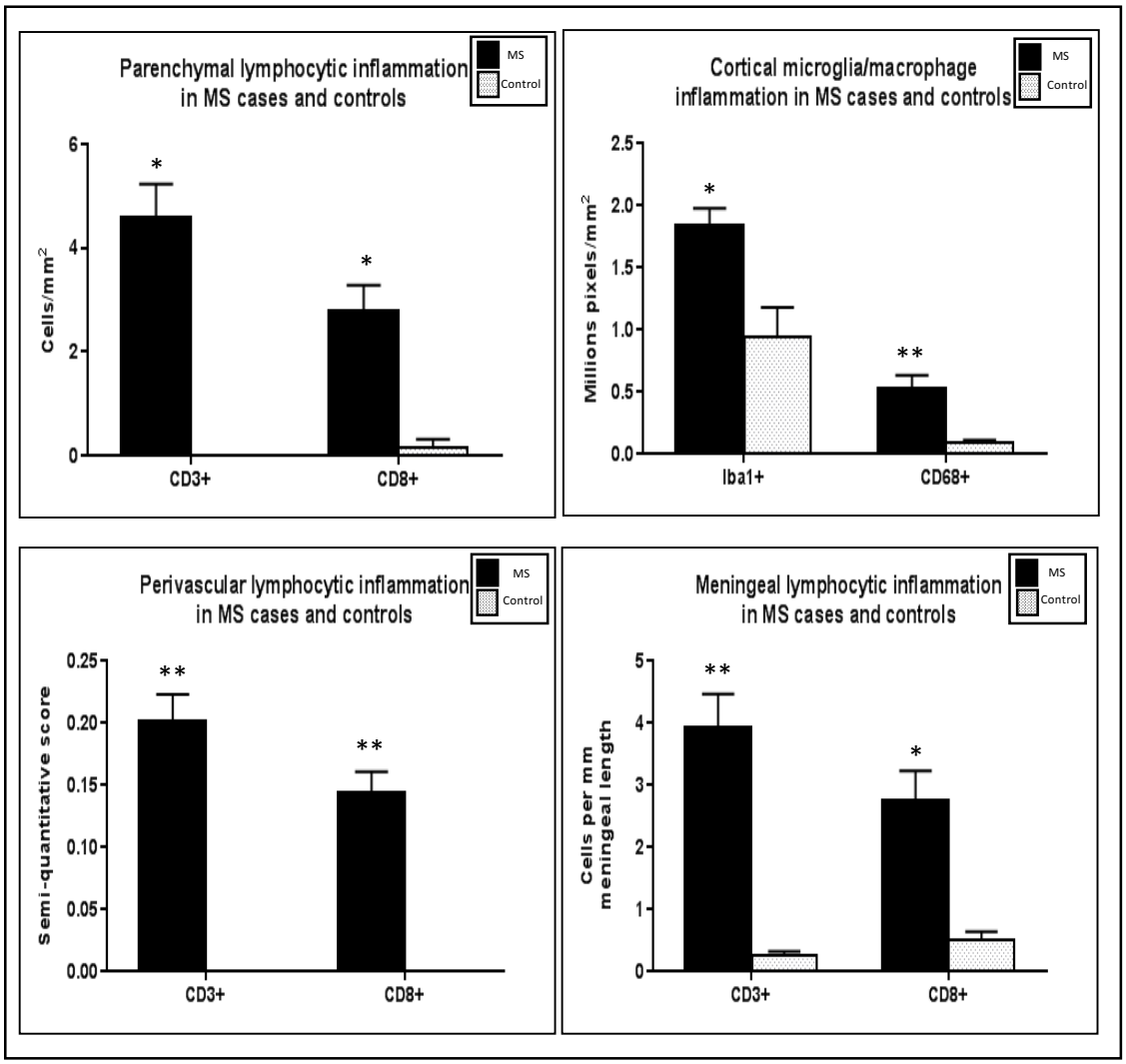


Figure 2.4: Motor cortical inflammation in MS cases and controls. Bar graphs showing the extent of motor cortical inflammation in normal appearing parenchyma, perivascular and meningeal compartments in MS cases and controls. * P<0.05 ** P<0.01

2.3.2.4. Relationship of motor cortical lesions, inflammation and demographic factors

Motor cortical lesion load inversely correlated with age (r=-0.337, p=0.021), independent of disease duration (Figure 2.5). The size of motor cortical lesions positively correlated with the extent of CD3+ cells within lesions (r=0.497, p=0.007). Whilst CD8+ T-cells constituted the majority of the total T-cell population within motor cortical lesions, they were rarely seen within lesional perivascular spaces. Meningeal T-cell and motor cortical microglia/macrophage inflammation were not associated with lesion size (meningeal CD3+: r=0.203, p=0.191; meningeal CD8+: r=0.190, p=0.223; parenchymal CD68+: r=0.228, p=0.263; parenchymal Iba1+: r=0.002, p=0.993).

2.3.3. Genetic-pathology relationships in MS

2.3.3.1. Demyelination

On consideration of all MS cases, *HLA-DRB1*15*+ cases did not have a significantly greater burden of motor cortical lesions compared to *HLA-DRB1*15*- cases (15+: 0.28 ± 0.098mm^2/mm motor cortical length versus 15-: 0.3 ± 0.073mm^2/mm motor cortical length, p=0.97). As motor cortical demyelination was more severe in younger cases, we assessed the influence of *HLA-DRB1*15* on the extent of demyelination in cases younger than the median age of the entire cohort (i.e. age < 62yrs). In this younger population, *HLA-DRB1*15*+ cases had significantly greater motor cortical lesion burden compared to *HLA-DRB1*15*- cases when controlling for gender, duration of disease and post-mortem interval (15+: 0.51 ± 0.219mm^2/mm motor cortical length versus 15-: 0.25 ± 0.087mm^2/mm cortical length, p=0.048) (Figure 2.5). *HLA-DRB1*15* status did

not appear to influence the number of motor cortical lesions in each case (15+: 1.5 ± 0.378 lesions/mm motor cortical length versus 15-: 1.81 ± 0.514/mm motor cortical length, p=0.969). In our cohort, only three cases were homozygous for *HLA-DRB1*15,* precluding further analysis of the effect of dose of this allele on the severity of motor cortical pathology.

The observed inverse relationship between age and extent of motor cortical lesion burden, noted in all MS cases, was significantly driven by cases bearing the *HLA-DRB1*15* allele (r=-0.56, p=0.008) (Figure 2.5). A sensitivity analysis (in which the most and least demyelinated case was excluded) showed this relationship to be robust (r=-0.466, p=0.044).

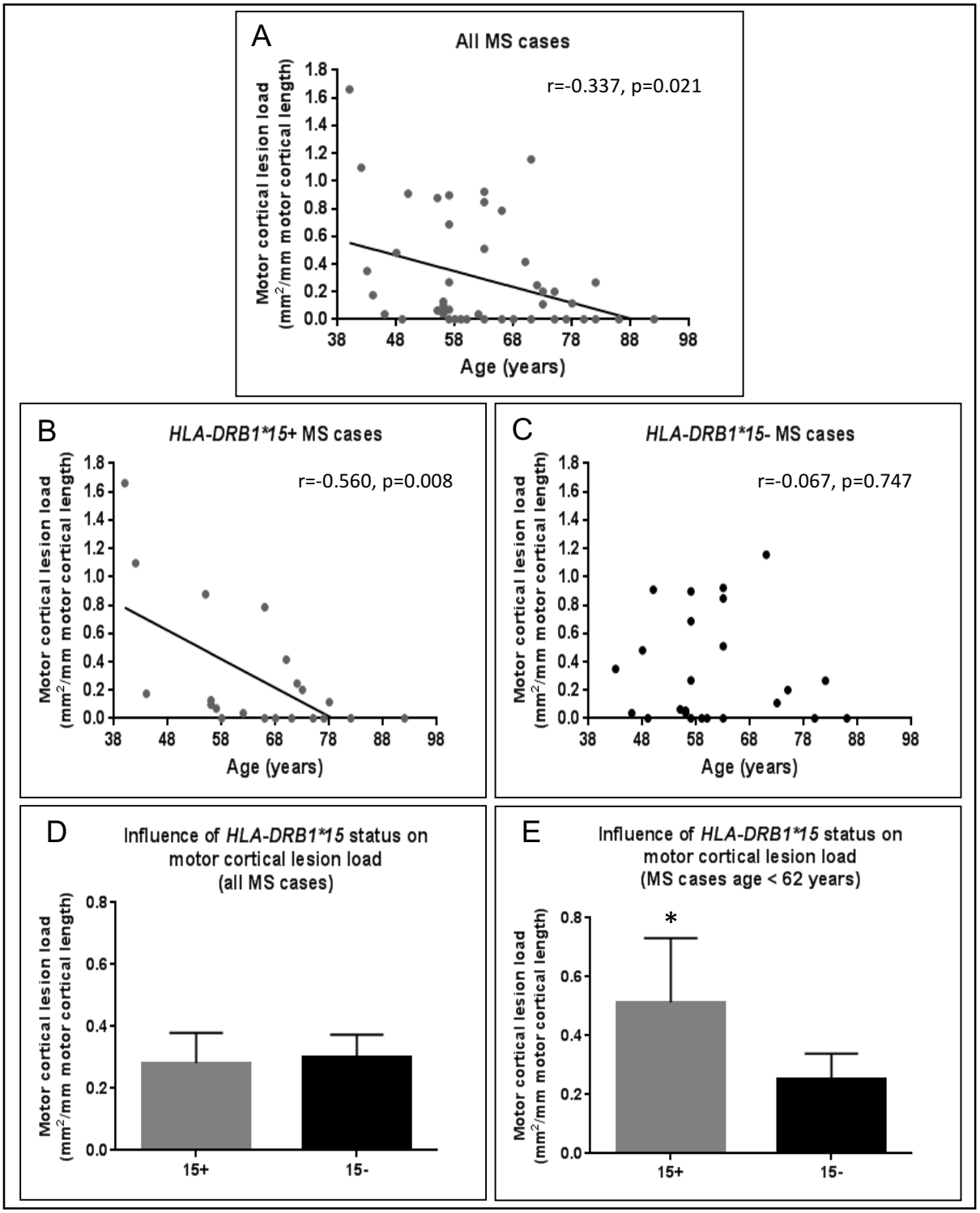


*Figure 2.5: Relationship of age, HLA-DRB1*15 status and motor cortical lesion load.* Panels A-C display scatter plots showing the influence of *HLA-DRB1*15* status on the relationship between age and motor cortical lesion load in all MS cases (A) *HLA-DRB1*15*+ cases (B) and *HLA-DRB1*15*- (C) cases. Panels D and E display bar charts showing the influence of *HLA-DRB1*15* status on motor cortical lesion burden. * P<0.05, ** P<0.01

2.3.3.2. Parenchymal lymphocytic inflammation

In all MS cases, *HLA-DRB1*15* status did not have a significant relationship with the extent of CD3+ T-cell inflammation within NAGM or the parenchyma of motor cortical lesions (NAGM: 15+: 4.71 ± 1.17 cells/mm^2 versus 15-: 3.89 ± 0.76 cells/mm^2, p=0.763; lesion: 15+: 6.03 ± 2.06 cells/mm^2 versus 15-: 2.81 ± 0.76 cells/mm^2, p=0.332). In contrast, again in all MS cases, *HLA-DRB1*15*+ cases demonstrated more severe CD8+ T-cell inflammation within both NAGM and lesional parenchyma compared to *HLA-DRB1*15*- cases (NAGM: 15+: 4.52 ± 1.33 cells/mm^2 versus 15-: 2.01 ± 0.53 cells/mm^2, p=0.042; lesion: 15+: 4.55 ± 1.46 cells/mm^2 versus 15-: 2.01 ± 0.55 cells/mm^2, p=0.047) (Figure 2.6).

In younger cases, *HLA-DRB1*15*+ cases had significantly more CD3+ and CD8+ T-cells within lesional parenchyma (CD3+: 15+: 13.57 ± 2.9 cells/mm^2 versus 2.38 ± 0.73 cells/mm^2, p=0.006; CD8+: 15+: 7.97 ± 3.17 cells/mm^2 versus 15-: 2.27 ± 0.84 cells/mm^2, p=0.054). In NAGM, *HLA-DRB1*15* status did not associate significantly with the extent of CD3+ or CD8+ T-cell inflammation (CD3+: 15+: 6.27 ± 1.96 cells/mm^2 versus 15-: 4.04 ± 1.16 cells/mm^2, p=0.278; CD8+: 15+: 6.49 ± 3.12 cells/mm^2 versus 15-: 2.1 ± 0.68 cells/mm^2, p=0.175) (Figure 2.6).

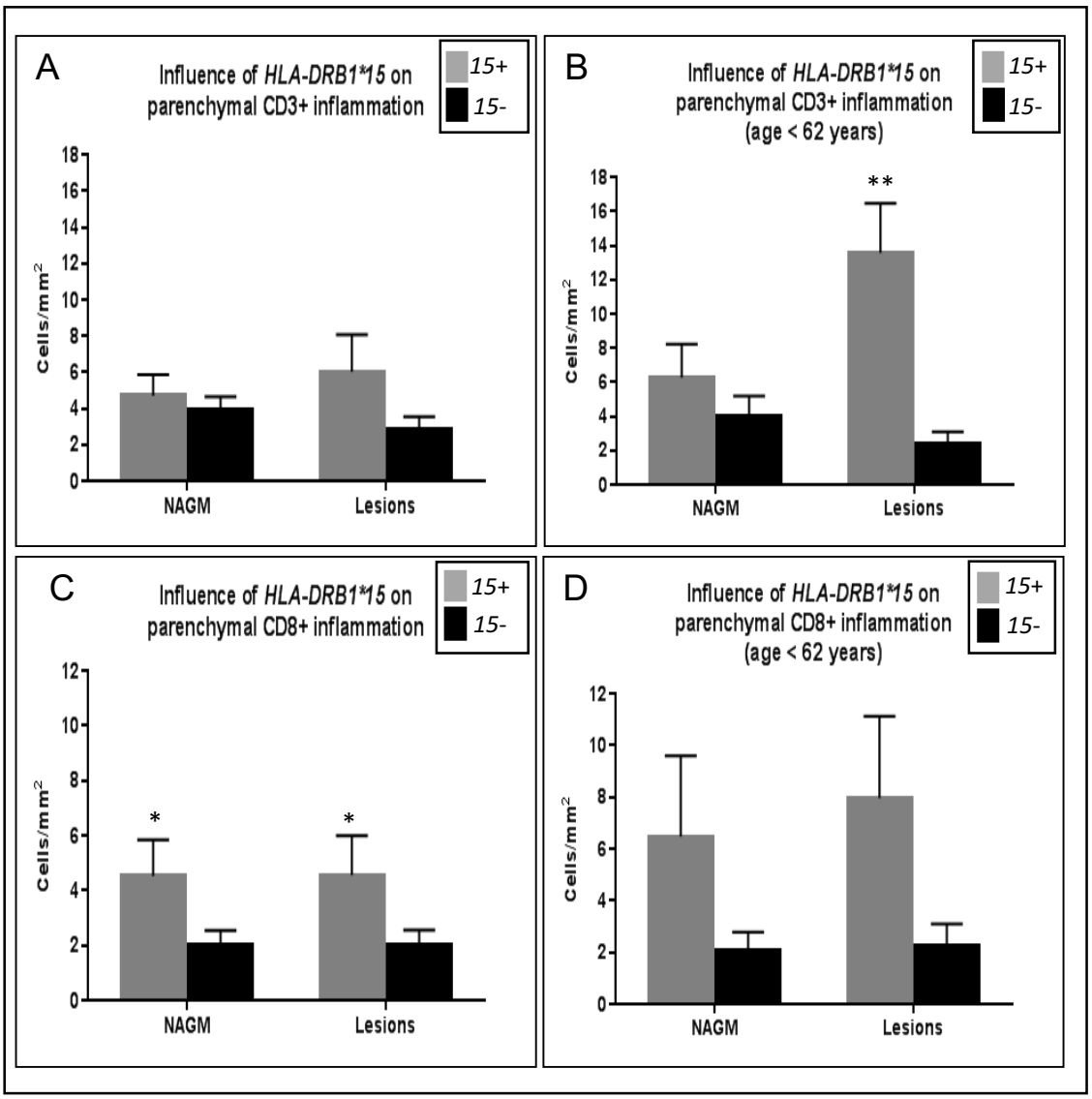


*Figure 2.6: HLA-DRB1*15 status and parenchymal T-cell inflammation*. Bar charts showing the influence of *HLA-DRB1*15* status on motor cortical parenchymal T-cell inflammation in MS.

* P<0.05 ** P<0.01

2.3.3.3. Perivascular lymphocytic inflammation

In all MS cases, *HLA-DRB1*15+* cases had significantly greater perivascular CD3+ and CD8+ T-cell inflammation within NAGM but not within motor cortical lesions compared to *HLA-DRB1*15-* cases (NAGM: CD3+: 15+: 0.24 ± 0.04 versus 15-: 0.17 ± 0.02, p=0.029; CD8+: 15+: 0.19 ± 0.03 versus 15-: 0.11 ± 0.01, p=0.011) (lesions: CD3+: 15+: 0.28 ± 0.13 versus 15-: 0.12 ± 0.05, p=0.289; CD8+: 15+: 0.08 ± 0.047 versus 15-: 0.01 ± 0.01, p=0.056). Similar findings were seen in younger cases where *HLA-DRB1*15* status influenced the extent of perivascular CD3+ and CD8+ T-cell inflammation within NAGM but not within motor cortical lesions (NAGM: CD3+: 15+: 0.32 ± 0.07 versus 15-: 0.19 ± 0.04, p=0.047; CD8+: 15+: 0.27 ± 0.09 versus 15-: 0.12 ± 0.02, p=0.05)(lesions: CD3+: 15+: 0.34 ± 0.19 versus 15-: 0.16 ± 0.07, p=0.406; CD8+: 15+: 0.21 ± 0.1 versus 15-: 0 ± 0, p=0.051) (Figure 2.7).

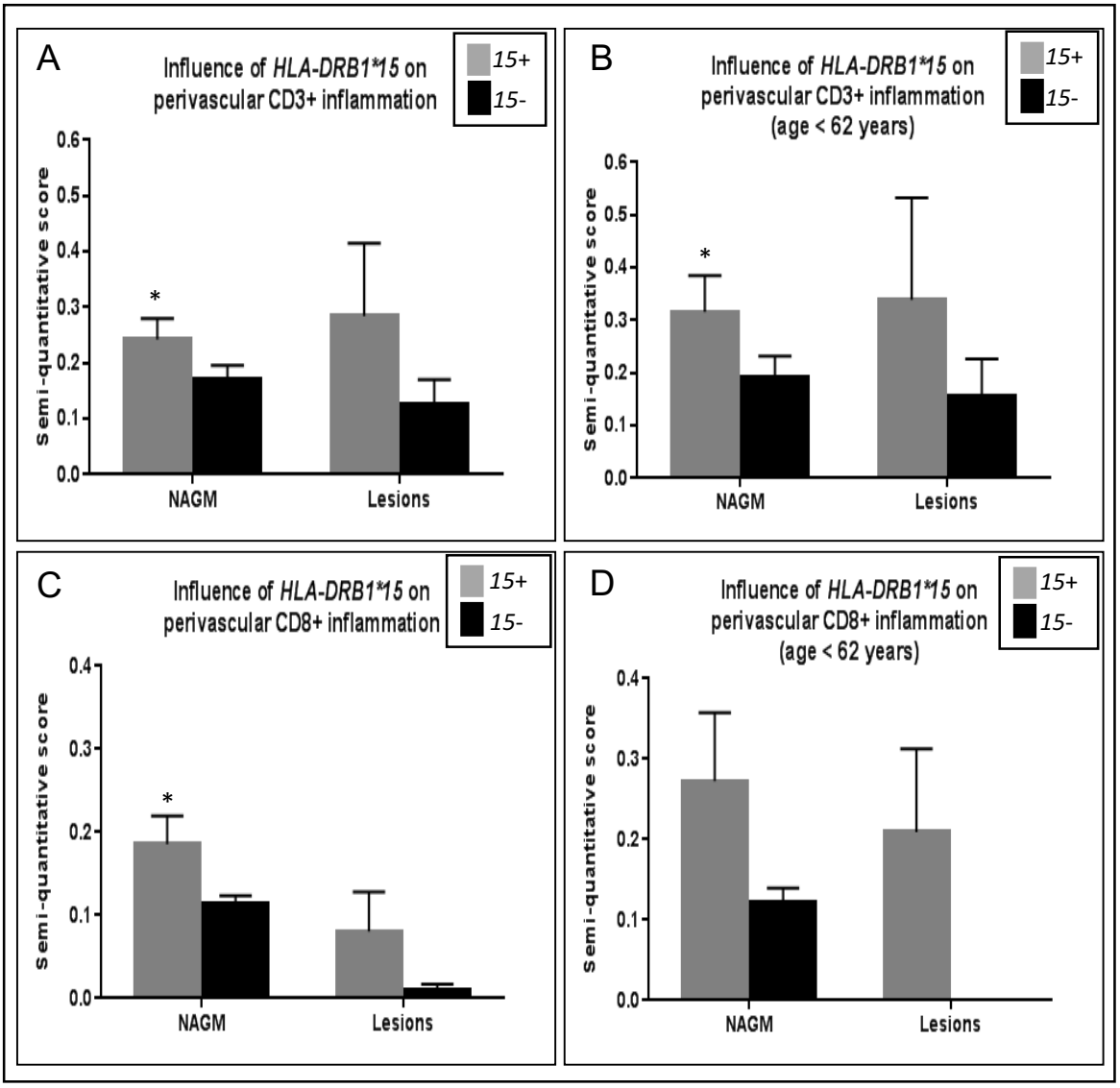


*Figure 2.7: HLA-DRB1*15 status and perivascular T-cell inflammation.* Bar charts showing the influence of *HLA-DRB1*15* status on motor cortical perivascular T-cell inflammation in MS. Note that only three MS cases younger than 62 years displayed perivascular CD8+ cells within lesions (D), hence the statistically insignificant result when comparing this compartment in younger MS cases (p=0.051). Data presented as mean ± SEM.

* P<0.05 ** P<0.01

2.3.3.4. Meningeal lymphocytic inflammation

*HLA-DRB1*15*+ cases had a significantly greater quantity of meningeal CD8+ cells when all MS cases were considered (15+: 3.66 ± 0.8 cells/mm meninges versus 15-: 1.88 ± 0.48 cells/mm meninges, p=0.049), though this was not the case in younger cases (15+: 4.6 ± 1.8 cells/mm meninges versus 15-: 2.21 ± 0.73 cells/mm meninges, p=0.622). In all cases, no statistically significant impact of *HLA-DRB1*15* on meningeal CD3+ inflammation was observed (15+: 4.39 ± 0.71 cells/mm meninges versus 15-: 3.46 ± 0.84 cells/mm meninges, p=0.155). The same was also true of younger cases (CD3: 15+: 4.36 ± 1.08 cells/mm meninges versus 15-: 4.45 ± 1.35 cells/mm meninges, p=0.837)

2.3.3.5. Microglial/macrophage inflammation

Upon consideration of all MS cases, *HLA-DRB1*15* status did not influence the severity of Iba1+ or CD68+ inflammation in NAGM (Iba1+: 15+: 1.77 ± 0.26 million pixels/mm^2 versus 15-: 1.87 ± 0.18 million pixels/mm^2, p=0.751) (CD68+: 15+: 0.7 ± 0.26 million pixels/mm^2 versus 15-: 0.4 ± 0.04 million pixels/mm^2, p=0.108) or in lesions (Iba1+: 15+: 2.3 ± 0.35 million pixels/mm^2 versus 15-: 1.61 ± 0.26 million pixels/mm^2, p=0.651) (CD68+: 15+: 0.71 ± 0.24 million pixels/mm^2 versus 15-: 0.31 ± 0.05 million pixels/mm^2, p=0.074).

In cases younger than 62 years, *HLA-DRB1*15*+ cases had significantly more Iba1+ cells within lesions (15+: 3.1 ± 0.44 million pixels/mm^2 versus 15-: 1.31 ± 0.14 million pixels/mm^2, p=0.002), but not in NAGM (15+: 2.24 ± 0.66 million pixels/mm^2 versus 15-: 1.81 ± 0.19 million pixels/mm^2, p=0.318). Also in young cases, *HLA-DRB1*15+* cases had significantly more severe CD68+ inflammation

within lesions (15+: 1.22 ± 0.53 million pixels/mm^2 versus 15-: 0.27 ± 0.06 million pixels/mm^2, p=0.009) and NAGM (15+: 1.35 ± 0.73 million pixels/mm^2 versus 15-: 0.41 ± 0.05 million pixels/mm^2, p=0.009) compared to their *HLA-DRB1*15*- counterparts (Figure 2.8).

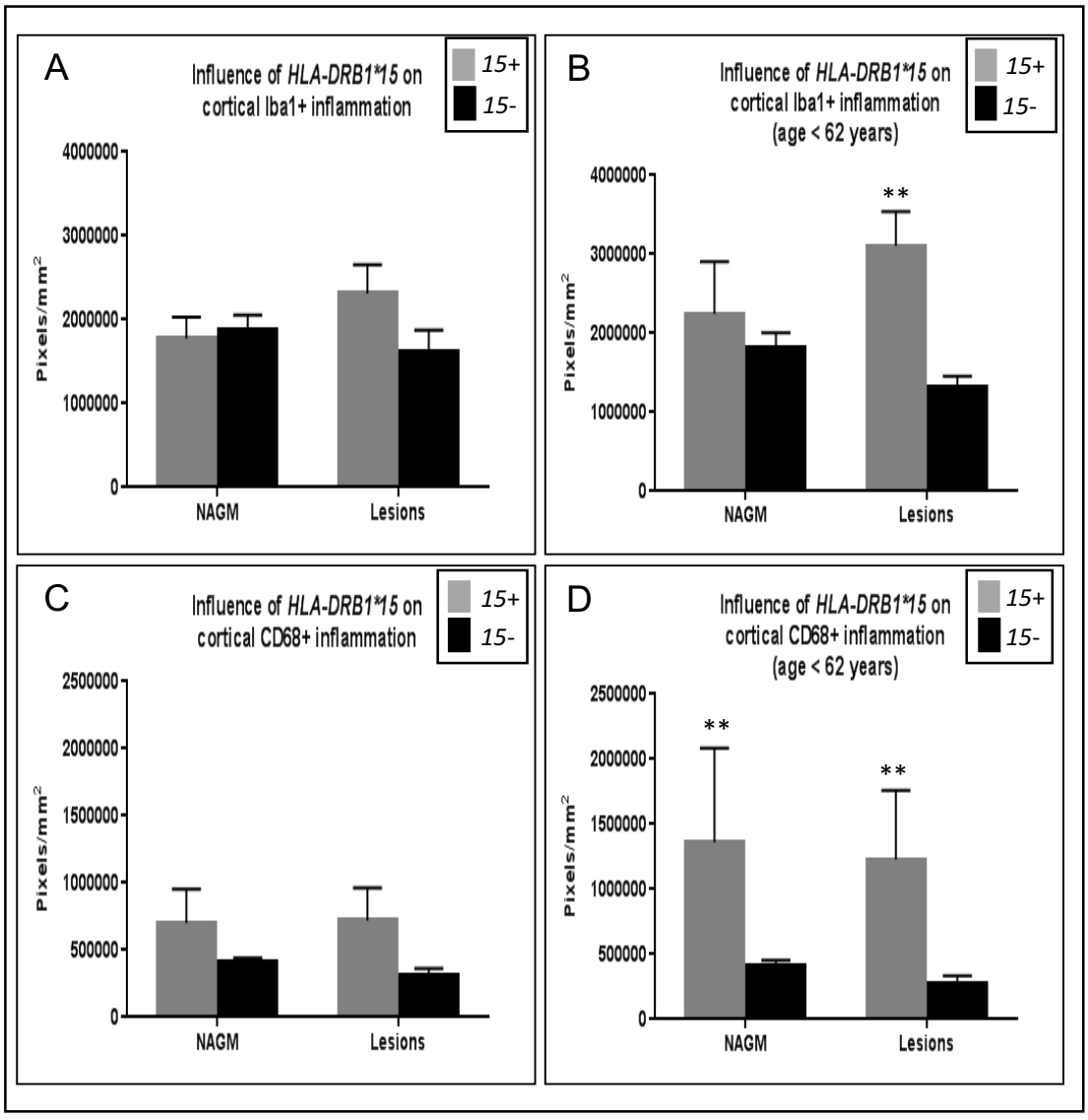


*Figure 2.8: HLA-DRB1*15 status and microglial/macrophage inflammation.* Bar charts showing the influence of *HLA-DRB1*15* status on motor cortical microglial/macrophage burden. Data presented as mean ± SEM. * P<0.05 ** P<0.01

2.3.4. Relationships between motor cortical lesion load, inflammation, demographic factors and *HLA-DRB1*15* status

A relationship between age and the severity of CD3+ T-cell inflammation in lesional parenchyma when considering all MS cases was not detected (r=-0.092, p=0.663). However, such a relationship emerged in cases bearing the *HLA-DRB1*15* allele (r=-0.767, p=0.002). Further, motor cortical lesion size correlated significantly with the extent of CD3+ T-cell inflammation in lesional parenchyma solely in *HLA-DRB1*15*+ cases (15+: r=0.623, p=0.023; 15-: r=0.310, p=0.260).

2.3.5. Correlations between motor cortical and spinal cord MS pathology, and the influence of *HLA-DRB1*15* status

We next compared motor cortical pathology with previously assessed spinal cord pathology derived from the same MS cases (DeLuca *et al.*, 2013).

2.3.5.1. Demyelination

Demyelination in the motor cortex did not correlate with demyelination found at each level of the spinal cord when total cord area was considered (cervical: r=0.094, p=0.592; thoracic: r=0.119, p=0.464; lumbar: r=0.025, p=0.883). *HLA-DRB1*15* status did not have a significant influence on the relationship of demyelination between motor cortex and spinal cord.

When evaluating the relationship between motor cortical demyelination and demyelination impinging on the anatomically relevant lateral corticospinal tracts (LCSTs), no correlations were observed when all cases were considered (cervical: r=0.177, p=0.239; thoracic: r=0.201, p=0.176; lumbar: r=0.176, p=0.238).

In contrast, a significant correlation between motor cortical demyelination and cervical cord LCST demyelination emerged in *HLA-DRB1*15+* cases only (15+: r=0.556, p=0.009; 15-: r=-0.172, p=0.412). *HLA-DRB1*15* status did not influence the relationship between motor cortical demyelination and thoracic or lumbar spinal cord LCST demyelination.

2.3.5.2. Parenchymal lymphocytic inflammation

Upon comparison of motor cortical NAGM and spinal cord NAGM it was observed that CD3+ and CD8+ inflammation significantly correlated at the lumbar (CD3+: r=0.460, p=0.008; CD8+: r=0.372 p=0.025) but not cervical (CD3+: r=0.247, p=0.205; CD8+: r=0.285, p=0.150) or thoracic (CD3+: r=-0.212, p=0.332; CD8+: r=0.118, p=0.566) levels.

*HLA-DRB1*15* status had no influence on the correlations of lymphocytic inflammation between motor cortical NAGM and cervical or thoracic spinal cord NAGM. However, CD3+ inflammation correlated between motor cortical NAGM and lumbar spinal cord NAGM only in *HLA-DRB1*15*+ cases (15+: r=0.613, p=0.015 versus 15-: r=0.240, p=0.354). *HLA-DRB1*15* status had no influence on the correlation of CD8+ inflammation between motor cortical NAGM and lumbar spinal cord NAGM. Similar findings were observed with comparisons between motor cortical NAGM and spinal cord NAWM T-cell inflammation.

2.3.5.3. Parenchymal microglia/macrophage inflammation

Correlations between motor cortical NAGM and spinal cord NAGM CD68+ microglial/macrophage inflammation were not observed, save for at the thoracic level (cervical: r=0.111, p=0.605; thoracic: r=0.406, p=0.049; lumbar: r=0.099,

p=0.601). There was no influence of *HLA-DRB1*15* status on these relationships between motor cortical NAGM and spinal cord NAGM CD68+ microglia/macrophage inflammation. Similar findings were observed with comparisons between motor cortical NAGM and spinal cord NAWM CD68+ microglia/macrophage inflammation.

2.3.5.4. Meningeal Inflammation

Significant correlations between motor cortical and spinal cord meningeal T-cell inflammation were observed throughout the length of the neuraxis (cervical: CD3+: r=0.589, p=0.001; CD8+: r=0.576, p=0.001; thoracic: CD3+: r=0.708, p<0.001; CD8+: r=0.792, p<0.001; lumbar: CD3+: r=0.735, p<0.001; CD8+: r=0.740, p<0.001). Motor cortical meningeal T-cell inflammation correlated significantly with lumbar spinal cord meningeal T-cell inflammation only in *HLA-DRB1*15*+ cases (15+: CD3: r=0.826, p<0.001; CD8: r=0.696, p=0.002 versus 15-: CD3: r=0.336, p=0.188; CD8: r=0.438, p=0.09). *HLA-DRB1*15* status did not influence correlations of meningeal inflammation between motor cortex and cervical or thoracic spinal cord.

2.4. Discussion

We have shown, for the first time, that *HLA-DRB1*15* influences the extent of pathology in the MS motor cortex. In line with previous work we observed that cortical demyelination in MS is common and heterogeneous (Kutzelnigg *et al.*, 2005; Staugaitis *et al.*, 2012), and provide clear evidence that cases with more severe cortical demyelinating disease tend to die at younger ages regardless of disease duration. Our data suggest that *HLA-DRB1*15* associates with more severe motor cortical inflammation, and demyelination in younger MS cases. These findings are novel and advance our understanding of the pathologic heterogeneity characteristic of this disease.

In our MS cohort, the landscape of motor cortical myelin loss was complex, varying considerably both within and between cases. Consistent with other reports, subpial cortical lesions were the predominant motor cortical lesion type (Bö *et al.*, 2006; Bø *et al.*, 2003; Peterson *et al.*, 2001). Lesion burden was most severe in younger cases, a finding that could reflect either more aggressive cortical disease in this population or more extensive cortical remyelination in older cases, as has been previously observed (Chang *et al.*, 2012). Even though lymphocytic inflammation was most severe in the meninges relative to the parenchyma and perivascular space, a direct relationship between subpial demyelination and meningeal T- or B-cell inflammation was not observed. It has been suggested previously that diffusion of disease relevant antibodies from ectopic B-cell follicles located within the meningeal space may contribute to cortical demyelination in MS (Magliozzi *et al.*, 2007, 2013). Whilst we did not

observe B-cell follicle-like structures in our series, this may reflect tissue ascertainment and/or methodological differences. That being said, the influence of inflammation on cortical demyelination is likely to be more complex.

Our findings highlight a key role for the T-cell in cortical lesion pathogenesis. CD3+ T-cells correlated significantly with motor cortical lesion size, with CD8+ being the predominant T-cell type. Interestingly, CD8+ T-cells were underrepresented in the perivascular spaces within cortical lesions. This is consistent with their efficient migration out of the perivascular compartment (Booss *et al.*, 1983), and/or their heightened proliferative potential relative to other adaptive immune cell types (Babbe *et al.*, 2000). The reported propensity of brain lesions to surround perivascular spaces (Mistry *et al.*, 2013), and the intimate anatomic relationship between meninges and Virchow Robin spaces (Esiri and Gay, 1990), suggest multiple immune-mediated mechanisms (i.e. meningeal, parenchymal, and perivascular inflammation) likely drive cortical demyelination in MS, even in the chronic phase of the disease when T-cell inflammation is known to be less severe.

*HLA-DRB1*15* status had a striking influence on the relationship between age and motor cortical lesion burden. Younger cases carrying the *HLA-DRB1*15* allele demonstrated significantly greater motor cortical lesion burden, an effect not observed in *HLA-DRB1*15*- cases. While it is to be expected that cases with more severe demyelination die at younger ages, our results show that *HLA-DRB1*15* status has a critical role in shaping this relationship. Given that the

HLA-DRB1 locus is involved in antigen presentation, immune-mediated mechanisms likely drive this finding.

As with other studies, cortical inflammation was relatively scarce in our MS cases but significantly greater than controls (L Bø *et al.*, 2003; Peterson *et al.*, 2001). We provide evidence that *HLA-DRB1*15* status has a significant impact on the distribution and extent of motor cortical inflammation within MS cases. Cases bearing the *HLA-DRB1*15* allele had significantly more severe T-cell inflammation in the perivascular, parenchymal, and meningeal compartments compared to *HLA-DRB1*15-* cases. T-cell inflammation was particularly remarkable within cortical lesions, where it was most severe in younger *HLA-DRB1*15+* cases. A further role for *HLA-DRB1*15* on the topography of motor cortical pathology is demonstrated by the observation that T-cell inflammation correlated significantly with lesional size only in *HLA-DRB1*15+* cases. Given that age inversely correlated with T-cell inflammation only in *HLA-DRB1*15+* cases, it is not surprising that young *HLA-DRB1*15+* cases had more severe motor cortical demyelination. These findings are in line with previous work which has shown that inflammation within the MS brain diminishes with advancing age (Frischer *et al.*, 2009; Khademi *et al.*, 2013). We provide additional evidence to support the notion that *HLA-DRB1*15* status may exaggerate this impact of age on the severity of motor cortical inflammation and therefore, subsequent demyelination in these MS cases.

It is interesting that *HLA-DRB1*15* influenced not only total T-cell population numbers, as quantified by CD3+ staining, but also CD8+ cells. It is plausible that *HLA-DRB1*15* influenced CD4+ T-cells to create a cytokine milieu amenable to CD8+ T-cell proliferation. In addition, CD8+ T-cells could also have been influenced by genetic variants in *HLA* class I alleles tagged within the extended *HLA-DRB1*15* risk haplotype (Chao *et al.*, 2008). We recognise that direct quantification of CD4+ T-cells would have been of value, but technical limitations arising from paraffin-embedded tissue precluded this.

In addition to its influence on adaptive cell-mediated immune responses, genetic variation also appears to impact the extent of innate immunity in the MS cortex, particularly in the young. Younger *HLA-DRB1*15*+ MS cases had significantly greater Iba1+ and CD68+ microglia/macrophages within motor cortical lesions, the latter also being overrepresented in NAGM of these cases compared to *HLA-DRB1*15*- cases. Iba1+ and CD68+ cells represent distinct microglia/macrophage phenotypes; the former being a marker of the total population and the latter being a marker of activated cells. The presence of upregulated activated microglia in the NAGM of *HLA-DRB1*15+* cases suggests that priming of these cells may be important in the initiation of cortical lesions. Microglia/macrophages upregulate HLA-DR when stimulated with interferon-gamma (Ulvestad *et al.*, 1994), representing a potential mechanism by which allelic variation in this locus could affect disease. Why this genotypic influence should be exaggerated in younger age groups is unclear, but could relate to the fact that microglia undergo age-related gene expression changes that alter their

activation potential in later years (Ma *et al.*, 2013). Further assessment of the impact of age on microglia/macrophage phenotypes in MS is now needed.

Motor cortical demyelination was largely distinct from that in the spinal cord save for cervical cord LCST demyelination, which positively correlated with motor cortical demyelination only in *HLA-DRB1*15*+ MS cases. Whilst additional correlations between motor cortical and spinal cord demyelination may have been found with more extensive sampling, the fact that the extent of demyelination correlated significantly between different levels of the spinal cord challenges this view (DeLuca *et al.*, 2013). The regional variation in the severity of demyelination between these CNS regions within the same case therefore raises the possibility that mechanisms of demyelination or capability of repair are unique to cortical and spinal cord regions. In contrast, the extent of meningeal inflammation correlated significantly between the motor cortex and spinal cord (especially at the lumbar level) consistent with the contiguity of the subarachnoid space along the length of the neuraxis. In addition, T-cell inflammation correlated between motor cortex and lumbar spinal cord. The relationship between motor cortical and spinal cord meningeal inflammation and between motor cortical parenchymal T-cell and lumbar spinal cord parenchymal T-cell inflammation was driven primarily by *HLA-DRB1*15*+ cases. Whilst this may relate to the propensity of *HLA-DRB1*15* restricted T-cells to undergo autologous proliferation within the CSF compartment before entering the parenchyma (Mohme *et al.*, 2013), experimental validation is required.

Our findings add further evidence to the notion that *HLA-DRB1*15* influences disease severity, as previously reported in clinical (Masterman *et al.*, 2000), radiographic (Okuda *et al.*, 2009), and pathologic series (DeLuca *et al.*, 2013). Cases bearing the *HLA-DRB1*15* allele have a younger age of onset (Masterman *et al.*, 2000), increased cognitive (Okuda, Srinivasan, *et al.*, 2009) and motor impairment (DeLuca *et al.*, 2007), greater MRI lesion burden in both the brain (Okuda *et al.*, 2009) and spinal cord (Sombekke *et al.*, 2009), and more severe inflammation and demyelination in the post-mortem spinal cord (DeLuca *et al.*, 2013). Future studies will now assess the mechanisms by which *HLA-DRB1*15* exerts its influence. One possible explanation is that *HLA-DRB1*15* influences CNS antigen presentation such that induction of immune tolerance to self fails. Alternatively, this allele may confer greater T-cell proliferation potential in response to *HLA-DRB1* ligation. This latter view is supported by studies that have shown an increased expression of *HLA-DRB1*15* in MS cases (Alcina *et al.*, 2012) and increased autologous proliferation of T-cells expressing this allele (Mohme *et al.*, 2013).

The current approach of studying the influence of genetic variation on robust, quantitative pathologic outcomes is powerful, as has been illustrated in other complex neurologic diseases (Pera *et al.*, 2013). The fact that we were able to detect significant differences between *HLA-DRB1*15* genotype groups in the extent of motor cortical inflammation, which is notably scarce, adds further credence to this claim. Our study also highlights the importance of studying younger cases with neurologic disease to dissect out the role of genetic factors

that may otherwise be diluted with pathologic changes that occur with disease evolution and ageing.

In summary, we provide clear evidence that *HLA-DRB1*15* significantly influences the severity of inflammation in the MS motor cortex, and the amount of demyelination in younger MS cases. These findings are the first to link the influence of genotype with pathology in the MS motor cortex and shed light onto the genetic substrate of the pathologic heterogeneity characteristic of this enigmatic disease.

3. Fibrinogen deposition associates with neurodegeneration in the multiple sclerosis motor cortex

3.1 Introduction

Cortical tissue injury is a key pathological feature of progressive multiple sclerosis (MS), and correlates with irreversible physical and cognitive decline (Calabrese *et al.*, 2012). A widely-held theory states that the progressive stage of MS is characterised by compartmentalisation of CNS inflammation behind a "closed" BBB (Lassmann *et al.*, 2012). According to this view, the inaccessibility of the CNS in progressive disease might explain why immunomodulatory compounds fail to produce clinical benefit. However, there is limited experimental evidence to support this explanation. A greater understanding of the pathogenesis of cortical injury in MS is fundamental for developing novel disease-modifying drugs that could slow or even halt disability accumulation in the progressive stage.

In chapter 2, we showed that *HLA-DRB1*15* status associates with the severity of motor cortical pathologic outcome. A disrupted BBB may help explain these findings, as greater leukocyte proliferation in the meninges could have a direct impact on parenchymal inflammation if the physiologic barrier to their migration into the brain was perturbed. In the current chapter, we therefore hypothesise that *HLA-DRB1*15* status has an impact on the integrity of the motor cortical BBB in MS.

Meningeal inflammation appears to be a central driver of cortical pathology in MS (Magliozzi *et al.*, 2010). However, the role of BBB disruption in this process has been relatively overlooked. Given the anatomic relationship between the subarachnoid compartment and penetrating perivascular spaces, BBB disruption and meningeal inflammation could both be intricately linked to the initiation and/or exacerbation of cortical pathology. To date, the evidence of cortical BBB disruption in MS has been limited. Endothelial tight junction abnormalities have been detected in cortical normal appearing grey matter (NAGM), a finding suggestive of BBB disruption (Leech *et al.*, 2007). However, attempts to detect surrogates of BBB disruption, such as extravasated plasma proteins, in post-mortem cortical MS tissue have so far failed (van Horssen *et al.*, 2007).

The serum protein fibrinogen is a good surrogate marker of BBB disruption due its abundance, large size (340 kDa), restriction to the intravascular compartment, and lack of expression in the healthy CNS. Fibrinogen is also part of a complex thrombolytic cascade that can stimulate inflammatory sequelae (Bardehle *et al.*, 2015; Davalos and Akassoglou, 2012). Thrombin mediates the polymerisation of fibrinogen to insoluble fibrin, and thus helps maintain vascular hemostasis. In turn, plasmin mediates the dissolution of fibrin, a process tightly regulated by plasminogen activator inhibitors (PAI), such as PAI-1.

Animal models of MS have implicated fibrinogen deposition and PAI-1 dysregulation in disease pathogenesis. In EAE, fibrinogen extravasation induces activation of microglia and subsequent axonal damage before the onset of clinical

signs, as well as promoting the recruitment of myelin specific T-cells (Davalos *et al.*, 2012; Ryu *et al.*, 2015). EAE can be ameliorated by inhibitors of the coagulation cascade: PAI-1 inhibitors cause a reduction in paralysis, demyelination, and axonal degeneration (Akassoglou *et al.*, 2004; Pelisch *et al.*, 2015).

Studies investigating fibrinogen and PAI-1 in animal models of MS are relevant to understanding MS in humans. The deposition of fibrin and/or fibrinogen is a feature of white and deep grey matter plaques, particularly those that are actively demyelinating (Gay and Esiri, 1991; Vercellino *et al.*, 2009). Proteomic assessment of such active plaques points to specific dysregulation of coagulation proteins (Han *et al.*, 2008). PAI-1 is up-regulated in acute white matter lesions but also in CSF and serum, where it has been linked to disease activity (Akenami *et al.*, 1997; Gveric *et al.*, 2003; Onodera *et al.*, 1999). The potential clinical relevance of elevated PAI-1 is highlighted by the recent observation that PAI-1 polymorphisms are linked to MS susceptibility (Zivković *et al.*, 2014). These observations provide a compelling rationale to revisit cortical fibrinogen deposition and PAI-1 expression and their relationships to neuronal damage in MS post-mortem tissue.

In the current study, we provide unequivocal evidence that fibrinogen deposition is common and extensive in MS cortex, and is significantly associated with neuronal loss. We reinforce these findings by showing that cortical PAI-1 is up-regulated in cases with abundant fibrinogen deposition. Altogether, these

findings suggest that fibrinogen deposition in the MS cortex may play an important role in cortical neurodegeneration, and therefore, contribute to irreversible disability progression.

3.2. Materials and Methods

3.2.1. Study population

Human archival material of MS (n=47) and control cases (n=10) from the UK MS tissue bank, Imperial College, London, and Oxford Brain Bank was used with appropriate ethical approval. Whilst the MS cohort used in this study is the same as that used in Chapter 2, a new control cohort was gained.

3.2.2. Tissue sampling

For each MS and control case, motor cortical tissue blocks from the mesial frontal cortex were sampled given the relevance of cortical pathology and lower limb motor system dysfunction to progressive MS. Motor cortical location was confirmed by the presence of Betz cells in cortical layer 5 identified by H&E staining. By matching the location of motor cortex between cases, intra-cortical pathologic heterogeneity was minimised. MS cases previously genotyped for *HLA-DRB1*15* status were used (as outlined in chapter 2).

3.2.3. Immunohistochemistry

Formalin-fixed paraffin-embedded tissue blocks were cut into 6μm thick adjacent sections and labelled with primary antibodies for myelin (PLP), fibrinogen (monoclonal and polyclonal), microglia/macrophages (Iba1), activated microglia/macrophages (CD68), neurons (NeuN) and PAI-1, using DAB

immunohistochemistry (Appendix 1). Sections were counterstained with haematoxylin. Fluorescent double-labelling for fibrinogen (monoclonal) and each of neurons (neurofilament), astrocytes (GFAP) and microglia/macrophages (Iba1) was also performed on a subset of cases to probe cellular localisation of fibrinogen using established protocols (Appendix 2). Experiments with omission of primary and secondary antibodies were used as negative controls. Full details of the antibodies used in this study can be found in Tables 3.1 and 3.2.

Table 3.1: Summary of antibodies used for DAB immunohistochemistry in chapter 3

Antibody	Clone	Classification	Pretreatment	Dilution	Supplier	Catalogue Number
PLP	plpc1	Monoclonal mouse	Microwave, citrate pH 6.0	1/1000	AbD Serotec	MCA8399
Fibrinogen (monoclonal)	aa31-130 of fibrinogen gamma	Monoclonal mouse	Autoclave, tris-EDTA pH 9.0	1/5000	Abcam	ab58207
Fibrinogen (polyclonal)		Polyclonal rabbit	Autoclave, tris-EDTA pH 9.0	1/50,000 O/N	Dako	A0080
Iba1		Polyclonal rabbit	Autoclave, tris-EDTA pH 9.0	1/1000	Wako	019-19741
CD68	PG-M1	Monoclonal mouse	Microwave, citrate pH 6.0	1/100	Dako	M0876
NeuN	A60	Monoclonal mouse	Autoclave, citrate pH 6.0	1/400	Millipore	MAB377
PAI-1		Rabbit Polyclonal	Autoclave, citrate pH 6.0	1/2000 O/N	Abcam	ab66705

Table 3.2: Summary of antibodies used for fluorescent immunohistochemistry in chapter 3

Antibody	Clone	Classification	Pretreatment	Dilution	Supplier	Catalogue Number
Fibrinogen (monoclonal)	aa31-130 of fibrinogen gamma	Monoclonal mouse	Autoclave, tris-EDTA pH 9.0	1/500 O/N	Abcam	ab58207
Neurofilament	N52	Monoclonal mouse	Autoclave, tris-EDTA pH 9.0	1/250 O/N	Sigma	N0142
GFAP		Polyclonal rabbit	Autoclave, tris-EDTA pH 9.0	1/8000 O/N	Dako	Z0334
Iba1		Polyclonal rabbit	Autoclave, tris-EDTA pH 9.0	1/3000 O/N	Wako	019-19741

3.2.4 Assessment of motor cortical demyelination

Foci of cortical demyelination were defined by complete loss of myelin in PLP-stained sections. A quantitative measure of cortical lesion burden area was related to total cortical length, as previously described in chapter 2.

3.2.5 Assessment of motor cortical fibrinogen deposition, microglial/macrophage inflammation, and neuronal density

Fibrinogen deposition (as assessed with the monoclonal antibody), microglial/macrophage inflammation, and neuronal density were quantified in MS cases and controls within consistently spaced trajectories perpendicular to the subpial surface of the cortex. Each trajectory consisted of 2 FOVs per cortical layer, with the exception of layer 3 which was sampled using 4 FOVs due to its relatively large size. Supragranular cortex was defined as cortical layers 1-3 and infragranular cortex was defined as cortical layers 4-6 (Figure 3.1).

Photomicrographs of each FOV were acquired using AxioVision software. Approximately 2,500 FOVs were assessed for each antigen under study across MS and control cohorts (>12,500 FOVs total), which were then analysed as outlined below. The distribution and extent of fibrinogen, as immunolabelled with the monoclonal antibody, was validated using an additional fibrinogen antibody that was polyclonal. Relationships between (monoclonal) fibrinogen and demyelination, microglial/macrophage inflammation, and neurons were explored.

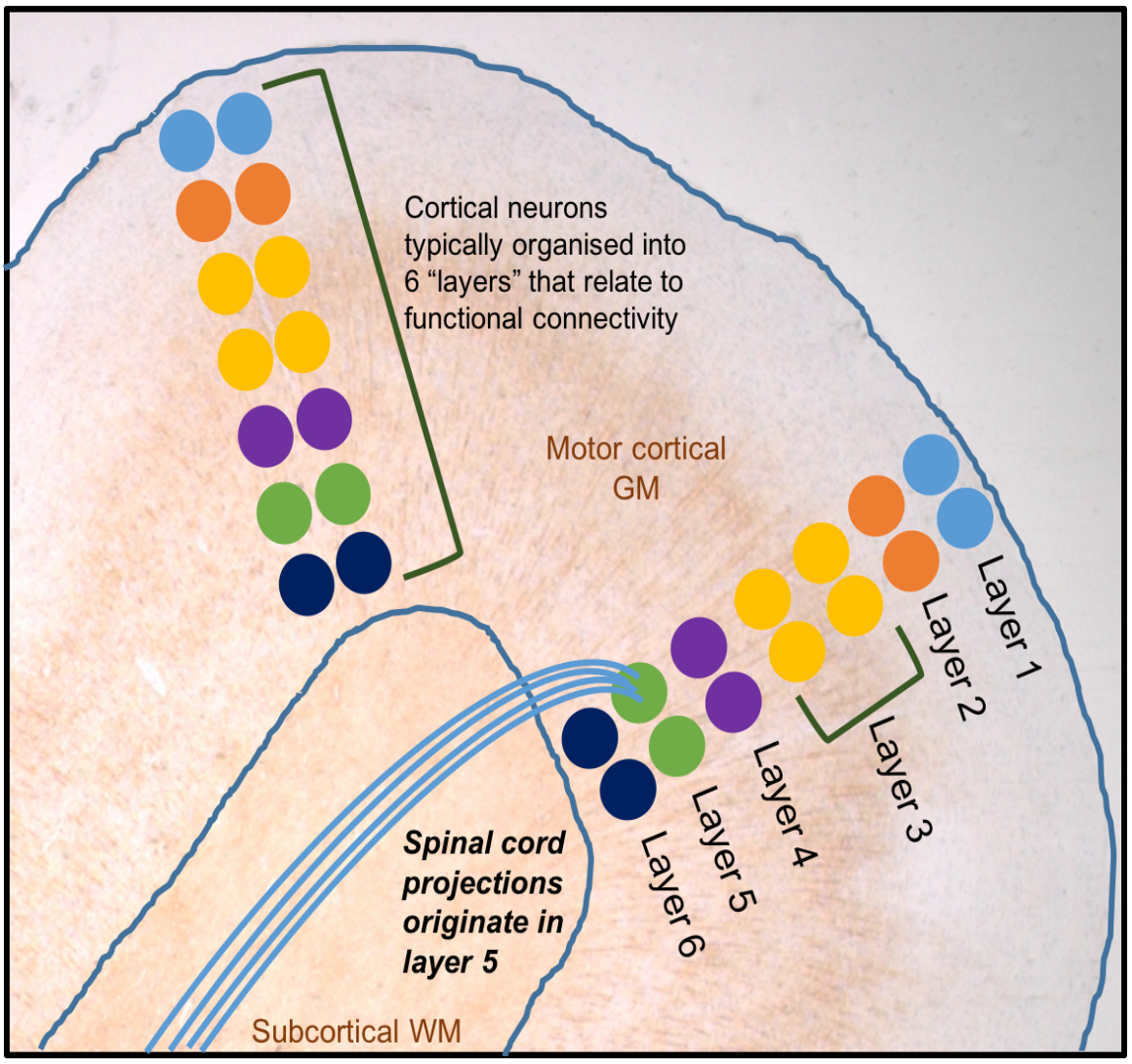


Figure 3.1: Assessment strategy of motor cortical pathology. Trajectories of analysis were spaced at systematic intervals perpendicular to the cortical surface. Two FOVs (coloured circles) in each cortical layer (four FOVs in layer 3 due to its relatively larger size) were photographed at 400x magnification. Approximately 2,500 images were acquired for each antibody under study. FOVs were analysed as outlined. Supragranular and infragranular cortex were defined as layers 1-3 and layers 4-6, respectively.

3.2.6. Quantitation of fibrinogen deposition

Total fibrinogen deposition was quantified in each FOV using a semi-automatic colour-based extraction method and is reported as chromogen positive pixels /mm^2, as previously published (Yates *et al.*, 2015). This method lacked the specificity needed to be able to quantify fibrinogen deposition in separate cortical compartments, i.e. extracellular spaces, cell bodies and neuritic/glial-processes. Therefore, a separate semi-quantitative score of the severity of fibrinogen deposition in each of the extracellular, cell body, and neuritic/glial process compartments in each FOV were used as follows: 0 (virtually absent), 1 (mild), 2 (moderate) or 3 (severe) (Figure 3.3).

3.2.7. Quantitation of microglial/macrophage inflammation

Microglial/macrophage inflammation (Iba1+, CD68+) was quantified in each FOV using semi-automatic colour-based extraction, and expressed as million pixels/mm^2.

3.2.8. Quantitation of neuronal density

Neuronal density was quantified in each FOV by manually counting the number of NeuN+ cells with a single nucleus and visible nucleolus (Figure 3.2). Across the cohort, we quantified approximately 70,000 neurons, expressed as neurons/mm^2.

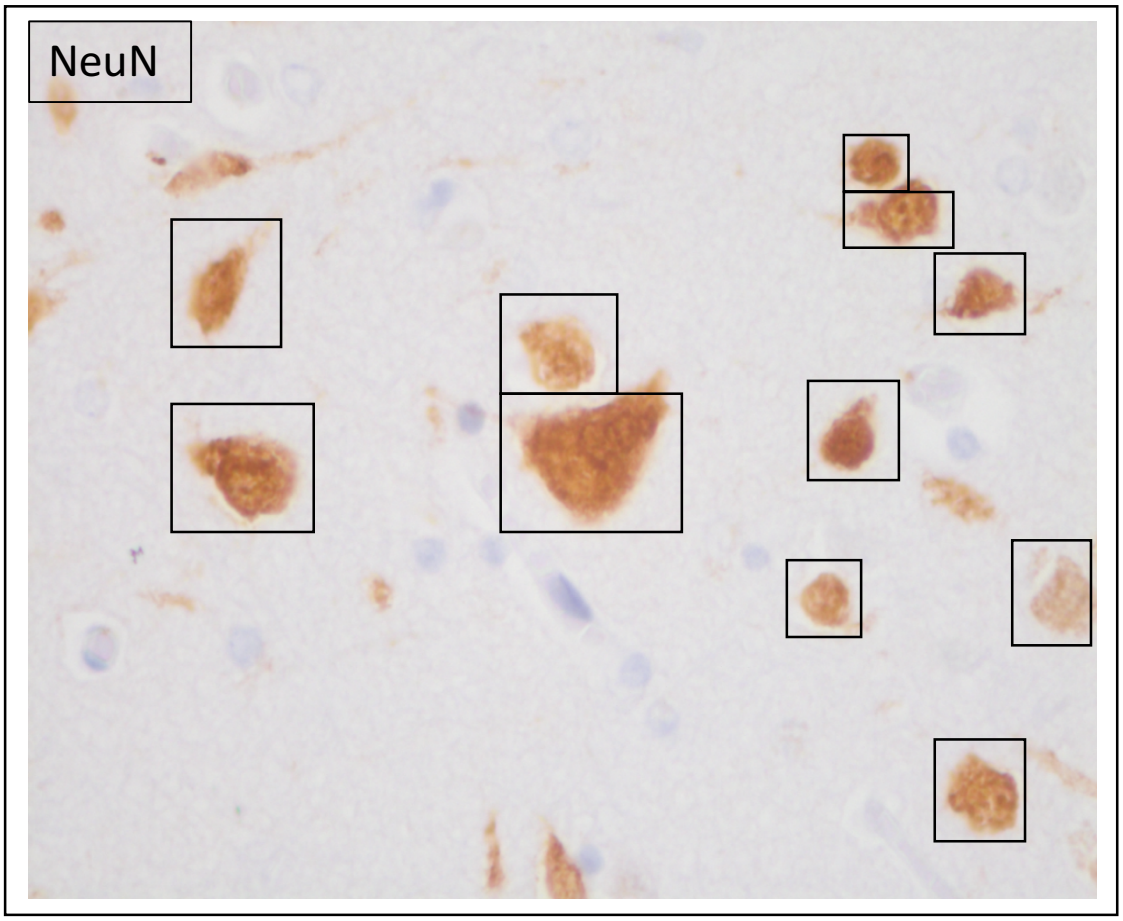


Figure 3.2: Quantitation of motor cortical neuronal density. Neuronal density was manually quantified by counting the number of NeuN+ cells with a single nucleus and visible nucleolus. The image above depicts an example FOV, with neurons delineated by black boxes. Approximately 70,000 neurons were quantified across MS and control cohorts, expressed as neurons/mm^2.

3.2.9. Assessment of motor cortical PAI-1

Motor cortical PAI-1 was assessed in all controls and a subset of MS cases lying at the extremes of extracellular fibrinogen (low: n=10; high: n=10) matched for age, sex, duration of disease, and PM interval. FOVs were examined in trajectories that were consistently spaced and perpendicular to the subpial surface, as described for previous analyses. FOVs were assessed by a semi-automatic colour based extraction method, with data presented as chromogen positive pixels/mm^2.

3.2.10. Statistical analyses

Quantitative differences in continuous pathologic variables between MS cases and controls was assessed using independent t-tests where data was normally distributed and Mann-Whitney U tests where data was not normally distributed. Kruskal-Wallis tests were used to compare data within MS and control cases where independent variables had more than one value (i.e. cortical layer 1-6) and data was not normally distributed. Dunn's tests were carried out post-hoc. For comparisons of normal data within MS cases, regression models were fitted with age, sex and post-mortem interval as covariates. The relationships between continuous pathologic variables were assessed using Spearman rank correlation coefficients. Comparisons of pathologic variables within MS cases, for example when comparing lesional with non-lesional parenchyma, were carried out using Wilcoxon signed ranks tests. Distribution of data was assessed analytically and graphically and transformed as required. Data are presented ± SEM. Two-sided tests were used to test hypotheses and P-values less than 0.05 were considered significant. Statistical analyses were done using SPSS v22 software.

3.3. Results

3.3.1. Demographic features of MS and control cohort

Clinical details of the cases used in this study are found in Table 3.3. For information regarding clinical details of *HLA-DRB1*15*+ and *HLA-DRB1*15*- MS cases, refer to Table 2.2

Table 3.3: Clinical details of cohort used in chapter 3

	MS cases (n=47)	**Controls (n=10)**
Age of death (yrs)	63 (range: 40-92)	74 (range: 57-91)
Duration of disease (yrs)	31 (range:11-58)	n/a
Sex	M=13, F=34	M=7, F=3
Clinical Course	PPMS:4, SPMS:38, RRMS:1, Unknown:4	n/a
Brain weight (g)	1157 (range: 894-1380)	1320 (range: 1072-1628)
PM interval (hrs)	18 (range: 7-38)	36.7 (range: 10-72)

3.3.2. Fibrinogen deposition: MS vs. controls

3.3.2.1. Distribution and extent of fibrinogen deposition

Total fibrinogen deposition was observed to a greater extent in MS motor cortex when compared to control cases (MS: 19.05 ± 3 million pixels/mm^2 vs. control: 1.64 ± 0.41 million pixels/mm^2, p=0.003). The extent of total fibrinogen deposition between cortical layers was significantly different within MS cases (p=0.001) but not controls (p=0.701) (Figure 3.4). In MS, total fibrinogen was greater in deep infragranular cortical layers compared to more superficial ones (layers 5 and 6 vs. layer 2, Dunn's non-parametric comparison: p<0.05).

Fibrinogen deposition was frequently observed to respect the boundary between white and grey matter. Indeed, extensive infragranular cortical deposition was often contrasted sharply with negative white matter immediately adjacent. Fibrinogen was deposited diffusively in extracellular spaces as well as cell bodies and neurites/glial-processes. The extent and distribution of fibrinogen deposition in these specific motor cortical compartments is outlined below.

3.3.2.2. Extracellular fibrinogen

The extent of extracellular deposition in MS was significantly greater than in controls (MS: 1.07 ± 0.12 vs. control: 0.24 ± 0.07, p=0.001). The extent of extracellular fibrinogen deposition differed significantly between cortical layers in MS cases (p<0.001) but not controls (p=0.189) (Figure 3.3A). In MS, it was again deeper infragranular cortical layers that demonstrated more extracellular fibrinogen deposition (layers 5 and 6 vs. layer 2, Dunn's non-parametric comparison: p<0.01).

3.3.2.3. Cell Body Fibrinogen

The extent of cell body deposition was significantly greater in MS cases than in controls (MS: 0.69 ± 0.08 vs. control: 0.19 ± 0.06, p=0.003). Unlike extracellular fibrinogen, the extent of fibrinogen within cell bodies did not differ between cortical layers within MS cases (p=0.157) or controls (p=0.517) (Figure 3.3B).

Double-labelling immunofluorescence experiments showed that astrocytic cell bodies often contained dense fibrinogen deposits in the subpial zone (Figure 3.5). In other cortical layers, fibrinogen co-localised with both neurons and astrocytes but not microglia/macrophages (Figure 3.5). In control cases, cell body fibrinogen deposition was scant but when present co-localised to occasional neurons and glia.

3.3.2.4. Neuritic/glial-process fibrinogen

The extent of neuritic/glial-process fibrinogen was significantly greater in MS cases than controls (MS: 0.51 ± 0.07 vs. control: 0.11 ± 0.07, p=0.004). The extent of neuritic/glial-process fibrinogen deposition was significantly different between cortical layers within MS cases (p<0.001) but not controls (p=0.733) (Figure 3.3C). In MS, fibrinogen in neuritic/glial processes was greater in superficial cortical layers compared to deeper ones (i.e. layers 1 and 2 vs. layers 4-6; Dunn's non-parametric comparison: p<0.05).

Double-labelling immunofluorescence experiments clearly demonstrated co-localisation of neuritic/glial-process fibrinogen with astrocytes in the subpial zone. However, much neuritic/glial-process fibrinogen was present outside of

astrocytes suggesting co-localisation within the neuritic compartment (Figure 3.5).

Total, extracellular, cell body, and neuritic/glial-process fibrinogen deposition in each motor cortical layer (1-6) in MS compared to control is summarised in Table 3.4.

Table 3.4: Summary of fibrinogen deposition in MS and control motor cortex

Cortical Layer	Total Fibrinogen (millions of pixels/mm²)			Extracellular Fibrinogen (SQ score)			Cell Body Fibrinogen (SQ score)			Neuritic/Glial-process Fibrinogen (SQ score)		
	MS	Control	p-value	MS	Control	p-value	MS	Control	p-value	MS	Control	p-value
1	11.88 ± 2.4	1.77 ± 0.85	**0.008**	0.79 ± 0.1	0.43 ± 0.16	0.095	0.65 ± 0.08	0.24 ± 0.11	**0.019**	1.0 ± 0.12	0.23 ± 0.15	**0.001**
2	6.46 ± 1.51	0.88 ± 0.18	**0.016**	0.69 ± 0.1	0.07 ± 0.03	**0.005**	0.64 ± 0.08	0.04 ± 0.03	**<0.001**	0.75 ± 0.09	0.13 ± 0.08	**0.002**
3	11.68 ± 2.8	1.42 ± 0.33	**0.022**	1.02 ± 0.12	0.12 ± 0.05	**0.001**	0.54 ± 0.08	0.12 ± 0.07	**0.003**	0.3 ± 0.06	0.06 ± 0.05	**0.015**
4	24.16 ± 4.4	1.95 ± 0.51	**0.013**	1.23 ± 0.14	0.28 ± 0.008	**0.005**	0.66 ± 0.069	0.23 ± 0.11	**0.028**	0.27 ± 0.06	0.09 ± 0.08	0.156
5	28.84 ± 4.82	1.92 ± 0.59	**0.006**	1.35 ± 0.14	0.26 ± 0.008	**0.002**	0.69 ± 0.09	0.21 ± 0.1	**0.02**	0.34 ± 0.07	0.09 ± 0.08	0.076
6	31.3 ± 4.84	1.9 ± 0.66	**0.006**	1.33 ± 0.14	0.27 ± 0.13	**0.002**	0.94 ± 0.1	0.26 ± 0.11	**0.007**	0.39 ± 0.08	0.08 ± 0.08	**0.026**

Table 3.4: Fibrinogen deposition was diffusively present throughout the motor cortex of MS cases and to a greater extent than in controls. Bold text highlights differences between MS and control that are statistically significant (p-values less than 0.05). SQ = semi-quantitative.

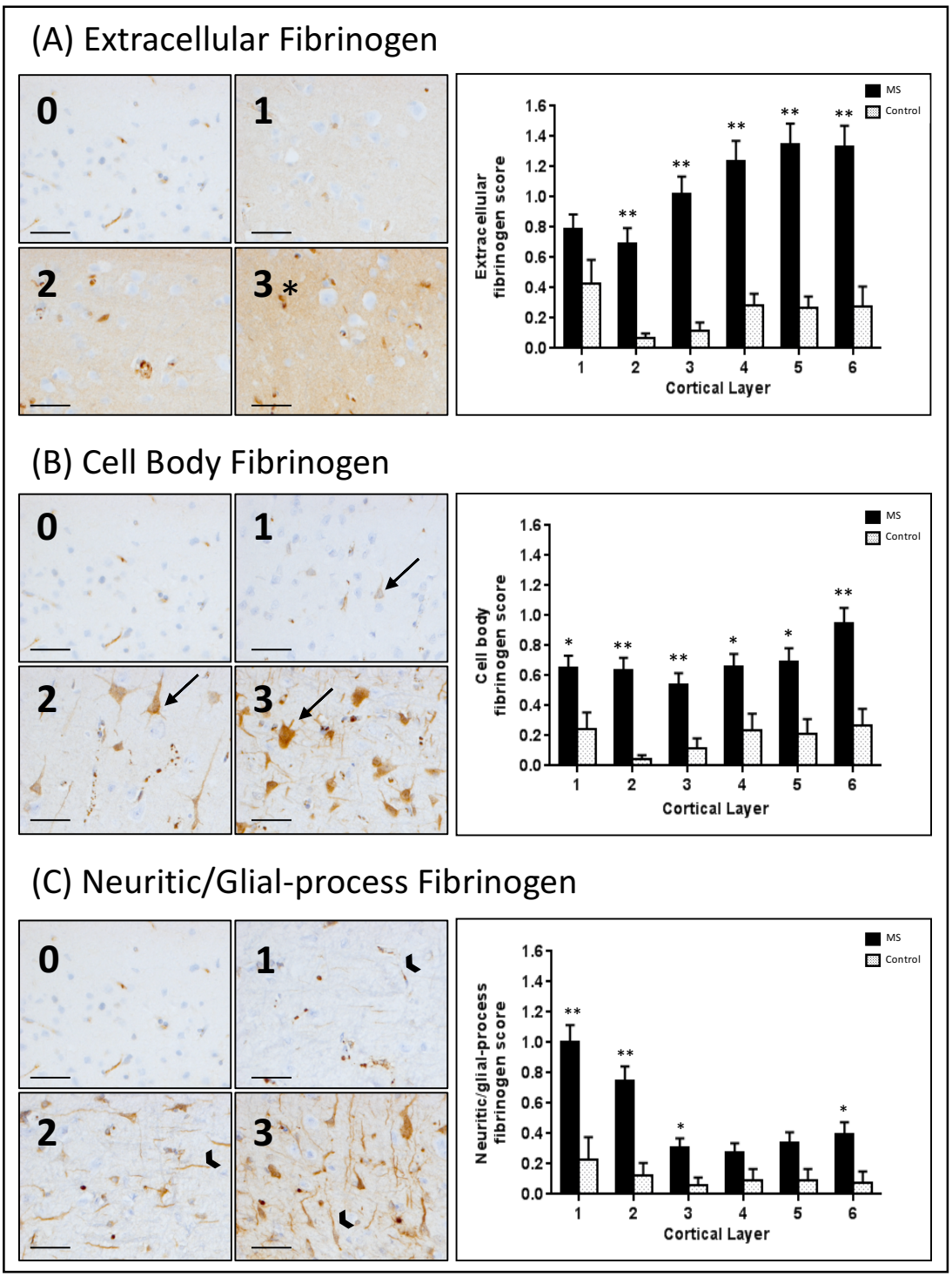


Figure 3.3: Semi-quantitative scoring of fibrinogen deposition. Automated quantification of total fibrinogen lacked the specificity to enable quantitation of deposition in separate cortical compartments. To circumvent this issue, we devised a semi-quantitative score for the severity of fibrinogen in each compartment, i.e. extracellular, cell body (black arrows) and neurites/glial-processes (arrow heads). Star denotes vascular fibrinogen. For each FOV analysed, fibrinogen deposited in each compartment (extracellular, cell bodies, neurites/glial-processes) was scored on a scale of 0 (no deposition), 1 (mild deposition), 2 (moderate deposition) and 3 (severe deposition). Extracellular fibrinogen was greater in MS throughout the cortical lamina but was concentrated in infragranular cortex (A). Cell body fibrinogen was also greater in MS but showed a consistent distribution throughout the cortical lamina (B). Neuritic/glial-process fibrinogen was greater in MS in cortical layers 1, 2 and 3, as well as layer 6 (C). * = $p<0.05$, ** = $p<0.01$

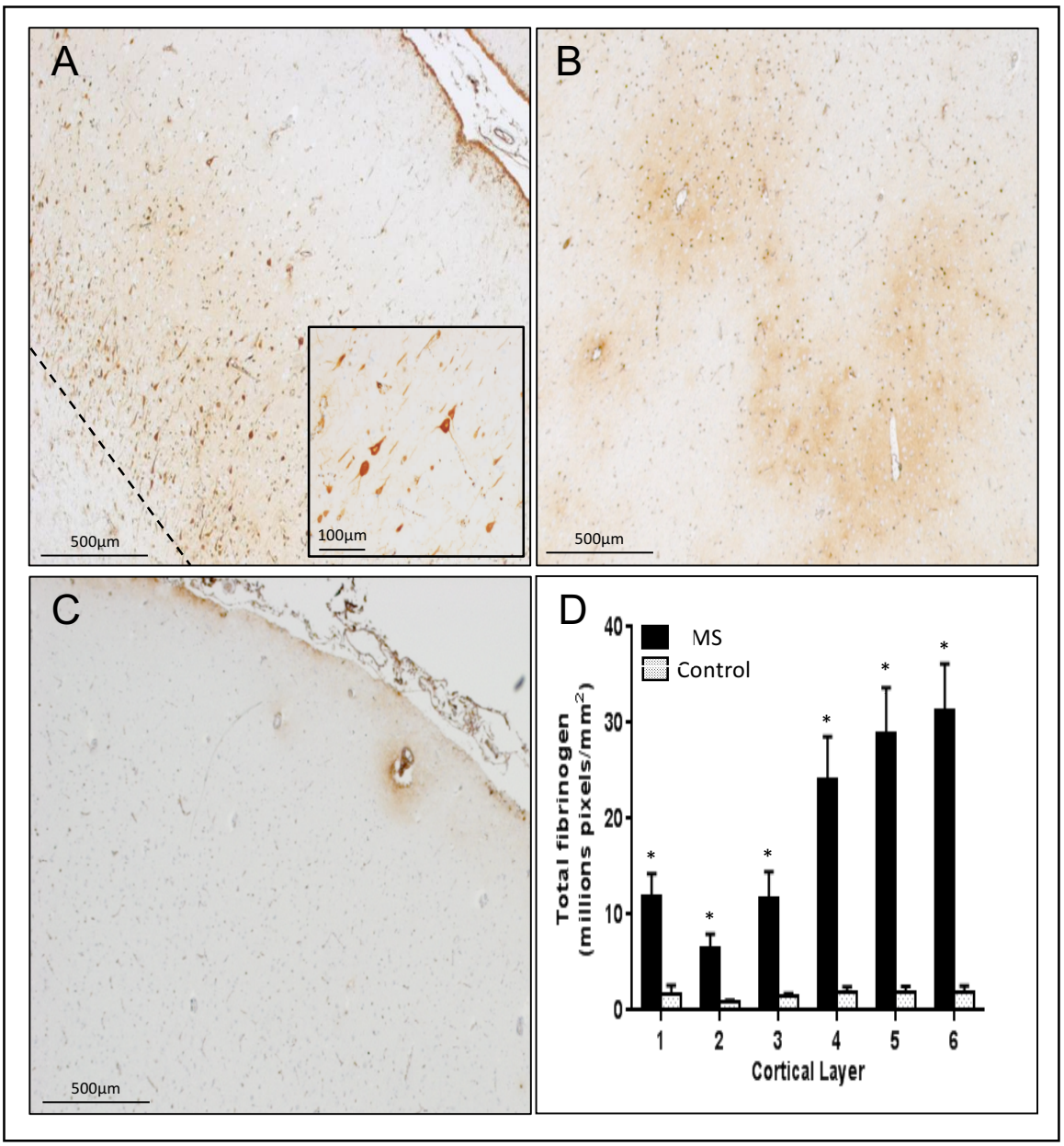


Figure 3.4: Fibrinogen deposition in the MS motor cortex. Fibrinogen was deposited diffusely in the MS motor cortex in both extracellular and intracellular spaces (A), and was commonly found to be vessel-associated (B). Parenchymal fibrinogen in control cases was typically confined to the perivasculature and subpial cortex (D). Quantitation of total fibrinogen in MS cases and controls, using a semi-automatic colour-based extraction algorithm, demonstrated more severe deposition in MS throughout the cortical lamina (D).
* = $p<0.05$, ** = $p<0.01$

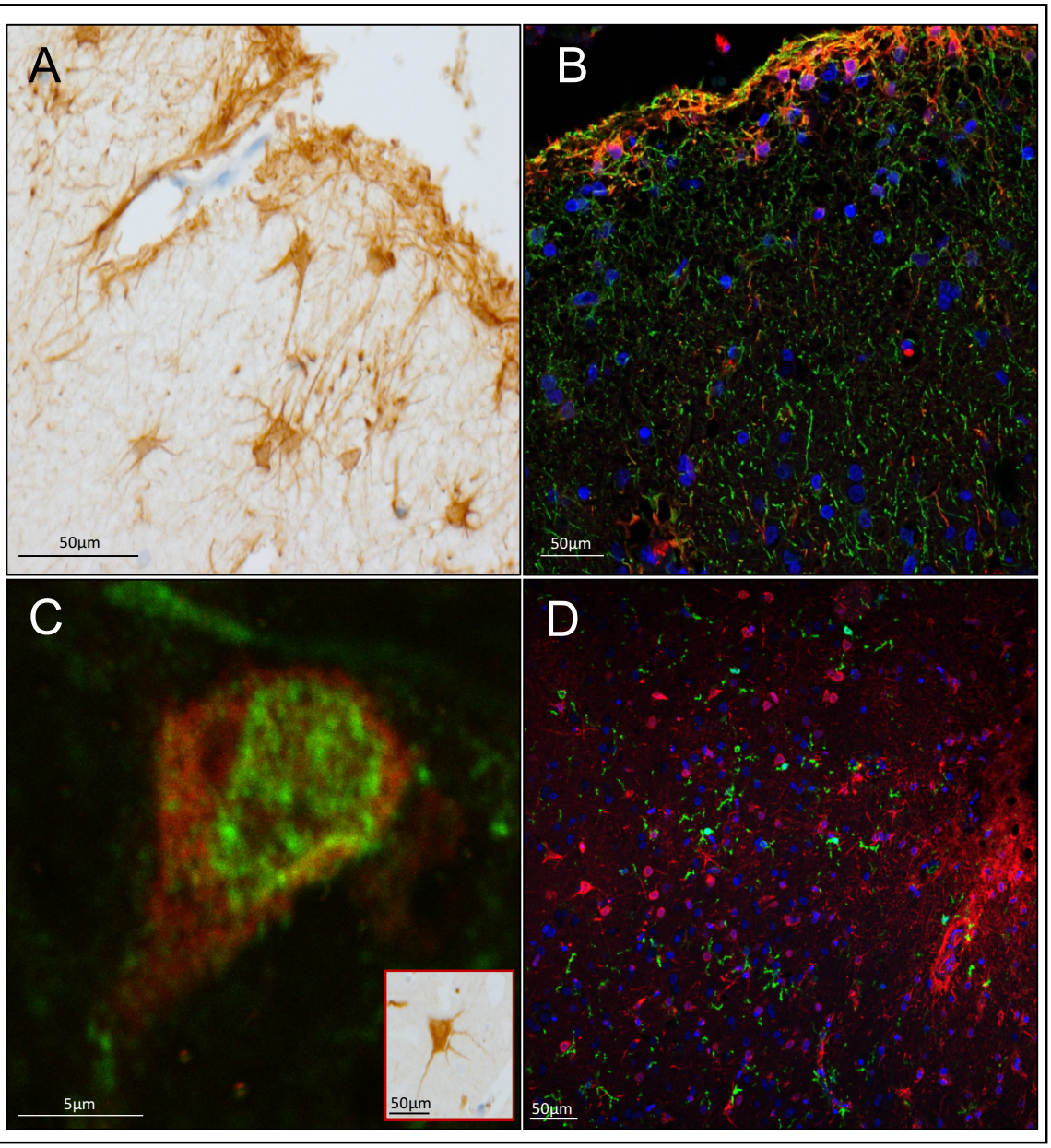


Figure 3.5: Fluorescent double-labelling of fibrinogen to demonstrate cellular localisation. Fibrinogen was found to affect different cell types using DAB immunohistochemistry (A). Cell body and neuritic/glial-process fibrinogen (red) appeared to associate with astrocytes (green) in the subpial glia limitans (B). Fibrinogen (red) also associated with neurofilament (green), a marker of neurons (C). In contrast, an assessment of fibrinogen (red) and Iba1+ microglia/macrophages (green) did not provide evidence of co-localisation (D).

3.3.2.5. Validation of (monoclonal) fibrinogen findings with additional (polyclonal) fibrinogen antibody

To verify the specificity of the (monoclonal) fibrinogen findings, we replicated our semi-quantitative scores with a second, polyclonal, antibody targeting fibrinogen. There was a significant correlation of fibrinogen scores between antibodies in the extracellular ($r=0.515$, $p<0.001$), cell body ($r=0.809$, $p<0.001$) and neuritic/glial-process ($r=0.76$, $p<0.001$) compartments in MS cases and controls. Fibrinogen was detected diffusively deposited throughout the motor cortex with a polyclonal antibody (Figure 3.6), with the localisation similar to our monoclonal antibody (Figure 3.7). The extent of fibrinogen, as assessed by this second polyclonal fibrinogen antibody, was also consistent with the results of our monoclonal antibody (Figure 3.8).

The polyclonal fibrinogen antibody demonstrated a greater level of background staining relative to the monoclonal fibrinogen antibody. As such, further analyses between fibrinogen and other metrics of cortical pathology were restricted to the more specific monoclonal fibrinogen antibody.

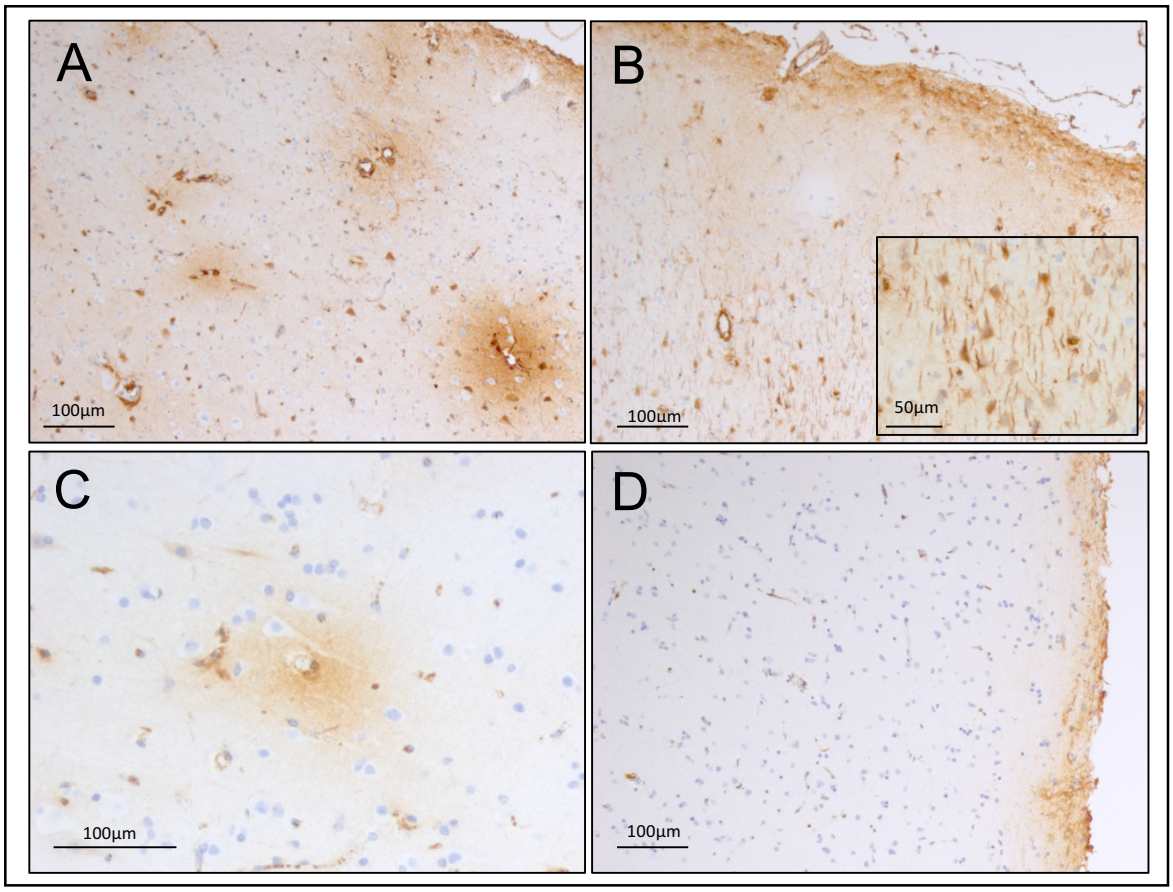


Figure 3.6: Fibrinogen deposition detected with polyclonal antibody. Fibrinogen was detected diffusively throughout the cortex with a polyclonal antibody. Extracellular, including perivascular, deposition was observed (A), as well as cell body and neuritic/glial-process fibrinogen (B). Control cases demonstrated small amounts of perivascular (C) and subpial deposition (D).

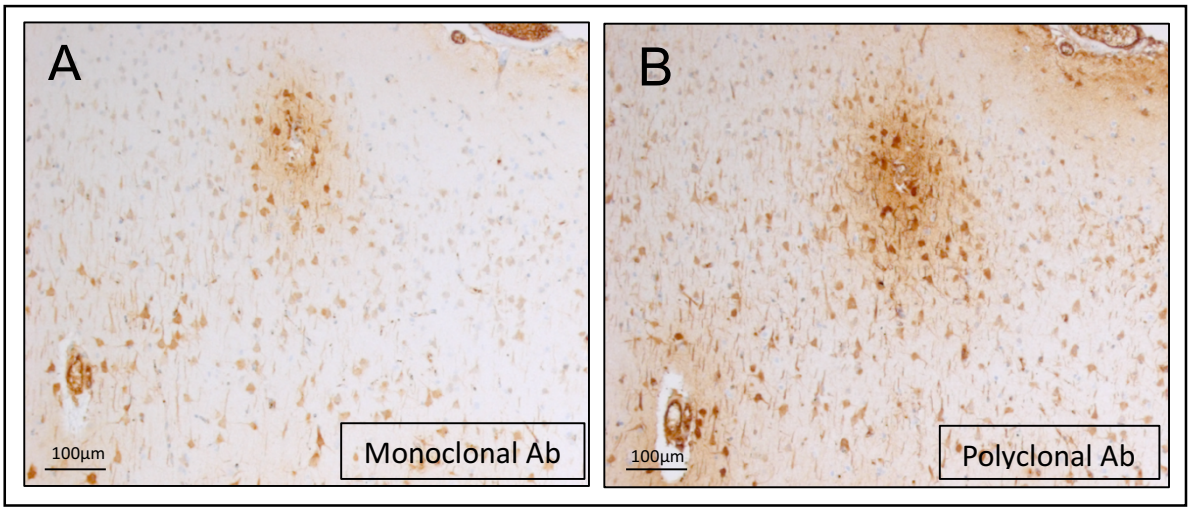


Figure 3.7: Direct Comparison of fibrinogen deposition detected with monoclonal and polyclonal antibodies. Monoclonal (A) and polyclonal (B) fibrinogen antibodies demonstrated consistent immunolabelling in adjacent sections of motor cortex

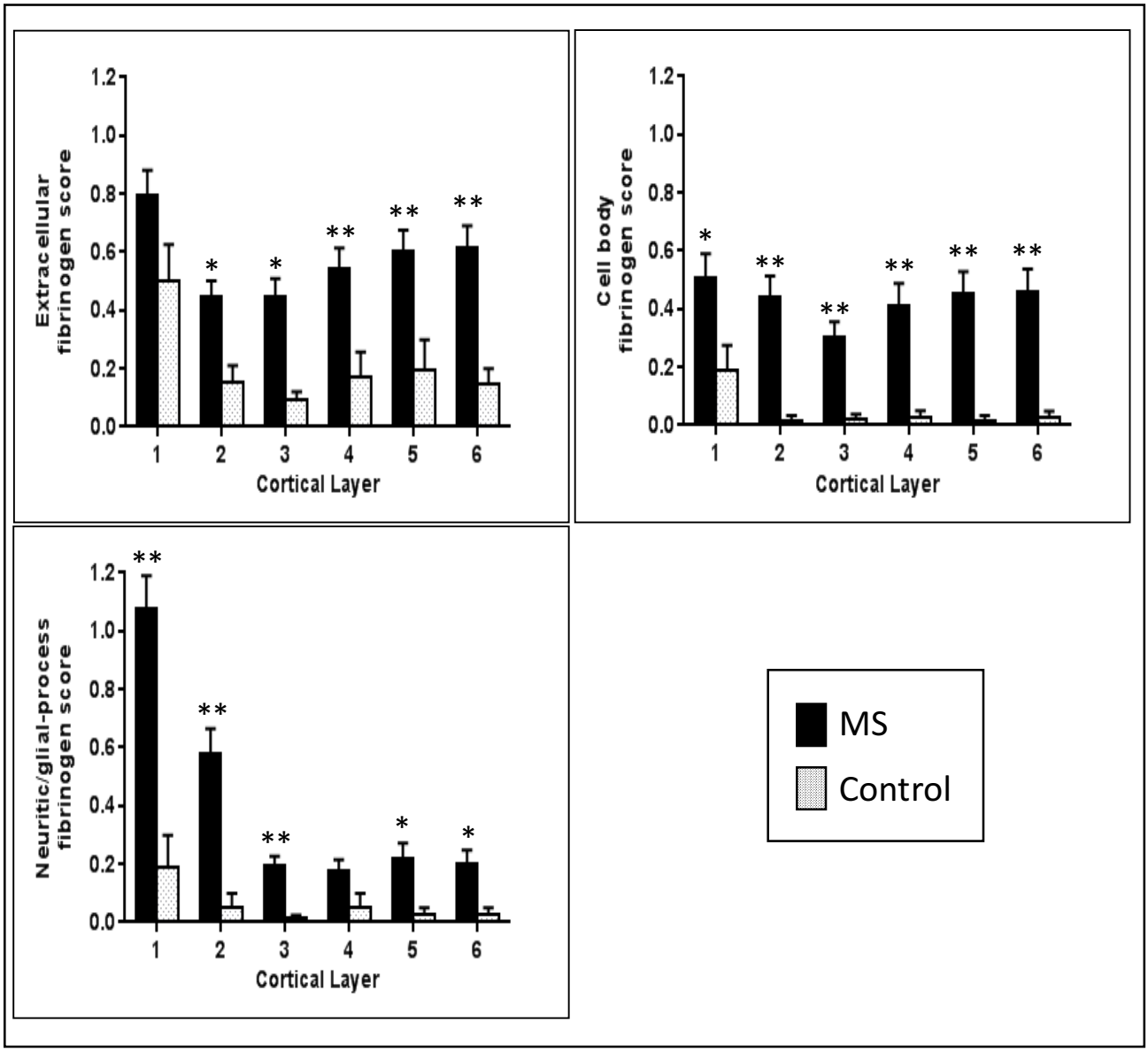


Figure 3.8: Quantitation of fibrinogen deposition using polyclonal fibrinogen antibody. Fibrinogen deposition, as assessed using a polyclonal antibody, was detected in significantly greater quantities in MS cases compared to controls. The distribution of deposition was consistent with our monoclonal antibody in the extracellular space (A), cell bodies (B) and neurites/glial-processes (C). * = $p<0.05$, ** = $p<0.01$

3.3.3. Influence of *HLA-DRB1*15* on motor cortical fibrinogen deposition

*HLA-DRB1*15* status did not appear to have an influence on total motor cortical fibrinogen deposition (15+: 21.1 ± 4 million pixels/mm^2 vs. 15-: 17.4 ± 4 million pixels/mm^2, p=0.544). This finding was consistent for extracellular fibrinogen (15+: 1.2 ± 0.17 vs 15-: 1.0 ± 0.14, p=0.475), cell body fibrinogen (15+: 0.75 ± 0.12 vs. 15-: 0.64 ± 0.09, p=0.576) and neuritic/glial-process fibrinogen (15+: 0.55 ± 0.1 vs. 15-: 0.48 ± 0.09, p=0.773) (Figure 3.9).

Given our findings of more severe inflammatory pathology in younger *HLA-DRB1*15*+ cases (outlined in chapter 2), we also compared the extent of fibrinogen in MS cases below the median age (age < 62 years). In this younger population, *HLA-DRB1*15* allele status did not appear to impact on the extent of total fibrinogen deposition (15+: 26.2 ± 6.3 million pixels/mm^2 vs. 15-: 16 ± 6.7 million pixels/mm^2, p=0.255). This finding was consistent for extracellular fibrinogen (15+: 1.4 ± 0.24 vs 15-: 0.88 ± 0.18, p=0.108), cell body fibrinogen (15+: 0.79 ± 0.16 vs. 15-: 0.58 ± 0.1, p=0.297) and neuritic/glial-process fibrinogen (15+: 0.62 ± 0.18 vs. 15-: 0.42 ± 0.08, p=0.266) (Figure 3.9).

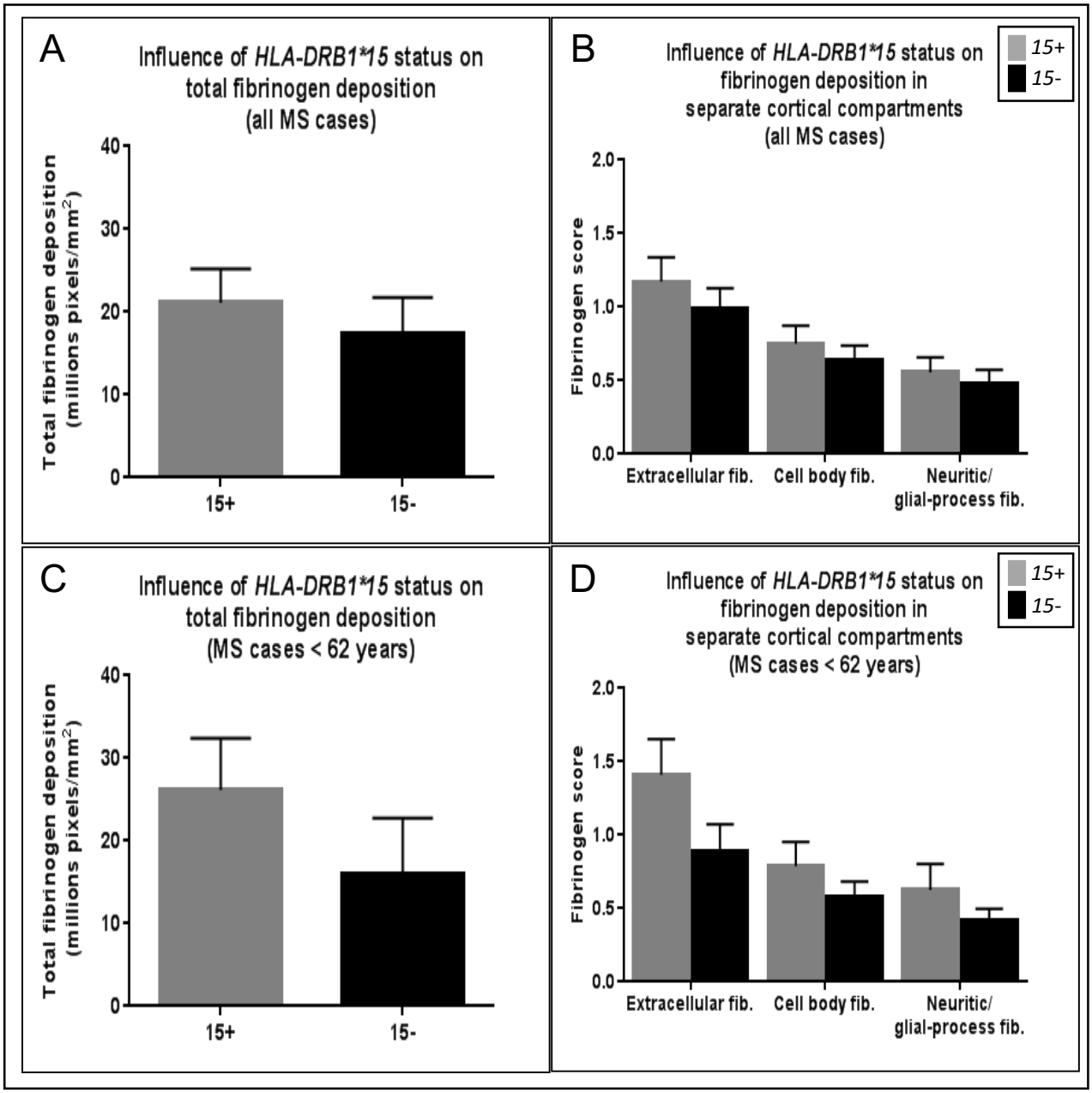


*Figure 3.9: Association of HLA-DRB1*15 status with fibrinogen deposition.* Association of *HLA-DRB1*15* status with total fibrinogen deposition in all MS cases (A), and younger MS cases (C), and association of *HLA-DRB1*15* status with extracellular, cell body and neuritic/glial-process fibrinogen in all MS cases (B), and younger MS cases (D).

3.3.4. Relationships between MS motor cortical pathology and fibrinogen deposition

Quantitative measures of demyelination, microglial/macrophage inflammation, and neuronal density were obtained in MS and controls. The results of these analyses, and relationships therein with fibrinogen deposition, are outlined below.

3.3.4.1. Demyelination and fibrinogen deposition

No relationship was observed between overall cortical lesional burden and total fibrinogen deposition (r=0.140, p=0.349). Further, no relationships were observed between cortical lesional burden and either extracellular (r=0.142, p=0.342), cell body (r=-0.001, p=0.993), or neuritic/glial-process fibrinogen deposition (r=-0.005, p=0.973) irrespective of cortical layer.

3.3.4.2. Microglial/macrophage inflammation and fibrinogen deposition

No difference in the extent of Iba1+ microglia/macrophage inflammation was detected between MS cases and the current control cohort (MS: 7.03 ± 0.68 million pixels/mm^2 vs. control: 6.16 ± 0.7 million pixels/mm^2, p=0.474), irrespective of cortical layer (Figure 3.10).

Similarly, no difference in the extent of CD68+ microglia/macrophage inflammation was detected between MS cases and the current control cohort (MS: 2.17 ± 0.45 million pixels/mm^2 vs. control: 1.35 ± 0.32 million pixels/mm^2, p=0.221), irrespective of cortical layer (Figure 3.11).

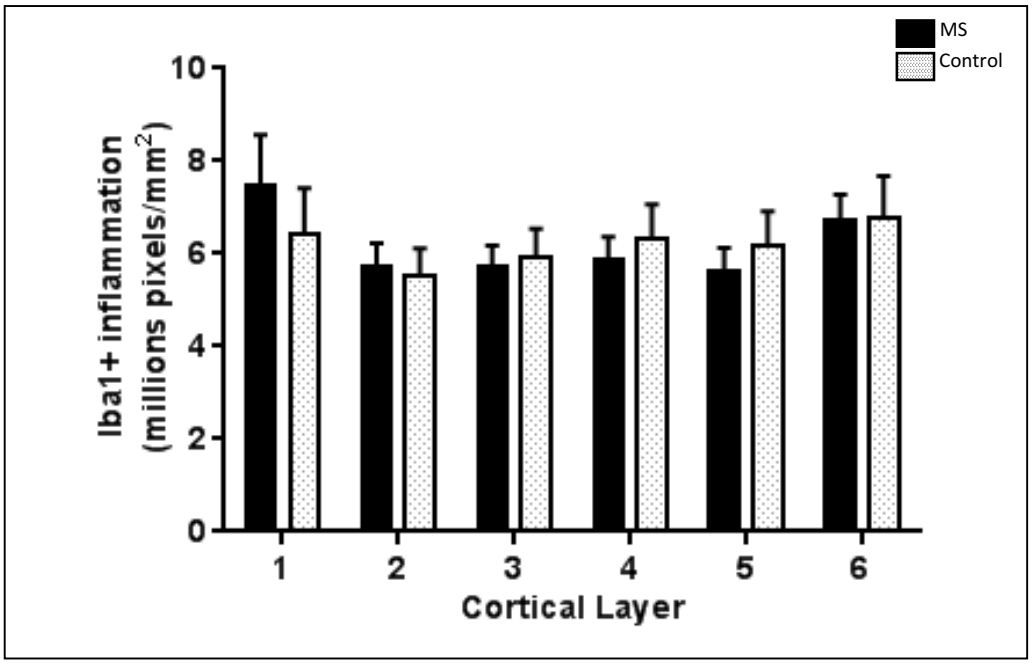


Figure 3.10: Iba1+ inflammation in MS and controls. No difference in the extent of Iba1+ inflammation was observed in any cortical layer between MS and control cases.

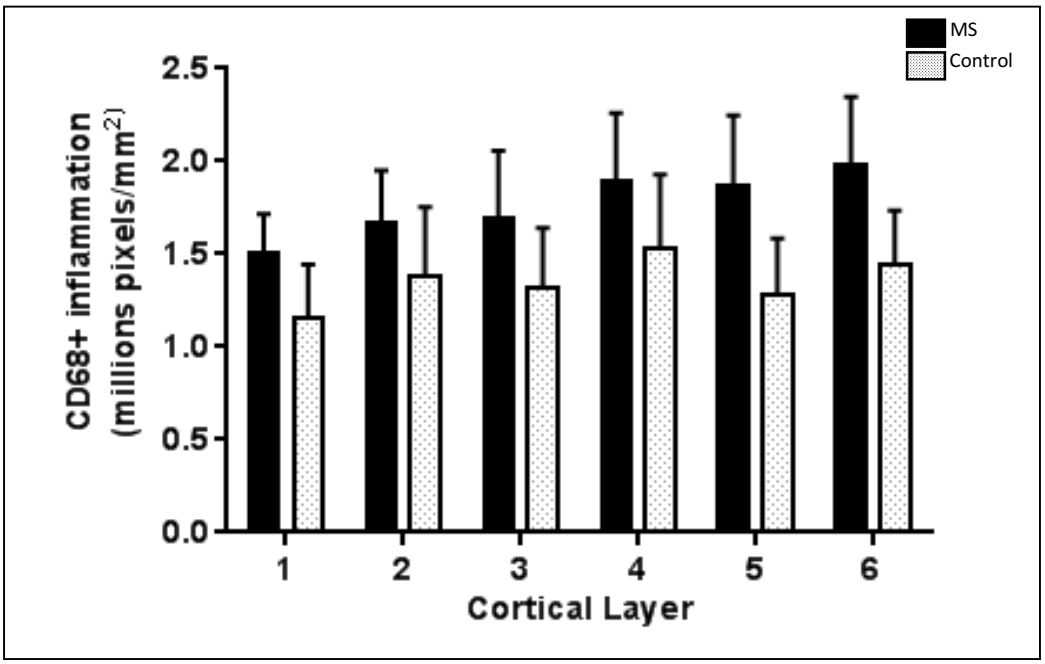


Figure 3.11: CD68+ inflammation in MS and controls. No difference in the extent of CD68+ inflammation was observed in any cortical layer between MS and control cases.

Within MS cases, no differences in microglia/macrophage inflammation was detected between lesions and NAGM (Wilcoxon: Iba1: z=1.538, p=0.124; CD68: z=1.823, p=0.068) (Figure 3.12).

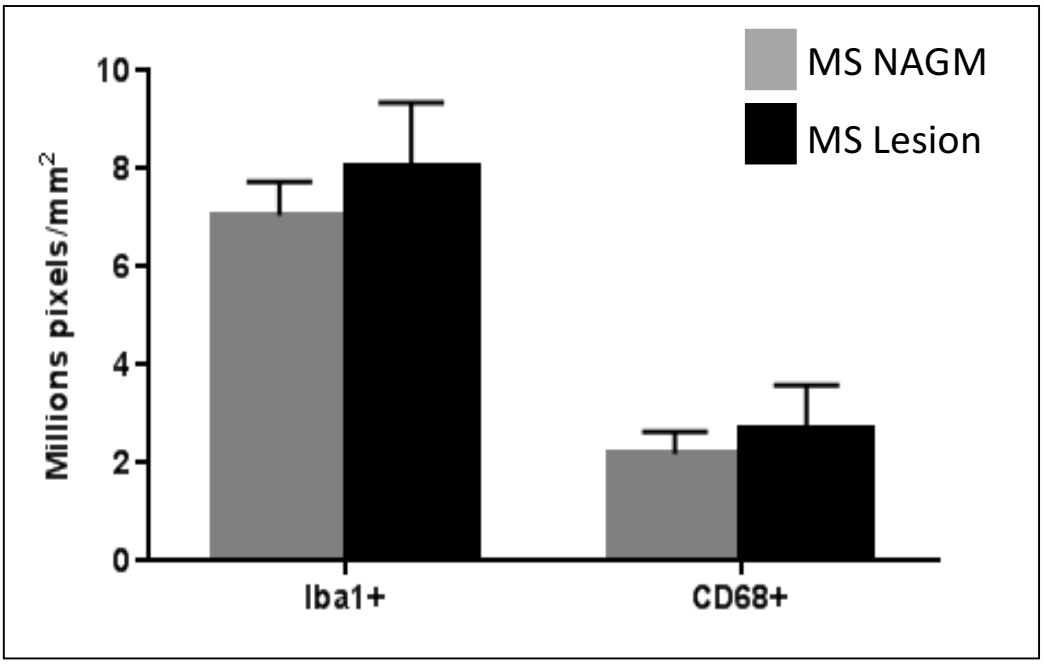


Figure 3.12: Microglial/macrophage inflammation in MS NAGM and lesions. No differences were detected in the extent of either Iba1+ or CD68+ inflammation in lesions compared to MS NAGM.

No relationship was observed between Iba1+ inflammation and total fibrinogen deposition (r=-0.145, p=0.337) nor CD68+ inflammation and total fibrinogen deposition (r=0.018, p=0.902). In addition, no relationships were observed between microglial/macrophage inflammation and either extracellular (Iba1+: r=-0.062, p=0.681; CD68+: r=0.104, p=0.485), cell body (Iba1+: r=-0.220, p=0.142; CD68+: r=-0.039, p=0.794) or neuritic/glial process-associated fibrinogen deposition (Iba1+: r=-0.258, p=0.084; CD68+: r=-0.097, p=0.516), irrespective of cortical layer or demyelination. Similar to MS cases, no

relationships between microglial/macrophage inflammation and fibrinogen deposition were observed in controls.

3.3.4.3. Neuronal density and fibrinogen deposition

No differences were detected in neuronal density between MS cases and controls (MS: 414 ± 17 neurons/mm^2 vs control: 431 ± 27 neurons/mm^2, p=0.909), irrespective of cortical layer (Figure 3.13). Within MS cases, no differences in neuronal density were observed within lesions compared to NAGM (Wilcoxon: z=1.282, p=0.200) (Figure 3.14).

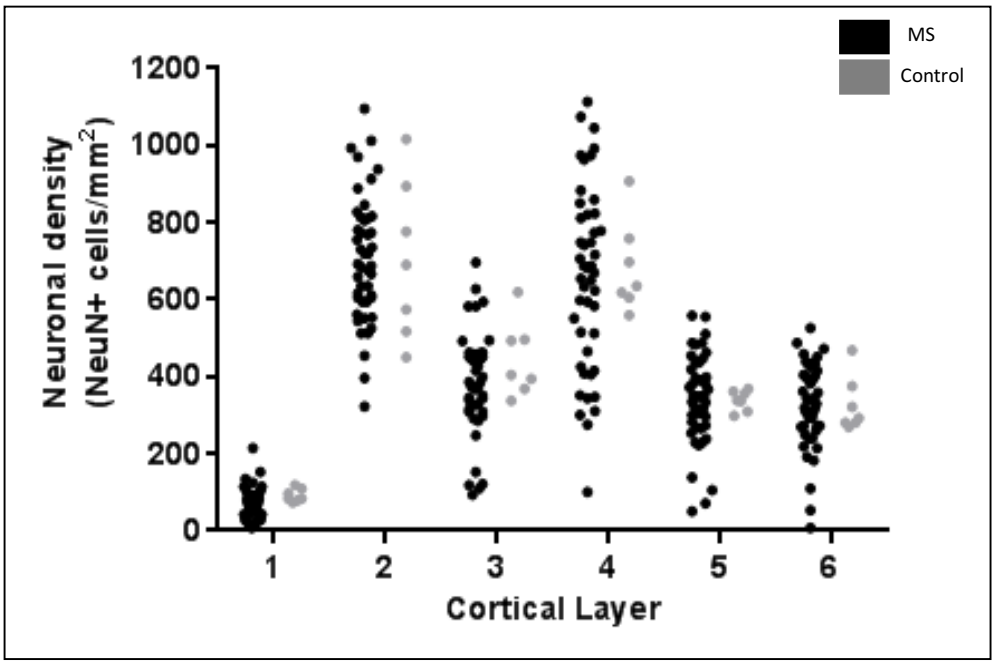


Figure 3.13: Neuronal density in MS and controls. No difference in neuronal density was observed in any cortical layer between MS and control cases.

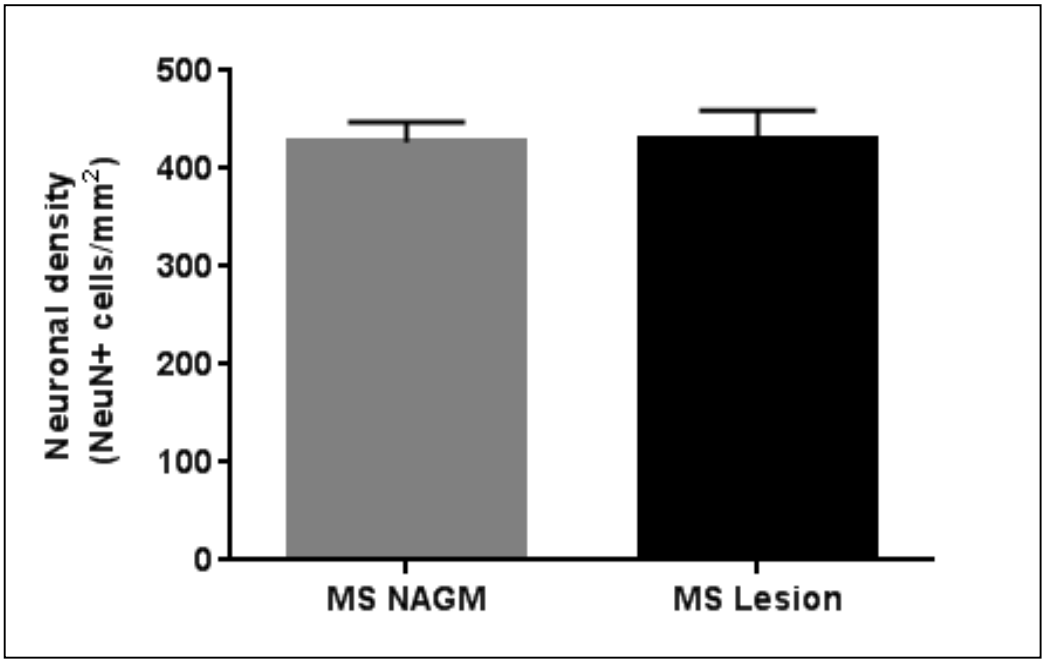


Figure 3.14: Neuronal density in MS NAGM and lesions. No difference in neuronal density was observed between MS NAGM and lesional parenchyma. * = p<0.05, ** = p<0.01

Whilst neuronal density was not statistically different between MS and controls, striking differences emerged within MS cases when considering the extent of fibrinogen. Neuronal density inversely correlated with total fibrinogen deposition (r=-0.401, p=0.006). This relationship was restricted to extracellular fibrinogen deposition (extracellular: r=-0.355, p=0.015; cell body: r=-0.284, 0.056; neuritic/glial process: r=-0.234, p=0.118). No relationship between fibrinogen deposition and neuronal density was observed in control cases (total: r=-0.250, p=0.589, extracellular: r=-0.679, p=0.094; cell body: r=-0.222, p=0.632; neuritic/glial-process: r=0.148, p=0.751).

To assess the impact of extracellular fibrinogen deposition on neuronal *loss* in the motor cortex, MS cases were divided into "high" and "low" fibrinogen groups based on the median value for extracellular fibrinogen in the relevant anatomic area under study. MS cases with an extracellular fibrinogen score equal to the median were excluded from the analysis to ensure an equal number of cases in each group.

MS cases with a high burden of extracellular fibrinogen (EC fib.) showed significantly greater neuronal loss when compared with MS cases with low fibrinogen, corrected for age, sex and PM interval (high EC fib: 13.8 % ± 4.3% neuronal loss vs. low EC fib: -5.2 ± 6.3% neuronal loss, p=0.017). These findings were limited to the infragranular cortex where fibrinogen deposition was more severe (high infragranular EC fib: 13.8 ± 5.26% infragranular neuronal loss vs. low infragranular EC fib: -8.49 ± 7.45% infragranular neuronal loss, p=0.039). Given the importance of layer 5 neurons for motor function, it is intriguing that neuronal loss in layer 5 was strikingly more severe in the high fibrinogen group (high layer 5 EC fib: 14.88 ± 5.4% layer 5 neuronal loss vs. low layer 5 EC fib: -19.56 ± 6.85% layer 5 neuronal loss, p=0.001).

Consistent with these findings, layer 5 neuronal density was also significantly reduced in the high fibrinogen group (high layer 5 EC fib: 288 ± 18 layer 5 neurons/mm^2 vs. low layer 5 EC fib: 404 ± 23 layer 5 neurons/mm^2, p=0.001) (Figure 3.15).

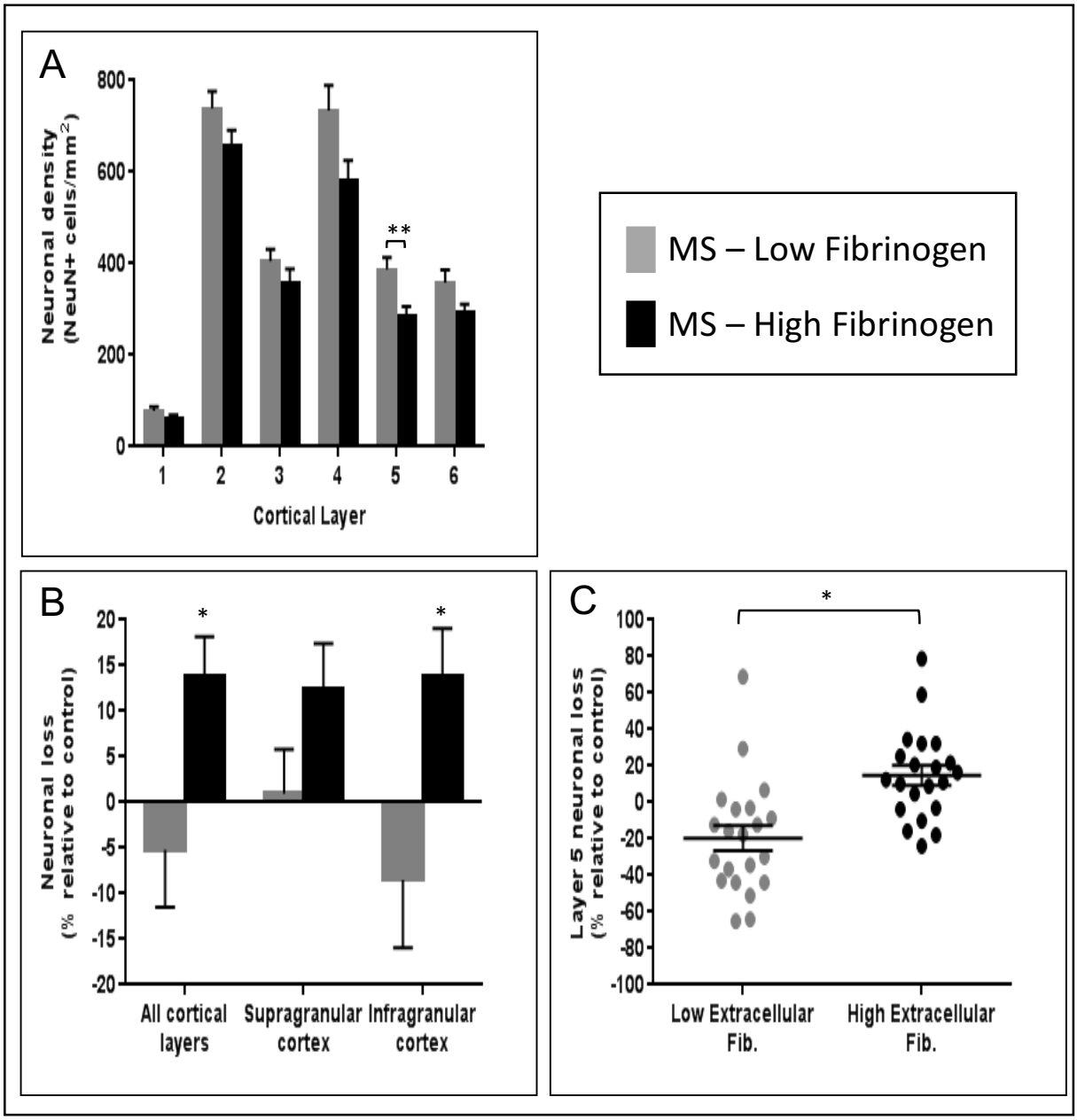


Figure 3.15: Association of fibrinogen deposition with motor cortical neuronal loss. MS cases were divided into "high" and "low" extracellular fibrinogen groups based on the median extracellular score for the MS cohort. A significant difference in neuronal density was detected in the functionally-relevant layer 5 when high and low fibrinogen MS groups were compared (A). When MS cases were divided based on the median of extracellular fibrinogen in supra- and infragranular cortex, a significant difference in neuronal loss was observed between high and low extracellular fibrinogen MS groups when all cortical layers were considered, with the effect being driven by differences in infragranular cortex (B). Further assessment of layer 5 showed more extensive neuronal loss in the MS group with high levels of extracellular fibrinogen (C). Whilst overall neuronal density did not differ in MS compared to control, that there are clear differences in neuronal *loss* between MS cases that demonstrate high versus low amounts of extracellular fibrinogen highlights the potential impact of fibrinogen deposition on neurodegeneration. * = $p<0.05$, ** = $p<0.01$

3.3.5. Assessment of motor cortical PAI-1 in MS cases and controls

PAI-1 was similarly distributed throughout all cortical layers in MS cases and control. However, the extent of PAI-1 expression differed significantly between "high fibrinogen" MS cases and controls in each cortical layer assessed (*layer 2*: MS: 33,147 ± 7,881 vs. control: 14,990 ± 4,862 pixels/mm^2, p=0.043; *layer 3*: MS: 40,839 ± 9,022 vs. control: 20,626 ± 8,954 pixels/mm^2, p=0.035; *layer 4*: MS: 42,148 ± 12,299 vs. control: 20,038 ± 10,103 pixels/mm^2, p=0.035; *layer 5*: 36,482 ± 10,650 vs. control: 17,539 ± 9,752 pixels/mm^2, p=0.035; *layer 6*: 31,766 ± 8,874 vs. control: 14,986 ± 9,00 pixels/mm^2, p=0.035) (Figure 3.16). Lesions had no influence on the extent of PAI-1 expression when compared to MS NAGM (Wilcoxon: z=0.105, p=0.917).

A

	MS – Low EC Fib. (n=10)	MS – High EC Fib. (n=10)
Age of death (yrs)	65.7 (55-82)	65.9 (55-82)
Duration of disease (yrs)	33.5 (19-50)	31.1 (12-50)
Sex	8F, 2M	8F, 2M
Clinical Course	SPMS=10	SPMS=10
Brain weight (g)	1,195 (1,000-1,380)	1,162 (1,045-1,370)
PM interval (hrs)	16.2 (7-25)	15.7 (7-21)

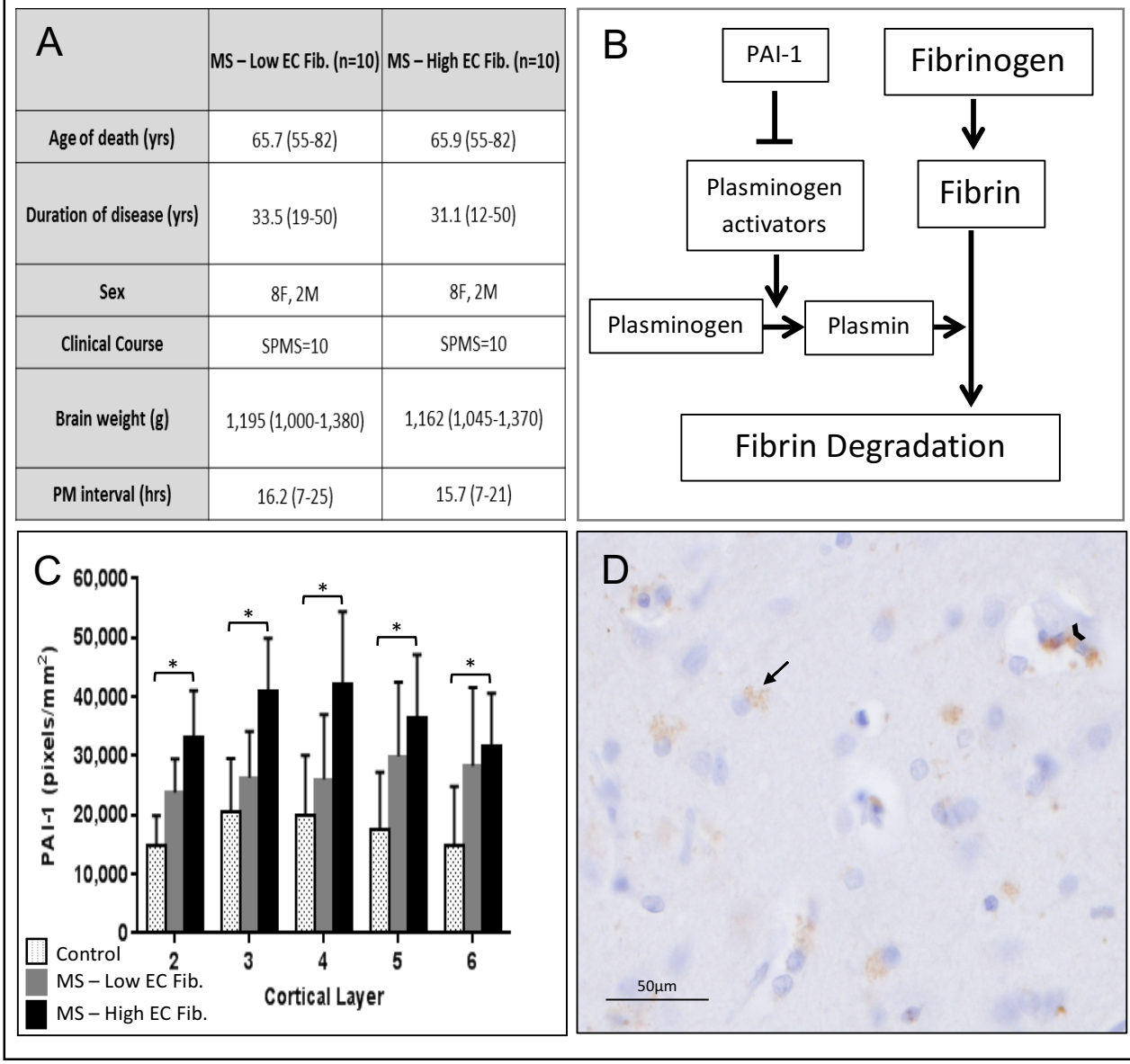


Figure 3.16: Motor cortical PAI-1. The extent of PAI-1 deposition was assessed in a subset of MS cases selected based on the extent of extracellular fibrinogen deposition (high: n=10; low: n=10) and controls (n=10) (A). Fibrinolysis is under the close control of PAI-1, via its inhibition of plasminogen activators. A greater expression of PAI-1 would therefore be expected to coincide with greater deposition of fibrin (B). In all cortical layers assessed, a significant difference was detected in the expression of PAI-1 in MS cases with the most extracellular fibrinogen deposition compared to controls. Layer 1 was not assessed due to consistent artefactual immunolabelling at the section edge (C). PAI-1 was expressed diffusively throughout the cortex, with microglia/macrophage-associated (arrow head) and extracellular deposition (arrow) observed (D). * = $p<0.05$, ** = $p<0.01$

3.4 Discussion

We provide unequivocal evidence that fibrinogen deposition in the MS cortex is frequent and extensive, appears independent of *HLA-DRB1*15* status, and relates to the extent of neuronal loss. This is the first study to link a parenchymal aspect of cortical pathology to neurodegeneration. Given the importance of cortical pathology to disease progression, the potential clinical relevance of these findings is substantial. Future investigations are now needed to elucidate the role of cortical fibrinogen on clinical outcome, and the impact of its elimination.

Our study identifies fibrinogen deposition as a novel component of MS cortical pathology. We found markedly elevated levels of fibrinogen in MS cases compared to controls. Fibrinogen was located in both the extracellular space and within cells and intracellular processes with varying distributions. Extracellular fibrinogen deposition was predominantly located in the deeper infragranular cortical layers. A perivascular distribution was common, though more extensive staining beyond vessels was also frequently observed. In contrast, an overexpression of fibrinogen within neuritic/glial-processes was observed in superficial cortical layers where neuritic and astrocytic labelling was seen. Intracellular fibrinogen was found within neurons and astrocytes throughout all cortical layers. Our findings challenge the idea that large molecular weight serum proteins are not deposited in the MS cortex (van Horssen *et al.*, 2007). The explanation for this inconsistency is not clear, but may relate to differences in tissue antigenicity that relate to fixation and/or processing protocols employed by different institutions.

The presence of fibrinogen in the MS cortex raises the question about its provenance. Fibrinogen accumulation may be caused by increased deposition (i.e. extravasation), impaired clearance, or both. The possibility that BBB disruption leads to increased fibrinogen extravasation in MS cortex is supported by Leech and colleagues, who demonstrated endothelial tight junction abnormalities in cortical grey matter in secondary progressive MS cases (Leech *et al.*, 2007). Together with our own observations, these findings suggest that BBB disruption may be a feature of MS cortical pathology in the progressive phase.

Impaired fibrin(ogen) clearance could also explain the excess fibrinogen burden seen in the cortex of our MS cohort. Impaired clearance may be a late consequence of BBB disruption in the 'early' phase of the disease. Several lines of evidence suggest that the coagulation pathway is perturbed in MS. Proteomic assessment of active plaques has shown specific dysregulation of coagulation proteins (Han *et al.*, 2008) and plasminogen activator inhibitor (PAI-1) is up-regulated in white matter lesions, where it has been associated with a failure of fibrinolysis (Gveric *et al.*, 2003). Interestingly, PAI-1 is also up-regulated in CSF and blood serum of MS patients, and polymorphisms of the PAI-1 gene have recently been linked to disease risk providing further support to suboptimal clearance of coagulation proteins in MS (Akenami *et al.*, 1997; Onodera *et al.*, 1999; Zivković *et al.*, 2014). Our finding of significant up-regulation of PAI-1 in MS cases in which fibrinogen deposition is most severe implies that dysregulation of PAI-1 might impair the clearance of fibrin(ogen) and allow its

pathologic accumulation in MS. Other possible sources of fibrinogen include synthesis by resident neurons and glia and/or retrograde transport in damaged axons in white matter areas exposed to accumulated serum proteins (Fabian and Petroff, 1987). Experimental evidence for these alternative cellular sources of fibrinogen is lacking.

The extent of fibrinogen deposition was not associated with *HLA-DRB1*15* status in our cohort, arguing against greater BBB disruption underlying observations of more inflammation and demyelination in *HLA-DRB1*15*+ cases. However, the observation of intrinsic abnormalities in fibrinogen clearance limits the interpretation of this finding, as we were unable to assess the age of deposited fibrinogen as a result. A genetic impact on BBB integrity may therefore dilute with disease evolution and ageing. Nonetheless, the extent of extracellular fibrinogen in our cohort significantly related to neuronal loss, suggesting a possible role for this protein in cortical neurodegeneration.

Whilst previous studies have demonstrated neuronal loss in the MS cortex, the reduction is typically slight and predominantly in superficial cortical layers where it is topographically associated with tertiary lymphoid-like aggregates in the meninges (Magliozzi *et al.*, 2010; Wegner *et al.*, 2006). In our MS cohort, extracellular fibrinogen correlated with the extent of neuronal loss. These differences were most exaggerated in the infragranular cortex, where fibrinogen deposition was most severe. Specific loss of layer 5 projection neurons also appeared to segregate with the extent of extracellular fibrinogen deposition.

These findings suggest that the cortical deposition of fibrinogen could be an important driver of disease progression, a finding supported by a wealth of experimental data (Davalos and Akassoglou, 2012).

A relationship between fibrinogen and neuroaxonal demise has been shown in disease relevant animal models. In EAE, fibrinogen activates microglia, which in turn mediates axonal damage even before the onset of clinical signs (Davalos *et al.*, 2012). The manipulation of the coagulation cascade to reduce CNS fibrin(ogen) deposition in these animal models leads to clinical improvement (Adams *et al.*, 2007; Akassoglou *et al.*, 2004; East *et al.*, 2008). Human *in vitro* experiments have confirmed that fibrinogen interacts with Toll-like receptors expressed by interferon-gamma activated macrophages leading to the secretion of neurotoxic products (Smiley *et al.*, 2001). Interferon-gamma can diffuse from the subarachnoid space into the subpial parenchyma (Gardner *et al.*, 2013). Given that the perivascular space is continuous with the subarachnoid space, microglia/macrophages activated by interferon-gamma may create a neurotoxic inflammatory milieu in the presence of fibrinogen even in cortical layers distant from the subpial surface. While we could not demonstrate a relationship between fibrinogen deposition and innate inflammation in our cohort, such relationships may be difficult to discern given that genetic factors, disease evolution and ageing likely impact the recognised phenotypic heterogeneity of microglial/macrophage inflammation (Caldeira *et al.*, 2014; Ritzel *et al.*, 2015; Yates *et al.*, 2015). Further, interactions of inflammatory mediators are likely short-lived and therefore impervious to detection in an autopsy cohort. In

contrast, the permanency of neuronal death allowed us to detect relationships between fibrinogen and neuronal loss.

Fibrinogen, as a potent activator of microglial/macrophage inflammation, might be a novel therapeutic target (Davalos and Akassoglou, 2012). Effective neutralisation of fibrinogen could enable the limitation of ongoing maladaptive innate immune responses thought to contribute to the diffuse neuroaxonal loss characteristic of progressive disease (Frischer *et al.*, 2015).

In summary, we introduce cortical fibrinogen deposition as a novel component of MS cortical pathology. We show that fibrinogen is extensively deposited in MS motor cortex where regulation of fibrinolysis appears perturbed. The relationship between neuronal loss and fibrinogen deposition in the MS motor cortex highlights the potential functional relevance of this protein in disease progression. Future studies aimed at elucidating the provenance and putative neuroaxonal toxicity of fibrinogen, and its potential impact on clinical disability, are urgently needed.

4. The influence of *HLA-DRB1*15* on motor cortical neurodegeneration in multiple sclerosis

4.1. Introduction

In chapter 2, we demonstrated that *HLA-DRB1*15*+ MS cases have more severe motor cortical demyelination and inflammation, particularly in younger cases. In chapter 3 we investigated whether cortical fibrinogen deposition, as a surrogate marker of BBB disruption, might be more severe in *HLA-DRB1*15*+ cases and therefore underpin divergent pathologic outcome. Whilst we did not any find evidence that fibrinogen deposition was associated with *HLA-DRB1*15* status, we detected striking associations between fibrinogen and cortical neuronal loss. Taken together, these findings highlight a role for genetic variation in pathologic heterogeneity and a critical importance of parenchymal factors in the initiation and/or exacerbation of cortical tissue injury in MS. In the current chapter, we therefore investigate the relationship between cortical parenchymal inflammation and neurodegeneration, and associations therein with *HLA-DRB1*15* status.

Neuronal loss is a documented feature of the MS cortex, but reports are conflicting as to its extent and determinant pathologic factors (Klaver *et al.*, 2015; Peterson *et al.*, 2001; Wegner *et al.*, 2006). In one of the largest assessments to date, significant neuronal loss was only observed in cases harbouring tertiary lymphoid-like follicles in the sub-arachnid space (Magliozzi *et al.*, 2010), suggesting that meningeal inflammation drives cortical

neurodegeneration via the diffusion of neurotoxic factors into the brain. The role of parenchymal inflammation in this process has been relatively overlooked, in part because lymphocytic inflammation and microglia/macrophage activation are not prominent features of progressive MS cortical pathology (L Bø *et al.*, 2003). However, the fact that genetic factors associated with disease susceptibility and clinical outcome can influence cortical parenchymal inflammation provides a persuasive justification to re-assess the impact of local inflammatory factors on cortical neurodegeneration in the context of *HLA-DRB1*15*.

The relationship between parenchymal inflammation and MS cortical neurodegeneration is likely to be complex. Lymphocytes populate perivascular spaces but are scarce in the cortical parenchyma (Peterson *et al.*, 2001). Microglial/macrophages, in contrast, are common in MS cortex. Whilst it is not currently possible to reliably distinguish resident microglia from extravasated macrophages, the lack of leukocyte infiltration into the MS cortex implicates microglia as the predominant myeloid population involved in cortical pathology. *In vitro* studies have demonstrated a marked heterogeneity in microglia/macrophage phenotype (Mills *et al.*, 2000). Both destructive immunity and stimulation of tissue repair has been reported (Kigerl *et al.*, 2009), including the promotion of remyelination in EAE (Miron *et al.*, 2013). Whilst evidence of microglia/macrophage heterogeneity is detected in MS post-mortem tissue (Peferoen *et al.*, 2015), the detection of any fixed dichotomy is lacking (Vogel *et al.*, 2013). Rather, it is likely that the relative activity of neurodegenerative

and/or neuroprotective microglia/macrophage functions are dynamically related to anatomic location and ageing (Ritzel *et al.*, 2015), as well as genetic variation (Yates *et al.*, 2015), and local inflammatory factors (Miron *et al.*, 2013).

Despite substantial demyelination in progressive MS (Kutzelnigg *et al.*, 2005) and chronic meningeal inflammation that may last several decades (Howell *et al.*, 2011), our cohort suggests that the majority of motor cortical neurons survive the MS disease process. This raises the possibility that microglia/macrophage-mediated neuroprotective strategies may be operative here. Trapp and colleagues have recently shown that microglia-mediated stripping of inhibitory GAD+ synapses protected neurons from apoptosis induced by toxic inflammatory mediators (Chen *et al.*, 2014). GAD catalyses the conversion of glutamate to GABA, and is therefore critical in inhibitory neurotransmission within the CNS. Removal of GAD+ synapses leads to up-regulation of excitatory neurotransmission and subsequent promotion of pro-survival gene expression (Chen *et al.*, 2014). GAD is also expressed in occasional neuronal cytoplasm (Pinal and Tobin, 1998), where its expression has been linked to trophic support of injured neurons after ischaemic stroke (Li *et al.*, 2010) and excitotoxicity (Falkenberg *et al.*, 1997). Whether microglia/macrophage inflammation promote neuroprotective mechanisms involving GAD in the MS cortex, and the impact of *HLA-DRB1*15* status therein, is not known.

In the current study, we assess the relationship between motor cortical parenchymal inflammation, GAD and neuronal density in the context of *HLA*-

*DRB1*15* status. We show that *HLA-DRB1*15* influences the relationship between parenchymal microglia/macrophage inflammation, but not lymphocytic inflammation, and neuronal density. We extend these findings by investigating motor cortical GAD, as a putative marker of neuroprotection, and provide evidence for inhibitory synaptic stripping by demonstrating a significant reduction in GAD+ synapses in the MS motor cortex. In addition, GAD+ layer 5 neurons appear to be smaller in MS, particularly in *HLA-DRB1*15*+ cases. Regarding cytoplasmic GAD expression, we find significant relationships with microglia/macrophage inflammation, but only in *HLA-DRB1*15*- MS cases. This study is the first to link a genetic factor to neurodegeneration in the MS cortex and provides evidence of disease-related changes to GAD expression that are relevant to cortical tissue injury.

4.2. Materials and Methods

4.2.1. Study population

The MS and control cohort used in this study is the same as that used in chapter 3. Briefly, a human autopsy cohort of pathologically confirmed MS cases (n=47) and control cases (n=10) was used. Primary motor cortex was sampled from mesial precentral gyrus and MS cases were previously genotyped for *HLA-DRB1*15* status, as outlined in chapter 3.

4.2.2. Immunohistochemistry and Immunofluorescence

Formalin-fixed paraffin-embedded tissue blocks were cut into 6uM thick sections and labelled with primary antibodies for microglia (Iba1), activated microglia (CD68), lymphocytes (CD3), cytotoxic lymphocytes (CD8), glutamic acid decarboxylase (GAD 65/67) and neurons (NeuN) using DAB immunohistochemistry (Table 4.1) (Appendix 1). Sections were counterstained with haematoxylin. Synaptic GAD was assessed by double-labelling sections with primary antibodies to GAD and neurons (neurofilament), conjugated respectively to Alexa-647 anti-rabbit and Alexa-488 anti-mouse fluorescent secondary antibodies (Table 4.2). Fluorescent sections were counterstained with DAPI (Appendix 2). Experiments with omission of primary and secondary antibodies were used as negative controls.

Table 4.1: Antibodies used for DAB immunohistochemistry in chapter 4

Antibody	Clone	Classification	Pretreatment	Dilution	Supplier	Catalogue Number
Iba1		Polyclonal rabbit	Autoclave, tris-EDTA pH 9.0	1/1000	Wako	019-19741
CD68	PG-M1	Monoclonal mouse	Microwave, citrate pH 6.0	1/100	Dako	M0876
CD3		Polyclonal rabbit	Autoclave, tris-EDTA pH 9.0	1/100	Dako	A0452
CD8	C8/C114B	Monoclonal mouse	Autoclave, citrate pH 6.0	1/5	Dako	IS623
GAD 65/67		Polyclonal rabbit	Autoclave, citrate pH 6.0	1/200	Millipore	AB1511
NeuN	A60	Monoclonal mouse	Autoclave, citrate pH 6.0	1/400	Millipore	MAB377

Table 4.2: Antibodies used for immunofluorescence in chapter 4

Antibody	Clone	Classification	Pretreatment	Dilution	Supplier	Catalogue Number
Neurofilament	N52	Monoclonal mouse	Autoclave, citrate pH 6.0	1/250 O/N	Sigma	N0142
GAD 65/67		Polyclonal rabbit	Autoclave, citrate pH 6.0	1/3000 O/N	Millipore	AB1511

4.2.3. Assessment strategy of motor cortical inflammation and neuronal density

Neuronal density (NeuN+), microglia/macrophage inflammation (Iba1+ and CD68+) and lymphocytic inflammation (CD3+ and CD8+) were quantified in each cortical layer along predefined and systematically spaced trajectories that were arranged perpendicular to the cortical surface, as outlined in chapter 3 (Figure 3.1).

4.2.3.1. Lymphocytic inflammation

Parenchymal lymphocytes (CD3+ and CD8+) were manually counted using light microscopy by quantifying positively labelled cells in each FOV, and are expressed as cells/mm^2. Within each FOV, one perivascular space (with the most severe inflammatory infiltration) was scored semi-quantitatively according to the following criteria: 0= no cells, 1= 1-3 cells, 2= 3+ cells, 3= one complete perivascular cuff.

4.2.3.2. Microglia/macrophage inflammation

Photomicrographs acquired of FOVs containing microglia/macrophage inflammation (Iba1+ and CD68+) were assessed using a semi-automatic colour-based extraction method and are reported as millions of pixels/mm^2, as described in previous chapters of this thesis (quantitation is outlined in Figure 2.2, sampling is outlined in Figure 3.1).

4.2.3.3. Neuronal density

Motor cortical neuronal density was assessed in each FOV by manually counting NeuN+ cells that had a single nucleus and visible nucleolus. In total, approximately 70,000 neurons were counted across the cohort and are expressed as neurons/mm^2, as outlined in chapter 3.

4.2.4. Assessment strategy of motor cortical meningeal inflammation

Meningeal lymphocytic and microglia/macrophage inflammation was assessed in available leptomeninges. Lymphocytes (CD3+ and CD8+) were manually counted and related to meningeal length (expressed as cells/mm meningeal length), as outlined in chapter 2. Microglia/macrophage inflammation could not be manually counted due to the complex morphology of Iba1+ and CD68+ cells that made resolving individual cells difficult. Instead, meningeal microglia/macrophage inflammation was scored for each case semi-quantitatively as either 0 (virtually absent), 1 (mild), 2 (moderate) or 3 (severe), as previously described (Howell *et al.*, 2015).

4.2.5. Assessment strategy of motor cortical GAD

Motor cortical GAD was assessed to probe putative neuroprotective mechanisms involving GABA neurotransmission and metabolism. GAD can localise to inhibitory synapses and/or neuronal cytoplasm (Figure 4.1). As such, the extent of synaptic and cytoplasmic GAD was assessed separately as outlined below.

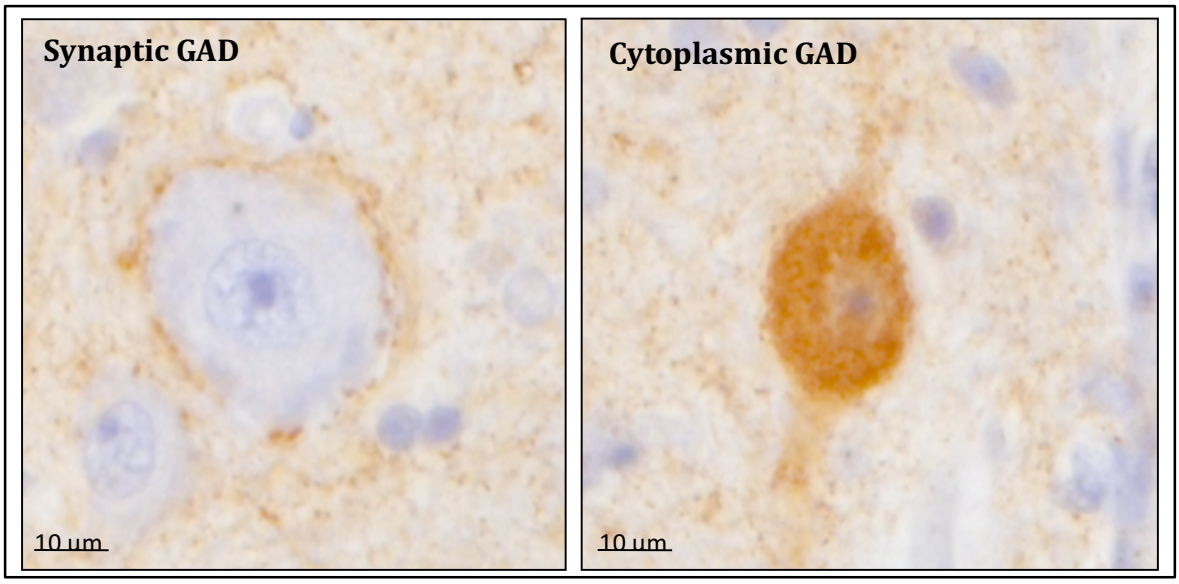


Figure 4.1: Immunolabelling of synaptic GAD (left) and cytoplasmic GAD (right). GAD can localise to both inhibitory synapses and neuronal cytoplasm. In both locations, GAD catalyses the production of GABA

4.2.5.1. Synaptic GAD

For all analyses involving synaptic GAD, a subset of MS cases (n=20) matched for age, disease duration, sex, post mortem interval and layer 5 neuronal density between *HLA-DRB1*15* genotype groups (i.e. *HLA-DRB1*15*+, n=10; *HLA-DRB1*15*-, n=10), and control cases (n=7), were studied (Table 4.4).

MS cases and controls double-labeled with GAD and neurofilament were imaged using a Leica 710 confocal microscope. We restricted our analysis to pyramidal neurons in layer 5 NAGM. Layer 5 was selected for its relevance to MS progression given the long axonal projections of this layer in the corticospinal system. Pyramidal neurons that showed clear evidence of GAD+ synapses were sampled by moving the microscope stage systematically through layer 5 of the motor cortex until n=30-40 neurons could be imaged for each case in areas of NAGM. A total of 883 neurons were photographed in MS cases and controls.

In order to quantify membrane-associated GAD+ synaptic density, images were subjected to an algorithm designed in collaboration with colleagues at the Institute of Biomedical Engineering, University of Oxford (Figure 4.2). Photographed neurons were segmented into neuronal perikarya and GAD+ synapses. A 1μm thick neuronal boundary was delineated based on a level-set algorithm and considered to be the neuronal membrane. In order to assess membrane-associated GAD+ synapses, fluorescent signal was segmented based on circularity and size constraints. Fluorescent signal that met appropriate size and circularity criteria, but that did not have adequate intensity to be reliably distinguished from background signal, was rejected. The value used to define minimum fluorescent signal intensity, above which synapses were quantified, was generated via the independent assessment of a range of thresholds by two observers who came to mutual agreement. The ability of the algorithm to robustly segment GAD+ synapses was verified using a set of images that were manually segmented (n=10).

Analysed images were quality controlled and neurons that failed to optimally segment were deleted. Of the 883 neurons photographed, 239 were deleted (27%), leaving 252 *HLA-DRB1*15*+ neurons, 240 *HLA-DRB1*15*- neurons, and 152 control neurons (644 neurons in total).

Membrane-associated GAD+ synaptic density was assessed in each case by quantifying GAD+ synapses overlapping the neuronal boundary, and is expressed as GAD+ synapses/μm^2 neuronal membrane. In addition to GAD synapses, GAD+

cell size was calculated by summating the area within the segmented neuronal boundary with the area of the delineated boundary, and is expressed as μm^2.

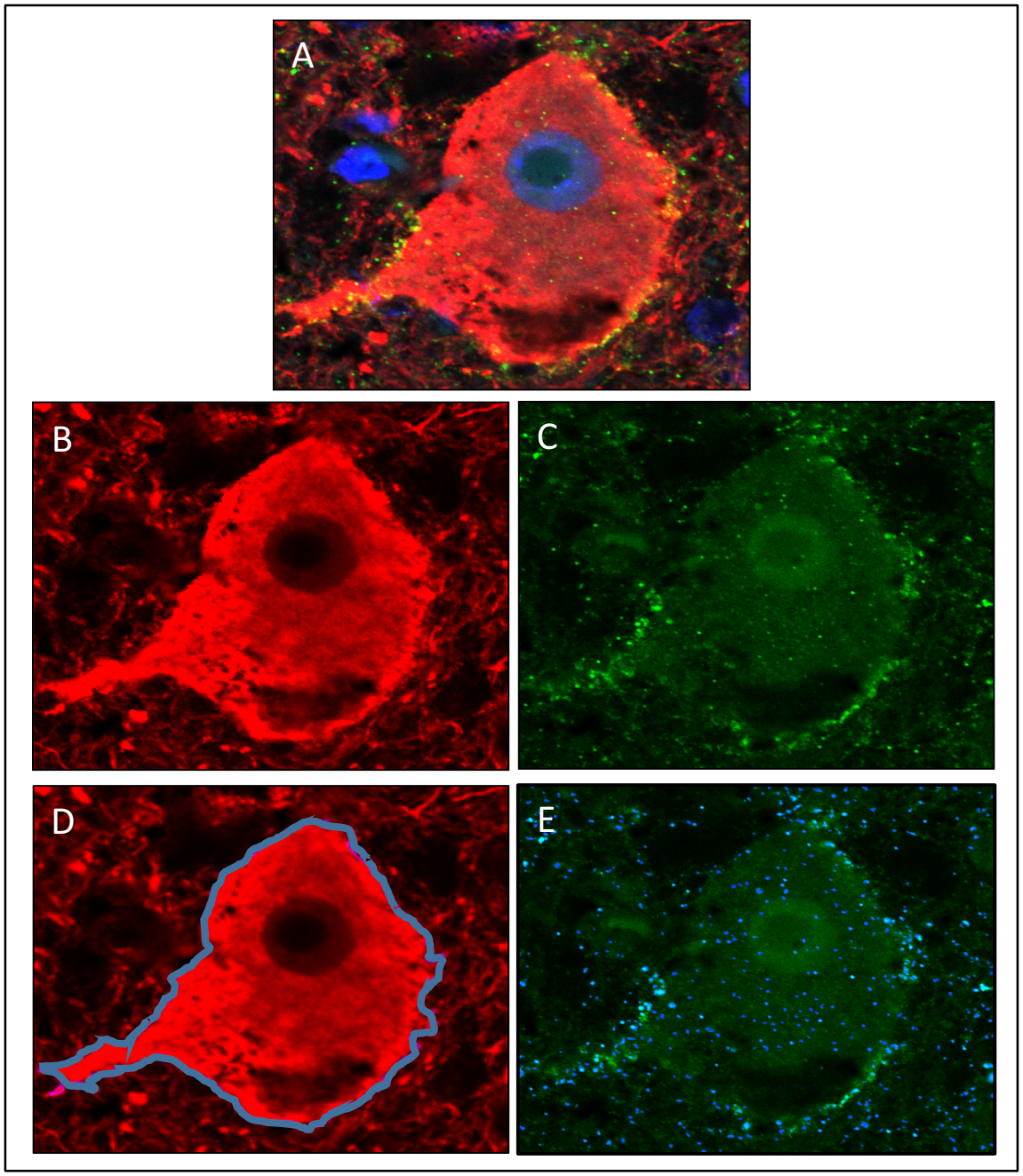


Figure 4.2: Quantitation of GAD+ synaptic coverage of layer 5 neurons. Confocal images were acquired of layer 5 pyramidal neurons double-labelled for neurofilament (neurons; red) and GAD 65/67 (GAD+ synapses; green), and counter-stained with DAPI (nuclei; blue) (A). Acquired images were split into their respective colour channels (B&C) before being subjected to a segmentation algorithm optimised in collaboration with colleagues at the Institute of Biomedical Engineering (Oxford). Neuronal perikarya (D; blue outline) and GAD+ synapses (E; blue overlay) were outlined and quantified as outlined in the main text.

4.2.5.2. Cytoplasmic GAD

MS cases (n=47) and controls (n=7) immunolabeled with GAD were scanned using an Aperio ScanScope slide scanner. A custom-made validated cell-counting algorithm within Aperio ImageScope software was used to quantify the density of cells with cytoplasmic GAD immunoreactivity within the available motor cortical area (Figure 4.3). A separate analysis was undertaken to compare cytoplasmic GAD density in lesions versus NAGM. Data is expressed as cytoplasmic GAD+ cells/mm^2.

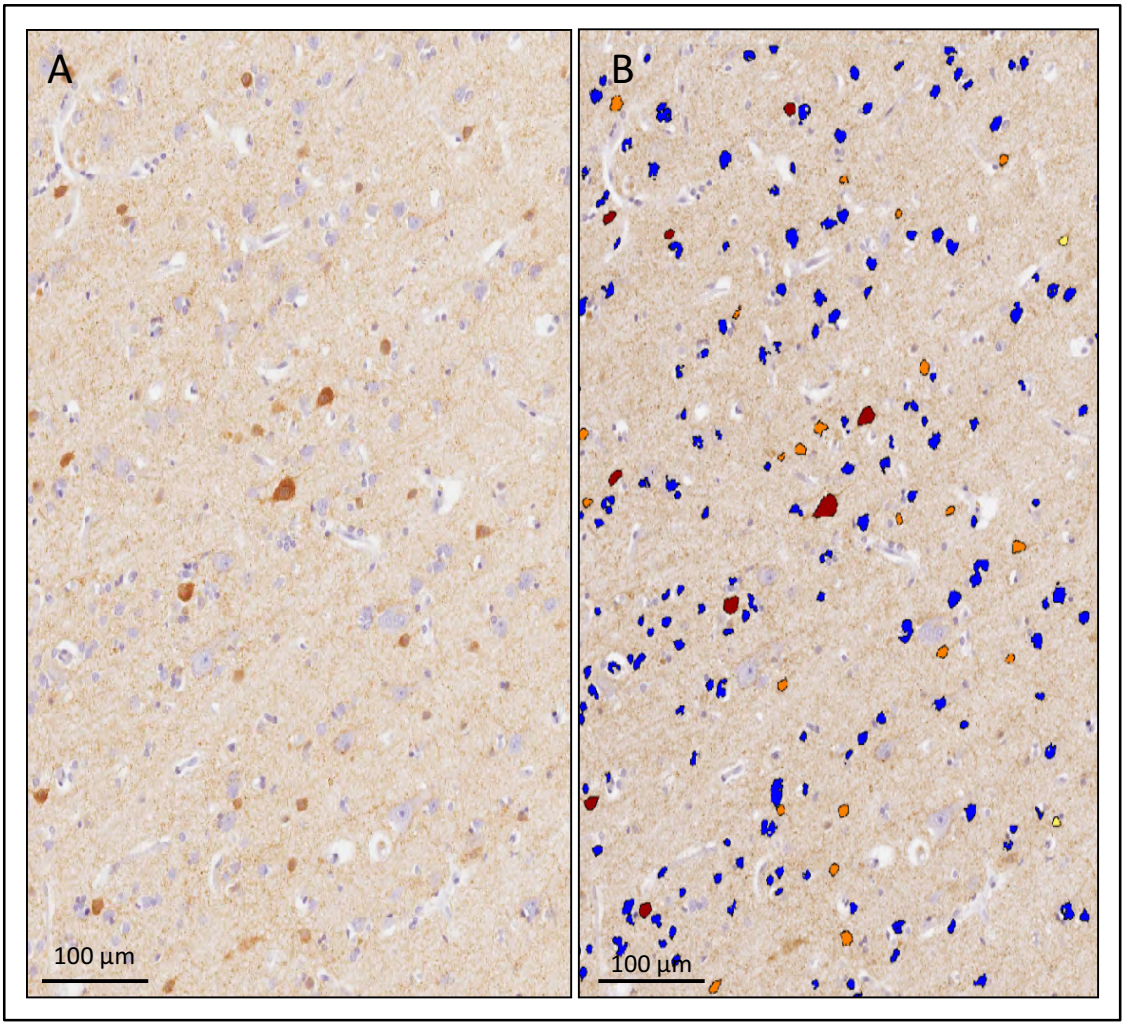


Figure 4.3: Cytoplasmic GAD quantitation. Example automation of cytoplasmic GAD quantitation input (A), and output (B). The following colour rules were used: red = strongly staining; orange = medium staining; yellow = weak staining; blue (or no colour mask) = negative staining. Only red and orange counts were included in analysis. Validation with manual counts was carried out in a subset of n=20 MS cases ($r=0.740$, $p<0.001$).

4.2.6. Statistical analyses

Relationships between continuous pathologic variables were assessed using Spearman rank correlation coefficients. Partial correlations were assessed on normally distributed data to correct for confounding variables. To evaluate the predictive value of inflammatory variables on neuronal density, multiple linear regression models were constructed, controlling for demographic factors as appropriate. Linear regression models were fitted to evaluate the influence of *HLA-DRB1*15* status on continuous pathologic outcome measures whilst controlling for age, sex and post-mortem interval, as appropriate. Distribution of data was assessed analytically and graphically and transformed as required. Data are presented ± SEM. All tests of hypotheses were carried out using two-sided tests. In all analyses, P-values less than 0.05 were considered significant. Statistical analyses were done using SPSS v21 software.

4.3. Results

4.3.1. Clinical features of MS cases and controls

Clinical details for the MS and control cohort used in this chapter can be found in Table 4.3. Clinical details for the MS and control cohort used in GAD+ synapse analyses can be found in Table 4.4.

Table 4.3: Clinical details of cohort used in chapter 4

	MS cases (n=47)	***HLA-DRB1*15*+ (n=21)**	***HLA-DRB1*15*- (n=26)**	**Controls (n=10)**
Age of death (yrs)	63 (range: 40-92)	65 (range: 40-92)	62 (range: 43-86)	74 (range: 57-91)
Duration of disease (yrs)	31 (range:11-58)	32 (range:12-58)	30 (range: 11-55)	n/a
Sex	M=13, F=34	M=7, F=14	M=6, F=20	M=7, F=3
Clinical Course	PPMS:4, SPMS:38, RRMS:1, Unknown:4	PPMS:3, SPMS:17, RRMS:0, Unknown:1	PPMS:1, SPMS:21, RRMS:1, Unknown:3	n/a
Brain weight (g)	1157 (range: 894-1380)	1163 (range: 1000-1364)	1152 (range: 894-1380)	1320 (range: 1072-1628)
PM interval (hrs)	18 (range: 7-38)	18 (range: 7-38)	18 (range: 8-28)	36.7 (range: 10-72)

Table 4.4: Clinical details of cohort for synaptic GAD analysis

	All MS cases (n=20)	***HLA-DRB1*15+*** **(n=10)**	***HLA-DRB1*15-*** **(n=10)**	**Controls (n=7)**
Age of death (yrs)	60.5 (range: 42-82)	60.7 (range: 42-82)	60.2 (range: 48-80)	78 (range: 68-91)
Duration of disease (yrs)	28.1 (range: 11-58)	27.4 (range: 12-58)	28.9 (range: 11-38)	n/a
Sex	18F, 2M	9F, 1M	9F, 1M	3F, 4M
PM interval	18.63 (range: 7-38)	18.8 (range: 7-38)	18.45 (range: 7.5-28)	28.4 (range: 10-52)
Layer 5 neuronal density/mm^2	358 (range: 138-595)	339 (range: 229-595)	377 (range: 138 - 555)	338 (range: 298-368)

4.3.2. Neuropathological findings: MS vs. controls

4.3.2.1. Parenchymal microglia/macrophage inflammation in MS versus control motor cortex

The extent of microglia/macrophage inflammation in the current MS and control cohort was outlined in chapter 3. Briefly, total and activated microglia/macrophage inflammation, Iba1+ and CD68+ cells respectively, were not significantly increased in the MS parenchyma when compared to controls (Figure 3.10 & 3.11), or in MS lesions compared to MS NAGM (Figure 3.12). In MS cases and controls, the extent of Iba1+ inflammation significantly correlated with the extent of CD68+ inflammation ($r=0.703$, $p<0.001$).

4.3.2.2. Parenchymal and perivascular lymphocytic inflammation in MS versus control motor cortex

CD3+ lymphocytic inflammation was more severe in MS cases than control, both in the parenchyma (MS: 4.2 ± 0.6 cells/mm2 vs. 0.9 ± 0.2 cells/mm2, $p<0.001$) and perivascular space (MS: 0.8 ± 0.01 vs. 0.01 ± 0.005, $p<0.001$). Similarly, CD8+ lymphocytic inflammation was also more severe in MS cases than control in both parenchyma (MS: 1.8 ± 0.3 cells/mm2 vs. 0.1 ± 0.07 cells/mm2, $p<0.001$) and perivascular spaces (MS: 0.04 ± 0.006 vs. 0.01 ± 0.006, $p=0.003$) (Figure 4.4)

Within each MS case, no difference was detected in parenchymal CD3+ inflammation in lesions compared to NAGM (Wilcoxon: $z=1.834$, $p=0.067$). Similarly, no significant increase in CD8+ inflammation in lesions was detected compared to NAGM (Wilcoxon: $z=0.443$, $p=0.658$).

Within each MS case, no differences were observed in perivascular lymphocytes in lesions compared to NAGM, both in terms of CD3+ cells (Wilcoxon: z= 0.411, p=0.681), or CD8+ cells (Wilcoxon: z=1.224, p=0.221) (Figure 4.4).

In MS cases, the extent of CD3+ inflammation correlated with the extent of CD8+ inflammation in the perivasculature (r=0.617, p<0.001) and parenchyma (r=0.559, p<0.001). In control cases, CD3+ cells correlated with CD8+ in the perivasculature (r=0.665, p=0.036), but not parenchyma (r=-0.426, p=0.220).

4.3.2.3. Meningeal inflammation in MS versus control motor cortex

Meningeal CD3+ and CD8+ inflammation was greater in MS than controls (CD3+: MS: 3.9 ± 0.5 cells/mm meningeal length vs. control: 1.4 ± 0.2 cells/mm meningeal length, p<0.001; CD8+: MS: 2.7 ± 0.5 cells/mm meningeal length vs. control: 1 ± 0.2 cells/mm meningeal length, p=0.001). Meningeal Iba1+ and CD68+ inflammation was significantly greater in MS than controls (Iba1+: MS: 1.275 ± 0.179 vs. control: 0.25 ± 0.164, p=0.002; CD68+: MS: 1.6 ± 0.174 vs. control: 0.25 ± 0.164, p<0.001) (Figure 4.4).

In MS cases, CD8+ meningeal inflammation correlated with meningeal microglia/macrophage inflammation (Iba1+: r=0.708, p<0.001; CD68+: r=0.676, p<0.001). Similar relationships were detected between CD3+ meningeal inflammation and meningeal microglia/macrophage inflammation (Iba1+: r=0.519, p=0.001; CD68+: r=0.383, p=0.015). In controls, no relationships were observed between meningeal CD8+ inflammation and meningeal microglia/macrophage inflammation (r=-0.126, p=0.766; CD68+: r=-0.126,

p=0.766), or between meningeal CD3+ inflammation and meningeal microglia/macrophage inflammation (r=-0.126, p=0.766; CD68+: r=-0.126, p=0.766).

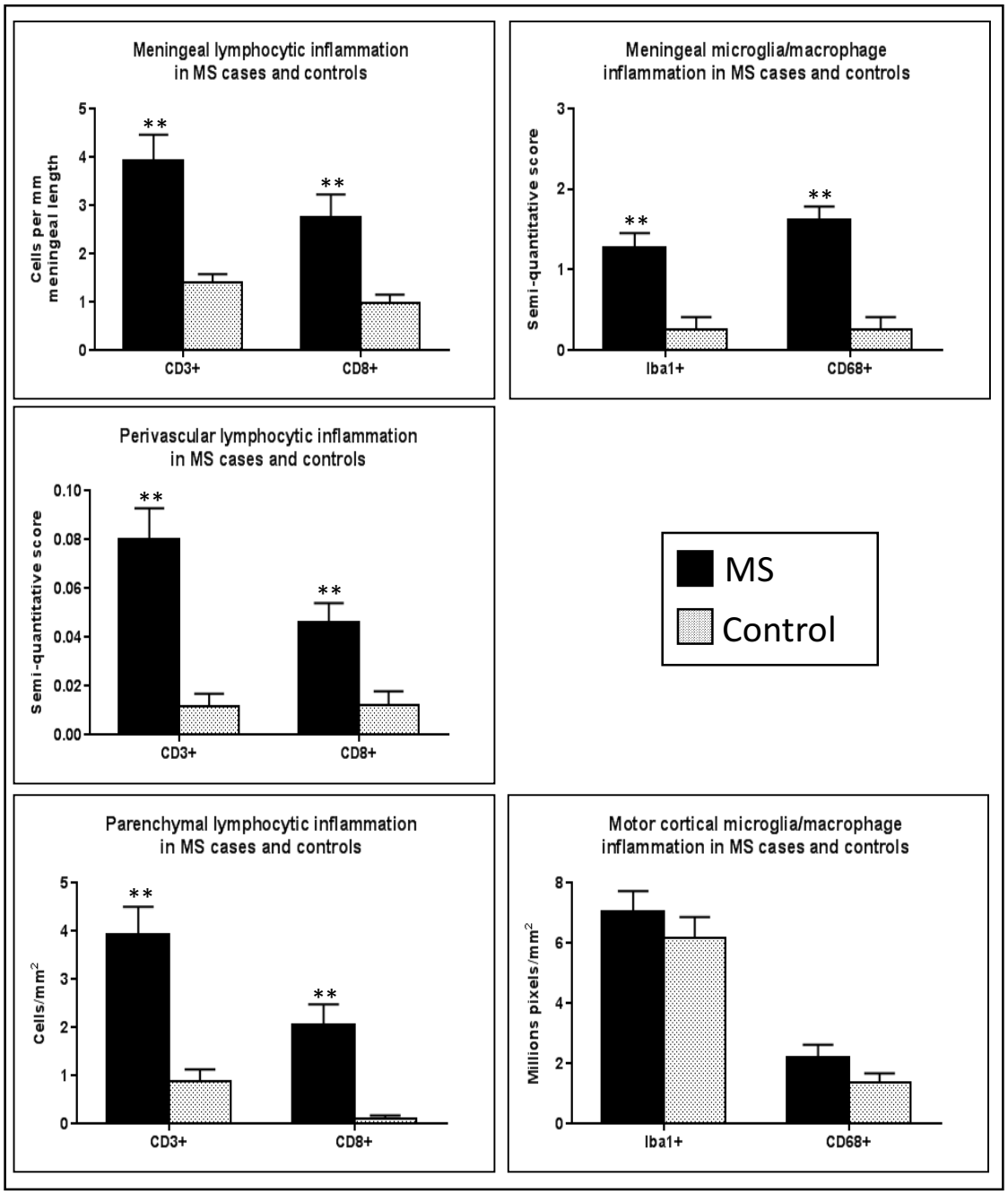


Figure 4.4: Meningeal, perivascular and parenchymal inflammation in MS cases and controls.

* = p<0.05, **=p<0.01

4.3.2.4. Neuronal density in MS versus control motor cortex

Neuronal density in this MS and control cohort was outlined in chapter 3. Briefly, neuronal density did not differ between MS and control (Figure 3.13) or in MS lesions compared to MS NAGM (Figure 3.14).

4.3.3. Relationships between meningeal, perivascular and parenchymal inflammation in MS and control

Meningeal lymphocytes correlate with perivascular lymphocytes, but not parenchymal lymphocytes, in MS

In MS cases, meningeal CD3+ inflammation significantly correlated with perivascular CD3+ inflammation ($r=0.563$, $p<0.001$), but not parenchymal CD3+ inflammation ($r=0.123$, $p=0.431$). Similarly, meningeal CD8+ inflammation significantly correlated with perivascular CD8+ inflammation ($r=0.502$, $p=0.01$), but not parenchymal CD8+ inflammation ($r=0.228$, $p=0.141$).

In control cases, meningeal CD3+ inflammation was not correlated with perivascular CD3+ ($r=0.230$, $p=0.584$), or parenchymal CD3+ cells ($r=-0.366$, $p=0.373$). Similarly, in control cases meningeal CD8+ inflammation was not correlated with perivascular CD8+ ($r=0.692$, $p=0.062$), or parenchymal CD8+ cells ($r=0.156$, $p=0.712$).

Meningeal microglia/macrophage inflammation correlates with parenchymal microglia/macrophages in MS

In MS cases, a weak correlation was observed between Iba1+ inflammation in the meninges and parenchyma ($r=0.312$, $p=0.05$). No relationship was observed

between CD68+ inflammation in the meninges and parenchyma (r=0.161, p=0.315).

In control cases, no relationships were observed between Iba1+ meningeal inflammation and Iba1+ parenchymal inflammation (r=0.504, p=0.203). Similarly, no relationships were detected in control cases between meningeal CD68+ and parenchymal CD68+ inflammation (r=0.252, p=0.547).

Meningeal lymphocytic inflammation correlates with parenchymal microglia/macrophage inflammation in MS

In MS cases, CD8+ meningeal inflammation was correlated with parenchymal Iba1+ (r=0.414, p=0.006) and CD68+ inflammation (r=0.407, p=0.007). Similar relationships were detected in MS cases between meningeal CD3+ inflammation and parenchymal microglia/macrophage inflammation (Iba1+: r=0.336, p=0.029; CD68+: r=0.291, p=0.058).

In controls, CD8+ meningeal inflammation was not associated with parenchymal microglia/macrophage inflammation (Iba1+: r=-0.143, p=0.736; CD68: r=-0.238, p=0.570). Similarly, no relationships were detected between meningeal CD3+ inflammation and parenchymal microglia/macrophage inflammation in controls (Iba1+: r=-0.286, p=0.493; CD68+: r=-0.619, p=0.102).

4.3.4. Relationships between parenchymal inflammation and neuronal density in MS and control motor cortex

In MS, microglia/macrophage inflammation (total and activated) positively correlated with neuronal density (Iba1+: r=0.470, p=0.001, CD68+: r=0.461, p=0.001) (Figure 4.5), a finding restricted to MS cases that died above the median age of the cohort (age > 62 years) (Iba1+: r=0.762, p<0.001; CD68+: r=0.691, p<0.001). No relationship between microglia/macrophage inflammation and neuronal density was found in cases below the median age (Iba1+: r=0.245, p=0.260; CD68+: r=0.284, p=0.190) (Figure 4.6).

In MS, no relationship was observed between lymphocytic inflammation and neuronal density (CD3+: r=-0.008, p=0.960; CD8+: r=0.184, p=0.221). This finding was consistent in MS cases under the age of 62 (CD3+: r=-0.082, p=0.710; CD8+ r=-0.100, p=0.650), and over the age of 62 (CD3+: r=-0.021, p=0.924; CD8+ r=-0.382, p=0.079).

In control cases, no relationship was detected between microglia/macrophage inflammation and neuronal density (Iba1+: r=-0.036, p=0.939; CD68+: r=0.179, p=0.702) or lymphocytic inflammation and neuronal density (CD3+: r=-0.216, p=0.641; CD8+: r=-0.134, p=0.775). The small size of our control cohort precluded the assessment of specific age groups.

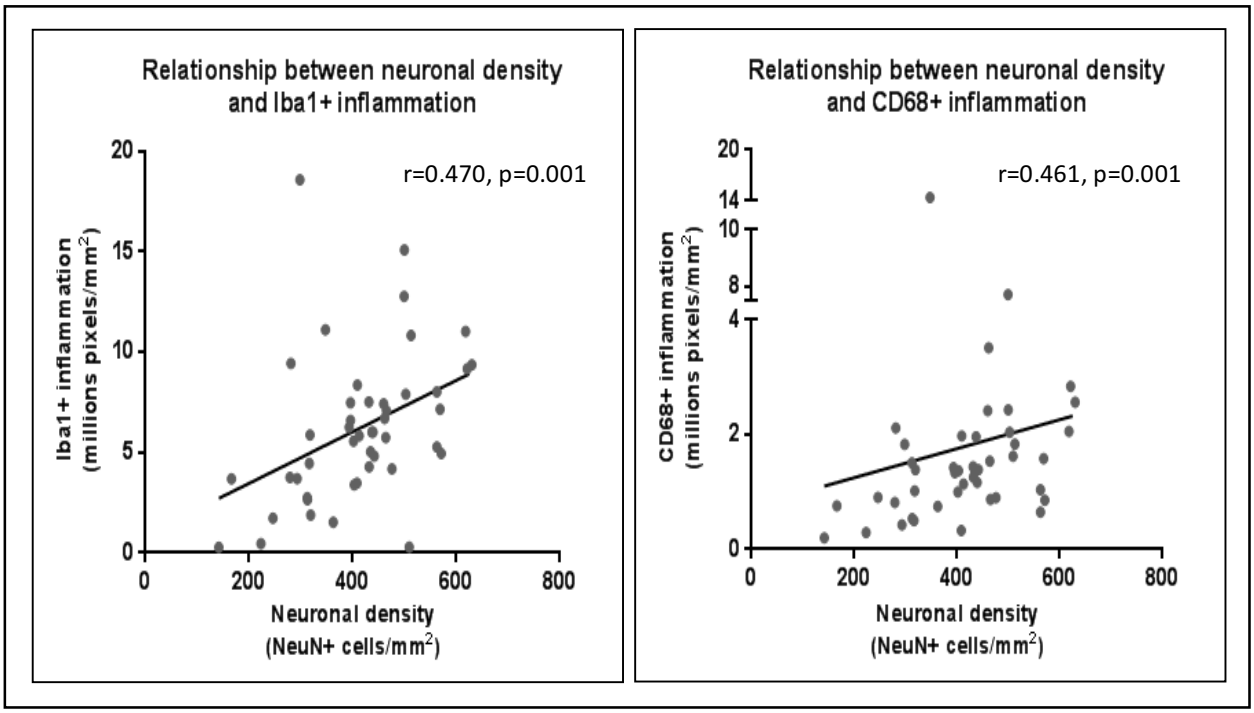


Figure 4.5: Relationship between microglia/macrophage inflammation and neuronal density

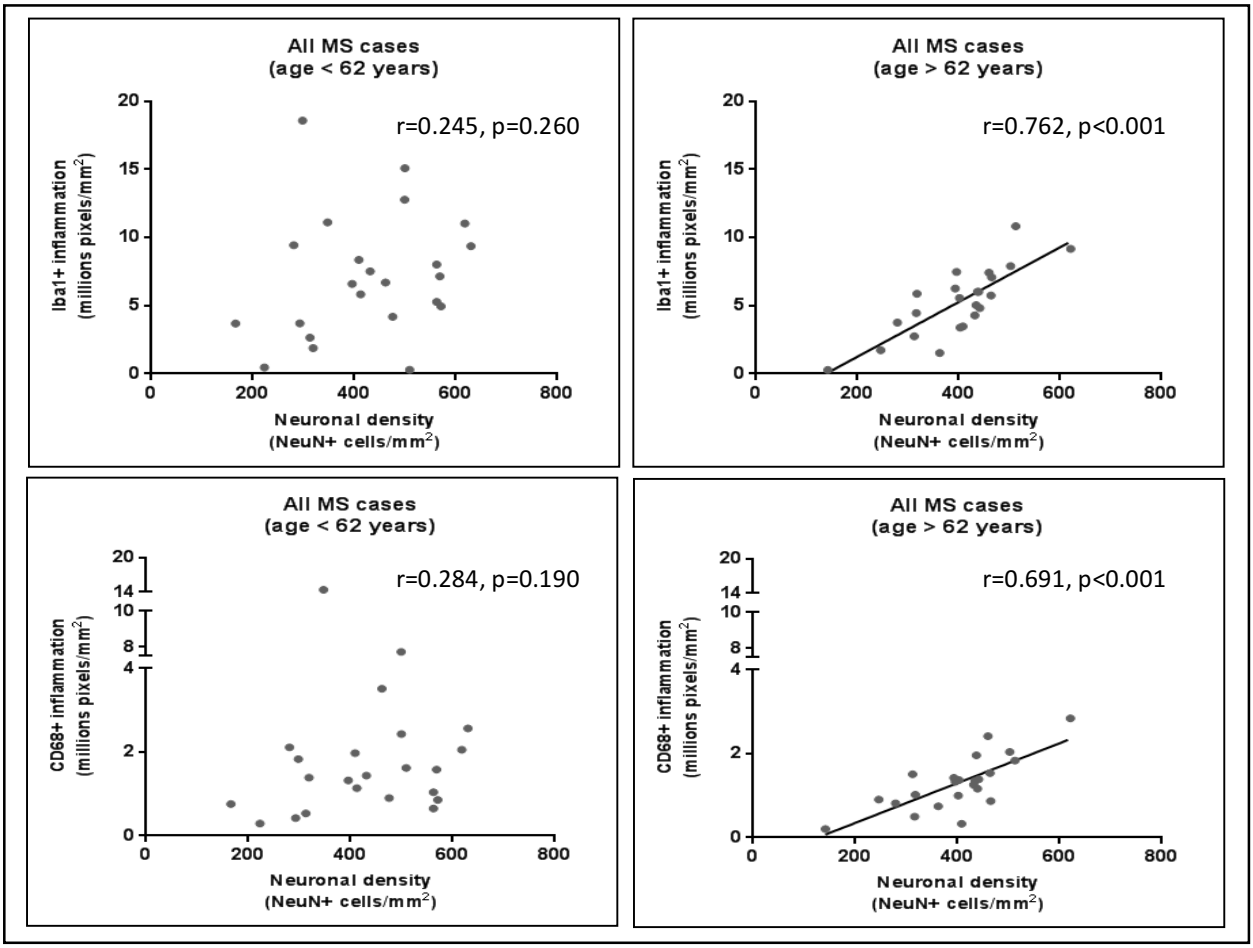


Figure 4.6: Relationship between microglia/macrophage inflammation and neuronal density in MS cases below and above the median age of the cohort (median age = 62 years)

4.3.5. Influence of *HLA-DRB1*15* status on the relationship between parenchymal microglia/macrophage inflammation and neuronal density

*HLA-DRB1*15* status had no impact on cortical neuronal density (15+: 417 ± 20 neurons/mm^2 vs. 15-: 411 ± 26 neurons/mm^2, p=0.766). This finding was consistent in cases under the age of 62 years (15+: 414 ± 44 neurons/mm^2 vs. 15-: 435 ± 35 neurons/mm^2, p=0.539) and over the age of 62 years (15+: 420 ± 20 neurons/mm^2 vs. 15-: 378 ± 39 neurons/mm^2, p=0.246) (figure 4.7).

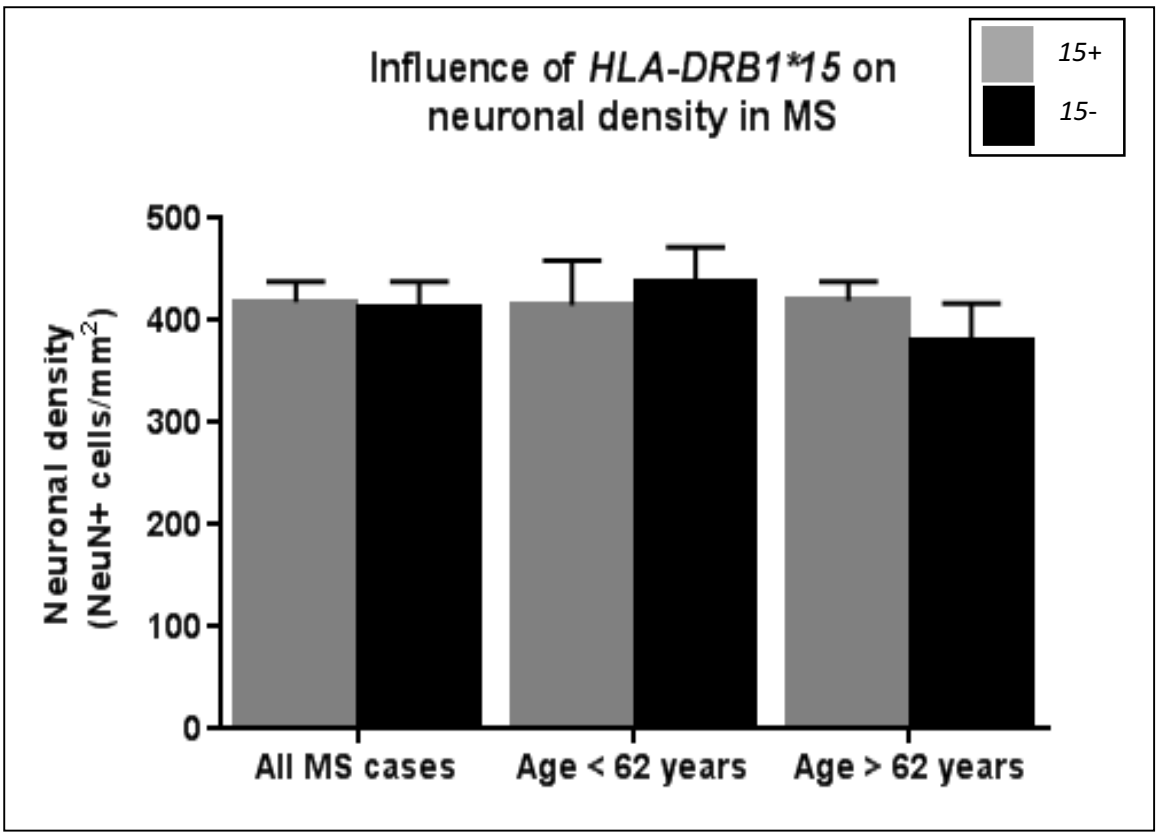


*Figure 4.7: Impact of HLA-DRB1*15 status on neuronal density in all MS cases, MS cases under 62 years, and MS cases over 62 years*

The relationship between microglia/macrophage inflammation and neuronal density was explored further in the context of *HLA-DRB1*15* status, given the striking age-related findings presented above, and the role of *HLA-DRB1*15* on the extent of inflammation as outlined in chapter 2. Microglia/macrophage

inflammation positively correlated with neuronal density in *HLA-DRB1*15*- MS cases only (Iba1+: r=0.722, p=0<0.001; CD68+: r=0.638, p<0.001). No relationship between microglia/macrophage inflammation and neuronal density was detected in *HLA-DRB1*15*+ MS cases (Iba1+: r=0.161, p=0.498; CD68+: r=0.211, p=0.373) (Figure 4.8).

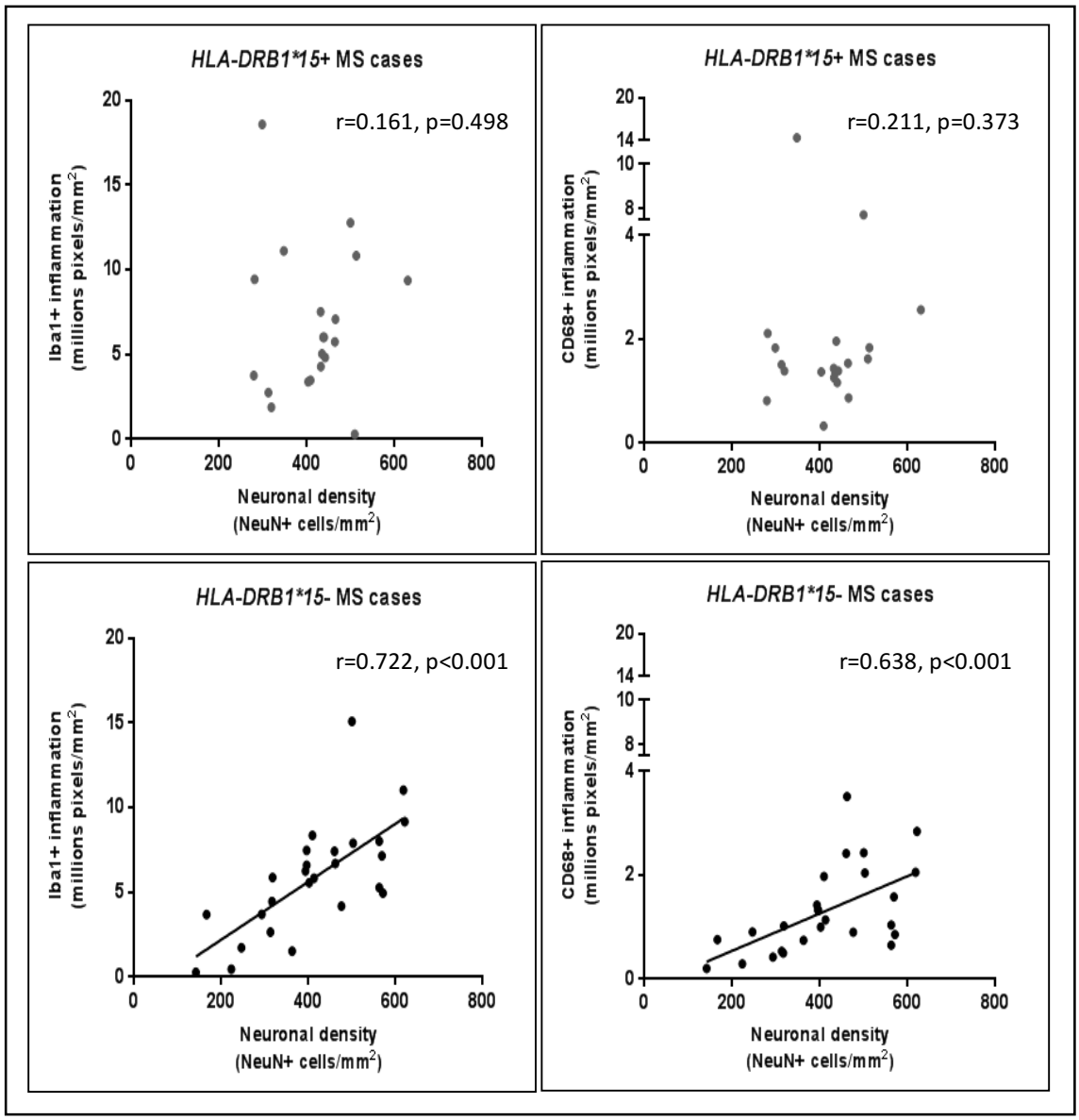


*Figure 4.8: Relationship between microglia/macrophage inflammation and neuronal density in HLA-DRB1*15+ and HLA-DRB1*15- genotype groups*

To compare the relationships between motor cortical microglia/macrophage inflammation and neuronal density in *HLA-DRB1*15* positive and negative genotype groups, multiple linear regression analyses were run with neuronal density used as the dependant variable. Demographic factors were added as independent variables and extracellular fibrinogen deposition was also included to factor out the impact of this variable given our findings in chapter 3.

The regression includes an interaction term between *HLA-DRB1*15* status and either Iba1+ inflammation or CD68+ inflammation, to allow comparisons between genotype groups within the same regression model (Tables 4.5 and 4.6). Given the way in which *HLA-DRB1*15* is coded in the regression (0=15+, 1=15-), this interaction term represents the impact of *HLA-DRB1*15*- cases only. The regression models show that both Iba1+ and CD68+ inflammation are associated with neuronal density in *HLA-DRB1*15*- MS cases, but not HLA-*DRB1*15*+ MS cases, after correction for demographic factors and extracellular fibrinogen deposition, and when the whole MS cohort is assessed.

Table 4.5: Multiple linear regression analysis showing the interaction of *HLA-DRB1*15* status and Iba1+ inflammation to predict neuronal density

	Unstandardised coefficients		Standardised coefficient	t	Sig.
Independent Variable	**B**	**Std. Error**	**Beta**		
Age	0.003	1.145	0	0.003	0.998
Sex	6.84	31.093	0.026	0.22	0.827
Post-mortem interval	2.83	2.153	0.168	1.314	0.197
Extracellular fibrinogen	-50.841	18.816	-0.317	-2.072	**0.01**
HLA-DRB1*15	-186	54.611	-0.805	-3.406	**0.002**
Iba1+ (millions of pixels)	-2.492	5.411	-0.095	-0.544	0.59
HLA-DRB1*15 **X Iba1+ inflammation**	28.963	7.521	0.95	3.851	**0.00044**

Dependant variable: neuronal density

Table 4.6: Multiple linear regression analysis showing the interaction *of HLA-DRB1*15* status and CD68+ inflammation to predict neuronal density

	Unstandardised coefficients		Standardised coefficient	t	Sig.
Independent Variable	**B**	**Std. Error**	**Beta**		
Age	-0.168	1.169	-0.018	-0.144	0.887
Sex	42.28	32.565	0.162	1.298	0.202
Post-mortem interval	3.661	2.558	0.218	1.431	0.161
Extracellular fibrinogen	-51.089	20.262	-0.319	-2.521	**0.016**
HLA-DRB1*15	-147.194	45.081	-0.637	-3.265	**0.002**
CD68+ (millions of pixels)	-5.453	8.256	-0.105	-0.661	0.513
***HLA-DRB1*15* X CD68+ inflammation**	94.11	24.135	0.733	3.899	**0.00038**

Dependent variable: neuronal density

Stratification of our MS cohort for both *HLA-DRB1*15* allele status *and* age revealed additional observations.

In *HLA-DRB1*15*+ cases that died under 62 years, no relationship was observed between neuronal density and Iba1+ or CD68+ inflammation (Iba1+: r=-0.357, p=0.385; CD68+: r=-0.167, p=0.693). In *HLA-DRB1*15*- cases that died under 62 years, neuronal density was correlated with Iba1+ inflammation (Iba1+: r=0.614, p=0.015), but not CD68+ inflammation, although this trended towards significance (CD68+: r=0.468, p=0.079) (Figure 4.9).

In *HLA-DRB1*15*+ cases that died over 62 years, a relationship was detected between neuronal density and Iba1+ inflammation (r=0.864, p=0.001), but not CD68+ inflammation (r=0.309, p=0.355). In *HLA-DRB1*15*- MS cases that died over 62 years, both Iba1+ and CD68+ inflammation was associated with neuronal density (Iba1: r=0.864, p=0.001, CD68+: r=0.873, p<0.001) (Figure 4.10).

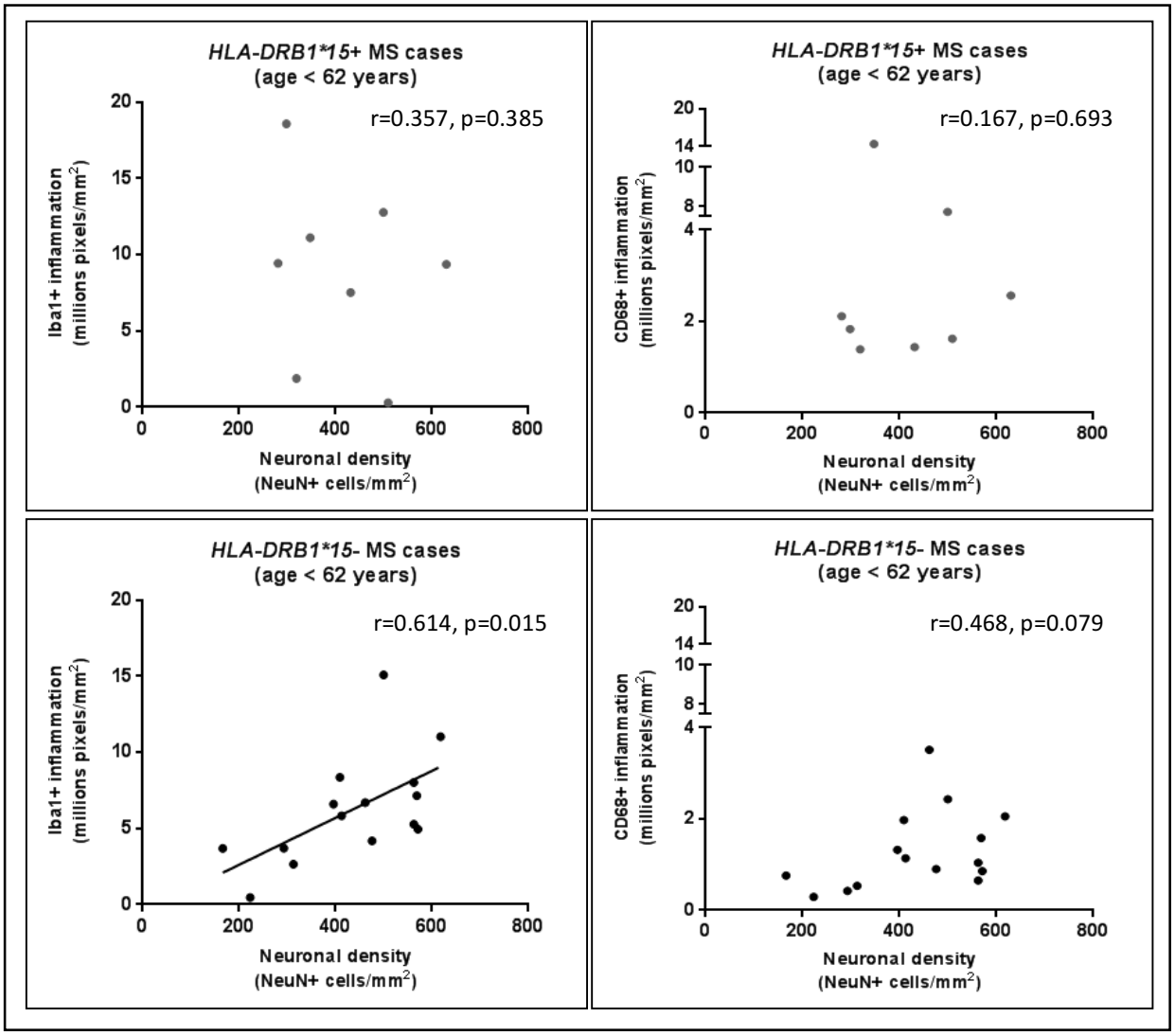


*Figure 4.9: Relationship between microglia/macrophage inflammation and neuronal density in HLA-DRB1*15+ and HLA-DRB1*15- MS cases under 62 years*

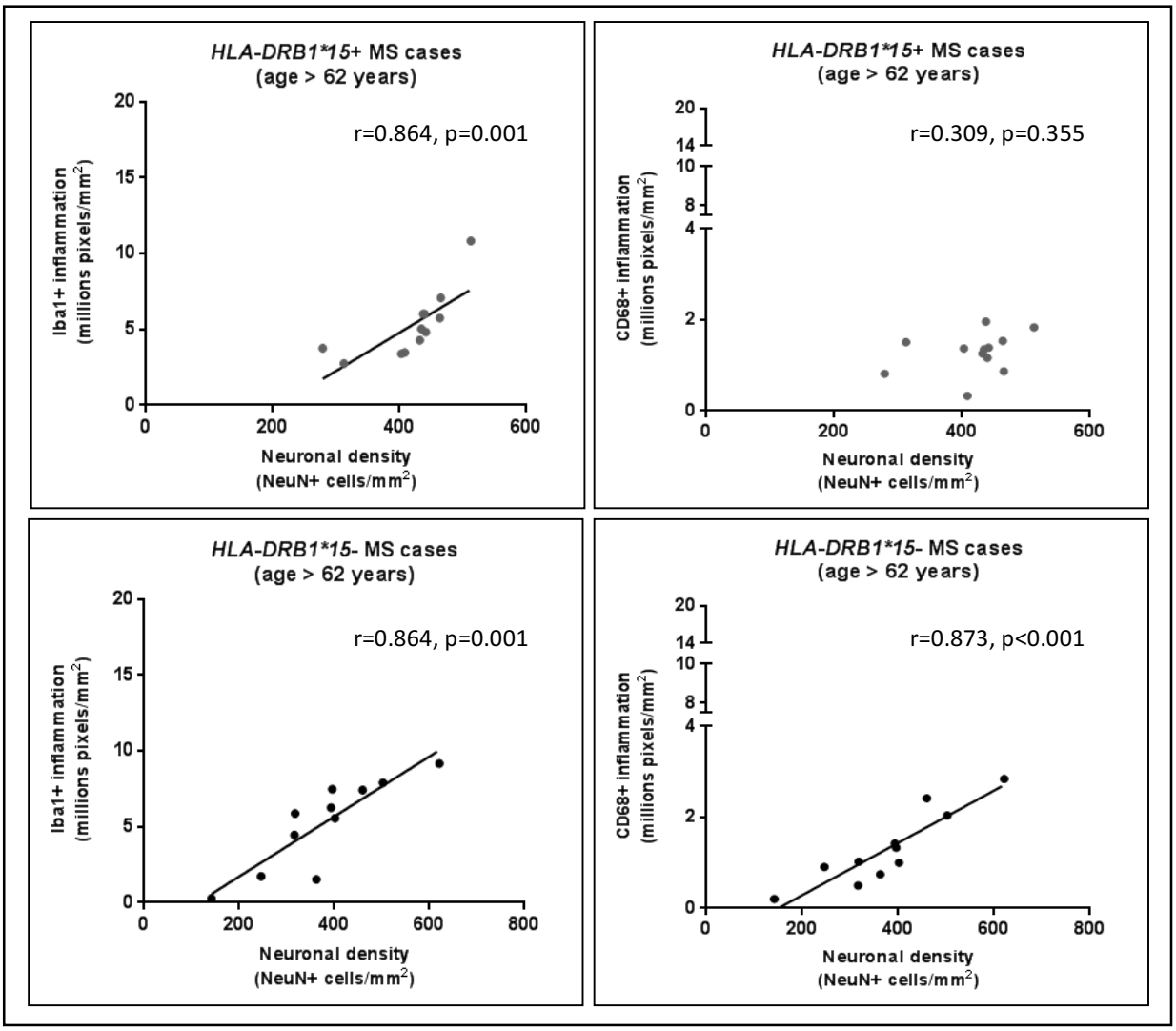


*Figure 4.10: Relationship between microglia/macrophage inflammation and neuronal density in HLA-DRB1*15+ and HLA-DRB1*15- MS cases over 62 years*

4.3.6. GAD in the MS motor cortex

The intriguing genotype- and age-dependant relationship between microglia/macrophage inflammation and neuronal density suggests that the contribution of microglia/macrophage inflammation to cortical neurodegeneration is complex in MS, and potentially beneficial in subgroups of cases. The expression of GAD has been linked to microglia/macrophage inflammation and neuroprotection. We therefore sought to assess the expression of motor cortical GAD, both at the synapse and within the cytoplasm.

Synaptic GAD+ neurons

4.3.6.1. Membrane-associated GAD+ synaptic density in MS and control

A 14% reduction in the density of membrane-associated GAD+ synapses was detected in MS compared to control (MS: 0.299 ± 0.006 synapses/μm^2 neuronal membrane vs. control: 0.348 ± 0.009 synapses/μm^2 neuronal membrane, p=0.005).

No difference in the density of membrane-associated GAD+ synapses was detected in *HLA-DRB1*15*+ MS cases compared to *HLA-DRB1*15*- MS cases (15+: 0.3 ± 0.008 synapses/μm^2 neuronal membrane vs. 15-: 0.297 ± 0.008 synapses/μm^2 neuronal membrane, p=0.493). As a result, membrane-associated GAD+ synapses were reduced relative to control in both *HLA-DRB1*15*+ (p=0.002) and *HLA-DRB1*15*- MS cases (p=0.017), when assessed separately (Figure 4.11A).

4.3.6.2. Relationships between membrane-associated GAD+ synaptic density, microglia/macrophage inflammation and neuronal density in MS and controls

In MS cases, membrane-associated GAD+ synaptic density was not correlated with either layer 5 microglia/macrophage inflammation (Iba1+: r=-0.036, p=0.880; CD68+: r=-0.012, p=0.960) or layer 5 neuronal density (r=0.164, p=0.490). *HLA-DRB1*15* status had no impact on the relationship between membrane-associated GAD+ synaptic density and layer 5 Iba1+ microglia/macrophage (15+: r=0.127, p=0.726; 15-: r=-0.042, p=0.907), layer 5 CD68 + microglia/macrophage (15+: r=-0.285, p=0.425; 15-: r=0.394, p=0.260), or layer 5 neuronal density (15+: r=0.127, p=0.726; 15-: r=0.067, p=0.855).

In controls, membrane-associated GAD+ synaptic density was not correlated with either layer 5 microglia/macrophage inflammation (Iba1+: r=0.107, p=0.819; CD68+: r=0.393, p=0.383) or layer 5 neuronal density (r=-0.393, p=0.383).

4.3.6.3. Assessment of GAD+ neuronal size

A 24% reduction in GAD+ neuronal size was detected in MS compared to control (MS: 403 ± 15 μm^2 vs. control: 531 ± 29 μm^2, p=0.001). *HLA-DRB1*15* status had a significant impact on GAD+ neuronal size, with *HLA-DRB1*15*+ neurons being 13% smaller than *HLA-DRB1*15*- neurons (15+: 376 ± 21 μm^2 vs. 15-: 432 ± 22 μm^2, p=0.018). When *HLA-DRB1*15*+ and *HLA-DRB1*15*- MS cases were assessed separately, only *HLA-DRB1*15*+ neurons demonstrated a significant reduction in GAD+ neuron size relative to control (15+: p<0.001; 15-: p=0.149) (Figure 4.11B).

4.3.6.4. Relationships between GAD+ neuronal size, microglia/macrophage inflammation, neuronal density, and GAD synapse in MS and controls

In MS cases, GAD+ neuronal size was not correlated with either layer 5 microglia/macrophage inflammation (Iba1+: r=-0.174, p=0.462; CD68+: r=0.143, p=0.548), layer 5 neuronal density (r=-0.371, p=0.107), or membrane-associated GAD synapse (r=0.054, p=0.230). *HLA-DRB1*15* status had no impact on the relationship between GAD+ neuronal size and layer 5 Iba1+ microglia/macrophage (15+: r=0.455, p=0.187; 15-: r=-0.248, p=0.489), layer 5 CD68 + microglia/macrophage (15+: r=0.394, p=0.260; 15-: r=-0.091, p=0.803), layer 5 neuronal density (15+: r=-0.188, p=0.603; 15-: r=-0.685, p=0.029), or membrane-associated GAD synapse (15+: r=0.104, p=0.099; 15-: r=0.008, p=0.902). In controls, GAD+ neuronal size was not correlated with either layer 5 microglia/macrophage inflammation (Iba1+: r=0.107, p=0.819; CD68+: r=0.357, p=0.432), layer 5 neuronal density (r=0.321, p=0.482), or membrane-associated GAD synapses (r=0.079, p=0.336).

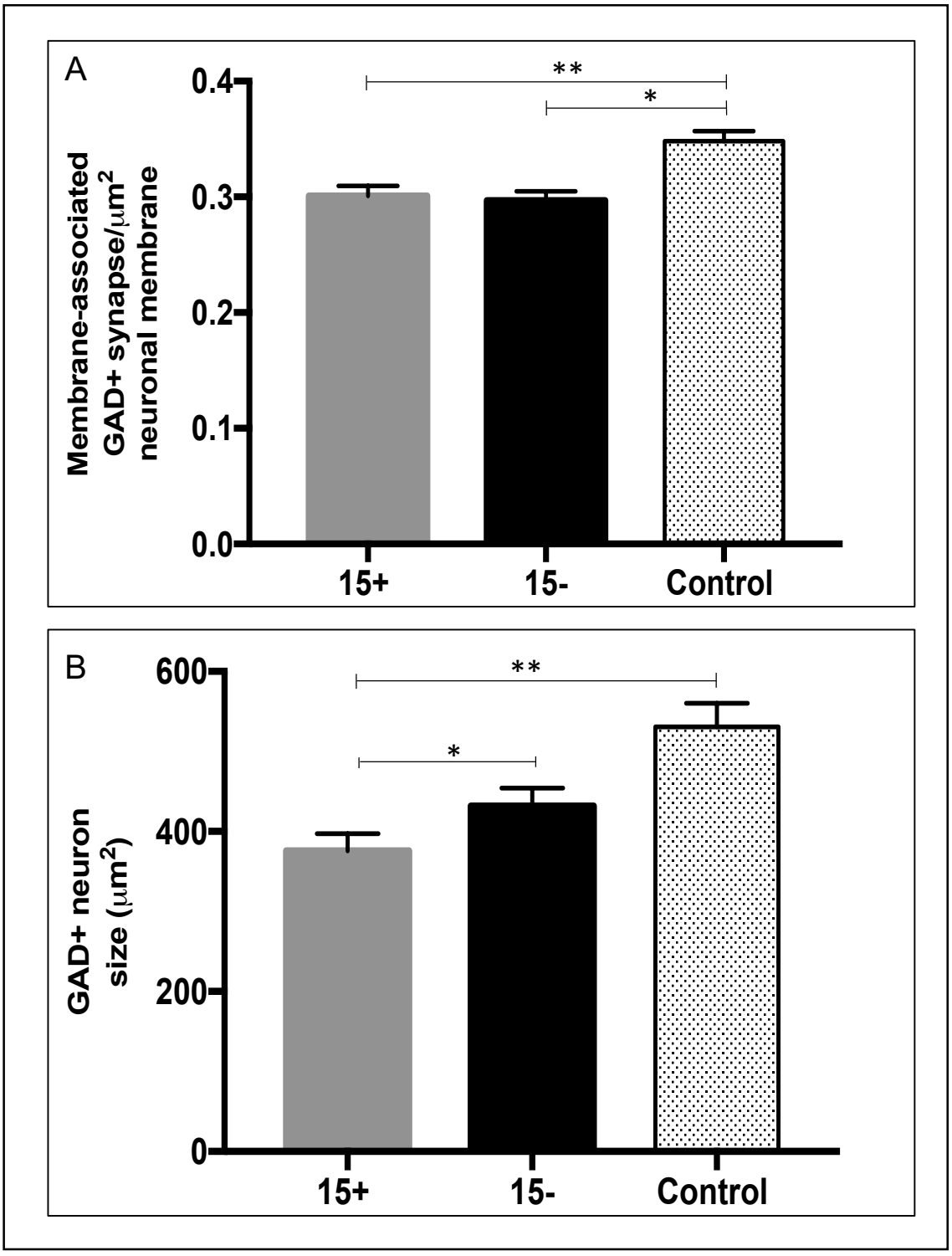


Figure 4.11: GAD+ neurons in MS and control. Membrane-associated GAD+ synapses were reduced in MS, regardless of *HLA-DRB1*15* genotype (A). GAD+ neurons were of smaller area in MS, particularly in the *HLA-DRB1*15*+ cohort (B). *=p<0.05 **=p<0.01

Cytoplasmic GAD+ neurons

4.3.6.5. Cytoplasmic GAD density in MS and control

There was no significant difference in the extent of GAD+ cytoplasmic density when MS cases were compared to controls (MS: 44 ± 3.5 cells/mm^2 vs. control: 42 ± 1.4 cells/mm^2, p=0.120). No significant difference in cytoplasmic GAD was detected in lesions compared to NAGM (Wilcoxon: z=0.571, p=0.568).

*HLA-DRB1*15* status had no impact on cytoplasmic GAD density (15+: 49 ± 5 GAD+/mm^2 vs. 15-: 41 ± 5 GAD+/mm^2, p=0.323). This finding was consistent both in cases under 62 years (15+: 41 ± 6 GAD+/mm^2 vs. 15-: 41 ± 6 GAD+/mm^2, p=0.573) and over 62 years (15+: 53 ± 8 GAD+/mm^2 vs. 15-: 41 ± 8 GAD+/mm^2, p=0.236).

4.3.6.6. Relationships between cytoplasmic GAD, microglia/macrophage inflammation and neuronal density in MS and controls

In MS cases, cytoplasmic GAD density positively correlated with neuronal density after correcting for Iba1+ and CD68+ inflammation in a partial correlation (r=0.459, p=0.002). In controls, there was no relationship between cytoplasmic GAD positivity and neuronal density, after correction for Iba1+ and CD68+ inflammation (r=0.500, p=0.253). With consideration of age, the relationship between cytoplasmic GAD and neuronal density was restricted to cases below 62 years (r=0.700, p<0.001). In contrast, no relationship between cytoplasmic GAD and neuronal density was observed in MS cases above 62 years (r=0.035, p=0.883). Similar relationships were not assessed in controls due to the small sample size precluding meaningful comparisons.

On considering relationships between inflammation and neurodegeneration in the MS cohort, microglia/macrophage inflammation was not correlated with cytoplasmic GAD, after correcting for neuronal density (Iba1: r=0.153, p=0.316; CD68: r=0.114, p=0.455). This finding was consistent both under 62 years (Iba1: r=0.290, p=0.190; CD68: r=0.353, p=0.107), and over 62 years (Iba1: r=0.365, p=0.104; CD68: r=-0.032, p=0.891). No relationship between microglia/macrophage inflammation and cytoplasmic GAD was detected in controls, after correcting for neuronal density (Iba1+r=-0.213, p=0.685; CD68: r=0.066, p=0.901).

*4.3.6.7. Influence of HLA-DRB1*15 on the relationship between cytoplasmic GAD and microglia/macrophage inflammation*

In *HLA-DRB1*15*- cases, cytoplasmic GAD was correlated with Iba1+ inflammation after correcting for neuronal density (r=0.446, p=0.025), given the positive relationship between cytoplasmic GAD positivity and neuronal density described previously (see 4.3.6.6). The relationship between Iba1+ inflammation and cytoplasmic GAD observed in the *HLA-DRB1*15*- cohort was driven by cases under 62 years (r=0.528, p=0.052), as no relationship was detected in cases over 62 years (r=0.469, p=0.172), after correcting for neuronal density. No relationship was observed between cytoplasmic GAD and CD68+ inflammation in *HLA-DRB1*15*- cases, after correction for neuronal density (r=0.273, p=0.186). This was consistent both for cases under 62 (r=0.310, p=0.281), and for cases over 62 (r=0.333, p=0.347).

In *HLA-DRB1*15*+ cases, no relationship between cytoplasmic GAD and microglia/macrophage inflammation was detected after correcting for neuronal density (Iba1+: r=-0.075, p=0.761; CD68: r=0.017, p=0.945). Similar results were observed in cases under 62 years (Iba1+: r=-0.003, p=0.995; CD68: r=0.600, p=0.154) and in cases over 62 years (Iba1+: r=-0.329, p=0.353; CD68: r=0.457, p=0.184).

4.4. Discussion

In the current study, we have comprehensively assessed the impact of parenchymal inflammation on neurodegeneration in the MS motor cortex. We show that the relationship between microglia/macrophage inflammation and neuronal density is influenced by age and *HLA-DRB1*15* status. We extend these findings by investigating motor cortical GAD, as a putative marker of neuroprotection. We show that membrane-associated GAD+ synapses are reduced in MS and that GAD+ neurons are smaller in MS compared to control cases, particularly within the *HLA-DRB1*15*+ cohort. We also report that cytoplasmic GAD expression is related to microglia/macrophage inflammation, but only in *HLA-DRB1*15*- MS cases. This study is therefore the first to link a genetic factor to neurodegeneration in the MS cortex and provides evidence of disease-related changes to GAD expression that are relevant to cortical tissue injury.

Neuronal loss is a characteristic feature of MS cortical pathology (Peterson *et al.*, 2001). This being said, there is no consensus on the extent to which neurons are lost, or determinant pathologic factors. Whilst some studies have detected subtle neuronal loss only in demyelinated cortical areas (Wegner *et al.*, 2006), others have reported substantial loss in NAGM (Klaver *et al.*, 2015) and evidence of oxidative injury and Wallerian degeneration (Haider *et al.*, 2016). In one of the largest assessments to date, significant neuronal loss was only observed in MS cases harbouring lymphoid-like structures in the sub-arachnoid space, wherein superficial neuronal loss implicated the presence of a diffusible neurotoxic factor

originating in the overlying meninges (Magliozzi *et al.*, 2010). However, the sub-arachnoid space is anatomically contiguous with penetrating perivascular spaces. The diffusion of factors into the brain parenchyma therefore likely influences MS pathology throughout the depth of the cortex. Consistent with this, in our cohort meningeal lymphocytic inflammation was associated with perivascular lymphocytic inflammation and parenchymal microglia/macrophage inflammation. The central role of HLA class II in lymphocyte activation suggests that genetic variation of relevant immune loci may influence T-cell activation and subsequent chemokine secretion in both meninges and the perivasculature to secondarily impact on parenchymal microglia/macrophage phenotypes (Goverman, 2009; Mantovani *et al.*, 2004).

In our series, we found that the relationship between microglia/macrophage inflammation and neuronal density was related to both ageing and *HLA-DRB1*15* status. Neurons were positively associated with microglia/macrophage inflammation except in younger cases, particularly within the *HLA-DRB1*15*+ cohort. These findings are therefore consistent with the notion that inflammation is more severe in *HLA-DRB1*15*+ cases, and further exemplifies the contribution of age to genetically-driven immune phenotypes. It has been demonstrated that microglia become more easily activated (VanGuilder *et al.*, 2011) and secrete greater amounts of pro-inflammatory cytokines during normal ageing (Sierra *et al.*, 2007), and lysosomal breakdown of damaged myelin has been shown to accelerate this process (Safaiyan *et al.*, 2016). Greater demyelination in young *HLA-DRB1*15*+ MS cases (as demonstrated in chapter 2)

may therefore lead to accelerated ageing of cortical microglia and a promotion of pro-inflammatory phenotypes that impacts on innate immune relationships with neurons. Together, these findings highlight the potentially contrasting contribution of microglia/macrophages to MS cortical pathology across different genetic backgrounds and at different ages.

Our data adds to the wealth of experimental evidence that has shown marked phenotypic heterogeneity in microglia/macrophage inflammation, with these cells implicated in both neurodegenerative and neuroprotective processes. Various reports have noted microglia/macrophage-mediated reactive oxygen (Fischer *et al.*, 2012), protease (Webster and Crowe, 2006) and inflammatory cytokine secretion (Kawanokuchi *et al.*, 2006), recruitment and activation of lymphocytes (Almolda *et al.*, 2015), and cytotoxicity (Takeuchi, 2010). Other studies have demonstrated microglia/macrophage-mediated promotion of axon (Batchelor *et al.*, 2002) and myelin regeneration (Miron *et al.*, 2013), clearance of cellular debris (Marín-Teva *et al.*, 2004), and secretion of neurotrophic factors (Bessis *et al.*, 2007). A preponderance of beneficial cortical microglia/macrophage inflammation in our cohort may explain why neurons exposed to chronic inflammation over many decades have largely survived (Chen and Trapp, 2016).

In a recent study, Trapp and colleagues demonstrated that microglia-mediated stripping of GAD+ synapses can protect neurons from inflammatory damage (Chen *et al.*, 2014). GAD catalyses the decarboxylation of glutamate to GABA, and

as such is the primary source of inhibitory neurotransmitter in the CNS. Reduced inhibitory innervation of motor neurons increases firing of synaptic NMDA and reduces cell death by stimulating phosphorylation of CREB and expression of BDNF to prevent apoptosis (Chen *et al.*, 2014). In our cohort, we investigated membrane-associated GAD synaptic density using a novel computational algorithm and found evidence of significant inhibitory synaptic loss in MS, consistent with previous reports that have detected disturbed inhibitory neurotransmission in MS cortex based on transcript analysis of GAD mRNA (Dutta *et al.*, 2006). Whilst we were unable to relate GAD synaptic density to microglia/macrophage inflammation or neuronal density, the fact that inhibitory synaptic stripping occurs on time-scales measured in days likely renders such relationships difficult to discern in human autopsy material (Chen *et al.*, 2014).

Whether loss of GAD synapses in MS represents a neuroprotective strategy is not clear. Increased neuronal firing will likely increase neuronal stress when ATP synthesis is already reduced through oxidative injury and mitochondrial dysfunction, as has been demonstrated in MS cortex (Fischer *et al.*, 2013). Whilst the reduction in GAD synapses in our cohort occurred in the apparent absence of substantial neuronal loss, functionally-relevant changes to cortical neurons likely extend beyond overt loss of cellularity. In the current study, we have demonstrated that layer 5 GAD+ neurons are smaller in MS, particularly in the *HLA-DRB1*15*+ cohort. This is consistent with the findings of a recent study that demonstrated reduced neuronal size in MS cortex (Klaver *et al.*, 2015). Whether changes to neuronal size correlate with motor deficit is unknown, and will

require additional investigation. However, the apparent exacerbating effect of carrying the *HLA-DRB1*15* allele again suggests that parenchymal inflammation plays a key role in dictating cortical neuronal outcome.

In addition to assessing relationships between synaptic GAD, microglia/macrophage inflammation and *HLA-DRB1*15* status, we also assessed associations with cytoplasmic GAD. The function of cytoplasmic GAD is poorly defined. However, its subcellular localisation probably reflects a role independent of neurotransmission (Pinal and Tobin, 1998). Intriguingly, cytoplasmic GAD is up-regulated after ischaemic stroke (Li *et al.*, 2010) and excitotoxic injury (Falkenberg *et al.*, 1997), wherein expression may provide trophic support to neurons (Pinal and Tobin, 1998). In our cohort, cytoplasmic GAD positively associated with neuronal density, and in *HLA-DRB1*15*- MS cases associated with microglia/macrophage inflammation. Previous work has shown a reduction in GAD-67 mRNA in cortical MS tissue (Dutta *et al.*, 2006), the majority of which would be expressed in neuronal cytoplasm. Whilst we did not detect a difference in cytoplasmic GAD in MS versus controls, this may relate to regional variation in the expression of cytoplasmic GAD throughout the cortex (Bowers *et al.*, 1998). Further work will now be necessary to probe the temporal dynamics of cytoplasmic GAD expression and parenchymal microglia/macrophage inflammation, and the genetic impact therein, in order to further our understanding of the influence of these relationships on cortical neurodegeneration in MS.

Our study provides evidence that ageing and genetic variation at the *HLA-DRB1* allele influences the relationship between microglia/macrophage inflammation and cortical neuronal density. We extend these findings by showing that neuroprotective strategies previously shown to be driven by microglia in rodents, may also be operative in the human MS cortex. We have detected significant inhibitory synaptic loss and show that cytoplasmic GAD is related to microglia/macrophage inflammation only in *HLA-DRB1*15*- cases. Taken together, these findings suggest that innate inflammation, *HLA-DRB1*15* status, and GAD, may interact in the MS cortex and have relevance to neuronal survival. Future studies will now assess the mechanism by which genetic variation at the *HLA-DRB1* locus influences motor cortical inflammation and GAD expression and the relevance of these disease mechanisms to clinical outcome.

5. MRI-pathology correlations in the multiple sclerosis corticospinal tract

5.1. Introduction

This thesis has provided substantial insight into the pathogenesis of motor cortical tissue injury in MS. We have found that *HLA-DRB1*15* status plays an important role in sculpting the severity of cortical demyelinating and inflammatory pathology, as well as relationships between microglia/macrophage inflammation and cortical neurons. We have also identified fibrinogen deposition as a novel component of cortical pathology that associates with neuronal loss. The results presented thus far have therefore improved our understanding of how genetic factors and parenchymal inflammation influence neuronal survival, and suggest that cortical demyelination does not in itself contribute to cortical neurodegeneration. However, MS is a diffuse disease of the entire CNS, and neurons in motor cortical layer 5 project axons into the CST before their eventual termination in the spinal cord. In the current chapter, we combine post-mortem MRI with quantitative histology to assess how global CST lesion burden impacts on neurodegeneration in motor cortical layer 5.

Many studies of MS neuropathology have assessed how the demyelinated plaque relates to neuroaxonal loss. Although axonal loss occurs in both acute (Trapp *et al.*, 1998) and chronic MS lesions (Lovas *et al.*, 2000), the conflation of evidence suggests that the correlation between global demyelination and

neurodegeneration is surprisingly weak (DeLuca *et al.*, 2006). Factors independent of plaque formation are therefore likely to play a key role in the progression of degenerative pathology in MS. The detection of extensive neuroaxonal loss in normally myelinated areas (Evangelou *et al.*, 2000; Klaver *et al.*, 2015), and the fact that current therapies fail to substantially reduce long-term disability outcome despite having a significant impact on lesion formation, supports this view (Coles *et al.*, 1999).

A limitation of many studies that have assessed the contribution of demyelination to neurodegeneration is that they fail to take into account the extensive connectivity of the CNS. Evidence suggests that the extent of neurodegeneration correlates between anatomically connected structures in MS (Kolasinski *et al.*, 2012), and that lesional burden can associate with distant NAWM axonal loss in anatomically eloquent structures such as the corpus callosum (Ciccarelli *et al.*, 2003; Evangelou *et al.*, 2000). Taken together, these observations suggest that neurodegeneration in MS may spread in a tract-specific pattern, and be linked to demyelination of connected white matter. Evidence of Wallerian degeneration has recently been detected in MS cortex, thus implicating these disease mechanisms in the progression of cortical pathology, of which the cause remains largely unknown (Haider *et al.*, 2016).

Investigating the association of pathology between distant anatomic sites in MS is technically challenging. Whilst histology provides sub-cellular resolution and the ability to quantify neuroaxonal loss, sampling is necessarily restricted by

limitations of time, available material and tissue-section thickness. MRI, in contrast, enables global assessments of white matter demyelinating pathology but lacks sufficient resolution to quantify complete disease burden. This is particularly true in the cortex, where demyelination is poorly resolved even with advance sequences (Kilsdonk *et al.*, 2016). In order to investigate this critical knowledge gap, it is therefore necessary to combine histology with MRI-derived metrics. Doing so provides a unique opportunity to assess neuropathological relationships between cortical and subcortical tissue injury that are impervious to either technique when used in isolation.

In the current study, we combine radiographic quantitation of lesion burden impinging on the cerebral hemispheres and spinal cord CST with a comprehensive histologic assessment of cortical demyelination, microglia/macrophage inflammation and neuronal density throughout the length of the motor cortex. We show that within MS cases motor cortical pathology does not vary significantly, despite there being substantial differences *between* MS cases. Radiographic lesional burden impinging on the CST is more severe in the spinal cord compared to the brain, but does not appear to relate to motor cortical neurodegeneration in either location. This is the first study to assess the contribution of radiographic lesional burden to cortical pathology in MS and suggests that motor cortical neurodegeneration may progress independently of diffuse injury within the CST.

5.2. Materials and Methods

5.2.1. Study population

This study was performed on formalin-fixed whole brains and spinal cords derived from patients with a pathologically confirmed diagnosis of MS (n=10). Material was obtained from the UK MS tissue bank, Imperial College London, and the Oxford Brain bank, Oxford.

5.2.2. Histology

5.2.2.1. Tissue sampling

Primary motor cortex was sampled by anatomic identification of the precentral gyrus by a qualified neuropathologist. Tissue blocks were sampled at consistent intervals from mesial to lateral precentral gyrus (i.e. n=5 per hemisphere; n=10 per case; n=100 total). In addition, n=2 spinal cords (MS1 and MS2) were assessed in detail to investigate whether relationships identified between microglia/macrophage inflammation and motor cortical neuronal density, as described in chapter 4, are maintained in the lateral corticospinal tract. Each spinal cord was sampled at 1cm intervals throughout the entire available length, creating n=20 tissue blocks for MS1 and n=19 tissue blocks for MS2.

5.2.2.2. Immunohistochemistry

Formalin-fixed paraffin-embedded tissue blocks were cut into 6μm thick sections and labelled with primary antibodies to myelin (PLP), microglia/macrophages (Iba1) and activated microglia/macrophages (CD68+) using DAB immunohistochemistry (Appendix 1). Sections were counter-stained with haematoxylin. H&E staining was performed to enable quantitation of motor

cortical neurons given the inability of antibodies targeting NeuN to reliably label long-fixed tissue (Gill *et al.*, 2005). Appropriate sampling of motor cortex was confirmed by the presence of Betz cells in cortical layer 5. Spinal cord sections cut at 10μm thickness were impregnated with Palmgren's silver to delineate axons, as previously described (DeLuca *et al.*, 2013).

5.2.2.3. Assessment of motor cortical demyelination

Demyelination in the motor cortex was defined as the complete absence of myelin. Areas of motor cortical demyelination were quantified and related to the sampled cortical length and reported as mm^2/mm cortical length, as described in chapter 2.

5.2.2.4. Assessment strategy of motor cortical layer 5 microglia/macrophage inflammation and neuronal density

To gather a more detailed assessment of the functionally relevant projection layer 5, specific motor cortical pathologic outputs (i.e microglia/macrophage inflammation and neurons) were examined. Photomicrographs were acquired in layer 5 at 400x magnification, within systematically spaced trajectories arranged perpendicular to the subpial surface. For each trajectory, n=4 images were acquired in cortical layer 5 for each analysis. Analyses were restricted to normal-appearing areas given that motor cortical lesions only rarely affected infragranular cortical layers (Lars Bø *et al.*, 2003). Approximately 1,700 images were acquired for each analyses (n=5,100 total). Acquired photomicrographs were analysed as outlined below.

5.2.2.5. Motor cortical layer 5 microglia/macrophage inflammation

Photomicrographs acquired of microglia/macrophage inflammation (Iba1+ and CD68+) were assessed using a semi-automatic colour-based extraction method and are reported as pixels/mm^2, as outlined in chapter 2 (Figure 2.2).

5.2.2.6. Motor cortical layer 5 neuronal density

Layer 5 neurons in H&E stained sections were quantified by manually identifying larger pyramidal cells with a prominent nucleolus in each acquired photomicrograph (Figure 5.1). In total, approximately 10,500 neurons were counted across the cohort and are expressed as neurons/mm^2.

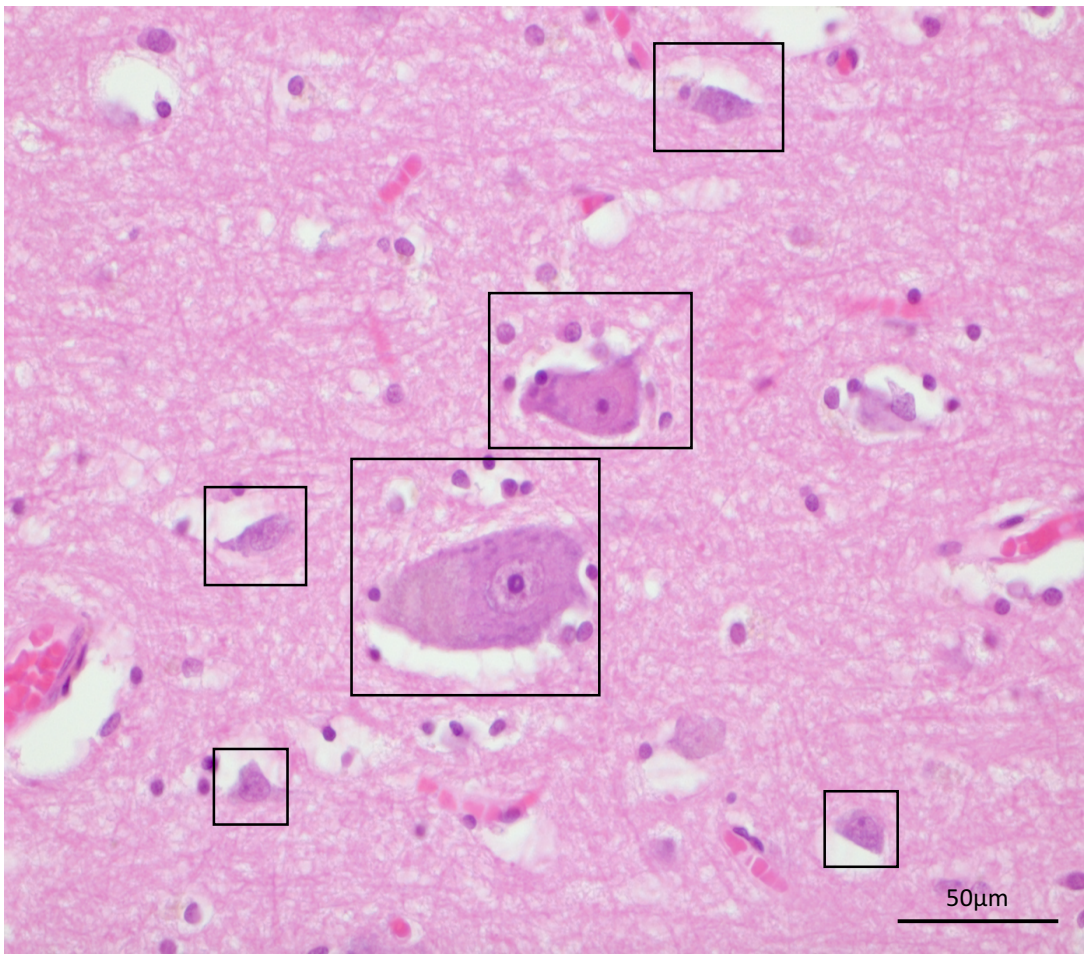


Figure 5.1: Neuronal counting method. Motor cortical neurons were manually identified on H&E-stained sections due to suboptimal neuronal labeling with NeuN in the current cohort. Neurons were defined as larger cells with a pyramidal morphology and prominent nucleolus, and are demonstrated with black borders in the image above.

5.2.2.7. Subgroup analysis of spinal cord LCST demyelination, microglia/macrophage inflammation and axonal density/number

The spinal cord LCST was defined as extending laterally from the posterior edge of the central grey to the edge of the cord. The mesial and posterior limits of the LCST were defined by the dorsal horn (Figure 5.2). Areas of LCST demyelination were quantified and related to notional LCST area. Pathologic outputs (i.e. Iba1+ microglia/macrophage inflammation and axonal density) were quantified in the LCST of each side of the cord. For each analysis, n=5 FOVs were systematically delineated creating approximately 200 FOVs per analysis per cord. For Iba1+ microglia/macrophage analysis, FOVs were drawn using Aperio ImageScope software, and analysed using a commercial pixel-counting algorithm, with data presented as millions of pixels/mm^2. For axonal density analysis, photomicrographs of each FOV were acquired at 400x magnification. Axonal density was quantified with a particle-counting algorithm within ImageJ software, expressed as axons/mm^2. Estimates of total LCST axonal number were gained by multiplying axonal density measures by total LCST notional area.

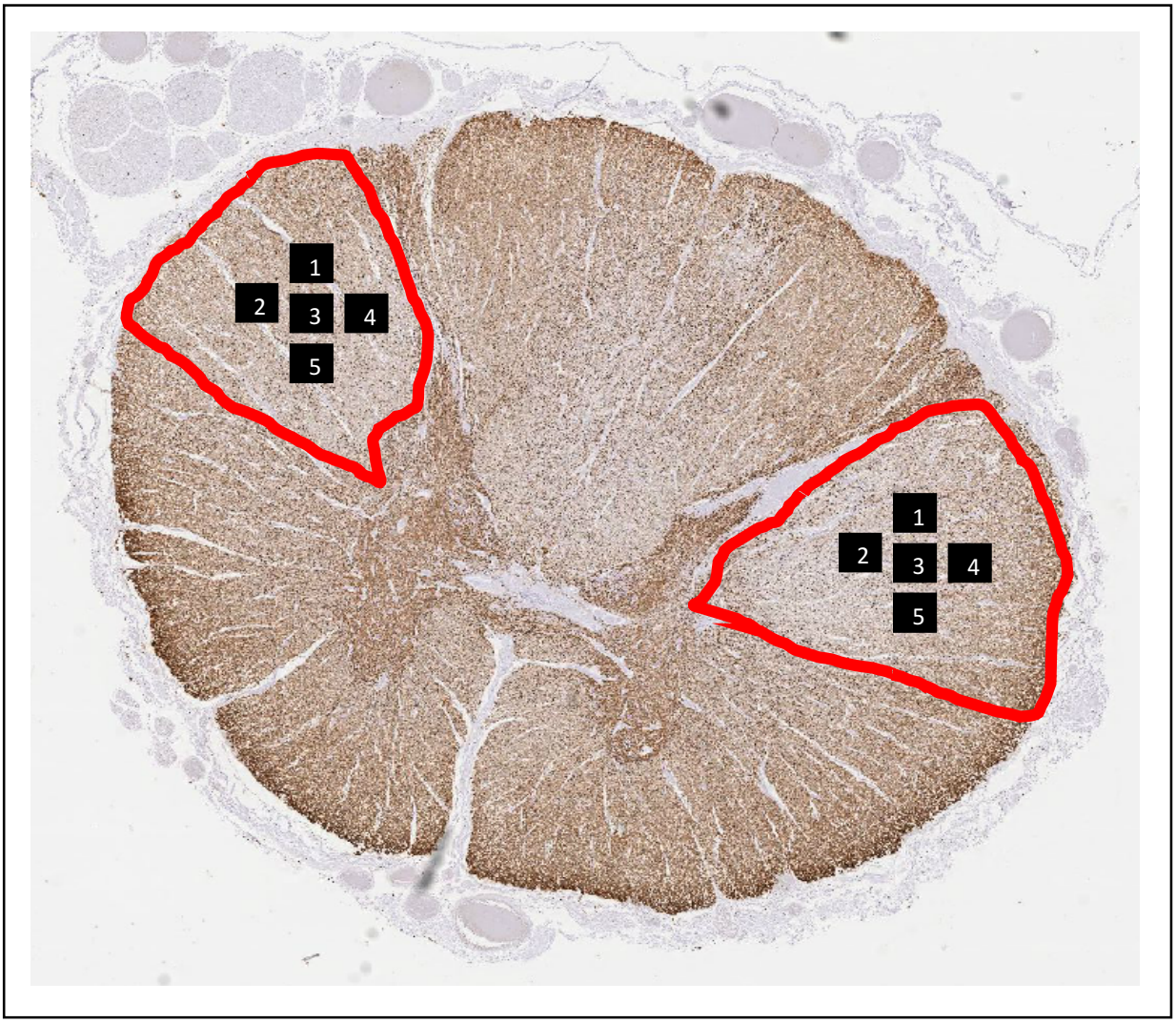


Figure 5.2: Spinal cord histology. The LCST (depicted in red) was delineated on each side of the spinal cord by identifying the posterior limit of the central grey and extending laterally to the edge of the cord. The mesial and posterior limits of the LCST were defined by the dorsal horn. LCST lesion burden was assessed by manually delineating areas of demyelination (not shown) and relating to notional LCST area (mm^2). Within each delineated LCST, n=5 field of views (black boxes) were spaced at systematic intervals for both Iba1+ microglia/macrophage and axonal density/number analyses, and analysed as outlined in the main text.

5.2.3. Cerebral hemispheric MRI

5.2.3.1. Cerebral hemispheric radiographic image acquisition

All cerebral hemispheric MRI data was acquired previously with a 3T Siemens scanner using a 12-channel head coil at FMRIB, Oxford, as reported (Kolasinski *et al.*, 2012). Structural data was acquired using a 3D balanced steady-state-free precession sequence (TR=7.4ms, TE=3.7ms, bandwidth=302 Hz/pixel, resolution=0.5x0.5x0.5mm). T_2-weighted B_0 volumes were acquired using diffusion-weighted MRI sequences (TR=530ms, TE=122ms, bandwidth=302 Hz/pixel, resolution=0.94x0.94x0.94) and were used in the current study to aid in the identification of cerebral hemispheric lesions given the strong hyper-intense signal emitted by plaques using this sequence.

5.2.3.2. Cerebral hemispheric radiographic image analysis

Cerebral hemispheric MRI images were analysed in order to quantify lesional burden impinging on the CST in both right and left cerebral hemispheres. Initial attempts to define the cerebral hemispheric CST using probabilistic tractography failed due to the suboptimal and highly variable diffusion of water in post-mortem fixed specimens. Registration of *in vivo* mapped tracts to our post-mortem cohort also failed due to inherent differences in tissue architecture of *in vivo* compared to post-mortem material. Cerebral hemispheric CST was therefore manually delineated, using *in vivo* mapped tracts and anatomic landmarks as a guide, on each structural cerebral hemispheric MRI slice. A second observer confirmed the anatomic localisation of the CST in the cerebral hemispheric MRI scans. Cerebral hemispheric CST was delineated in the medullary pyramids, pons and cerebral peduncles of the brainstem before

entering the posterior limb of the internal capsule. Passage of the CST through the cerebrum was guided by the posterior aspects of putamen, thalamus and then caudate. Beyond the cerebral ventricles, CST delineation proceeded in a rostral vertical line until reaching the precentral gyrus.

Cerebral hemispheric lesions were defined as distinct areas of hyper-intense signal on T_2-weighted B_0 scans, as previously described (Kolasinski *et al.*, 2012). Identified lesions were masked on structural volumes due to the greater anatomic accuracy allowed by this higher-resolution acquisition. Lesion burden impinging on the CST was quantified by computing lesion/CST overlay and relating this to total CST area for each hemisphere, and is expressed as percent cerebral hemispheric CST radiographic lesional burden.

5.2.4. Spinal cord MRI

5.2.4.1. Spinal cord radiographic image acquisition

Whole spinal cord material was scanned in a custom built holder (Figure 5.3). Spinal cords were imaged with a 7T Siemens scanner using a 24-channel receive coil in collaboration with colleagues at FMRIB, Oxford. Specimens were placed into the spinal cord holder and submerged in fluorinert. Proton-density-weighted structural data was acquired using a 2D spin-echo sequence (TR=3500ms, TE=15ms, bandwidth=200Hz/px, resolution=0.12x0.12x1mm). Whole spinal cord data was acquired in two or three acquisitions depending on the size of each cord. Stitching together of each acquisition was completed manually and with automated affine registration using the FSL software library to derive a single output of whole spinal cord for each case.

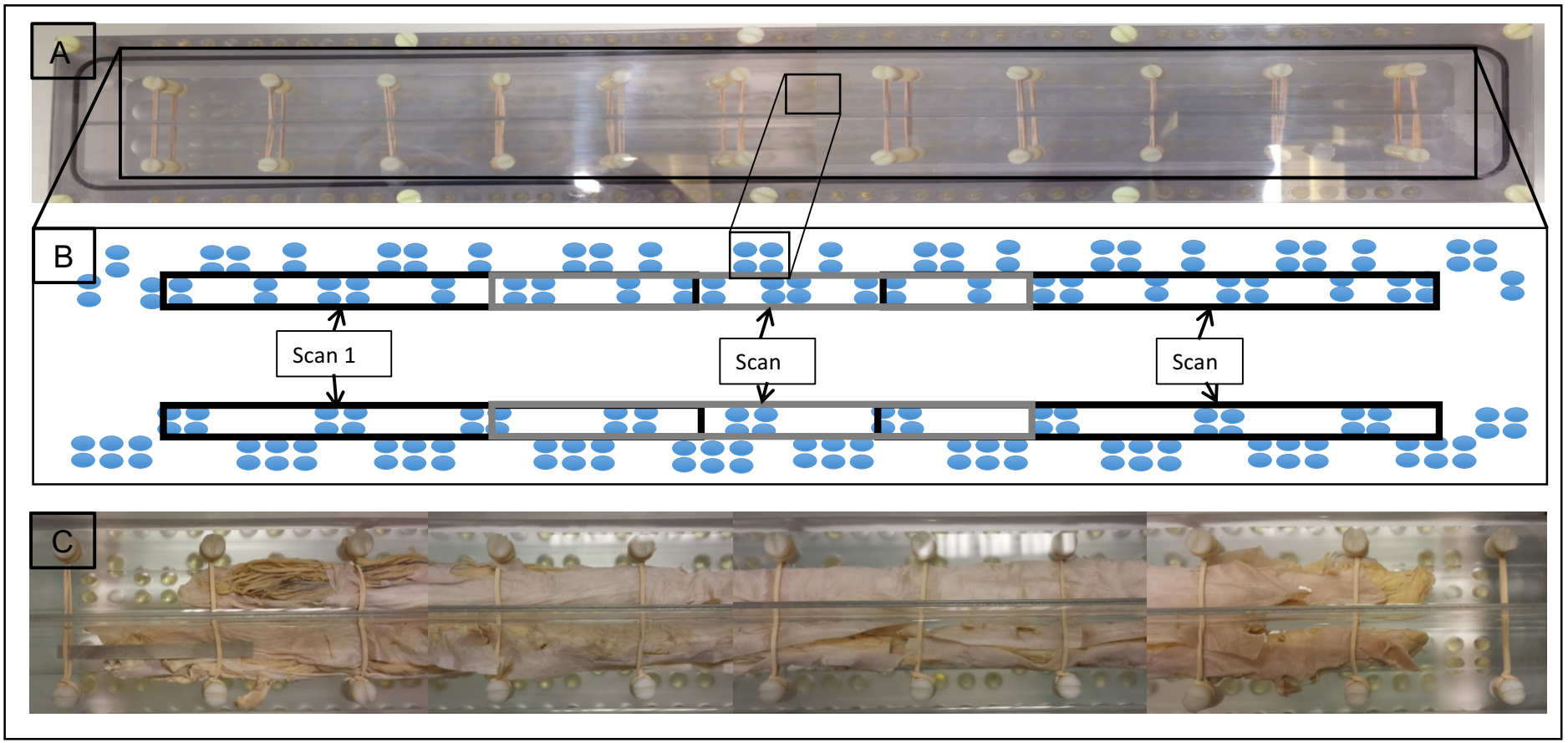


Figure 5.3: Spinal cord MRI acquisition. MRI acquisition of whole post-mortem spinal cord (SC) material necessitated the use of a novel SC holder (A), constructed by colleagues in the Department of Physics, Oxford, and based on designs by the current author. A schematic representation of the SC holder is shown in (B). The design of the SC holder included the provision of fiducial markings (vitamin D tablets; blue circles) that allow MRI data to be correlated with pathologic outputs as a result of hyper-intense signal arising from vitamin D after exposure to RF pulses. MRI data was acquired in two of three scans depending on the size of each SC, with scans necessarily overlapping (B). Data was stitched together after acquisition to derive complete, non-overlapping, proton-density-weighted images for each SC that were then analysed as outlined in the main text. An example of two SCs housed in the holder awaiting MRI acquisition is given in (C).

5.2.4.2. Spinal cord image analysis

Spinal cord MRI images were analysed in order to quantify lesional burden impinging on the LCST of each side of available spinal cord. The LCST was manually delineated on each proton-density-weighted MRI slice throughout the length of available cord. The anterior limit of the LCST was defined by the posterior edge of the central grey, extending laterally to the edge of the cord. The posterior and mesial limits of the LCST were defined by the dorsal horn.

Spinal cord lesions were defined as distinct areas of hyper-intense signal on proton-density-weighted scans. Identified lesions were masked and overlaid onto each predefined LCST. Total LCST lesional burden was quantified by relating proton-density–weighted hyper-intensity area that overlapped the LCST to total LCST area, expressed as percent spinal cord LCST radiographic lesional burden.

Spinal cord lesional burden was combined with cerebral hemispheric lesional burden to generate a combined metric encompassing the entire subcortical CST, and is expressed as “percent global CST radiographic lesional burden”.

CST radiographic lesion burden in both the cerebral hemispheres and in the spinal cord, as well as our “global” score, was related to motor cortical pathologic outputs (i.e. demyelination, microglia/macrophage inflammation and neuronal density) (Figure 5.4).

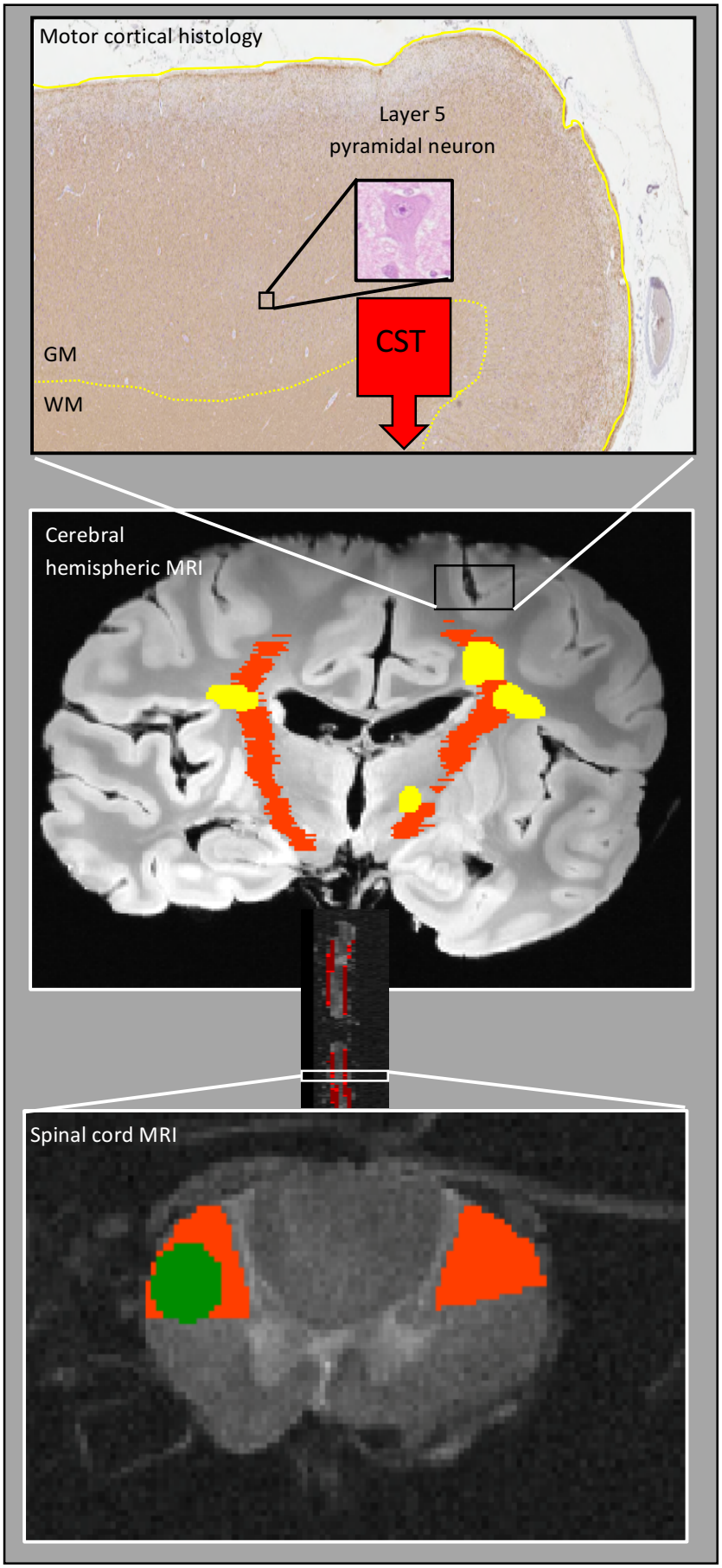


Figure 5.4: Summary of analysis strategy for motor cortex, cerebral hemispheres, and spinal cord. Neuronal density (visualised with H&E) was assessed in layer 5 of the motor cortex. Within each MS case, radiographic lesions impinging on the cerebral hemispheric CST and spinal cord LCST were quantified and related to motor cortical neuronal density. Red masks represent the CST in brain and spinal cord. Yellow and green masks represent radiographic lesions in the brain and spinal cord, respectively. In addition to neuronal density, demyelination and microglia/macrophage inflammation were quantified in the motor cortex, but are omitted from the figure for simplicity.

CST = corticospinal tract, GM = grey matter, WM = white matter

5.2.5. Statistical analyses

Relationships between continuous pathologic variables were assessed using Spearman rank correlation coefficients. Distribution of data was assessed analytically and graphically and transformed as required. Data are presented ± SEM. ANOVAs were used to compare data within MS cases where independent variables had more than one value (i.e. cortical regions 1-5). All tests of hypotheses were carried out using two-sided tests. In all analyses, P-values less than 0.05 were considered significant. Statistical analyses were done using SPSS v21 software.

5.3. Results

5.3.1. Demographic features of cohort

Demographic features of the cohort are found in table 5.1 below.

Table 5.1: Clinical details of cohort used in chapter 5

Case	Post-mortem interval (hrs)	Age (yrs)	Sex	Clinical phenotype	Disease duration (yrs)	Cause of death
MS1	30	60	F	SPMS	36	Pneumonia
MS2	48	64	M	RRMS (unclear if disease progressed)	43	Thrombo-embolism
MS3	26	79	F	SPMS	55	Pneumonia
MS4	59	72	M	SPMS	28	Pneumonia
MS5	69	50	F	SPMS	22	Metastatic breast cancer
MS6	37	66	M	SPMS	15	Prostate cancer
MS7	54	86	F	PPMS	54	Lymphoma
MS8	21	60	F	SPMS	11	MS
MS9	66	69	F	SPMS	37	MS
MS10	40	74	F	PPMS	33	Sepsis

MS = multiple sclerosis, SPMS = secondary progressive MS, PPMS = primary progressive MS, M = male, F = female

5.3.2. Motor cortical neuropathological findings

5.3.2.1. Cortical lesions

Motor cortical demyelination was observed in 8/10 cases, with significant variability detected between cases (mean: 0.185 ± 0.155 mm^2/mm cortical length; between-case ANOVA $p<0.001$). Within a given case where demyelination was detected, there was no significant difference in lesional burden between sampled motor cortical regions (between-region ANOVA within a given case: MS1, p=0.168; MS3, p=0.623; MS4, p=0.503; MS5, p=0.101; MS6, p=0.645; MS8, p=0.922; MS9, p=0.444; MS10, p=0.47) (Figure 5.5). Across the whole cohort, the motor cortical regions sampled demonstrated similar levels of demyelination regardless of the anatomic location (between-region ANOVA across whole cohort: p=0.983) (Figure 5.9).

5.3.2.2. Layer 5 microglia/macrophage inflammation

A comparison of layer 5 motor cortical microglia/macrophage inflammation between cases showed that there was significant variability in both Iba1+ (mean=0.336 ± 0.026 million pixels/mm^2, between-case ANOVA $p<0.001$) and CD68+ inflammation (mean=0.036 ± 0.005 million pixels/mm2, between-case ANOVA $p<0.001$). Within a given case, Iba1+ inflammation did not differ between motor cortical blocks, with the exception of MS9 where this was marginally significant (between-region ANOVA within a given case: MS1, p=0.800; MS2, p=0.524; MS3, p=0.282; MS4, p=0.314; MS5, p=0.107; MS6, p=0.867; MS7, p=0.525; MS8, p=0.502; MS9, p=0.022; MS10, p=0.167) (Figure 5.6). Similarly, CD68+ inflammation did not differ between motor blocks in any case studied (between-region ANOVA within a given case: MS1, p=0.478; MS2, p=0.764; MS3,

p=0.691; MS4, p=0.709; MS5, p=0.368; MS6, p=0.562; MS7, p=0.830; MS8, p=0.218; MS9, p=0.453; MS10, p=0.844) (Figure 5.7). Across the whole cohort, the motor cortical regions sampled demonstrated similar levels of microglia/macrophage inflammation (between-region ANOVA across whole cohort: Iba1+, p=0.489; CD68+, p=0.981) (Figure 5.9).

5.3.2.3. Layer 5 Neuronal density

A comparison of motor cortical layer 5 neuronal density between MS cases showed that there was significant variability in neuronal density (mean=64 ± 3 neurons/mm^2, between-case ANOVA p<0.001). However, within each case, no significant differences in layer 5 neuronal density was detected between motor cortical blocks, with the exception of MS1 and MS7 (between-region ANOVA within a given case: MS1, p=0.023; MS2, p=0.390; MS3, p=0.562; MS4, p=0.182; MS5, p=0.677; MS6, p=0.789; MS7, p=0.004; MS8, p=0.926; MS9, p=0.911; MS10, p=0.282) (Figure 5.8). Across the whole cohort, the motor cortical regions sampled demonstrated similar neuronal densities (between-region ANOVA across whole cohort: p=0.983) (Figure 5.9).

5.3.2.4. Relationships between cortical lesions and layer 5 microglia/macrophage inflammation and neuronal density

Cortical lesional burden significantly correlated with both Iba1+ (r=0.233, p=0.019) and CD68+ inflammation (r=0.232, p=0.02), but not neuronal density (r=0.029, p=777). Iba1+ inflammation significantly correlated with CD68+ inflammation (r=0.356, p<0.001). Neuronal density positively correlated with both Iba1+ (r=0.230, p=0.022) and CD68+ inflammation (r=0.289, p=0.004).

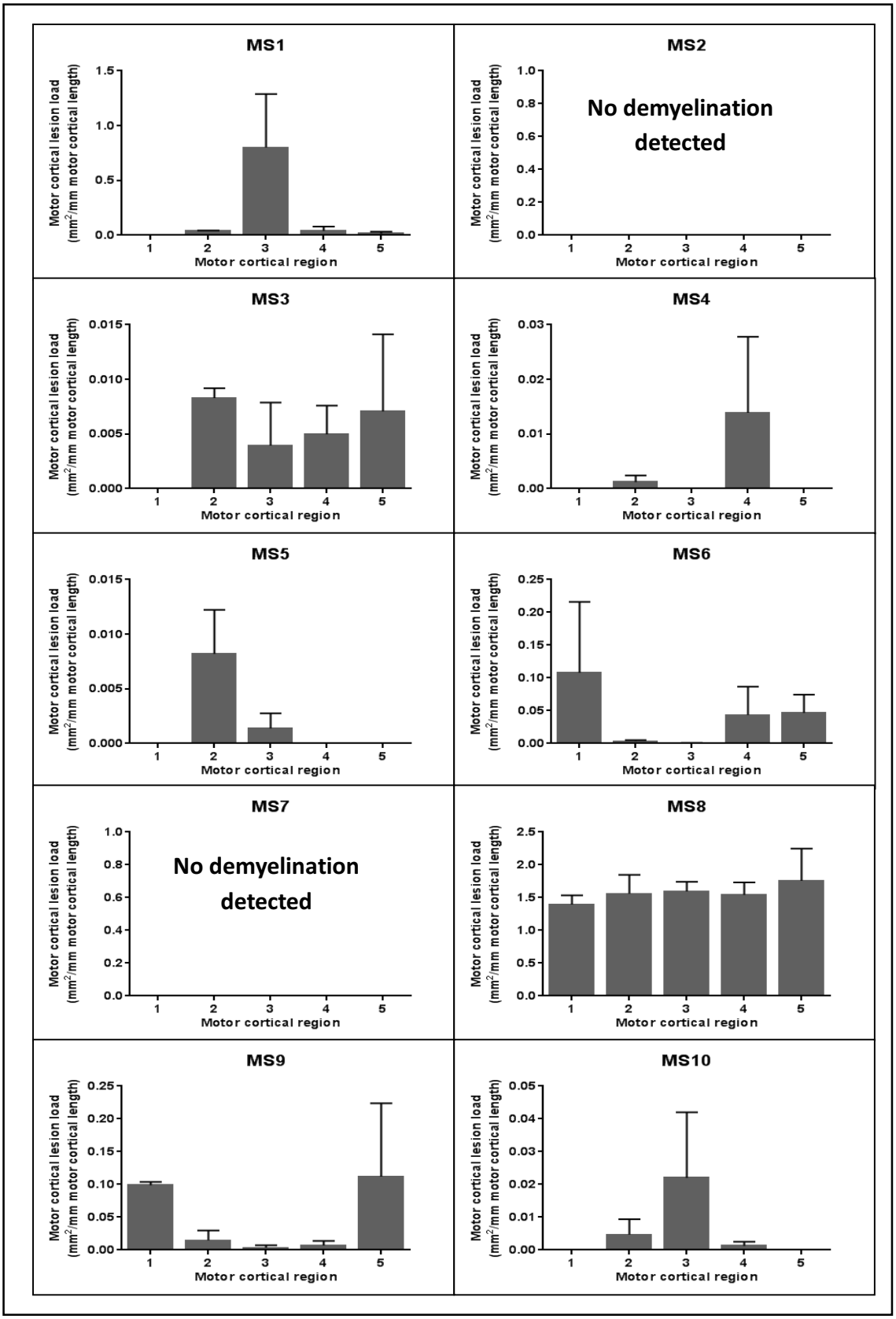


Figure 5.5: Demyelination in different motor cortical regions (1 being most mesial, 5 being most lateral). Note that y-axis scale bars are different due to marked variability between cases in the extent of demyelination. MS2 and MS7 are included for the sake of completeness, but no demyelination was detected in these cases.

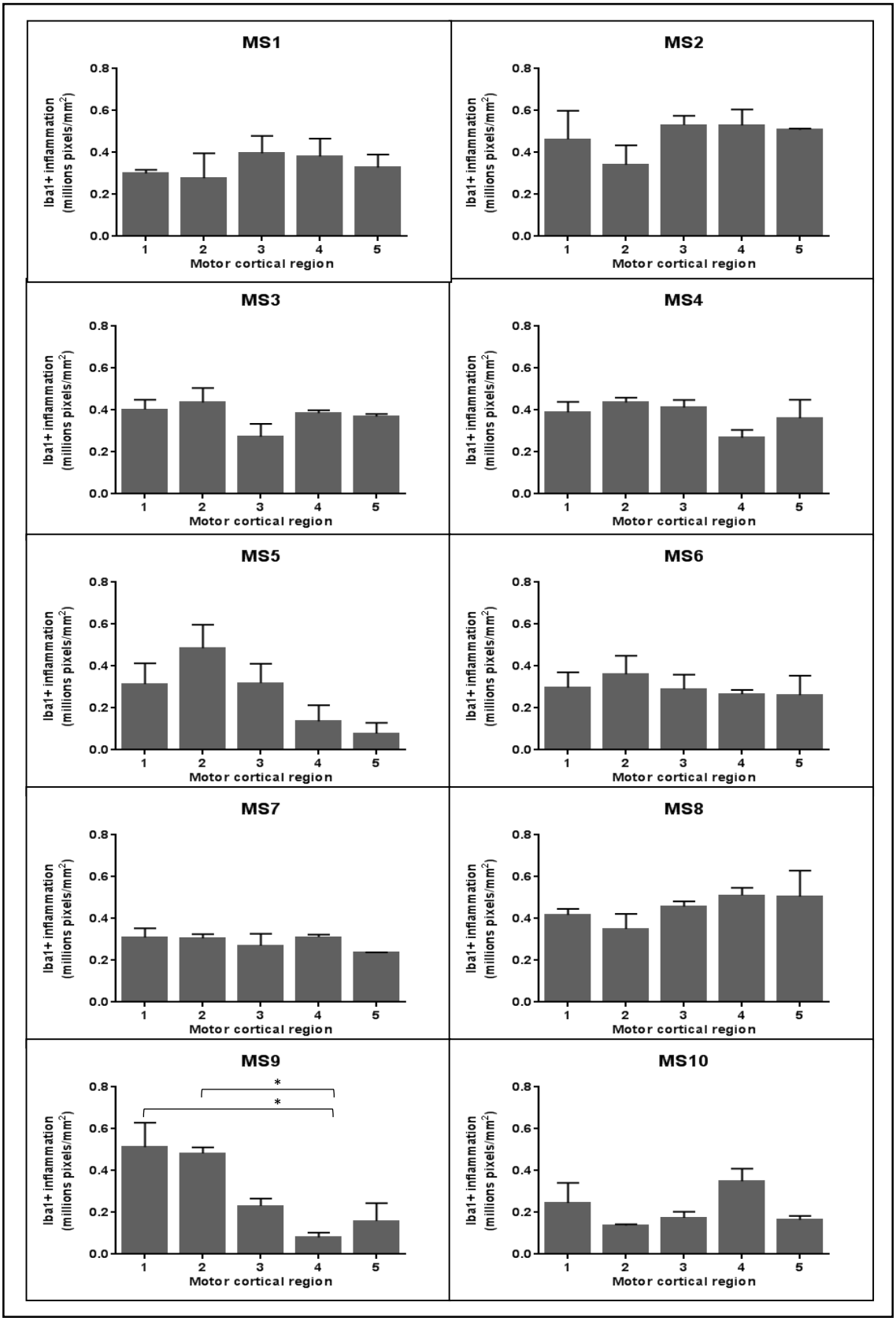


Figure 5.6: Iba1+ inflammation in different motor cortical regions (1 being most mesial, 5 being most lateral). With the exception of MS9, variation of Iba1+ inflammation was minimal within motor cortical regions of the same MS case. *=p<0.05, **=p<0.01

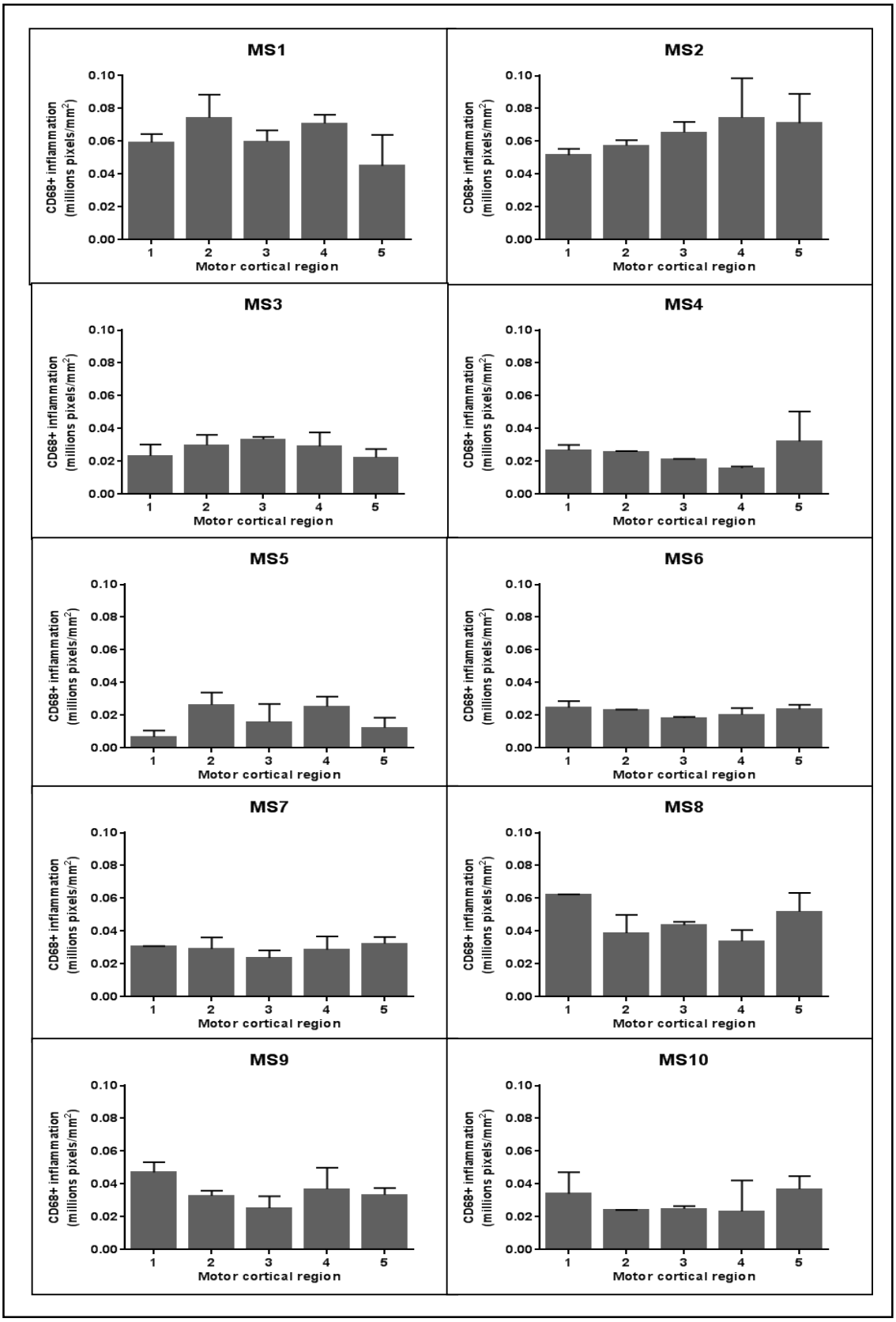


Figure 5.7: CD68+ inflammation in different motor cortical regions (1 being most mesial, 5 being most lateral). Variation of CD68+ inflammation was minimal within motor cortical regions of the same MS case.

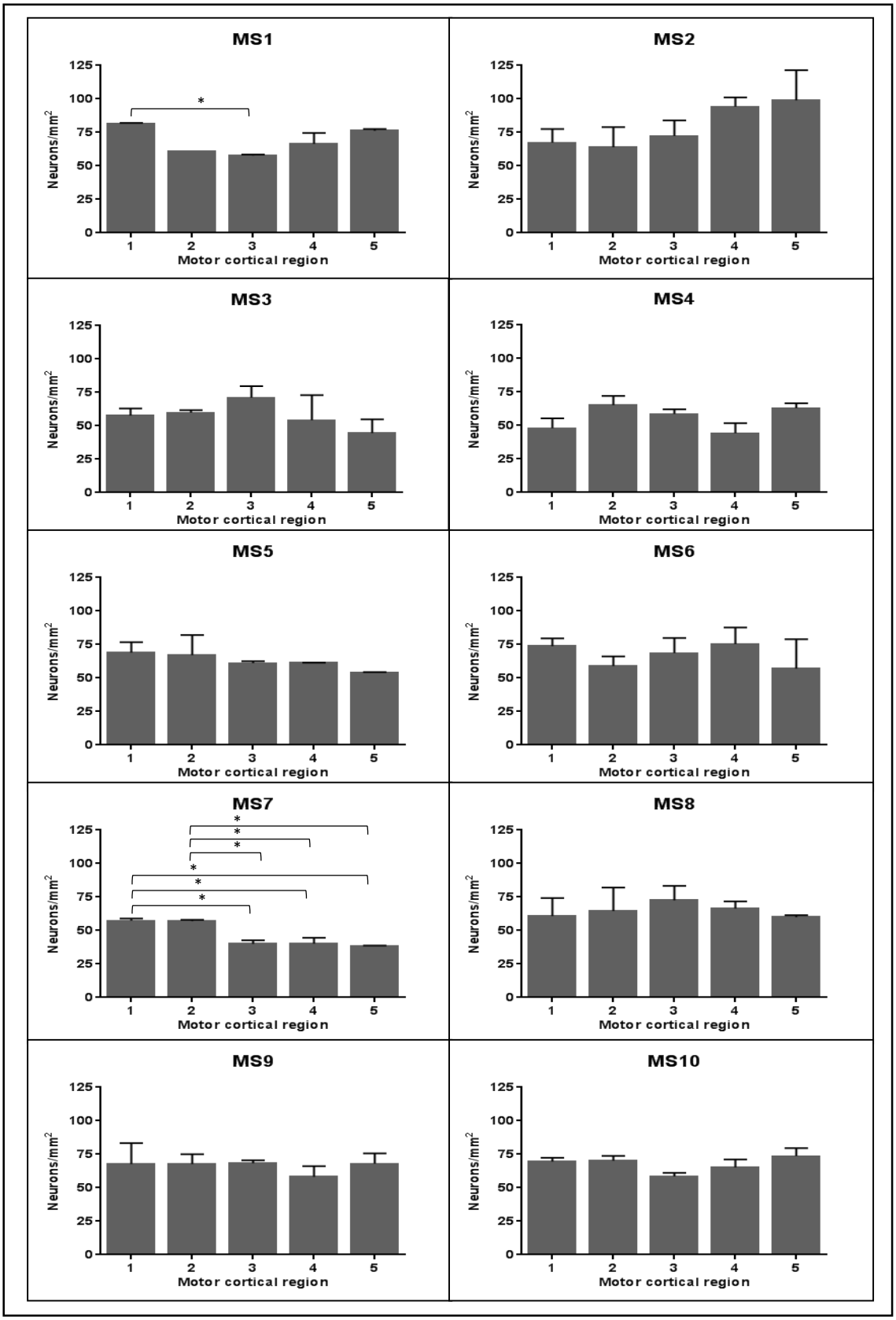


Figure 5.8: Neuronal density in different motor cortical regions (1 being most mesial, 5 being most lateral). With the exception of MS1 and MS7, variation in neuronal density was minimal within motor cortical regions of the same MS case. *=p<0.05, **=p<0.01

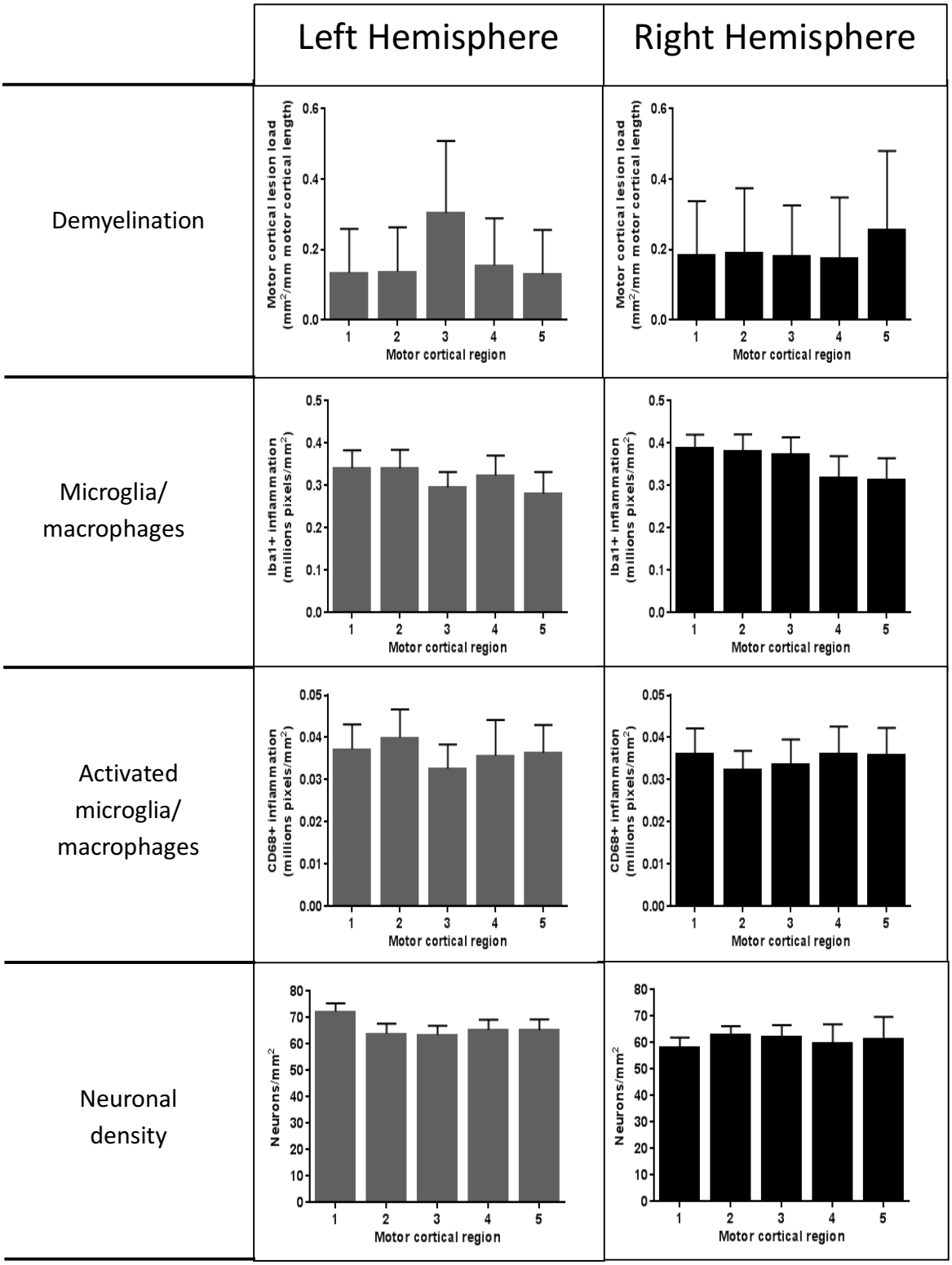


Figure 5.9: Pathologic outcomes throughout the length of the motor cortex. Grey bars represent left hemisphere, black bars represent right hemisphere. No motor cortical region demonstrated a predilection for demyelination, microglia/macrophage inflammation or neuronal loss in either hemisphere.

5.3.3. Spinal cord sub-group analysis

Given the significant positive correlation between microglia/macrophage inflammation and neurons (a finding shown to be influenced by *HLA-DRB1*15* status in chapter 4), we sought to extend these observations in the spinal cords of the two MS cases that demonstrated the most divergent relationship in terms of motor cortical layer 5 Iba1+ microglia/macrophage inflammation and neuronal density (MS1: r=-0.064, p=0.861; MS2: r=0.624, p=0.05). For these two cases, we comprehensively characterised the relationship between microglia/macrophage inflammation and axonal density throughout the entire length of the spinal cord LCST.

5.3.3.1. Radiographic and pathologic characteristics of MS1 and MS2

MS1 had severe radiographic lesional burden in both the cerebral hemispheres (left hemisphere: 22% CST lesion; right hemisphere: 19% CST lesion) and in the spinal cord (left side: 78% LCST lesion; right side: 73% LCST lesion), and cortical lesions in 6/10 motor cortical blocks (mean=0.281 ± 0.172 mm^2/mm motor cortical length). MS2 had several cerebral hemispheric radiographic lesions (left hemisphere: 11% CST lesion; right hemisphere: 7% CST lesion) but virtually no involvement of the spinal cord (left side: 2% LCST lesion; right side: 1% LCST lesion) and no motor cortical demyelination. Motor cortical layer 5 neuronal density did not differ significantly between the two cases (MS1: 69 ± 3 neurons/mm^2 vs MS2: 79 ± 7 neurons/mm^2, p=0.170). However, there was a significant difference in spinal cord LCST axonal density (MS1: 7,831 ± 320 axons/mm^2 vs MS2: 14,429 ± 226 axons/mm^2, p<0.001) as well as total estimated LCST axonal number (MS1: 27,625 ± 2,310 LCST axons vs MS2: 65,483

± 3,437 LCST axons, p<0.001). Within MS1, there was no difference in axonal density in NAGM compared to lesional parenchyma (NAGM: 7,584 ± 472 axons/mm^2 vs lesion: 8,325 ± 633 axons/mm^2, p=0.351), or total estimated LCST axonal number (NAGM: 26,717 ± 3,607 LCST axons vs lesion: 29,173 ± 4,127 LCST axons, p=0.461). The small amount of plaque burden impinging on the spinal cord LCST of MS2 precluded a lesional analysis of this case.

5.3.3.2. Relationship between microglia/macrophage inflammation and axonal density in MS1 and MS2

In the spinal cords of MS1 and MS2, motor cortical relationships between microglia/macrophages and neurons were maintained in the spinal cord. In MS1, no relationship between Iba1+ microglia/macrophages and LCST axonal density was detected in NAGM (r=200, p=493) or lesions (r=400, p=140). In contrast, Iba1+ microglia/macrophages positively correlated with LCST axonal density in MS2 in NAGM (r=0.763, p<0.001) (Figure 5.10). Lack of LCST demyelination in MS2 precluded a lesional assessment of this case.

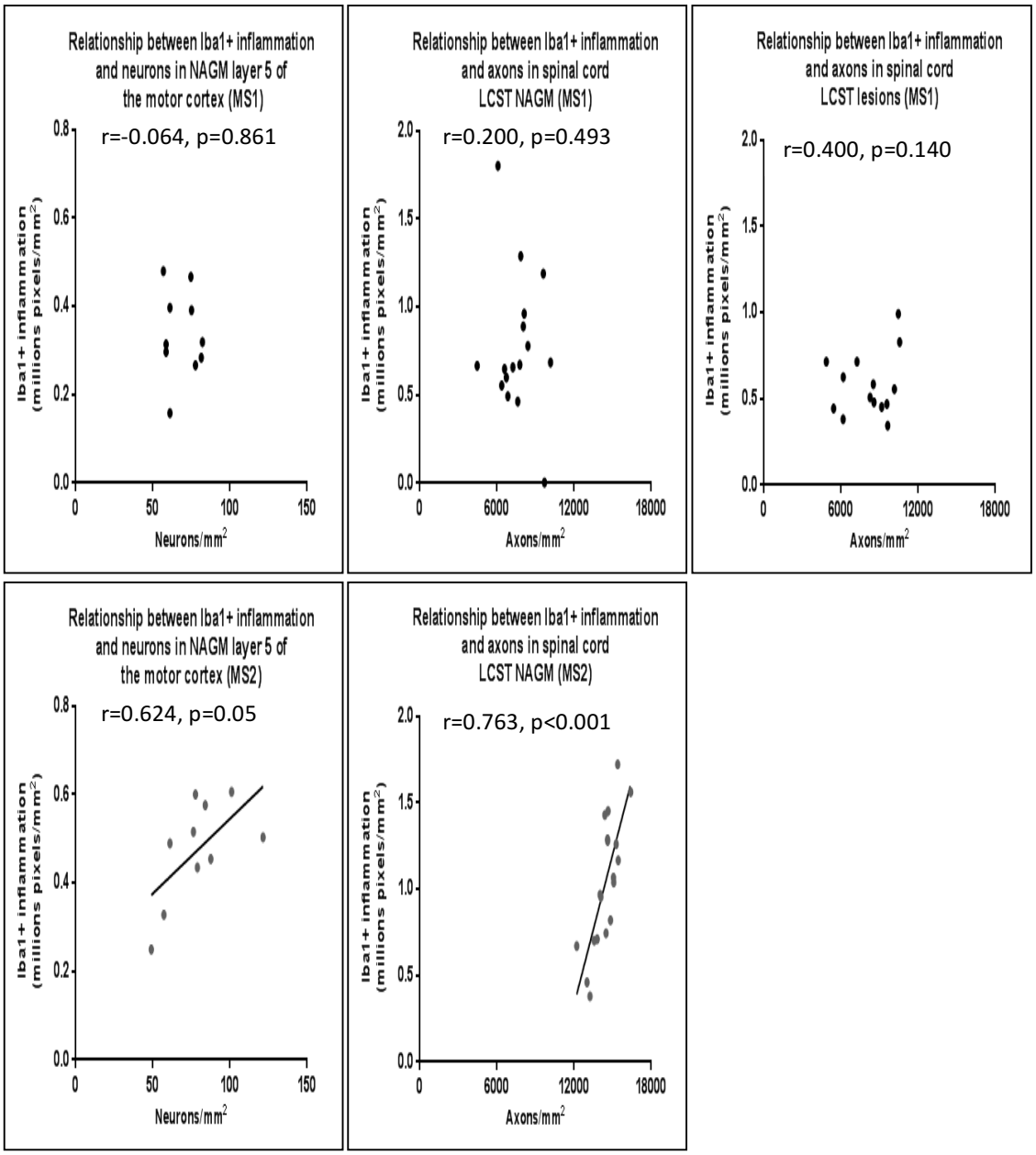


Figure 5.10: Comparison of microglia/macrophage and neuronal relationships in motor cortex and spinal cord. The presence of a positive relationship between Iba1+ inflammation and neuronal density in the motor cortex was maintained throughout the length of the spinal cord in the LCST of the same MS case.

5.3.4. Cerebral hemispheric CST radiographic findings

Cerebral hemispheric radiographic CST lesions, delineated on post-mortem MRI, were detected in 7/10 MS cases, although in one of these cases only 0.03% of the cerebral hemispheric CST was affected. Cerebral hemispheric CST lesional burden was variable between the MS cases in our cohort, ranging from 0.03% to 19% (mean cerebral hemispheric CST radiographic lesional burden: 4.5 ± 1.5%). No significant difference in lesional burden was detected in the right versus left hemisphere across the whole cohort (left: 5 ± 2% vs. right: 4 ± 2%, p=0.840) (Figure 5.11A and Figure 5.11B).

5.3.5. Spinal cord LCST radiographic findings

Spinal cord LCST lesions, delineated on post-mortem spinal cord MRI, were detected in 9/10 MS cases, ranging from 1.4% to 76% (mean spinal cord LCST lesional burden: 20.7 ± 5.7%). There was no significant difference in the extent of spinal cord LCST radiographic lesion burden on the right side of the cord versus the left side across the whole cohort (left: 22 ± 8% vs right: 20 ± 9%, p=0.897) (Figure 5.11C and Figure 5.11D).

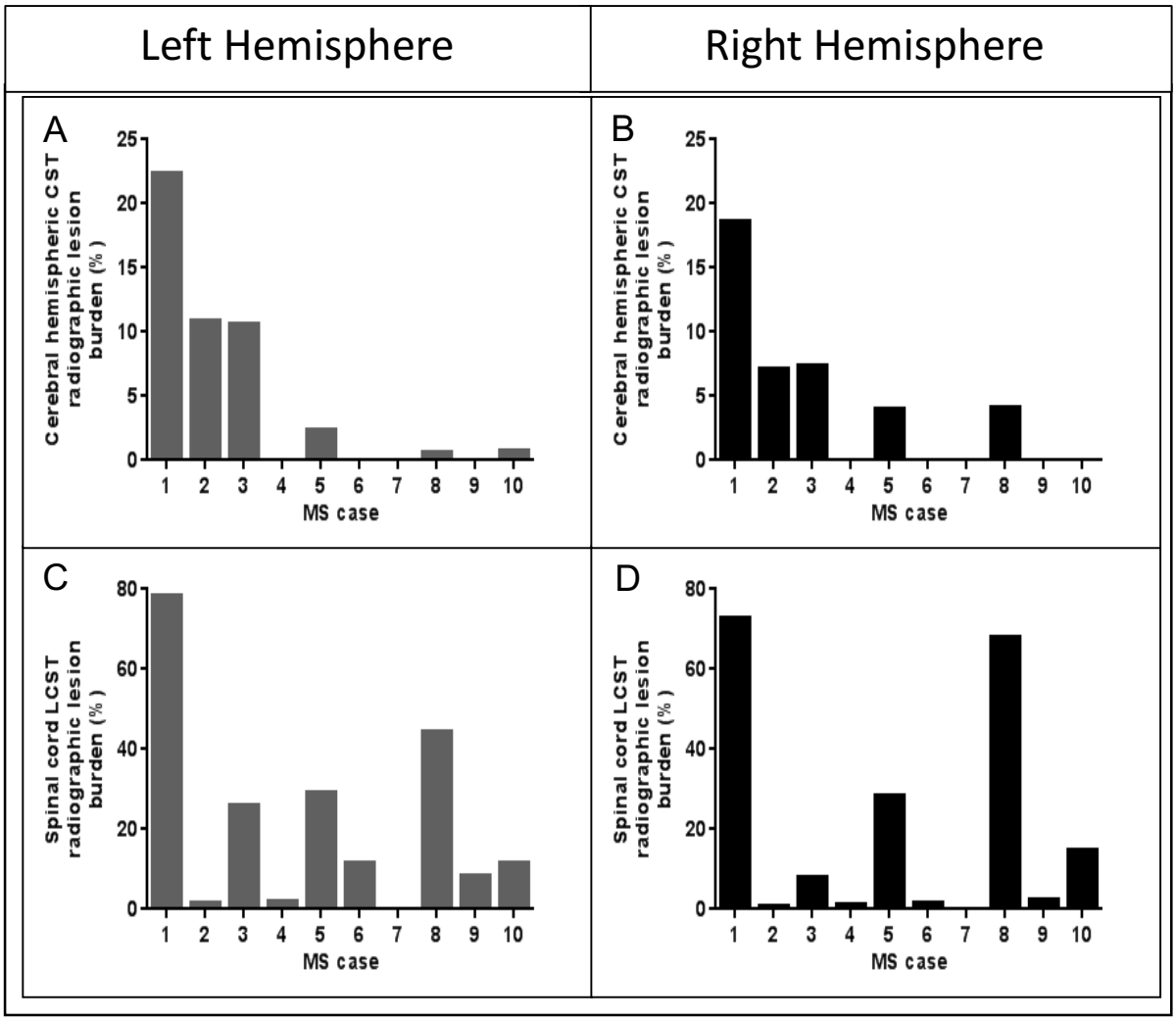


Figure 5.11: Comparison of radiographic lesion burden impinging on the CST of the brain and spinal cord. Grey bars represent left hemisphere, black bars represent right hemisphere, of both brain (A&B) and spinal cord (C&D)

5.3.6. Relationship between motor cortical histology and CST radiographic findings

5.3.6.1. Relationship between motor cortical demyelination and CST radiographic lesional burden

Upon assessment of the whole cohort, no relationship was observed between motor cortical demyelination and cerebral hemispheric CST radiographic lesional burden (r=0.086, p=0.813). Motor cortical demyelination was correlated significantly with spinal cord LCST radiographic lesional burden (r=0.681, p=0.03). However, this finding appeared to be driven by two outlying cases, as no

relationship was observed after their removal (r=0.395, p=0.333). No relationship was detected between motor cortical demyelination and global CST radiographic lesional burden (r=0.213, p=0.555).

A trending relationship was observed between cerebral hemispheric CST and spinal cord LCST radiographic lesional burden (r=0.583, p=0.077). However, this also appeared to be driven by an outlying case with severe radiographic lesional burden throughout the neuraxis, as no relationship was observed after its removal (r=0.424, p=0.256).

5.3.6.2. Relationship between motor cortical neuropathology and CST radiographic lesional burden

Global CST radiographic lesional burden was not associated with motor cortical layer 5 Iba1+ (r=0.200, p=0.580), CD68+ (r=0.212, p=0.556) or neuronal density (r=0.455, p=0.187) (Figure 5.12A).

Cerebral hemispheric CST radiographic lesional burden was not associated with motor cortical layer 5 Iba1+ (r=0.399, p=0.254), CD68+ (r=0.362, p=0.304) or neuronal density (r=0.558, p=0.093) (Figure 5.12B). Spinal cord LCST radiographic lesional burden was not associated with motor cortical layer 5 Iba1+ (r=0.018, p=0.960), CD68+ (r=-0.018, p=0.960) or neuronal density (r=0.236, p=0.511) (Figure 5.12C).

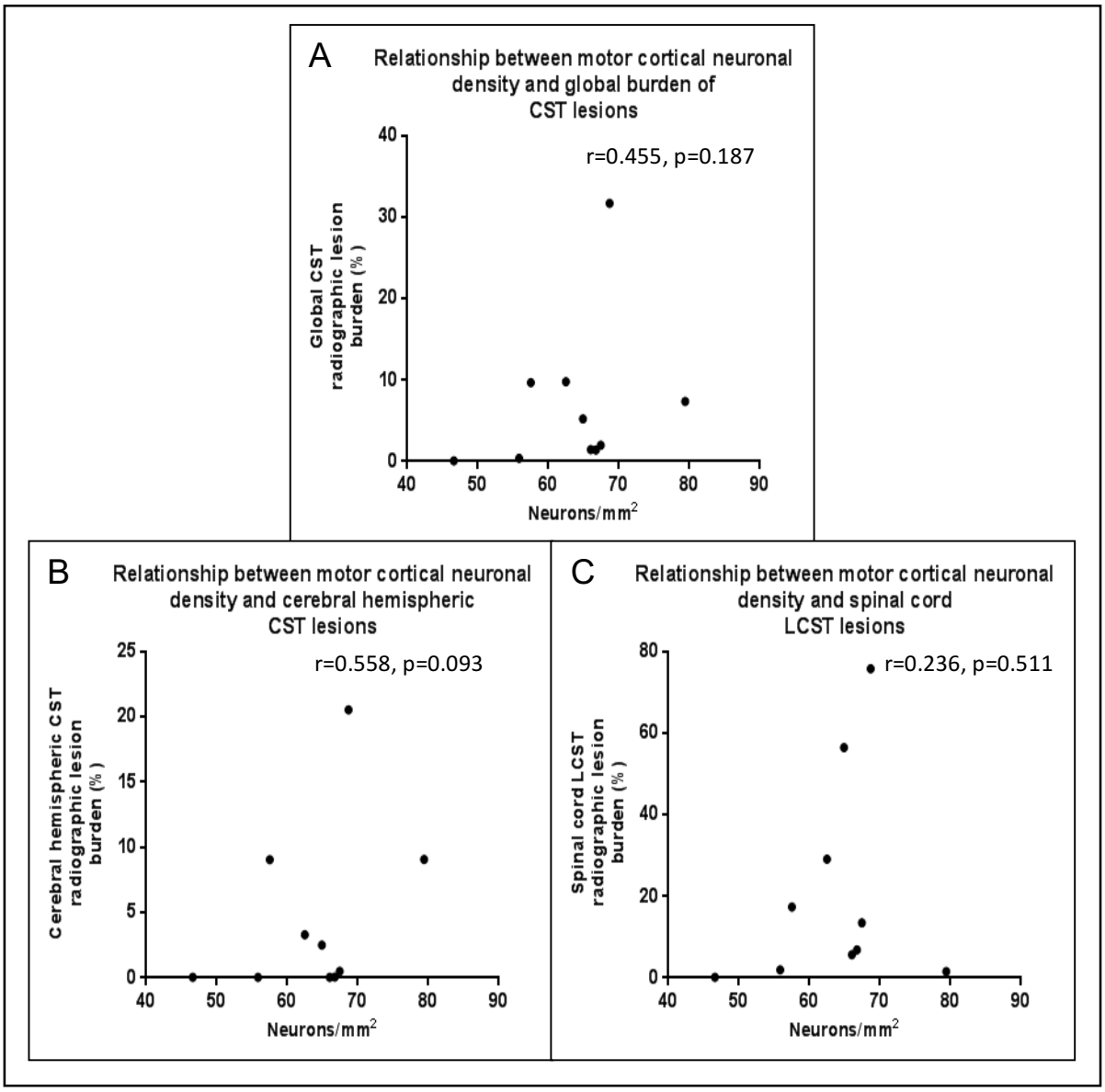


Figure 5.12: Relationships between CST radiographic lesional burden and motor cortical layer 5 neuronal density. No associations were observed between motor cortical layer 5 neuronal density and global CST radiographic lesional burden (A), cerebral hemispheric CST radiographic lesional burden (B), or spinal cord LCST radiographic lesional burden (C)

5.4. Discussion

In the current study, we have systematically quantified the extent of demyelination, microglia/macrophage inflammation and neuronal density throughout the entire length of the motor cortex, and related these metrics to CST radiographic lesional burden in both cerebral hemispheres and spinal cord. We show that whilst motor cortical MS pathology is highly variable between MS cases, minimal variation is observed within a given case in different motor cortical regions. Lesion burden impinging on the motor cortex, brain CST and spinal cord LCST is similar in both hemispheres of a given case, yet apparently independent from each other within the same hemisphere. Relevant to disability accrual, CST lesional burden does not appear to impact on motor cortical neurons. This is first study to assess the contribution of global CST lesional burden to motor cortical pathologic outcome, and suggests that motor cortical neurodegeneration proceeds independently of white matter lesions in connected tracts.

This thesis has shed important new light onto cortical disease processes in MS. We have shown that *HLA-DRB1*15* status impacts the extent of inflammatory demyelination in the motor cortex, as well as relationships between innate inflammation and neurons. We have also described fibrinogen deposition as a novel component of cortical MS pathology that associates with neurodegeneration. However, a potential limitation of previous chapters is that, whilst detailed, sampling was necessarily restricted to one tissue block per case. In the current chapter, we sought to quantify pathologic outcome throughout the

length of the motor cortex in order to validate our sampling approach in previous chapters. This comprehensive analysis strategy also allowed a complete assessment of relationships between CST lesion burden and motor cortical pathologic outcome.

We show that motor cortical pathologic outcome does not vary significantly within the same case, when different regions of motor cortex are sampled. Given data in previous chapters demonstrating that microglia/macrophage inflammation and neuronal density do not differ substantially from control cases in progressive MS, this finding may reflect the paucity of microglia/macrophage inflammation in the MS cortex, and anatomic homogeneity in neuronal populations. That being said, we did not find significant variation in lesional burden between motor cortical regions of the same case either. Previous reports have suggested that cortical lesional burden demonstrates marked intra-individual cortical heterogeneity between more distant anatomic areas (Kutzelnigg and Lassmann, 2006). Current consensus suggests that meningeal inflammatory infiltrates (Howell *et al.*, 2011), that might be more troublesome in areas of CSF stasis (Magliozzi *et al.*, 2010), drive cortical demyelination in MS. Given that we have sampled lateral to mesial motor cortical areas, where CSF flow likely differs, our data challenge this view. Rather, it appears that a diffuse meningeal and perivascular inflammatory process drives MS pathology in the progressive stage that affects motor cortical areas of the precentral gyrus similarly. Unfortunately, technical factors precluded analysis of fibrinogen in

different motor cortical regions, and future investigations will be needed to assess intra-cortical variation in fibrinogen deposition in optimally-fixed tissue.

An intriguing finding of this thesis has been the detection of a relationship between microglia/macrophage inflammation and neurons. The availability of two complete spinal cord cases for detailed histologic analyses allowed a comprehensive assessment of this relationship to be undertaken in the LCST. Interestingly, when a positive relationship between microglia/macrophages and neurons was observed in the motor cortex it was also observed in the spinal cord (with axons), and vice versa. These findings add credence to the notion that microglia/macrophages are physiologically linked to neuronal/axonal populations in a relationship that becomes disturbed in MS. Given our data in chapter 4, which has convincingly demonstrated that the relationship between microglia/macrophage inflammation and neuronal density appears related to *HLA-DRB1*15* status when a large cohort of cases is assessed, it is plausible that a similar genotype related effect may be operative here. Future work characterising the relationship between microglia/macrophage inflammation and axonal loss in a larger cohort of MS cases that are genotyped for *HLA-DRB1*15* status would be of interest. Regardless, our data adds further support to the view that therapeutic modulation of innate immune cells may be beneficial to neuroaxonal survival in MS.

The importance of improving our understanding of pathologic factors associated with cortical neurodegeneration was further outlined in the current cohort,

wherein motor cortical demyelination did not associate with neuronal density. The lack of association is consistent with previous findings in this thesis and adds further to a wealth of evidence suggesting that demyelination does not fully account for the extent of neurodegeneration in MS (DeLuca *et al.*, 2006; Klaver *et al.*, 2015). However, demyelination may impact on neurodegeneration in distant connected (and normally myelinated) structures via a retrograde spread of pathology.

Previous studies have associated CST tissue injury with cortical changes in MS (Gorgoraptis *et al.*, 2010). However, this study did not investigate spinal cord material and relied on radiographic imaging surrogates of cortical damage (Gorgoraptis *et al.*, 2010). MRI remains poor at detecting cortical demyelination (Kilsdonk *et al.*, 2016), and does not have the resolution necessary to reliably quantify inflammation and/or neurodegeneration. The paucity of complete specimens available to both MRI and post-mortem histologic analyses has limited the number of MRI-pathology correlational studies and impeded advance in our understanding of how global CST injury relates to motor cortical pathology in MS.

In the current study, we have used a unique cohort of MS cases to quantify radiographic lesion burden impinging on the cerebral hemispheric and spinal cord CST, that we have then related to robust and quantitative motor cortical pathologic outputs. In our series, both brain and spinal cord CST radiographic lesions were common. CST lesions were more common in the spinal cord than in

the cerebral hemispheres (as a function of complete lesional area), an expected finding given the propensity of the lateral columns to demyelination and the proportionately large spinal cord area that the LCST occupies. We have also found that both cerebral hemispheres of the same MS case, and both sides of the spinal cord, experience a similar level of CST lesional burden. However, the extent of radiographic lesional burden in the cerebral hemispheres does not necessarily correlate with the spinal cord. This finding is consistent with previous studies that have assessed spinal cord pathology *in vivo* and adds support to the view that brain and spinal cord pathology progress somewhat independently in MS (Kearney *et al.*, 2015), and that different inflammatory mechanisms may predominant in spinal cord that are not a feature of brain pathology (Stromnes *et al.*, 2008).

Pertinent to long-term clinical outcome, we found no evidence that the extent of CST radiographic lesional burden was related to motor cortical demyelination, microglia/macrophage inflammation or neuronal density. Previous work has suggested the presence of tract-specific diffuse degenerative processes in MS (Kolasinski *et al.*, 2012), and Wallerian degeneration in anatomically eloquent structures (Ciccarelli *et al.*, 2003; Evangelou, Konz, *et al.*, 2000). However, this is the first study to assess the link between CST-specific radiographic lesions and pathologically defined cortical tissue injury in MS. Our data suggests that motor cortical neurodegeneration is not associated with diffuse CST damage, as resolvable on MRI. Given our data in previous chapters demonstrating convincing relationships between parenchymal factors and neurons, we

therefore propose that local inflammatory factors (in combination with meningeal pathology) predominantly drive motor cortical neuronal loss in MS. This being said, a critical limitation of the current work should be noted. That is, that the histologic correlates of radiographic signal change are not well described. We have therefore been unable to segregate radiographic lesions into their respective pathologic correlates (Filippi *et al.*, 2012). Future work aimed at improving our understanding of how MRI signal change relates to specific aspects of MS pathology is urgently needed.

In summary, this chapter has further added to our understanding of motor cortical pathology in MS. We have shown that pathologic outcome does not vary markedly within different regions of the same MS case, and that motor cortical neurodegeneration is not influenced by radiographic CST lesions. Future work aimed at investigating the pathologic correlates of MRI signal change, and how specific components of MS pathology relate to tissue injury of distant connected structures is now required.

6. Summary

The general aims of this thesis were to (i) assess the influence of *HLA-DRB1*15* allele status on motor cortical pathologic heterogeneity and (ii) assess the contribution of global CST radiographic lesional burden on motor cortical MS pathology. This has been achieved by associating carriage of *HLA-DRB1*15* with robust and quantitative motor cortical pathologic outputs, and through the use of a unique MS cohort available for post-mortem MRI and motor cortical histologic analyses. The principal findings of each results chapter of this thesis are summarised below.

6.1 The influence of *HLA-DRB1*15* on motor cortical inflammatory pathology in multiple sclerosis

Cortical tissue injury is a feature of the earliest stages of MS (Giorgio *et al.*, 2011), is most prevalent in the progressive stage (Kutzelnigg *et al.*, 2005), and appears to associate with cognitive and physical decline (Calabrese *et al.*, 2012). Studies that have assessed the distribution of cortical pathology in MS have identified a prominent involvement of the motor cortex (M Calabrese *et al.*, 2010). Understanding genetic determinants of motor cortical pathologic outcome may therefore improve our understanding of MS progression, identify novel drug targets, and create the possibility of more targeted therapeutic modulation of select patient groups.

In chapter 2, we sought to elucidate the impact of *HLA-DRB1*15* status on motor cortical pathologic outcome in a large cohort (n=47) of MS cases. We found that

*HLA-DRB1*15* significantly associates with the extent of inflammation in the MS motor cortex, and the extent of demyelination in younger cases. These findings are the first to associate a genetic factor to the severity of MS cortical pathology and enhance our understanding of the pathologic heterogeneity characteristic of this disease.

Our conclusions in chapter 2 provide important insight into the pathogenesis of motor cortical pathology. In the progressive stage of MS, cortical parenchymal inflammation is scarce (L Bø *et al.*, 2003), yet demyelination can be diffuse and severe (Kutzelnigg *et al.*, 2005). This has led the predominant view that parenchymal factors do not play a substantial role in cortical tissue injury. Instead, focus has shifted to diffusible factors originating from inflammation in the sub-arachnoid space (Howell *et al.*, 2011). Our findings in chapter 2 suggest that a genetic locus relevant to disease susceptibility and clinical outcome is also associated with the severity of parenchymal and perivascular cortical inflammation, and also highlight the key role of age in dictating the severity of MS pathology. These findings therefore implicate the presence of age-related and genetically-divergent disease mechanisms occurring within the cortical parenchyma in MS, despite an apparent paucity of peripheral inflammatory infiltration.

Our results in chapter 2 are consistent with previous observations that *HLA-DRB1*15* impacts disease severity, as demonstrated in clinical (DeLuca *et al.*, 2007), radiographic (Okuda *et al.*, 2009), and pathologic series (DeLuca *et al.*,

2013). A possible explanation for these findings is that *HLA-DRB1*15* influences CNS antigen presentation such that induction of immune tolerance to self fails (Altmann *et al.*, 1995). Alternatively, this allele may confer greater T-cell proliferation potential in response to *HLA-DRB1* ligation (Mohme *et al.*, 2013). Whilst this latter point may not be consistent with the lack of lymphocytes in the cortical parenchyma, it is likely that fulminant meningeal inflammation is in part the result of extensive T-cell proliferation within the sub-arachnoid space. Greater extravasation of meningeal T-cells into the cortical parenchyma, as we have observed in *HLA-DRB1*15*+ cases, could directly impact on resident microglial inflammation and influence disease processes relevant to disease progression (Frischer *et al.*, 2015).

In summary, our findings shed light onto the genetic substrate of the pathologic heterogeneity characteristic of MS, and suggest that disease mechanisms occurring within the cortical parenchyma are important determinants of cortical tissue injury.

6.2. Fibrinogen deposition associates with neurodegeneration in the multiple sclerosis motor cortex

A prevailing view of MS pathology states that the progressive phase is characterised by compartmentalisation of the CNS parenchyma behind a closed BBB (Hochmeister *et al.*, 2006). Indeed, efforts to detect surrogate markers of BBB disruption, such as extravasated serum protein, have so far failed in post-mortem cortical tissue (van Horssen *et al.*, 2007). However, the detection of

endothelial tight junction abnormalities in cortical NAGM suggest that BBB disruption may be an important feature of MS cortical pathology that has heretofore been overlooked (Leech *et al.*, 2007).

Chapter 2 showed that lymphocytic and microglia/macrophage inflammation is greater in *HLA-DRB1*15*+ cases. A disrupted BBB may help explain these findings, as greater leukocyte proliferation in the meninges could have a direct impact on parenchymal inflammation if the physiologic barrier to their migration into the brain was perturbed. In addition, animal models of MS have shown that fibrinogen, a protein not found in the healthy brain but abundant in plasma, can activate resident microglia and cause downstream axonal injury (Davalos *et al.*, 2012). We have therefore assessed the extent of cortical fibrinogen deposition, as a disease-relevant surrogate marker of BBB disruption, and relationships therein with *HLA-DRB1*15* and neurodegeneration.

Our results in chapter 3 show that fibrinogen deposition is frequent and extensive in the MS motor cortex, suggesting that diffuse and chronic BBB disruption may be a fundamental component of cortical pathology. This being said, other sources of fibrinogen deposition must also be considered. Our observation of increased expression of PAI-1 in MS cases with the most fibrinogen depositions suggests that fibrinogen clearance is also perturbed in MS, as reported previously in white matter lesions (Gveric *et al.*, 2003). Synthesis of fibrinogen by resident neurons and glia and/or retrograde transport by damaged axons exposed to fibrinogen in acute white matter lesions are further

possible sources, but experimental evidence is lacking (Fabian and Petroff, 1987).

The extent of fibrinogen deposition was not associated with *HLA-DRB1*15* status in our cohort, arguing against greater BBB disruption underlying observations of more inflammation and demyelination in *HLA-DRB1*15*+ cases. However, the observation of intrinsic abnormalities in fibrinogen clearance limits the interpretation of this finding, as we were unable to assess the age of deposited fibrinogen as a result. A genetic impact on BBB integrity may therefore dilute with disease evolution and ageing.

Consistent with *in vitro* (Smiley *et al.*, 2001) and animal model data (Davalos *et al.*, 2012), fibrinogen deposition was associated with motor cortical neuronal loss. However, we did not detect a relationship between fibrinogen deposition and microglia/macrophage inflammation. This latter observation likely relates to short-lived interactions between inflammatory mediators being impervious to detection in an autopsy cohort, as a wealth of experimental data has shown fibrinogen to be a potent activator of innate inflammation (Davalos and Akassoglou, 2012). The fact that deposited fibrinogen may not be removed due to abnormalities in its clearance adds further complexity to this relationship (Gveric *et al.*, 2003). Nonetheless, emerging evidence suggests that perturbed microglia/macrophage inflammation may contribute to the diffuse neuroaxonal loss characteristic of progressive disease (Frischer *et al.*, 2015). Fibrinogen

deposition in the motor cortex may therefore be a novel therapeutic target with the potential to reduce disability accrual.

6.3. The influence of *HLA-DRB1*15* on neurodegeneration in the multiple sclerosis motor cortex

In the first two results chapters of this thesis, we demonstrated that (i) genetic variation at the *HLA-DRB1* locus impacts on motor cortical demyelination and inflammation and (ii) fibrinogen deposition in the cortex significantly associates with neuronal loss. These findings highlight the fundamental role of genetic variation in pathologic heterogeneity and the critical importance of parenchymal factors in the initiation and/or exacerbation of cortical tissue injury in MS. In chapter 4, we therefore investigated the relationship between motor cortical parenchymal inflammation and neurodegeneration, and associations therein with *HLA-DRB1*15*.

An intriguing finding of previous neuropathology studies that have assessed MS cortex is the apparently modest loss of neurons (Klaver *et al.*, 2015; Magliozzi *et al.*, 2010; Wegner *et al.*, 2006). This is despite cortical atrophy that can be detected from disease onset (Calabrese *et al.*, 2007), as well as typically substantive meningeal inflammation (Howell *et al.*, 2011) and cortical demyelination that characterises the progressive stage (Kutzelnigg *et al.*, 2005). Given then that cortical neurons are exposed to a chronic inflammatory milieu, endogenous neuroprotective mechanisms might play a key role in neuronal

survival. Recent work has shown that microglia inflammation can protect cortical neurons from apoptosis in a model of CNS inflammation by influencing GAD expression (Chen *et al.*, 2014). We hypothesised that relationships between microglia/macrophage inflammation, GAD expression, and neuronal density in MS might be influenced by *HLA-DRB1*15* status.

In chapter 4 we show that the association between microglia/macrophage inflammation and neuronal density is influenced by both age and *HLA-DRB1*15* status. Neurons were positively associated with microglia/macrophage inflammation, except in young cases and particularly within the *HLA-DRB1*15*+ cohort. This finding adds support to the notion that younger age and carriage of *HLA-DRB1*15* leads to more severe pathologic outcome in MS, and highlights the potentially contrasting contribution of microglia/macrophages to cortical neurodegeneration across different genetic backgrounds and at different ages. One explanation for these findings is that neuroprotective strategies employed by microglia/macrophage inflammation are also influenced by *HLA-DRB1*15* status.

In our cohort, we detected evidence of GAD synaptic loss in MS, suggesting that neuroprotective mechanisms involving inhibitory synaptic stripping might be operative in human MS cortex. We also observed a relationship between cytoplasmic GAD expression and microglia/macrophage inflammation, but only in *HLA-DRB1*15*- MS cases. Whilst cytoplasmic GAD expression has been suggested to provide trophic support to neurons (Pinal and Tobin, 1998), this is

not well described. Further work will therefore now be necessary to probe the temporal dynamics of cortical GAD expression and parenchymal microglia/macrophage inflammation, and the genetic impact therein, in order to further our understanding of the influence of these relationships on cortical neurodegeneration in MS.

Chapter 4 adds to the wealth of experimental evidence that has shown marked phenotypic heterogeneity in microglia/macrophage inflammation, with these cells implicated in both neurodegenerative (Fischer *et al.*, 2012) and neuroprotective processes (Chen *et al.*, 2014). The determinants of microglia/macrophage heterogeneity in MS are elusive, but will likely have important therapeutic implications. Microglia make up the predominant inflammatory cell type resident in the brain, but their role in the progression of MS pathology is not understood (Mishra and Wee Yong, 2016). That a genetic locus known to impact both disease risk and clinical outcome should also impact on relationships relevant to permanent disability accrual is likely an important clue to the underlying pathophysiology of progressive disease.

6.4. MRI-pathology correlations in the MS corticospinal tract

This thesis has shed light onto motor cortical parenchymal disease mechanisms relevant to neurodegeneration. However, MS is a global disease of the entire CNS and motor cortical neurons project axons into the corticospinal tract before their eventual termination in the spinal cord. Pathology of structures connected to the motor cortex could therefore impact on cortical neurodegeneration via a retrograde spread of pathology. In chapter 5, we quantified complete CST radiographic lesional burden and related this to pathologic outcome throughout the length of the motor cortex. Our comprehensive sampling of the motor cortex in chapter 5, from lateral to mesial precentral gyrus, also provides additional context to our findings in previous chapters in which only one tissue block was available per case.

Our findings in chapter 5 show that cortical lesional burden, microglia/macrophage inflammation, and neuronal density do not substantially vary throughout the motor cortex, regardless of a significant difference in measures between cases. This observation provides support to the validity of our sampling strategy in previous chapters, and provides important information about the scale of intra-cortical pathologic heterogeneity. Previous reports have reported large differences in lesional burden in different cortical areas, including notable sites of predilection (Kutzelnigg and Lassmann, 2006). Our findings suggest that disease processes in progressive MS do not markedly differ within the same gyrus and is consistent with the presence of a diffuse inflammatory process driving MS pathology in later disease stages (Magliozzi *et al.*, 2010).

Our results in chapter 5 show that radiographic lesional burden does not appear to associate with motor cortical neurodegeneration, and builds on a wealth of experimental evidence suggesting that radiographic lesions do not fully account for neuroaxonal loss in MS (DeLuca *et al.*, 2006). However, it is important to note that histologic substrates of MRI signal change are not well described, and it will therefore be necessary to correlate radiographic findings with pathologic outputs before definitive conclusions can be made (Filippi *et al.*, 2012). Nevertheless, our findings in chapter 5 lend support to the notion that MS cortical pathology is predominantly driven by local inflammatory factors in the meninges, perivascular space, and parenchyma, as shown in previous chapters of this thesis.

7. Future work

7.1. Genetic-pathology correlations

It is clear that carriage of *HLA-DRB1*15* impacts the severity of MS pathologic outcome, and relationships therein between motor cortical microglia/macrophage inflammation and neurodegeneration. Future work should now focus on elucidating the mechanism by which genetic variation at the *HLA-DRB1* locus impacts on MS pathologic (DeLuca *et al.*, 2013; Yates *et al.*, 2015), radiographic (Okuda, Srinivasan, *et al.*, 2009) and clinical heterogeneity (DeLuca *et al.*, 2007).

Given our motor cortical observations of more severe inflammation and demyelination in *HLA-DRB1*15*+ MS cases, and a divergent relationship between microglia/macrophage inflammation and neuronal density, we hypothesise that *HLA-DRB1*15* status heightens vulnerability to inflammatory demyelination and degeneration via an influence at the proteomic level. To investigate this hypothesis, it will be necessary to initially characterise and compare proteomes of lesional and non-lesional motor cortical parenchyma in *HLA-DRB1*15* positive and negative genotype groups. Cases should be chosen at the extremes of cortical lesional burden, whilst controlling for demographic factors. Only cases with lesional and non-lesional parenchyma within the same section should be used, and should also be matched for cortical layer. Material would be micro-dissected and subjected to liquid-chromatography tandem mass spectrometry (LC-

MS/MS) to allow identification of proteomic profiles that correlate with histologic metrics in each genotype group.

In addition to this initial analysis, it will also be pertinent to specifically assess the proteomic profile of microglia/macrophage inflammation given their divergent relationship with neuronal density according to *HLA-DRB1*15* status. Due to the functional relevance of layer 5 to motor control, investigation should focus on this cortical layer. Cases should be selected at the extremes of cortical neuronal density within each genotype group and matched for demographic factors. Material would be micro-dissected and subjected to LC-MS/MS to allow identification of proteomic profiles that associate with microglia/macrophage phenotype in *HLA-DRB1*15* positive and negative genotype groups.

Using proteomic data gained both from lesional/non-lesional analyses and microglia/macrophage inflammation, a *priori* hypotheses could be generated about the molecular substrates of immune and neurodegenerative pathology that might be influenced by genetic variation, which can then be tested *in vitro*. Lymphocytes and macrophages could be isolated from peripheral whole blood derived from untreated MS patients and controls that have been genotyped for *HLA-DRB1*15 status. Peptides identified from our initial proteomic assessment of post-mortem material that diverge according to *HLA-DRB1*15* status could be presented to lymphocytes by autologous macrophages. The proteomic profile of the resultant supernatant derived from each genotype group could then be characterised by LC-MS/MS and validated histologically.

7.2. Fibrinogen deposition and BBB disruption

This thesis has identified fibrinogen deposition as a novel component of MS cortical pathology that associates with neurodegeneration. Previous studies have shown that fibrinogen deposition is an early feature of MS-like pathology in EAE (Davalos *et al.*, 2012) and is neurotoxic *in vitro* (Smiley *et al.*, 2001). Future work should therefore focus on the relevance of BBB disruption and fibrinogen deposition to MS progression. This could be achieved with a comprehensive immunohistochemical study of the cortical vasculature in progressive MS cases and controls. Components of the BBB, such as astrocytic end feet, endothelial tight junctions and pericytes could be assessed and related to the extent of parenchymal fibrinogen deposition. Another approach would be to define novel imaging surrogates of subtle BBB perturbations so that vascular changes can be assessed at all disease stages. Work in this area has already shown promise, with evidence of pre-enhancement MRI signal change in a subset of lesions that likely relates to BBB changes relevant to lesion aetiology (Absinta *et al.*, 2015).

Possible aetiologies of BBB disruption could be assessed by micro-dissecting brain parenchymal tissue from perivascular spaces of disrupted vessels and comparing proteomic profiles to immediately adjacent vasculature that is apparently normal. Given recent work showing that bacterial toxin exposure can disrupt the BBB and lead to MS-like signs in rodents (Linden *et al.*, 2015), assessment of non-human proteins should also be considered.

7.3. MRI-pathology correlations

In the final part of this thesis, we assessed the association between global CST radiographic lesion burden and motor cortical neurodegeneration. However, a limitation of this study was that pathologic correlates of MRI signal change remain poorly defined. For this reason, comprehensive histologic assessment of our brain and spinal cord cohort (n=10) should be undertaken to investigate how demyelination and inflammation correlate with radiographic lesional burden, as defined in this thesis. In addition, we should also take further advantage of this unique cohort by investigating the pathologic correlates of novel non-conventional MRI modalities, such as myelin water imaging (MWI) (Laule *et al.*, 2016) and NODDI (Grussu *et al.*, 2016), that have recently been optimised in post-mortem specimens. In so doing, we have the opportunity to improve our understanding of how clinically–relevant MRI signal change reflects tissue integrity, and define novel imaging surrogates of pathologic change that extends beyond the resolution of conventional scans. Eventually, this work will improve our ability to monitor MS progression during life.

8. Bibliography

Van der Aa A, Hellings N, Bernard CCA, Raus J, Stinissen P. Functional properties of myelin oligodendrocyte glycoprotein-reactive T cells in multiple sclerosis patients and controls. J. Neuroimmunol. 2003; 137: 164–76.

Absinta M, Nair G, Sati P, Cortese ICM, Filippi M, Reich DS. Direct MRI detection of impending plaque development in multiple sclerosis. Neurol. Neuroimmunol. neuroinflammation 2015; 2: e145.

Acheson ED, Bachrach CA, Wright FM. Some comments on the relationship of the distribution of multiple sclerosis to latitude, solar radiation, and other variables. Acta Psychiatr. Scand. Suppl. 1960; 35: 132–47.

Adams RA, Bauer J, Flick MJ, Sikorski SL, Nuriel T, Lassmann H, et al. The fibrin-derived gamma377-395 peptide inhibits microglia activation and suppresses relapsing paralysis in central nervous system autoimmune disease. J. Exp. Med. 2007; 204: 571–82.

Ajami B, Bennett JL, Krieger C, Tetzlaff W, Rossi FM V. Local self-renewal can sustain CNS microglia maintenance and function throughout adult life. Nat. Neurosci. 2007; 10: 1538–43.

Akassoglou K, Adams RA, Bauer J, Mercado P, Tseveleki V, Lassmann H, et al. Fibrin depletion decreases inflammation and delays the onset of demyelination in a tumor necrosis factor transgenic mouse model for multiple sclerosis. Proc. Natl. Acad. Sci. U. S. A. 2004; 101: 6698–703.

Akenami FO, Koskiniemi M, Färkkilä M, Vaheri A. Cerebrospinal fluid plasminogen activator inhibitor-1 in patients with neurological disease. J. Clin. Pathol. 1997; 50: 157–60.

Alcina A, Abad-Grau MDM, Fedetz M, Izquierdo G, Lucas M, Fernández O, et al. Multiple sclerosis risk variant HLA-DRB1*1501 associates with high expression of DRB1 gene in different human populations. PLoS One 2012; 7: e29819.

Almerighi C, Sinistro A, Cavazza A, Ciaprini C, Rocchi G, Bergamini A. 1Alpha,25-dihydroxyvitamin D3 inhibits CD40L-induced pro-inflammatory and immunomodulatory activity in human monocytes. Cytokine 2009; 45: 190–7.

Almolda B, González B, Castellano B. Are Microglial Cells the Regulators of Lymphocyte Responses in the CNS? Front. Cell. Neurosci. 2015; 9: 440.

Altmann DM, Douek DC, Frater AJ, Hetherington CM, Inoko H, Elliott JI. The T cell response of HLA-DR transgenic mice to human myelin basic protein and other antigens in the presence and absence of human CD4. J. Exp. Med. 1995; 181: 867–75.

Alves-Leon S V, Papais-Alvarenga R, Magalhães M, Alvarenga M, Thuler LCS, Fernández y Fernandez O. Ethnicity-dependent association of HLA DRB1-DQA1-DQB1 alleles in Brazilian multiple sclerosis patients. Acta Neurol. Scand. 2007; 115: 306–11.

Androdias G, Reynolds R, Chanal M, Ritleng C, Confavreux C, Nataf S. Meningeal T cells associate with diffuse axonal loss in multiple sclerosis spinal cords. Ann. Neurol. 2010; 68: 465–76.

Ascherio A, Munch M. Epstein-Barr virus and multiple sclerosis. Epidemiology 2000; 11: 220–4.

Babbe H, Roers A, Waisman A, Lassmann H, Goebels N, Hohlfeld R, et al. Clonal expansions of CD8(+) T cells dominate the T cell infiltrate in active multiple sclerosis lesions as shown by micromanipulation and single cell polymerase chain reaction. J. Exp. Med. 2000; 192: 393–404.

Barcellos LF, Oksenberg JR, Begovich AB, Martin ER, Schmidt S, Vittinghoff E, et al. HLA-DR2 dose effect on susceptibility to multiple sclerosis and influence on disease course. Am. J. Hum. Genet. 2003; 72: 710–6.

Barcellos LF, Sawcer S, Ramsay PP, Baranzini SE, Thomson G, Briggs F, et al. Heterogeneity at the HLA-DRB1 locus and risk for multiple sclerosis. Hum. Mol. Genet. 2006; 15: 2813–24.

Bardehle S, Rafalski VA, Akassoglou K. Breaking boundaries-coagulation and fibrinolysis at the neurovascular interface. Front. Cell. Neurosci. 2015; 9: 354.

Bartholomäus I, Kawakami N, Odoardi F, Schläger C, Miljkovic D, Ellwart JW, et al. Effector T cell interactions with meningeal vascular structures in nascent autoimmune CNS lesions. Nature 2009; 462: 94–8.

Batchelor PE, Porritt MJ, Martinello P, Parish CL, Liberatore GT, Donnan GA, et al. Macrophages and Microglia Produce Local Trophic Gradients That Stimulate Axonal Sprouting Toward but Not beyond the Wound Edge. Mol. Cell. Neurosci. 2002; 21: 436–53.

Beecham AH, Patsopoulos NA, Xifara DK, Davis MF, Kemppinen A, Cotsapas C, et

al. Analysis of immune-related loci identifies 48 new susceptibility variants for multiple sclerosis. Nat. Genet. 2013; 45: 1353–60.

Benedict RHB, Bruce JM, Dwyer MG, Abdelrahman N, Hussein S, Weinstock-Guttman B, et al. Neocortical atrophy, third ventricular width, and cognitive dysfunction in multiple sclerosis. Arch. Neurol. 2006; 63: 1301–6.

Bessis A, Béchade C, Bernard D, Roumier A. Microglial control of neuronal death and synaptic properties. Glia 2007; 55: 233–8.

Bitsch A, Schuchardt J, Bunkowski S, Kuhlmann T, Brück W. Acute axonal injury in multiple sclerosis. Correlation with demyelination and inflammation. Brain 2000; 123 (Pt 6: 1174–83.

Bjartmar C, Kidd G, Mörk S, Rudick R, Trapp BD. Neurological disability correlates with spinal cord axonal loss and reduced N-acetyl aspartate in chronic multiple sclerosis patients. Ann. Neurol. 2000; 48: 893–901.

Bö L, Geurts JJG, Mörk SJ, van der Valk P. Grey matter pathology in multiple sclerosis. Acta Neurol. Scand. Suppl. 2006; 183: 48–50.

Bö L, Mörk S, Kong PA, Nyland H, Pardo CA, Trapp BD. Detection of MHC class II-antigens on macrophages and microglia, but not on astrocytes and endothelia in active multiple sclerosis lesions. J. Neuroimmunol. 1994; 51: 135–46.

Bø L, Vedeler CA, Nyland H, Trapp BD, Mørk SJ. Intracortical multiple sclerosis lesions are not associated with increased lymphocyte infiltration. Mult. Scler. 2003; 9: 323–31.

Bø L, Vedeler CA, Nyland HI, Trapp BD, Mørk SJ. Subpial demyelination in the cerebral cortex of multiple sclerosis patients. J. Neuropathol. Exp. Neurol. 2003; 62: 723–32.

Bogie JFJ, Stinissen P, Hendriks JJA. Macrophage subsets and microglia in multiple sclerosis. Acta Neuropathol. 2014; 128: 191–213.

Bonin S, Petrera F, Niccolini B, Stanta G. PCR analysis in archival postmortem tissues. Mol. Pathol. 2003; 56: 184–6.

Booss J, Esiri MM, Tourtellotte WW, Mason DY. Immunohistological analysis of T lymphocyte subsets in the central nervous system in chronic progressive multiple sclerosis. J. Neurol. Sci. 1983; 62: 219–32.

Bowers G, Cullinan WE, Herman JP. Region-specific regulation of glutamic acid decarboxylase (GAD) mRNA expression in central stress circuits. J. Neurosci. 1998; 18: 5938–47.

Bramow S, Frischer JM, Lassmann H, Koch-Henriksen N, Lucchinetti CF, Sørensen PS, et al. Demyelination versus remyelination in progressive multiple sclerosis. Brain 2010; 133: 2983–98.

Brändle SM, Obermeier B, Senel M, Bruder J, Mentele R, Khademi M, et al. Distinct oligoclonal band antibodies in multiple sclerosis recognize ubiquitous self-proteins. Proc. Natl. Acad. Sci. U. S. A. 2016; 113: 7864–9.

Brickshawana A, Hinson SR, Romero MF, Lucchinetti CF, Guo Y, Buttmann M, et al. Investigation of the KIR4.1 potassium channel as a putative antigen in patients with multiple sclerosis: a comparative study. Lancet. Neurol. 2014; 13: 795–806.

Brownwell B, Hughes JT. The distribution of plaques in the cerebrum in multiple sclerosis. J. Neurol. Neurosurg. Psychiatry 1962; 25: 315–20.

Brück W, Porada P, Poser S, Rieckmann P, Hanefeld F, Kretzschmar HA, et al. Monocyte/macrophage differentiation in early multiple sclerosis lesions. Ann. Neurol. 1995; 38: 788–96.

Calabrese M, Agosta F, Rinaldi F, Mattisi I, Grossi P, Favaretto A, et al. Cortical lesions and atrophy associated with cognitive impairment in relapsing-remitting multiple sclerosis. Arch. Neurol. 2009; 66: 1144–50.

Calabrese M, Atzori M, Bernardi V, Morra A, Romualdi C, Rinaldi L, et al. Cortical atrophy is relevant in multiple sclerosis at clinical onset. J. Neurol. 2007; 254: 1212–20.

Calabrese M, Battaglini M, Giorgio A, Atzori M, Bernardi V, Mattisi I, et al. Imaging distribution and frequency of cortical lesions in patients with multiple sclerosis. Neurology 2010; 75: 1234–40.

Calabrese M, Gallo P. Magnetic resonance evidence of cortical onset of multiple sclerosis. Mult. Scler. 2009; 15: 933–41.

Calabrese M, Poretto V, Favaretto A, Alessio S, Bernardi V, Romualdi C, et al. Cortical lesion load associates with progression of disability in multiple sclerosis. Brain 2012; 135: 2952–61.

Calabrese M, Rocca MA, Atzori M, Mattisi I, Favaretto A, Perini P, et al. A 3-year magnetic resonance imaging study of cortical lesions in relapse-onset multiple sclerosis. Ann. Neurol. 2010; 67: 376–83.

Caldeira C, Oliveira AF, Cunha C, Vaz AR, Falcão AS, Fernandes A, et al. Microglia change from a reactive to an age-like phenotype with the time in culture. Front. Cell. Neurosci. 2014; 8: 152.

Cantorna MT, Hayes CE, DeLuca HF. 1,25-Dihydroxyvitamin D3 reversibly blocks the progression of relapsing encephalomyelitis, a model of multiple sclerosis. Proc. Natl. Acad. Sci. U. S. A. 1996; 93: 7861–4.

Chang A, Smith MC, Yin X, Fox RJ, Staugaitis SM, Trapp BD. Neurogenesis in the chronic lesions of multiple sclerosis. Brain 2008; 131: 2366–75.

Chang A, Staugaitis SM, Dutta R, Batt CE, Easley KE, Chomyk AM, et al. Cortical remyelination: a new target for repair therapies in multiple sclerosis. Ann. Neurol. 2012; 72: 918–26.

Chao MJ, Barnardo MCNM, Lincoln MR, Ramagopalan S V, Herrera BM, Dyment DA, et al. HLA class I alleles tag HLA-DRB1*1501 haplotypes for differential risk in multiple sclerosis susceptibility. Proc. Natl. Acad. Sci. U. S. A. 2008; 105: 13069–74.

Chard DT, Griffin CM, Parker GJM, Kapoor R, Thompson AJ, Miller DH. Brain atrophy in clinically early relapsing-remitting multiple sclerosis. Brain 2002; 125: 327–37.

Chen Z, Jalabi W, Hu W, Park H-J, Gale JT, Kidd GJ, et al. Microglial displacement of inhibitory synapses provides neuroprotection in the adult brain. Nat. Commun. 2014; 5: 4486.

Chen Z, Trapp BD. Microglia and neuroprotection. J. Neurochem. 2016; 136

Suppl: 10–7.

Chu AB, Sever JL, Madden DL, Iivanainen M, Leon M, Wallen W, et al. Oligoclonal IgG bands in cerebrospinal fluid in various neurological diseases. Ann. Neurol. 1983; 13: 434–9.

Ciccarelli O, Chen JT. MS cortical lesions on double inversion recovery MRI: few but true. Neurology 2012; 78: 296–7.

Ciccarelli O, Werring DJ, Barker GJ, Griffin CM, Wheeler-Kingshott CAM, Miller DH, et al. A study of the mechanisms of normal-appearing white matter damage in multiple sclerosis using diffusion tensor imaging--evidence of Wallerian degeneration. J. Neurol. 2003; 250: 287–92.

Ciccarelli O, Werring DJ, Wheeler-Kingshott CA, Barker GJ, Parker GJ, Thompson AJ, et al. Investigation of MS normal-appearing brain using diffusion tensor MRI with clinical correlations. Neurology 2001; 56: 926–33.

Cifelli A, Arridge M, Jezzard P, Esiri MM, Palace J, Matthews PM. Thalamic neurodegeneration in multiple sclerosis. Ann. Neurol. 2002; 52: 650–3.

Coles AJ, Wing MG, Molyneux P, Paolillo A, Davie CM, Hale G, et al. Monoclonal antibody treatment exposes three mechanisms underlying the clinical course of multiple sclerosis. Ann. Neurol. 1999; 46: 296–304.

Colton CA, Gilbert DL. Microglia, an in vivo source of reactive oxygen species in the brain. Adv. Neurol. 1993; 59: 321–6.

Compston A, Coles A. Multiple sclerosis. Lancet 2008; 372: 1502–17.

Confavreux C, Vukusic S, Moreau T, Adeleine P. Relapses and Progression of Disability in Multiple Sclerosis. N. Engl. J. Med. 2000; 343: 1430–1438.

Cotton F, Weiner HL, Jolesz FA, Guttmann CRG. MRI contrast uptake in new lesions in relapsing-remitting MS followed at weekly intervals. Neurology 2003; 60: 640–6.

Croxford AL, Kurschus FC, Waisman A. Mouse models for multiple sclerosis: historical facts and future implications. Biochim. Biophys. Acta 2011; 1812: 177–83.

Davalos D, Akassoglou K. Fibrinogen as a key regulator of inflammation in disease. Semin. Immunopathol. 2012; 34: 43–62.

Davalos D, Ryu JK, Merlini M, Baeten KM, Le Moan N, Petersen MA, et al. Fibrinogen-induced perivascular microglial clustering is required for the development of axonal damage in neuroinflammation. Nat. Commun. 2012; 3: 1227.

Dean G, Elian M. Age at immigration to England of Asian and Caribbean immigrants and the risk of developing multiple sclerosis. J. Neurol. Neurosurg. Psychiatry 1997; 63: 565–8.

DeLuca GC, Alterman R, Martin JL, Mittal A, Blundell S, Bird S, et al. Casting light on multiple sclerosis heterogeneity: the role of HLA-DRB1 on spinal cord pathology. Brain 2013; 136: 1025–34.

DeLuca GC, Ebers GC, Esiri MM. Axonal loss in multiple sclerosis: a pathological survey of the corticospinal and sensory tracts. Brain 2004; 127: 1009–18.

DeLuca GC, Ramagopalan S V, Herrera BM, Dyment DA, Lincoln MR, Montpetit A, et al. An extremes of outcome strategy provides evidence that multiple sclerosis severity is determined by alleles at the HLA-DRB1 locus. Proc. Natl. Acad. Sci. U. S. A. 2007; 104: 20896–901.

DeLuca GC, Williams K, Evangelou N, Ebers GC, Esiri MM. The contribution of demyelination to axonal loss in multiple sclerosis. Brain 2006; 129: 1507–16.

Desai RA, Davies AL, Tachrount M, Kasti M, Laulund F, Golay X, et al. Cause and prevention of demyelination in a model multiple sclerosis lesion. Ann. Neurol. 2016; 79: 591–604.

Duquette P, Décary F, Pleines J, Boivin D, Lamoureux G, Cosgrove JB, et al. Clinical sub-groups of multiple sclerosis in relation to HLA: DR alleles as possible markers of disease progression. Can. J. Neurol. Sci. 1985; 12: 106–10.

Dutta R, McDonough J, Yin X, Peterson J, Chang A, Torres T, et al. Mitochondrial dysfunction as a cause of axonal degeneration in multiple sclerosis patients. Ann. Neurol. 2006; 59: 478–89.

Dyment DA, Herrera BM, Cader MZ, Willer CJ, Lincoln MR, Sadovnick AD, et al. Complex interactions among MHC haplotypes in multiple sclerosis: susceptibility and resistance. Hum. Mol. Genet. 2005; 14: 2019–26.

Dyment DA, Yee IML, Ebers GC, Sadovnick AD. Multiple sclerosis in stepsiblings: recurrence risk and ascertainment. J. Neurol. Neurosurg. Psychiatry 2006; 77: 258–9.

East E, Gverić D, Baker D, Pryce G, Lijnen HR, Cuzner ML. Chronic relapsing

experimental allergic encephalomyelitis (CREAE) in plasminogen activator inhibitor-1 knockout mice: the effect of fibrinolysis during neuroinflammation. Neuropathol. Appl. Neurobiol. 2008; 34: 216–30.

Ebers GC. Natural history of primary progressive multiple sclerosis. Mult. Scler. 2004; 10 Suppl 1: S8-13–5.

Ebers GC, Sadovnick AD, Dyment DA, Yee IML, Willer CJ, Risch N. Parent-of-origin effect in multiple sclerosis: observations in half-siblings. Lancet (London, England) 2004; 363: 1773–4.

Ebers GC, Sadovnick AD, Risch NJ. A genetic basis for familial aggregation in multiple sclerosis. Canadian Collaborative Study Group. Nature 1995; 377: 150–1.

Eikelenboom MJ, Petzold A, Lazeron RHC, Silber E, Sharief M, Thompson EJ, et al. Multiple sclerosis: Neurofilament light chain antibodies are correlated to cerebral atrophy. Neurology 2003; 60: 219–23.

Esiri MM. Immunoglobulin-containing cells in multiple-sclerosis plaques. Lancet (London, England) 1977; 2: 478.

Esiri MM, Gay D. Immunological and neuropathological significance of the Virchow-Robin space. J. Neurol. Sci. 1990; 100: 3–8.

Evangelou N, Esiri MM, Smith S, Palace J, Matthews PM. Quantitative pathological evidence for axonal loss in normal appearing white matter in multiple sclerosis. Ann. Neurol. 2000; 47: 391–5.

Evangelou N, Konz D, Esiri MM, Smith S, Palace J, Matthews PM. Regional axonal loss in the corpus callosum correlates with cerebral white matter lesion volume and distribution in multiple sclerosis. Brain 2000; 123 (Pt 9: 1845–9.

Fabian RH, Petroff G. Intraneuronal IgG in the central nervous system: uptake by retrograde axonal transport. Neurology 1987; 37: 1780–4.

Falkenberg T, Lindefors N, O'Connor WT, Zachrisson O, Camilli F, Ungerstedt U. GABA release and GAD67 mRNA expression in rat hippocampus following entorhinal cortex activation. Brain Res. Mol. Brain Res. 1997; 48: 413–6.

Fazekas F, Barkhof F, Filippi M, Grossman RI, Li DK, McDonald WI, et al. The contribution of magnetic resonance imaging to the diagnosis of multiple sclerosis. Neurology 1999; 53: 448–56.

Ferguson B, Matyszak MK, Esiri MM, Perry VH. Axonal damage in acute multiple sclerosis lesions. Brain 1997; 120 (Pt 3: 393–9.

Filippi M, Agosta F. Magnetization transfer MRI in multiple sclerosis. J. Neuroimaging 2007; 17 Suppl 1: 22S–26S.

Filippi M, Rocca MA, Barkhof F, Brück W, Chen JT, Comi G, et al. Association between pathological and MRI findings in multiple sclerosis. Lancet. Neurol. 2012; 11: 349–60.

Fischer MT, Sharma R, Lim JL, Haider L, Frischer JM, Drexhage J, et al. NADPH oxidase expression in active multiple sclerosis lesions in relation to oxidative tissue damage and mitochondrial injury. Brain 2012; 135: 886–99.

Fischer MT, Wimmer I, Höftberger R, Gerlach S, Haider L, Zrzavy T, et al. Disease-specific molecular events in cortical multiple sclerosis lesions. Brain 2013; 136: 1799–815.

Fisniku LK, Brex PA, Altmann DR, Miszkiel KA, Benton CE, Lanyon R, et al. Disability and T2 MRI lesions: a 20-year follow-up of patients with relapse onset of multiple sclerosis. Brain 2008; 131: 808–17.

Flügel A, Odoardi F, Nosov M, Kawakami N. Autoaggressive effector T cells in the course of experimental autoimmune encephalomyelitis visualized in the light of two-photon microscopy. J. Neuroimmunol. 2007; 191: 86–97.

Fogdell A, Hillert J, Sachs C, Olerup O. The multiple sclerosis- and narcolepsy-associated HLA class II haplotype includes the DRB5*0101 allele. Tissue Antigens 1995; 46: 333–6.

Franklin RJM. Why does remyelination fail in multiple sclerosis? Nat. Rev. Neurosci. 2002; 3: 705–14.

Frischer JM, Bramow S, Dal-Bianco A, Lucchinetti CF, Rauschka H, Schmidbauer M, et al. The relation between inflammation and neurodegeneration in multiple sclerosis brains. Brain 2009; 132: 1175–89.

Frischer JM, Weigand SD, Guo Y, Kale N, Parisi JE, Pirko I, et al. Clinical and pathological insights into the dynamic nature of the white matter multiple sclerosis plaque. Ann. Neurol. 2015; 78: 710–21.

Fu L, Matthews PM, De Stefano N, Worsley KJ, Narayanan S, Francis GS, et al. Imaging axonal damage of normal-appearing white matter in multiple sclerosis.

Brain 1998; 121 (Pt 1: 103–13.

Gardner C, Magliozzi R, Durrenberger PF, Howell OW, Rundle J, Reynolds R. Cortical grey matter demyelination can be induced by elevated pro-inflammatory cytokines in the subarachnoid space of MOG-immunized rats. Brain 2013; 136: 3596–608.

Gay D, Esiri M. Blood-brain barrier damage in acute multiple sclerosis plaques. An immunocytological study. Brain 1991; 114 (Pt 1: 557–72.

Geurts JJG, Bö L, Pouwels PJW, Castelijns JA, Polman CH, Barkhof F. Cortical lesions in multiple sclerosis: combined postmortem MR imaging and histopathology. AJNR. Am. J. Neuroradiol. 2005; 26: 572–7.

Geurts JJG, Calabrese M, Fisher E, Rudick RA. Measurement and clinical effect of grey matter pathology in multiple sclerosis. Lancet. Neurol. 2012; 11: 1082–92.

Gill SK, Ishak M, Rylett RJ. Exposure of nuclear antigens in formalin-fixed, paraffin-embedded necropsy human spinal cord tissue: detection of NeuN. J. Neurosci. Methods 2005; 148: 26–35.

Giorgio A, Stromillo ML, Rossi F, Battaglini M, Hakiki B, Portaccio E, et al. Cortical lesions in radiologically isolated syndrome. Neurology 2011; 77: 1896–9.

Gorgoraptis N, Wheeler-Kingshott CAM, Jenkins TM, Altmann DR, Miller DH, Thompson AJ, et al. Combining tractography and cortical measures to test system-specific hypotheses in multiple sclerosis. Mult. Scler. 2010; 16: 555–65.

Goulden R, Ibrahim T, Wolfson C. Is high socioeconomic status a risk factor for

multiple sclerosis? A systematic review. Eur. J. Neurol. 2015; 22: 899–911.

Gourraud P-A, Sdika M, Khankhanian P, Henry RG, Beheshtian A, Matthews PM, et al. A genome-wide association study of brain lesion distribution in multiple sclerosis. Brain 2013; 136: 1012–24.

Goverman J. Autoimmune T cell responses in the central nervous system. Nat. Rev. Immunol. 2009; 9: 393–407.

Grabert K, Michoel T, Karavolos MH, Clohisey S, Baillie JK, Stevens MP, et al. Microglial brain region-dependent diversity and selective regional sensitivities to aging. Nat. Neurosci. 2016; 19: 504–516.

De Groot CJ, Bergers E, Kamphorst W, Ravid R, Polman CH, Barkhof F, et al. Post-mortem MRI-guided sampling of multiple sclerosis brain lesions: increased yield of active demyelinating and (p)reactive lesions. Brain 2001; 124: 1635–45.

Grossman RI, Gonzalez-Scarano F, Atlas SW, Galetta S, Silberberg DH. Multiple sclerosis: gadolinium enhancement in MR imaging. Radiology 1986; 161: 721–5.

Grussu F, Schneider T, Yates RL, Zhang H, Wheeler-Kingshott CAMG, DeLuca GC, et al. A framework for optimal whole-sample histological quantification of neurite orientation dispersion in the human spinal cord. J. Neurosci. Methods 2016; 273: 20–32.

Gveric D, Herrera B, Petzold A, Lawrence DA, Cuzner ML. Impaired fibrinolysis in multiple sclerosis: a role for tissue plasminogen activator inhibitors. Brain 2003; 126: 1590–8.

Haider L, Fischer MT, Frischer JM, Bauer J, Höftberger R, Botond G, et al. Oxidative damage in multiple sclerosis lesions. Brain 2011; 134: 1914–24.

Haider L, Zrzavy T, Hametner S, Höftberger R, Bagnato F, Grabner G, et al. The topograpy of demyelination and neurodegeneration in the multiple sclerosis brain. Brain 2016; 139: 807–15.

Hametner S, Wimmer I, Haider L, Pfeifenbring S, Brück W, Lassmann H. Iron and neurodegeneration in the multiple sclerosis brain. Ann. Neurol. 2013; 74: 848–61.

Hammond SR, English DR, McLeod JG. The age-range of risk of developing multiple sclerosis: evidence from a migrant population in Australia. Brain 2000: 968–74.

Han MH, Hwang S-I, Roy DB, Lundgren DH, Price J V, Ousman SS, et al. Proteomic analysis of active multiple sclerosis lesions reveals therapeutic targets. Nature 2008; 451: 1076–81.

Handunnetthi L, Ramagopalan S V, Ebers GC. Multiple sclerosis, vitamin D, and HLA-DRB1*15. Neurology 2010; 74: 1905–10.

Hanisch U-K, Kettenmann H. Microglia: active sensor and versatile effector cells in the normal and pathologic brain. Nat. Neurosci. 2007; 10: 1387–94.

Harel A, Ceccarelli A, Farrell C, Fabian M, Howard J, Riley C, et al. Phase-Sensitive Inversion-Recovery MRI Improves Longitudinal Cortical Lesion Detection in Progressive MS. PLoS One 2016; 11: e0152180.

Harrison DM, Oh J, Roy S, Wood ET, Whetstone A, Seigo MA, et al. Thalamic lesions in multiple sclerosis by 7T MRI: Clinical implications and relationship to cortical pathology. Mult. Scler. 2015; 21: 1139–50.

Harrison DM, Roy S, Oh J, Izbudak I, Pham D, Courtney S, et al. Association of Cortical Lesion Burden on 7-T Magnetic Resonance Imaging With Cognition and Disability in Multiple Sclerosis. JAMA Neurol. 2015; 72: 1004–12.

Harvey L, Burne THJ, McGrath JJ, Eyles DW. Developmental vitamin D3 deficiency induces alterations in immune organ morphology and function in adult offspring. J. Steroid Biochem. Mol. Biol. 2010; 121: 239–242.

Hauser SL, Waubant E, Arnold DL, Vollmer T, Antel J, Fox RJ, et al. B-cell depletion with rituximab in relapsing-remitting multiple sclerosis. N. Engl. J. Med. 2008; 358: 676–88.

Healy BC, Ali EN, Guttmann CRG, Chitnis T, Glanz BI, Buckle G, et al. Smoking and disease progression in multiple sclerosis. Arch. Neurol. 2009; 66: 858–64.

Hedström AK, Hillert J, Olsson T, Alfredsson L. Smoking and multiple sclerosis susceptibility. Eur. J. Epidemiol. 2013; 28: 867–74.

Hensiek AE, Sawcer SJ, Feakes R, Deans J, Mander A, Akesson E, et al. HLA-DR 15 is associated with female sex and younger age at diagnosis in multiple sclerosis. J. Neurol. Neurosurg. Psychiatry 2002; 72: 184–7.

Hochmeister S, Grundtner R, Bauer J, Engelhardt B, Lyck R, Gordon G, et al. Dysferlin is a new marker for leaky brain blood vessels in multiple sclerosis. J. Neuropathol. Exp. Neurol. 2006; 65: 855–65.

Holick MF. Vitamin D deficiency. N. Engl. J. Med. 2007; 357: 266–81.

Holness CL, Simmons DL. Molecular cloning of CD68, a human macrophage marker related to lysosomal glycoproteins. Blood 1993; 81: 1607–13.

Horakova D, Zivadinov R, Weinstock-Guttman B, Havrdova E, Tamaño-Blanco M, Tyblova M, et al. HLA DRB1*1501 is only modestly associated with lesion burden at the first demyelinating event. J. Neuroimmunol. 2011; 236: 76–80.

Horsfield MA, Barker GJ, Barkhof F, Miller DH, Thompson AJ, Filippi M. Guidelines for using quantitative magnetization transfer magnetic resonance imaging for monitoring treatment of multiple sclerosis. J. Magn. Reson. Imaging 2003; 17: 389–97.

van Horssen J, Brink BP, de Vries HE, van der Valk P, Bø L. The blood-brain barrier in cortical multiple sclerosis lesions. J. Neuropathol. Exp. Neurol. 2007; 66: 321–8.

Howell OW, Reeves CA, Nicholas R, Carassiti D, Radotra B, Gentleman SM, et al. Meningeal inflammation is widespread and linked to cortical pathology in multiple sclerosis. Brain 2011; 134: 2755–71.

Howell OW, Schulz-Trieglaff EK, Carassiti D, Gentleman SM, Nicholas R, Roncaroli F, et al. Extensive grey matter pathology in the cerebellum in multiple sclerosis is linked to inflammation in the subarachnoid space. Neuropathol. Appl. Neurobiol. 2015; 41: 798–813.

Idiman E, Ozakbas S, Dogan Y, Kosehasanogullari G. The significance of oligoclonal bands in multiple sclerosis: relevance of demographic and clinical

features, and immunogenetic backgrounds. J. Neuroimmunol. 2009; 212: 121–4.

Ingle GT, Sastre-Garriga J, Miller DH, Thompson AJ. Is inflammation important in early PPMS? a longitudinal MRI study. J. Neurol. Neurosurg. Psychiatry 2005; 76: 1255–8.

Isobe N, Keshavan A, Gourraud P-A, Zhu AH, Datta E, Schlaeger R, et al. Association of HLA Genetic Risk Burden With Disease Phenotypes in Multiple Sclerosis. JAMA Neurol. 2016; 73: 795–802.

Jangi S, Gandhi R, Cox LM, Li N, von Glehn F, Yan R, et al. Alterations of the human gut microbiome in multiple sclerosis. Nat. Commun. 2016; 7: 12015.

Kawanokuchi J, Mizuno T, Takeuchi H, Kato H, Wang J, Mitsuma N, et al. Production of interferon-gamma by microglia. Mult. Scler. 2006; 12: 558–64.

Kearney H, Miller DH, Ciccarelli O. Spinal cord MRI in multiple sclerosis[mdash]diagnostic, prognostic and clinical value. Nat. Rev. Neurol. 2015; 11: 327.

Kettenmann H, Kirchhoff F, Verkhratsky A. Microglia: new roles for the synaptic stripper. Neuron 2013; 77: 10–8.

Khademi M, Dring AM, Gilthorpe JD, Wuolikainen A, Al Nimer F, Harris RA, et al. Intense inflammation and nerve damage in early multiple sclerosis subsides at older age: a reflection by cerebrospinal fluid biomarkers. PLoS One 2013; 8: e63172.

Kigerl KA, Gensel JC, Ankeny DP, Alexander JK, Donnelly DJ, Popovich PG.

Identification of two distinct macrophage subsets with divergent effects causing either neurotoxicity or regeneration in the injured mouse spinal cord. J. Neurosci. 2009; 29: 13435–44.

Kilsdonk ID, Jonkman LE, Klaver R, van Veluw SJ, Zwanenburg JJM, Kuijer JPA, et al. Increased cortical grey matter lesion detection in multiple sclerosis with 7 T MRI: a post-mortem verification study. Brain 2016; 139: 1472–81.

Kirk J, Plumb J, Mirakhur M, McQuaid S. Tight junctional abnormality in multiple sclerosis white matter affects all calibres of vessel and is associated with blood-brain barrier leakage and active demyelination. J. Pathol. 2003; 201: 319–27.

Klaver R, Popescu V, Voorn P, Galis-de Graaf Y, van der Valk P, de Vries HE, et al. Neuronal and axonal loss in normal-appearing gray matter and subpial lesions in multiple sclerosis. J. Neuropathol. Exp. Neurol. 2015; 74: 453–8.

Kleinewietfeld M, Manzel A, Titze J, Kvakan H, Yosef N, Linker RA, et al. Sodium chloride drives autoimmune disease by the induction of pathogenic TH17 cells. Nature 2013; 496: 518–22.

Koch M, Kingwell E, Rieckmann P, Tremlett H. The natural history of primary progressive multiple sclerosis. Neurology 2009; 73: 1996–2002.

Kolasinski J, Stagg CJ, Chance SA, Deluca GC, Esiri MM, Chang E-H, et al. A combined post-mortem magnetic resonance imaging and quantitative histological study of multiple sclerosis pathology. Brain 2012; 135: 2938–51.

Kooi E-J, Geurts JJG, van Horssen J, Bø L, van der Valk P. Meningeal inflammation is not associated with cortical demyelination in chronic multiple sclerosis. J.

Neuropathol. Exp. Neurol. 2009; 68: 1021–8.

Kornek B, Storch MK, Weissert R, Wallstroem E, Stefferl A, Olsson T, et al. Multiple sclerosis and chronic autoimmune encephalomyelitis: a comparative quantitative study of axonal injury in active, inactive, and remyelinated lesions. Am. J. Pathol. 2000; 157: 267–76.

Kremenchutzky M, Rice GPA, Baskerville J, Wingerchuk DM, Ebers GC. The natural history of multiple sclerosis: a geographically based study 9: observations on the progressive phase of the disease. Brain 2006; 129: 584–94.

Kurtzke JF. Epidemiology and etiology of multiple sclerosis. Phys. Med. Rehabil. Clin. N. Am. 2005; 16: 327–49.

Kutzelnigg A, Faber-Rod JC, Bauer J, Lucchinetti CF, Sorensen PS, Laursen H, et al. Widespread demyelination in the cerebellar cortex in multiple sclerosis. Brain Pathol. 2007; 17: 38–44.

Kutzelnigg A, Lassmann H. Cortical lesions and brain atrophy in MS. J. Neurol. Sci. 2005; 233: 55–9.

Kutzelnigg A, Lassmann H. Cortical demyelination in multiple sclerosis: a substrate for cognitive deficits? J. Neurol. Sci. 2006; 245: 123–6.

Kutzelnigg A, Lucchinetti CF, Stadelmann C, Brück W, Rauschka H, Bergmann M, et al. Cortical demyelination and diffuse white matter injury in multiple sclerosis. Brain 2005; 128: 2705–12.

Lassmann H. Experimental models of multiple sclerosis. Rev. Neurol. (Paris).

2007; 163: 651–5.

Lassmann H, van Horssen J, Mahad D. Progressive multiple sclerosis: pathology and pathogenesis. Nat. Rev. Neurol. 2012; 8: 647–56.

Laule C, Vavasour IM, Leung E, Li DKB, Kozlowski P, Traboulsee AL, et al. Pathological basis of diffusely abnormal white matter: insights from magnetic resonance imaging and histology. Mult. Scler. 2011; 17: 144–50.

Laule C, Yung A, Pavolva V, Bohnet B, Kozlowski P, Hashimoto SA, et al. High-resolution myelin water imaging in post-mortem multiple sclerosis spinal cord: A case report. Mult. Scler. 2016

Leech S, Kirk J, Plumb J, McQuaid S. Persistent endothelial abnormalities and blood-brain barrier leak in primary and secondary progressive multiple sclerosis. Neuropathol. Appl. Neurobiol. 2007; 33: 86–98.

Lemire JM, Archer DC. 1,25-dihydroxyvitamin D3 prevents the in vivo induction of murine experimental autoimmune encephalomyelitis. J. Clin. Invest. 1991; 87: 1103–7.

Li Y, Blanco GD, Lei Z, Xu ZC. Increased GAD expression in the striatum after transient cerebral ischemia. Mol. Cell. Neurosci. 2010; 45: 370–7.

Linden JR, Ma Y, Zhao B, Harris JM, Rumah KR, Schaeren-Wiemers N, et al. Clostridium perfringens Epsilon Toxin Causes Selective Death of Mature Oligodendrocytes and Central Nervous System Demyelination. MBio 2015; 6: e02513-14.

Loevner LA, Grossman RI, Cohen JA, Lexa FJ, Kessler D, Kolson DL. Microscopic disease in normal-appearing white matter on conventional MR images in patients with multiple sclerosis: assessment with magnetization-transfer measurements. Radiology 1995; 196: 511–5.

Lovas G, Szilágyi N, Majtényi K, Palkovits M, Komoly S. Axonal changes in chronic demyelinated cervical spinal cord plaques. Brain 2000: 308–17.

Lublin FD, Reingold SC, Cohen JA, Cutter GR, Sørensen PS, Thompson AJ, et al. Defining the clinical course of multiple sclerosis: the 2013 revisions. Neurology 2014; 83: 278–86.

Lucchinetti CF, Popescu BFG, Bunyan RF, Moll NM, Roemer SF, Lassmann H, et al. Inflammatory cortical demyelination in early multiple sclerosis. N. Engl. J. Med. 2011; 365: 2188–97.

Lycklama à Nijeholt GJ, Bergers E, Kamphorst W, Bot J, Nicolay K, Castelijns JA, et al. Post-mortem high-resolution MRI of the spinal cord in multiple sclerosis A correlative study with conventional MRI, histopathology and clinical phenotype. Brain 2001; 124: 154–166.

Ma W, Cojocaru R, Gotoh N, Gieser L, Villasmil R, Cogliati T, et al. Gene expression changes in aging retinal microglia: relationship to microglial support functions and regulation of activation. Neurobiol. Aging 2013; 34: 2310–21.

Madsen LS, Andersson EC, Jansson L, krogsgaard M, Andersen CB, Engberg J, et al. A humanized model for multiple sclerosis using HLA-DR2 and a human T-cell receptor. Nat. Genet. 1999; 23: 343–7.

Magliozzi R, Howell O, Vora A, Serafini B, Nicholas R, Puopolo M, et al. Meningeal B-cell follicles in secondary progressive multiple sclerosis associate with early onset of disease and severe cortical pathology. Brain 2007; 130: 1089–104.

Magliozzi R, Howell OW, Reeves C, Roncaroli F, Nicholas R, Serafini B, et al. A Gradient of neuronal loss and meningeal inflammation in multiple sclerosis. Ann. Neurol. 2010; 68: 477–93.

Magliozzi R, Serafini B, Rosicarelli B, Chiappetta G, Veroni C, Reynolds R, et al. B-cell enrichment and Epstein-Barr virus infection in inflammatory cortical lesions in secondary progressive multiple sclerosis. J. Neuropathol. Exp. Neurol. 2013; 72: 29–41.

Mahad D, Ziabreva I, Lassmann H, Turnbull D. Mitochondrial defects in acute multiple sclerosis lesions. Brain 2008; 131: 1722–35.

Mameli G, Cossu D, Cocco E, Masala S, Frau J, Marrosu MG, et al. Epstein-Barr virus and Mycobacterium avium subsp. paratuberculosis peptides are cross recognized by anti-myelin basic protein antibodies in multiple sclerosis patients. J. Neuroimmunol. 2014; 270: 51–5.

Mantovani A, Sica A, Sozzani S, Allavena P, Vecchi A, Locati M. The chemokine system in diverse forms of macrophage activation and polarization. Trends Immunol. 2004; 25: 677–86.

Marín-Teva JL, Dusart I, Colin C, Gervais A, van Rooijen N, Mallat M. Microglia promote the death of developing Purkinje cells. Neuron 2004; 41: 535–47.

Markovic-Plese S, Cortese I, Wandinger KP, McFarland HF, Martin R. CD4+CD28-

costimulation-independent T cells in multiple sclerosis. J. Clin. Invest. 2001; 108: 1185–94.

Masterman T, Ligers A, Olsson T, Andersson M, Olerup O, Hillert J. HLA-DR15 is associated with lower age at onset in multiple sclerosis. Ann. Neurol. 2000; 48: 211–9.

Matthews PM, Roncaroli F, Waldman A, Sormani MP, De Stefano N, Giovannoni G, et al. A practical review of the neuropathology and neuroimaging of multiple sclerosis. Pract. Neurol. 2016; 16: 279–87.

Meehan TF, DeLuca HF. The vitamin D receptor is necessary for 1alpha,25-dihydroxyvitamin D(3) to suppress experimental autoimmune encephalomyelitis in mice. Arch. Biochem. Biophys. 2002; 408: 200–4.

Mikaeloff Y, Caridade G, Tardieu M, Suissa S. Parental smoking at home and the risk of childhood-onset multiple sclerosis in children. Brain 2007; 130: 2589–95.

Miller DH, Barkhof F, Frank JA, Parker GJM, Thompson AJ. Measurement of atrophy in multiple sclerosis: pathological basis, methodological aspects and clinical relevance. Brain 2002; 125: 1676–95.

Miller DH, Chard DT, Ciccarelli O. Clinically isolated syndromes. Lancet. Neurol. 2012; 11: 157–69.

Miller DH, Hammond SR, McLeod JG, Purdie G, Skegg DC. Multiple sclerosis in Australia and New Zealand: are the determinants genetic or environmental? J. Neurol. Neurosurg. Psychiatry 1990; 53: 903–5.

Mills CD, Kincaid K, Alt JM, Heilman MJ, Hill AM. M-1/M-2 macrophages and the Th1/Th2 paradigm. J. Immunol. 2000; 164: 6166–73.

Milo R, Kahana E. Multiple sclerosis: geoepidemiology, genetics and the environment. Autoimmun. Rev. 2010; 9: A387-94.

Miron VE, Boyd A, Zhao J-W, Yuen TJ, Ruckh JM, Shadrach JL, et al. M2 microglia and macrophages drive oligodendrocyte differentiation during CNS remyelination. Nat. Neurosci. 2013; 16: 1211–8.

Mishra MK, Wee Yong V. Myeloid cells — targets of medication in multiple sclerosis. Nat. Publ. Gr. 2016; 12

Mistry N, Dixon J, Tallantyre E, Tench C, Abdel-Fahim R, Jaspan T, et al. Central veins in brain lesions visualized with high-field magnetic resonance imaging: a pathologically specific diagnostic biomarker for inflammatory demyelination in the brain. JAMA Neurol. 2013; 70: 623–8.

Mohme M, Hotz C, Stevanovic S, Binder T, Lee J-H, Okoniewski M, et al. HLA-DR15-derived self-peptides are involved in increased autologous T cell proliferation in multiple sclerosis. Brain 2013; 136: 1783–98.

Mottershead JP, Schmierer K, Clemence M, Thornton JS, Scaravilli F, Barker GJ, et al. High field MRI correlates of myelin content and axonal density in multiple sclerosis--a post-mortem study of the spinal cord. J. Neurol. 2003; 250: 1293–301.

Munger KL, Chitnis T, Ascherio A. Body size and risk of MS in two cohorts of US women. Neurology 2009; 73: 1543–50.

Munger KL, Levin LI, Hollis BW, Howard NS, Ascherio A. Serum 25-Hydroxyvitamin D Levels and Risk of Multiple Sclerosis. JAMA 2006; 296: 2832.

Munger KL, Zhang SM, O'Reilly E, Hernán MA, Olek MJ, Willett WC, et al. Vitamin D intake and incidence of multiple sclerosis. Neurology 2004; 62: 60–5.

Nelson F, Datta S, Garcia N, Rozario NL, Perez F, Cutter G, et al. Intracortical lesions by 3T magnetic resonance imaging and correlation with cognitive impairment in multiple sclerosis. Mult. Scler. 2011; 17: 1122–9.

Nimmerjahn A, Kirchhoff F, Helmchen F. Resting microglial cells are highly dynamic surveillants of brain parenchyma in vivo. Science 2005; 308: 1314–8.

Noseworthy JH, Lucchinetti C, Rodriguez M, Weinshenker BG. Multiple sclerosis. N. Engl. J. Med. 2000; 343: 938–52.

Öckinger J, Hagemann-Jensen M, Kullberg S, Engvall B, Eklund A, Grunewald J, et al. T-cell activation and HLA-regulated response to smoking in the deep airways of patients with multiple sclerosis. Clin. Immunol. 2016; 169: 114–20.

Odoardi F, Sie C, Streyl K, Ulaganathan VK, Schläger C, Lodygin D, et al. T cells become licensed in the lung to enter the central nervous system. Nature 2012; 488: 675–9.

Oksenberg JR, Barcellos LF, Cree BAC, Baranzini SE, Bugawan TL, Khan O, et al. Mapping multiple sclerosis susceptibility to the HLA-DR locus in African Americans. Am. J. Hum. Genet. 2004; 74: 160–7.

Okuda DT, Mowry EM, Beheshtian A, Waubant E, Baranzini SE, Goodin DS, et al.

Incidental MRI anomalies suggestive of multiple sclerosis: the radiologically isolated syndrome. Neurology 2009; 72: 800–5.

Okuda DT, Mowry EM, Cree BAC, Crabtree EC, Goodin DS, Waubant E, et al. Asymptomatic spinal cord lesions predict disease progression in radiologically isolated syndrome. Neurology 2011; 76: 686–92.

Okuda DT, Srinivasan R, Oksenberg JR, Goodin DS, Baranzini SE, Beheshtian A, et al. Genotype-Phenotype correlations in multiple sclerosis: HLA genes influence disease severity inferred by 1HMR spectroscopy and MRI measures. Brain 2009; 132: 250–9.

Onodera H, Nakashima I, Fujihara K, Nagata T, Itoyama Y. Elevated plasma level of plasminogen activator inhibitor-1 (PAI-1) in patients with relapsing-remitting multiple sclerosis. Tohoku J. Exp. Med. 1999; 189: 259–65.

Orton S-M, Herrera BM, Yee IM, Valdar W, Ramagopalan S V, Sadovnick AD, et al. Sex ratio of multiple sclerosis in Canada: a longitudinal study. Lancet. Neurol. 2006; 5: 932–6.

Pakpoor J, Disanto G, Gerber JE, Dobson R, Meier UC, Giovannoni G, et al. The risk of developing multiple sclerosis in individuals seronegative for Epstein-Barr virus: a meta-analysis. Mult. Scler. 2013; 19: 162–6.

Parker Harp CR, Archambault AS, Sim J, Ferris ST, Mikesell RJ, Koni PA, et al. B Cell Antigen Presentation Is Sufficient To Drive Neuroinflammation in an Animal Model of Multiple Sclerosis. J. Immunol. 2015; 194: 5077–5084.

Patani R, Balaratnam M, Vora A, Reynolds R. Remyelination can be extensive in

multiple sclerosis despite a long disease course. Neuropathol. Appl. Neurobiol. 2007; 33: 277–87.

Patrikios P, Stadelmann C, Kutzelnigg A, Rauschka H, Schmidbauer M, Laursen H, et al. Remyelination is extensive in a subset of multiple sclerosis patients. Brain 2006; 129: 3165–72.

Peferoen LAN, Vogel DYS, Ummenthum K, Breur M, Heijnen PDAM, Gerritsen WH, et al. Activation status of human microglia is dependent on lesion formation stage and remyelination in multiple sclerosis. J. Neuropathol. Exp. Neurol. 2015; 74: 48–63.

Pelisch N, Dan T, Ichimura A, Sekiguchi H, Vaughan DE, van Ypersele de Strihou C, et al. Plasminogen Activator Inhibitor-1 Antagonist TM5484 Attenuates Demyelination and Axonal Degeneration in a Mice Model of Multiple Sclerosis. PLoS One 2015; 10: e0124510.

Pera M, Alcolea D, Sánchez-Valle R, Guardia-Laguarta C, Colom-Cadena M, Badiola N, et al. Distinct patterns of APP processing in the CNS in autosomal-dominant and sporadic Alzheimer disease. Acta Neuropathol. 2013; 125: 201–13.

Peterson JW, Bö L, Mörk S, Chang A, Trapp BD. Transected neurites, apoptotic neurons, and reduced inflammation in cortical multiple sclerosis lesions. Ann. Neurol. 2001; 50: 389–400.

Pinal CS, Tobin AJ. Uniqueness and redundancy in GABA production. Perspect. Dev. Neurobiol. 1998; 5: 109–18.

Pitt D, Werner P, Raine CS. Glutamate excitotoxicity in a model of multiple

sclerosis. Nat. Med. 2000; 6: 67–70.

Popescu BFG, Bunyan RF, Parisi JE, Ransohoff RM, Lucchinetti CF. A case of multiple sclerosis presenting with inflammatory cortical demyelination. Neurology 2011; 76: 1705–10.

Pugliatti M, Sotgiu S, Rosati G. The worldwide prevalence of multiple sclerosis. Clin. Neurol. Neurosurg. 2002; 104: 182–91.

Ramagopalan S V, Deluca GC, Degenhardt A, Ebers GC. The genetics of clinical outcome in multiple sclerosis. J. Neuroimmunol. 2008; 201–202: 183–99.

Ramagopalan S V, Maugeri NJ, Handunnetthi L, Lincoln MR, Orton S-M, Dyment DA, et al. Expression of the multiple sclerosis-associated MHC class II Allele HLA-DRB1*1501 is regulated by vitamin D. PLoS Genet. 2009; 5: e1000369.

Ransohoff RM, Engelhardt B. The anatomical and cellular basis of immune surveillance in the central nervous system. Nat. Rev. Immunol. 2012; 12: 623–35.

Reynolds R, Roncaroli F, Nicholas R, Radotra B, Gveric D, Howell O. The neuropathological basis of clinical progression in multiple sclerosis. Acta Neuropathol. 2011; 122: 155–70.

Rich C, Link JM, Zamora A, Jacobsen H, Meza-Romero R, Offner H, et al. Myelin oligodendrocyte glycoprotein-35-55 peptide induces severe chronic experimental autoimmune encephalomyelitis in HLA-DR2-transgenic mice. Eur. J. Immunol. 2004; 34: 1251–61.

Ritzel RM, Patel AR, Pan S, Crapser J, Hammond M, Jellison E, et al. Age- and

location-related changes in microglial function. Neurobiol. Aging 2015; 36: 2153–63.

Rodríguez Cruz PM, Matthews L, Boggild M, Cavey A, Constantinescu CS, Evangelou N, et al. Time- and Region-Specific Season of Birth Effects in Multiple Sclerosis in the United Kingdom. JAMA Neurol. 2016; 73: 954–60.

Rosati G. The prevalence of multiple sclerosis in the world: an update. Neurol. Sci. 2001; 22: 117–39.

Rumah KR, Linden J, Fischetti VA, Vartanian T. Isolation of Clostridium perfringens type B in an individual at first clinical presentation of multiple sclerosis provides clues for environmental triggers of the disease. PLoS One 2013; 8: e76359.

Ryu JK, Petersen MA, Murray SG, Baeten KM, Meyer-Franke A, Chan JP, et al. Blood coagulation protein fibrinogen promotes autoimmunity and demyelination via chemokine release and antigen presentation. Nat. Commun. 2015; 6: 8164.

Sadovnick AD, Armstrong H, Rice GP, Bulman D, Hashimoto L, Paty DW, et al. A population-based study of multiple sclerosis in twins: update. Ann. Neurol. 1993; 33: 281–5.

Safaiyan S, Kannaiyan N, Snaidero N, Brioschi S, Biber K, Yona S, et al. Age-related myelin degradation burdens the clearance function of microglia during aging. Nat. Neurosci. 2016; 19: 995–998.

Sajja BR, Wolinsky JS, Narayana PA. Proton magnetic resonance spectroscopy in

multiple sclerosis. Neuroimaging Clin. N. Am. 2009; 19: 45–58.

Salari M, Janghorbani M, Etemadifar M, Dehghani A, Razmjoo H, Naderian G. Effects of vitamin D on retinal nerve fiber layer in vitamin D deficient patients with optic neuritis: Preliminary findings of a randomized, placebo-controlled trial. J. Res. Med. Sci. 2015; 20: 372–8.

Sanfilipo MP, Benedict RHB, Sharma J, Weinstock-Guttman B, Bakshi R. The relationship between whole brain volume and disability in multiple sclerosis: a comparison of normalized gray vs. white matter with misclassification correction. Neuroimage 2005; 26: 1068–77.

Sawcer S, Hellenthal G, Pirinen M, Spencer CCA, Patsopoulos NA, Moutsianas L, et al. Genetic risk and a primary role for cell-mediated immune mechanisms in multiple sclerosis. Nature 2011; 476: 214–9.

Scalfari A, Neuhaus A, Degenhardt A, Rice GP, Muraro PA, Daumer M, et al. The natural history of multiple sclerosis: a geographically based study 10: relapses and long-term disability. Brain 2010; 133: 1914–29.

Schläger C, Körner H, Krueger M, Vidoli S, Haberl M, Mielke D, et al. Effector T-cell trafficking between the leptomeninges and the cerebrospinal fluid. Nature 2016; 530: 349–353.

Schmierer K, Parkes HG, So P-W, An SF, Brandner S, Ordidge RJ, et al. High field (9.4 Tesla) magnetic resonance imaging of cortical grey matter lesions in multiple sclerosis. Brain 2010; 133: 858–67.

Seewann A, Kooi E-J, Roosendaal SD, Pouwels PJW, Wattjes MP, van der Valk P, et

al. Postmortem verification of MS cortical lesion detection with 3D DIR. Neurology 2012; 78: 302–8.

Seewann A, Vrenken H, Kooi E-J, van der Valk P, Knol DL, Polman CH, et al. Imaging the tip of the iceberg: visualization of cortical lesions in multiple sclerosis. Mult. Scler. 2011; 17: 1202–10.

Sierra A, Gottfried-Blackmore AC, McEwen BS, Bulloch K. Microglia derived from aging mice exhibit an altered inflammatory profile. Glia 2007; 55: 412–24.

Simon KC, van der Mei IAF, Munger KL, Ponsonby A, Dickinson J, Dwyer T, et al. Combined effects of smoking, anti-EBNA antibodies, and HLA-DRB1*1501 on multiple sclerosis risk. Neurology 2010; 74: 1365–71.

Smestad C, Brynedal B, Jonasdottir G, Lorentzen AR, Masterman T, Akesson E, et al. The impact of HLA-A and -DRB1 on age at onset, disease course and severity in Scandinavian multiple sclerosis patients. Eur. J. Neurol. 2007; 14: 835–40.

Smiley ST, King JA, Hancock WW. Fibrinogen stimulates macrophage chemokine secretion through toll-like receptor 4. J. Immunol. 2001; 167: 2887–94.

Sombekke MH, Lukas C, Crusius JBA, Tejedor D, Killestein J, Arteta D, et al. HLA-DRB1*1501 and spinal cord magnetic resonance imaging lesions in multiple sclerosis. Arch. Neurol. 2009; 66: 1531–6.

Sotirchos ES, Bhargava P, Eckstein C, Van Haren K, Baynes M, Ntranos A, et al. Safety and immunologic effects of high- vs low-dose cholecalciferol in multiple sclerosis. Neurology 2016; 86: 382–90.

Sriram S, Steiner I. Experimental allergic encephalomyelitis: a misleading model of multiple sclerosis. Ann. Neurol. 2005; 58: 939–45.

Sriram S, Stratton CW, Yao S, Tharp A, Ding L, Bannan JD, et al. Chlamydia pneumoniae infection of the central nervous system in multiple sclerosis. Ann. Neurol. 1999; 46: 6–14.

Srivastava R, Aslam M, Kalluri SR, Schirmer L, Buck D, Tackenberg B, et al. Potassium channel KIR4.1 as an immune target in multiple sclerosis. N. Engl. J. Med. 2012; 367: 115–23.

Staugaitis SM, Chang A, Trapp BD. Cortical pathology in multiple sclerosis: experimental approaches to studies on the mechanisms of demyelination and remyelination. Acta Neurol. Scand. Suppl. 2012: 97–102.

De Stefano N, Matthews PM, Fu L, Narayanan S, Stanley J, Francis GS, et al. Axonal damage correlates with disability in patients with relapsing-remitting multiple sclerosis. Results of a longitudinal magnetic resonance spectroscopy study. Brain 1998; 121 (Pt 8: 1469–77.

Stromnes IM, Cerretti LM, Liggitt D, Harris RA, Goverman JM. Differential regulation of central nervous system autoimmunity by T(H)1 and T(H)17 cells. Nat. Med. 2008; 14: 337–42.

Stys PK. Pathoetiology of multiple sclerosis: are we barking up the wrong tree? F1000Prime Rep. 2013; 5: 20.

Sun J, Link H, Olsson T, Xiao BG, Andersson G, Ekre HP, et al. T and B cell responses to myelin-oligodendrocyte glycoprotein in multiple sclerosis. J.

Immunol. 1991; 146: 1490–5.

Takeuchi H. Neurotoxicity by microglia: Mechanisms and potential therapeutic strategy. Clin. Exp. Neuroimmunol. 2010; 1: 12–21.

Tallantyre EC, Bø L, Al-Rawashdeh O, Owens T, Polman CH, Lowe JS, et al. Clinico-pathological evidence that axonal loss underlies disability in progressive multiple sclerosis. Mult. Scler. 2010; 16: 406–11.

Teitelbaum D, Meshorer A, Hirshfeld T, Arnon R, Sela M. Suppression of experimental allergic encephalomyelitis by a synthetic polypeptide. Eur. J. Immunol. 1971; 1: 242–8.

Thacker E, Mirzaei F, Ascherio A. Infectious mononucleosis and risk for multiple sclerosis: a meta-analysis. Ann. Neurol. 2006; 59: 499–503.

Trapp BD, Peterson J, Ransohoff RM, Rudick R, Mörk S, Bö L. Axonal transection in the lesions of multiple sclerosis. N. Engl. J. Med. 1998; 338: 278–85.

Tur C, Ramagopalan S, Altmann DR, Bodini B, Cercignani M, Khaleeli Z, et al. HLA-DRB1*15 influences the development of brain tissue damage in early PPMS. Neurology 2014; 83: 1712–8.

Ulvestad E, Williams K, Bø L, Trapp B, Antel J, Mørk S. HLA class II molecules (HLA-DR, -DP, -DQ) on cells in the human CNS studied in situ and in vitro. Immunology 1994; 82: 535–41.

VanGuilder HD, Bixler G V, Brucklacher RM, Farley JA, Yan H, Warrington JP, et al. Concurrent hippocampal induction of MHC II pathway components and glial

activation with advanced aging is not correlated with cognitive impairment. J. Neuroinflammation 2011; 8: 138.

Vercellino M, Masera S, Lorenzatti M, Condello C, Merola A, Mattioda A, et al. Demyelination, inflammation, and neurodegeneration in multiple sclerosis deep gray matter. J. Neuropathol. Exp. Neurol. 2009; 68: 489–502.

Vercellino M, Plano F, Votta B, Mutani R, Giordana MT, Cavalla P. Grey matter pathology in multiple sclerosis. J. Neuropathol. Exp. Neurol. 2005; 64: 1101–7.

Vogel DY, Vereyken EJ, Glim JE, Heijnen PD, Moeton M, van der Valk P, et al. Macrophages in inflammatory multiple sclerosis lesions have an intermediate activation status. J. Neuroinflammation 2013; 10: 35.

Voumvourakis KI, Kitsos DK, Tsiodras S, Petrikkos G, Stamboulis E. Human herpesvirus 6 infection as a trigger of multiple sclerosis. Mayo Clin. Proc. 2010; 85: 1023–30.

van Waesberghe JH, Kamphorst W, De Groot CJ, van Walderveen MA, Castelijns JA, Ravid R, et al. Axonal loss in multiple sclerosis lesions: magnetic resonance imaging insights into substrates of disability. Ann. Neurol. 1999; 46: 747–54.

Webster NL, Crowe SM. Matrix metalloproteinases, their production by monocytes and macrophages and their potential role in HIV-related diseases. J. Leukoc. Biol. 2006; 80: 1052–66.

Wegner C, Esiri MM, Chance SA, Palace J, Matthews PM. Neocortical neuronal, synaptic, and glial loss in multiple sclerosis. Neurology 2006; 67: 960–7.

Wergeland S, Myhr K-M, Løken-Amsrud KI, Beiske AG, Bjerve KS, Hovdal H, et al. Vitamin D, HLA-DRB1 and Epstein-Barr virus antibody levels in a prospective cohort of multiple sclerosis patients. Eur. J. Neurol. 2016; 23: 1064–70.

Witte ME, Mahad DJ, Lassmann H, van Horssen J. Mitochondrial dysfunction contributes to neurodegeneration in multiple sclerosis. Trends Mol. Med. 2014; 20: 179–87.

Xu J, Ling EA. Upregulation and induction of surface antigens with special reference to MHC class II expression in microglia in postnatal rat brain following intravenous or intraperitoneal injections of lipopolysaccharide. J. Anat. 1994: 285–96.

Yaldizli Ö, Sethi V, Pardini M, Tur C, Mok KY, Muhlert N, et al. HLA-DRB*1501 associations with magnetic resonance imaging measures of grey matter pathology in multiple sclerosis. Mult. Scler. Relat. Disord. 2016; 7: 47–52.

Yates RL, DeLuca GC. Comment: HLA-DRB1*1501 associations with magnetic resonance imaging measures of grey matter pathology in multiple sclerosis. Mult. Scler. Relat. Disord. 2016

Yates RL, Esiri MM, Palace J, Mittal A, DeLuca GC. The influence of HLA-DRB1*15 on motor cortical pathology in multiple sclerosis. Neuropathol. Appl. Neurobiol. 2015; 41: 371–84.

Yednock TA, Cannon C, Fritz LC, Sanchez-Madrid F, Steinman L, Karin N. Prevention of experimental autoimmune encephalomyelitis by antibodies against alpha 4 beta 1 integrin. Nature 1992; 356: 63–6.

Zivković M, Starčević Čizmarević N, Lovrečić L, Klupka-Sarić I, Stanković A, Gašparović I, et al. The role of TPA I/D and PAI-1 4G/5G polymorphisms in multiple sclerosis. Dis. Markers 2014; 2014: 362708.

Zozulya AL, Wiendl H. The role of regulatory T cells in multiple sclerosis. Nat. Clin. Pract. Neurol. 2008; 4: 384–98.

Appendix 1 - Protocol for DAB immunohistochemistry

1. De-wax sections in histoclear and and rehydrate in alcohol series
2. Incubate slides with 3% hydrogen peroxide (diluted in phosphate buffered saline) for 30 minutes
3. Perform heat-mediated antigen retrieval, as optimised
4. Mount slides onto sequenzas
5. Wash slides with TBS/T (2 x 5 minutes)
6. Apply primary antibody, as optimised, and incubate for 1 hour at room temperature, or overnight (O/N), as optimised
7. Wash slides with TBS/T (2 x 5 minutes)
8. Apply secondary antibody (neat) contained within commercial autostainer kit (Dako; catalogue number: K5007) and incubate for 40 minutes at room temperature
9. Wash slides with TBS/T (2 x 5 minutes)
10. Apply DAB chromogen (1/50 dilution) for 5 minutes at room temperature
11. Wash slides with TBS/T (2 x 5 minutes)
12. Remove slides from sequenzas and place in distilled water
13. Place slides in filtered haemotoxylin for 40 seconds at room temperature
14. Place slides in running tap water for 3 minutes
15. Dehydrate slides in alcohol series
16. Coverslip slides from histoclear

Appendix 2 - Protocol for immunofluorescence

1. De-wax sections in histoclear and and rehydrate in alcohol series
2. Perform heat-mediated antigen retrieval, as optimised
3. Mount slides onto sequenzas
4. Wash slides with TBS/T (2 x 5 minutes)
5. Apply primary antibody, as optimised, and incubate overnight at 4 degrees Celsius
6. Wash slides with TBS/T (2 x 5 minutes)
7. Apply fluorescent secondary antibody, as optimised, for 1 hour at room temperature
8. Wash slides with TBS/T (2 x 5 minutes)
9. Incubate slides with DAPI solution (0.5µg/ml) for 5 minutes at room temperature
10. Wash slides with TBS/T (2 x 5 minutes)
11. Remove slides from sequenzas and place into phosphate buffered saline
12. Incubate slides with Sudan Black solution (0.2% w/v) for 10 minutes at room temperature
13. Wash slides with TBS/T (2 x 5 minutes)
14. Coverslip slides from phosphate buffered saline using fluorescent mounting medium